THIN FILM SENSOR TECHNIQUES FOR THE INSTRUMENTATION OF CERAMIC/ METAL INTERFACES IN NEXT GENERATION AERO GAS TURBINES

Richard Stephen Shepherd

Centre for Advanced Materials and Surface Engineering
University of Salford, Salford, UK

Submitted in partial fulfilment of the requirements of the degree of Doctor of Philosophy, July 1999

Preface

This report is submitted as partial fulfilment of a Total Technology PhD course. The aims of the Total Technology course are to bring together the best aspects of a conventional PhD with the commercial focus generated by linking the research with a major industrial enterprise. The practice of engineering comprises people, planning, research, development, design, production, finance and marketing. These aspects of industry-based research projects are recognised by a Total Technology course. The situation may naturally arise that the needs of the company are reasonably taken into account when formulating the overall research programme. In this case the author is a full time employee of Rolls-Royce based in Derby. The author's responsibility includes the setting up and day-to-day management of a corporate facility for the production of thin film sensors. This involves the application of low temperature sensors when required by engine development projects and the co-ordination of the research strategy for high temperature research.

The high temperature research on which this submission is based is strongly influenced by the developing needs of the company. This has produced a broad area of research covering a number of materials and techniques aimed at the assembly of a complex sensor package for the measurement of temperature and strain on next generation aero gas turbines. This work was partially funded by the Ministry of Defence.

TABLE OF CONTENTS

LIST OF TABLES

LIST OF ILLUSTRATIONS

ACKNOWLEDGEMENTS

The author particularly wishes to thank Professor R. D. Arnell and Mr. P. Loftus for their support throughout the project.

The author is grateful to his local and senior management at Rolls-Royce for the opportunity and funding to pursue this work as a three year Ph.D. Financial support from the E.P.S.R.C is also acknowledged. The advice and support of the author's colleagues at Rolls-Royce has been greatly appreciated on many occasions. Particular thanks go to Mr. J. Gent and Mr. M. Keogh for their assistance with the NiCoCrAlY deposition trials, Mr. E. Brown and Mr. B. Hollingworth for their assistance with the sensor patterning works and Mr. M. Marshall for assistance in running the thin film facility. Also the author would like to thank Dr. G.W. Critchlow from Loughborough University for this assistance with the Auger analysis.

The author would like to thank his family and friends for their encouragement throughout the study. The support of the author's partner Juliet during the write up phase of the project is most gratefully acknowledged.

NOMENCLATURE		Units
ATP	Absolute Thermoelectric Power (Chapter 3)	μV/°C
B	Magnetic Flux Density	Tesla
E	electron charge	Coulomb
D	strain gauge wire diameter	m
EMF	Electromotive force	V
H	Magnetic Intensity	kA/m
I	Gauge excitation current	Amps
l	Gauge length	m
m	Mass of an electron	kg
r	radius of electron orbit	m
R	Electrical resistance	Ω
R_a	Average surface roughness	m
S_t	Gauge sensitivity	dimensionless
t	Time	s
T	Temperature	°C
ΔT	Temperature change	°C
T_c	Cold thermocouple junction temperature	°C
T_h	Hold thermocouple junction temperature	°C
T_m	Melting temperature	°C
V	Target potential	Volt
α	Temperature coefficient of electrical resistance	Ω/Ω/°C
Δε	Apparent strain	dimensionless
d	Wire gauge diameter	m
I	Excitation current	Ampere
ρ	Gauge resistivity	Ωm
β_w	Temperature coefficient of expansion of gauge element	m/m/°C
β_m	Temperature coefficient of expansion of substrate	m/m/°C

ABBREVIATIONS USED

AES	Auger Electron Spectroscopy
ATP	Approved Technical Package (Chapter 6)
DC	Direct Current
CAD	Computer Aided Design
CMSX-4	Cannon-Muskegon Single crystal no. 4 material
EDM	Electro Discharge Machining
EDS	Energy Dispersive Spectroscopy
GE	General Electric Inc, USA
HP	High pressure
IHI	Ishikawajima-Harima Heavy Industries, Japan
INCO	Inconel blade alloy
Karma	Trade name for nickel chromium alloy with other additives
IPM	Institute of Precious Metals, China
LP	Low pressure
ME	Measuring element
MSRR	Rolls-Royce material specification
MTU	Motoren-und Turbinen-Union, Germany
NASA	National Aeronautical and Space Administration, USA
NiCoCrAlY	Nickel-Cobalt-Chromium-Aluminium-Yttrium alloy
ONERA	Office National d'Etudes et de Recherches Aerspatiales, France
PVD	Physical vapour deposition
RF	Radio frequency (13.56 MHz)
SEM	Scanning electron microscope
TBC	Thermal barrier coating
VPS	Vacuum Plasma Spray
Zone I-III	Movchan-Demchishin zones from Thornton model
A-F	Parameters or interactions in experiment design
a-f	use of parameter in experiment where parameter is a high level

ABSTRACT

The growth of thrust and improved aeroengine efficiency has been gained by increased temperatures throughout the engine. This has been achieved by improved material technology and the continuous cooling of components complemented by the addition of thermal barrier coatings (TBC) to turbine and combustion chamber components. The aggressive nature of the application process of the TBC has previously made the measurement of metal surface temperature and strain exceedingly difficult on components to which it is applied.

In the present study magnetron sputter-deposited thin film sensor techniques have been developed specifically for compressor and turbine applications of noble metal thermocouples and strain gauges. The deposition, patterning and evaluation of reactively sputtered aluminium oxide, type R platinum thermocouples as well as PdCr and PtW dynamic strain gauges is reported. A sputtered NiCoCrAlY coating has been developed to replace the vacuum plasma spray process currently used in the TBC system. The most favourable location for the thin film sensor is at the metal/ceramic interface of the TBC system. However, in order to protect the sensor from the aggressive TBC process, the sensor has been deposited in a novel installation between two layers of NiCoCrAlY bond coat. Several trials have been performed to fabricate this package on turbine blade material substrates.

This work has demonstrated that the proposed sensor structure is feasible. However there are problems with delamination due to contamination and residual stress and with poor electrical insulation and these have limited the high temperature testing that could be performed. The novel techniques developed are already being utilised in measurement applications on components without TBCs. This work has been performed in an industrial context. The extensive project and risk management activities are reported.

AIMS AND OBJECTIVES

The work was carried out as a total technology PhD and was therefore broad in basis. In this case, the aim was to develop a solution to the problem of measuring temperature and strain on thermal barrier coated components. The solution identified and studied in this work involved developing a process to apply thin film sensors to the turbine components prior to the application of thermal barrier coatings.

In order to achieve this, a number of supporting processes needed to be developed. These included:

1. The magnetron sputtering of several layers of NiCoCrAlY to replace the currently used VPS process.

2. The development of a defect free high temperature electrical insulation layer based on the reactive sputtering of aluminium oxide.

3. The deposition, patterning and evaluation of Pt-8%W & Pd-13%Cr for high temperature dynamic strain gauges.

4. The deposition, patterning and evaluation of Pt/PtRh thin film thermocouples for turbine temperature measurements.

5. Improvement of the sensor patterning technique and more specifically the development of a lift-off patterning technique.

6. The integration of these processes into a sensor package

7. The improved patterning technique and sensor materials were also used for lower temperature applications for the acquisition of data on gas turbine aeroengines.

Chapter 1: Introduction

1.1 Introduction

The rapid expansion in civilian air transport since the 1950's has been, in part, due to the development of the gas turbine (jet) engine enabling easier long distance travel. This has fuelled a boom in tourism, both for commercial and leisure purposes. Developed in the 1930's for military uses, the jet engine now forms the basis for long distance transportation on fixed wing aircraft, short haul transport (with helicopters) and has been adapted for military ship propulsion, power generation and industrial oil and gas compression pumping.

Rolls-Royce is one of the world leaders in the design and manufacture of aero gas turbines. Founded in 1906 by the Hon. Charles Stuart Rolls and Henry Royce, the company initially produced high quality motor cars but diversified into aircraft propulsion through internal combustion driven propeller engines, then later gas turbine engines. Now a multinational company operating in a number of sectors due to the acquisition of other companies, Rolls-Royce has a multibillion pound turnover.

Derby, the original site of the car producing company, is now the centre for commercial aero gas turbine development and production. Here, new engines for airframes such as Boeing and Airbus are designed and tested through to civil and federal aviation authority certification.

The gas turbine is one of the most complex mechanical products produced today, comprising in excess of 40,000 components. To stay competitive requires continual product development, but in a mature market such as this, technical cost and development risk must be kept to a minimum. This demands a continuous improvement in the design process and evolutionary, rather than revolutionary design progression.

A key element in this, is development testing of new and existing engines. This is the main function of the experimental site. It is necessary to extract the maximum amount of information about the engine performance as early as possible in the test programme in order to reduce the number of tests required and the cost of the programme. It is also necessary to rigorously verify computer models of component performance on research rigs, in order to improve the design method and obtain a better product. Associated with this is a vast range of support services, one of which is the use (research, design and production) of sensor technology.

The environment in the engine can be quite arduous, with temperatures, for the latest Trent engine, ranging from -50°C to around 1480°C at the first turbine stage. The blades experience centripetal accelerations up to around 100,000g and dust particles impacting the surface at high velocity.

One area which has received a great deal of attention over the years has been aerofoil mounted instrumentation which provides information on, for example, temperature and strain. Lately, increased effort has been put into minimising the disturbance to the flow passing over the sensor, and to the component under test. A requirement had previously been established to develop a new sensor application technique, thin film sensors, to apply dynamic strain gauge sensors to compressor components. A corporate facility was set up by the author to research this technique and provide a sensor fabrication service using techniques that had previously been demonstrated by several subcontractors.

A new and growing requirement is to measure component temperature and strain on TBC components. This cannot be done using the conventional methods currently available. Without this, the risk to new engine development programmes, such as the Trent 500 engine for the Airbus A340, is increased.

The aim of this study was to develop the existing thin film sensor techniques to extend the current capability to those experienced in the turbine, using new materials and processes. Secondly, it was intended to fabricate a sensor package able to

withstand the subsequent application of the TBC and the conditions; temperature and vibration, found in the High Pressure (HP) turbine (see figure 1.01).

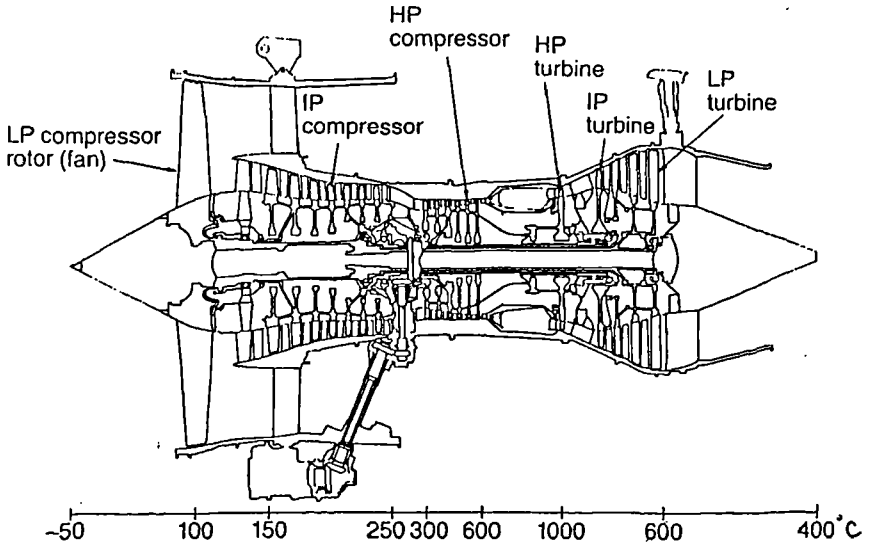

Figure 1.01: General layout and temperatures of an older RB211 engine (taken from Loftus[1])

The current strain gauge and thermocouple methods were reviewed. The limitations of these sensors for high temperature turbine use were assessed, with particular reference to instrumentation on thermally barrier coated components. The benefits of thin film sensors for strain and temperature measurement were reviewed and a brief description of the application processes given.

A proposal was made for the application of thin film sensors on thermal barrier coated components. The individual coating and techniques necessary to fabricate a sensor package were developed. The processes were then integrated to form the final sensor package. Throughout the work, project management activities were performed to ensure that the risk to the scheduled engine test from delays or inaccurate data was understood. Where possible, mitigation plans were in place to minimise the risk. The reasons for making measurements during gas turbine development is now discussed in greater detail.

1.2 Use of measurement techniques during aero gas turbine development

1.2.1 Temperature measurements

The growth of engine thrusts and improvement in thermal propulsive engine efficiency, have been partially gained by increased temperatures throughout the engine. This has been achieved by improved material technology and the continuous cooling of components so that operating temperatures can be increased without affecting blade and vane integrity (see figure 1.02). The component cooling is complemented by the addition of TBC to the turbine and combustion chamber.

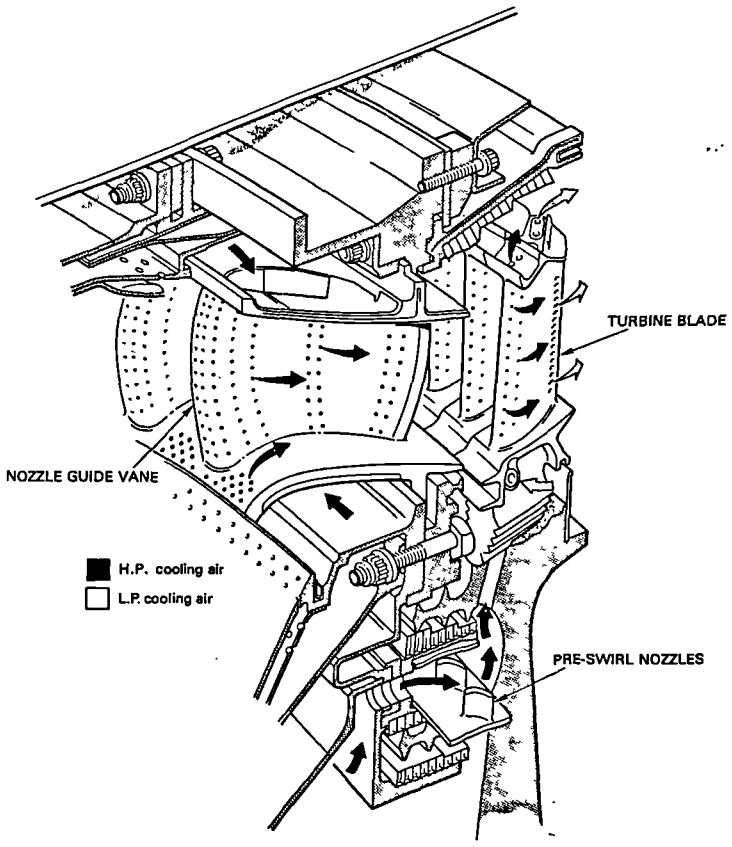

Figure 1.02: Blade cooling arrangement on a turbine component (taken from The Jet Engine[2])

Other improvements in engine design have been gained from 3-D compressor blades, manufacturing techniques such as the wide chord fan blade and the reduction in weight throughout the engine.

The measurement of surface metal temperatures can therefore asses the performance of these cooling measures and highlight hot spots in the combustion and turbine area. Future designs will increasingly involve reduced component cross-section and complexity of the cooling techniques. Most of the conventional methods for measuring surface temperature perturb the heat flow to and within the component. TBCs are also becoming increasingly used in modern engines to complement the air cooling of components. The aggressive nature of the bond coat process and temperature and atmosphere of the TBC process have previously made the measurement of metal surface temperature exceedingly difficult on components to which it is applied.

1.2.2 Vibration measurements

One of the most widely used measurement techniques at Rolls-Royce is component vibration analysis, normally by strain gauging. The main aim is to avoid any serious failures in the engine development process and to validate models on component behaviour that are used to set life in service figures. The secondary damage from a component failure in the multistage axial flow compressor or turbine of an aeroengine can be very severe. However, requirements for reducing vibration come into conflict with those of improving efficiency and reducing weight, the selling points of engines. Components are designed, for maximum efficiency, to have the minimum amount of airflow blockage and to be as light as possible. This makes them susceptible to high cycle fatigue.

The solution to the dilemma of vibration problems stems largely from the ability to predict the natural frequencies and damping of the vibrating systems in the operating environment of high and varying temperature and centrifugal force. The question

then becomes "which resonances can be lived with, and which are intolerable[3]". Remedial action must then be taken to move the intolerable resonant frequencies.

Each rotating blade is clamped at the root and will have a number of natural vibration modes. The modes have discrete vibration frequencies and deflected shapes. The mode shapes can be flap, bowstring, torsion and edgewise. (See figure 1.03). Some modes involve platform deflections as well as aerofoil deflections. Stationary stator vanes also have vibration modes, but these are bowstring-based because the stator is fixed at both ends. The vibration modes can be computer modelled for each component design, and the node positions and frequencies predicted. However, these frequencies can change whilst running-in an engine. The component material stiffness will reduce with increasing temperature. Therefore, the vibration frequency reduces with engine speed for small hot compressor components. Large cool blades experience stiffening under rotational forces. In this case flap frequencies increase with speed but torsion modes remain unaffected.

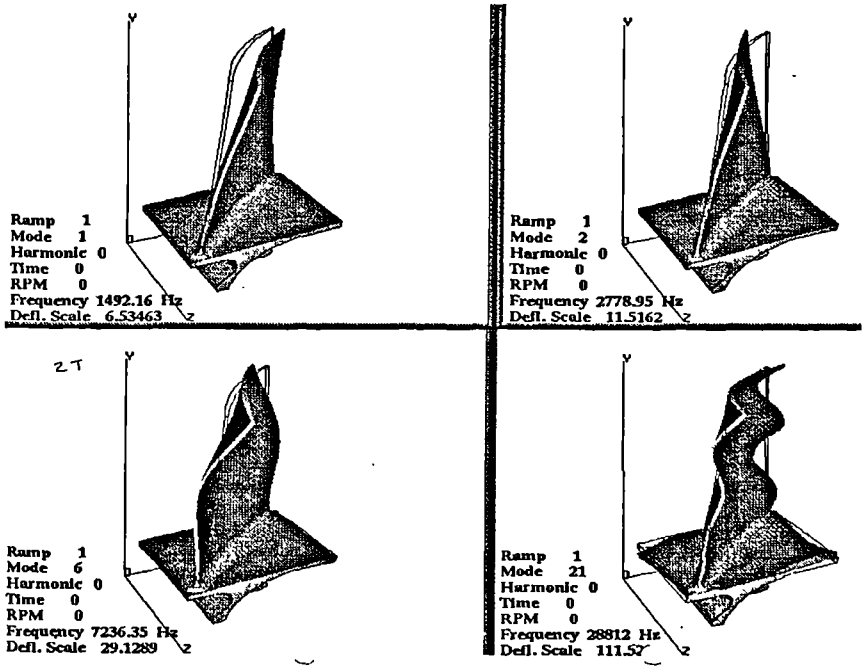

Figure 1.03: Vibration modes for a compressor blade (taken from Smailes[3])

The components can be excited in a number of ways. Interactions with other stages will be considered in this introduction. These can be predicted using vibration models. Other types of excitation, such as flutter (self excited vibration), acoustic

resonance, compressor surge and component stall are less easy to predict, either in terms of the point of occurrence or the effect on the components. This necessitates experimental testing of the engine through the entire range of possible running conditions with a number of strain gauges fitted for safety monitoring of each blade vibration mode.

The components are excited at a number of frequencies, which are engine speed related. Each component will be excited by wakes of the stages upstream of it and interactions from components downstream. The number of components in the stage and engine speed determines the frequency of excitation. Each stage normally has different component numbers to avoid these problems. The number of components in a stage gives the 'engine order' number. The most significant engine orders are normally generated by rotor/stator interactions.

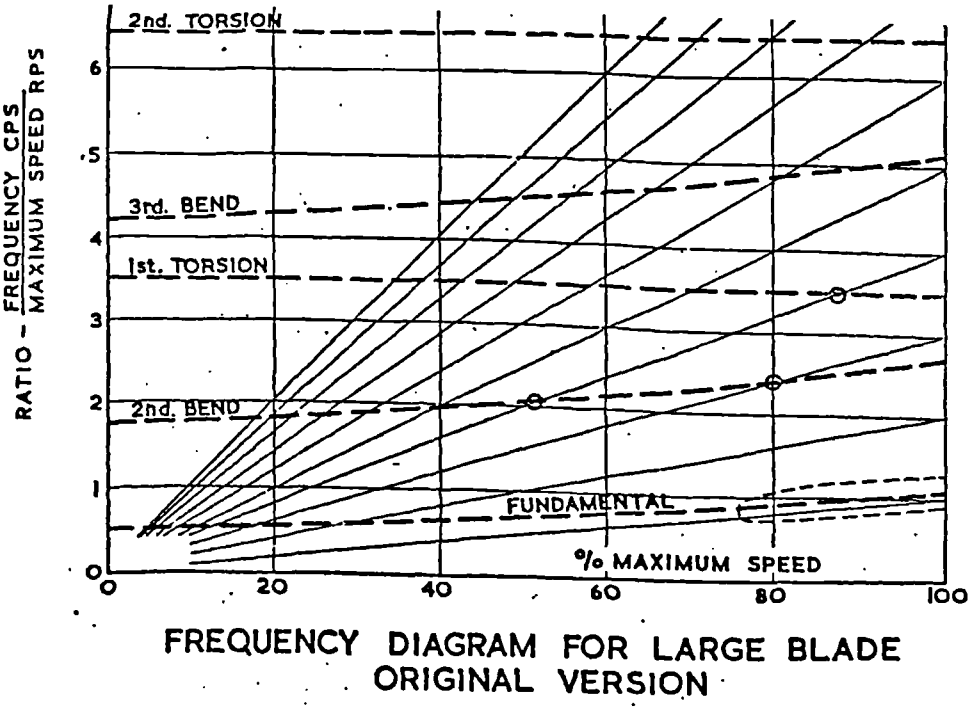

Figure 1.04: Campbell diagram of vibration frequencies against engine speed (taken from Smailes[3])

Engine order frequencies start at 0 Hz for 0 rpm and may cross component nodal frequencies causing resonance. During engine acceleration, components will exhibit

a number of modes. Also, interactions; the sum and differences of engine orders will excite the component. Therefore two, rotor stages with 31 and 38 blades will produce engine orders of 31, 38, 7 and 69. Engine orders and interactions with stages far upstream or downstream are normally less likely to excite a component. Because the wakes of the components are non-sinusoidal, harmonics will also be present.

The engine orders and modes are represented on a Campbell diagram as shown in figure 1.04[3]. This shows a Campbell diagram for a large blade. The torsion modes can be seen to remain constant with engine speed while the flap modes increase in frequency with speed. The engine orders are seen increasing with engine speed. Many resonance positions are shown. Usually the higher frequency events are dismissed. This is because the exciting force tends to diminish with frequency. Also for high frequency modes the components are split into a number of zones which move in different directions. Generally, the forces on a component increase with airflow velocity or engine speed. Attention is thus focused on the lower right side of the Campbell diagram.

Of particular concern here would be the following:

1. The fundamental frequency approaches the engine rotational frequency.
2. The second bending mode is in resonance with two engine orders.
3. The 1st torsion mode is in resonance at 87% speed.

The seriousness of these events would depend on the vibration amplitudes obtained in these modes during engine running. If necessary the mode frequency could be moved through a redesign of the blade although this is an expensive exercise.

Chapter 2: Review of strain gauges and materials

2.1 Principles of a strain gauge

The electrical resistance (R) of a metal is, amongst other parameters, a function of its state of strain. This phenomenon has found applications in electrical resistance strain gauges, pressure transducers and load cells.

A strain gauge consists of a measuring element (ME), a backing material and cement to bond the package to the component under test (See figure 2.01). The gauge has maximum sensitivity in the direction of the grid elements. The large area at the end of each grid element reduces the resistance that would cause cross-sensitivity of the gauge.

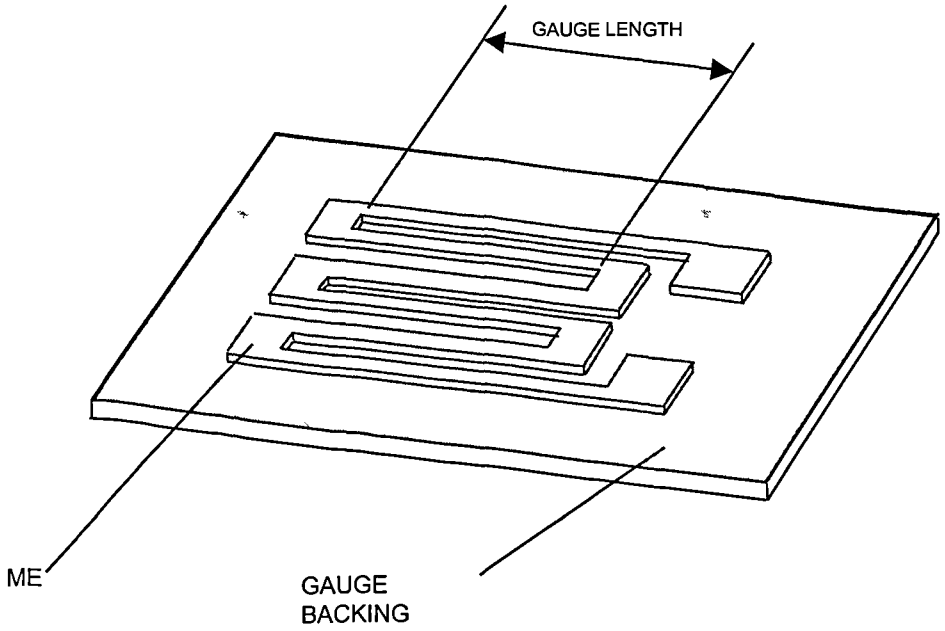

Figure 2.01: General view of a strain gauge

A suitable alloy should be used that ideally has all of the following properties: The alloy should have a high electrical resistivity (ρ). If this were not the case the leadout wires would have a significant resistance compared to the sensor and contribute to the sensitivity of the installation; The alloy should have a low temperature coefficient

of resistance (α) to minimise variations in apparent strain due to changes in temperature. The resistance/temperature relationship should remain linear over the operating range and should be reproducible over many cycles of heating and cooling; The alloy should have good resistance to oxidation; It should have a high sensitivity to strain (S_t), which should remain constant over the whole strain range and; The strain sensitivity /temperature relationship should be linear and reproducible.

None of today's materials meet all of these criteria, especially over the temperature range required by Rolls-Royce (ambient to above 1000°C). Therefore, several different materials are used to cover the range of operating temperatures[4].

The sensitivity (S_t) or Gauge Factor of the gauge is defined as:

$$S_t = \frac{\Delta R/R}{\Delta l/l} \qquad \text{Equation 1.}$$

Where R is the resistance of the strain gauge and l is the gauge length. This is one of the design characteristics of a strain gauge. There are two contributions to this [5]:

(i) The geometrical contribution, resulting from the changes in the ME geometry, which is almost equal in all metals, and;
(ii) The physical contribution, resulting from the changes in the resistivity of the measuring element with strain. This is very material sensitive.

The gauge backing should have the following virtues:

(i) Transfer the strain accurately and repeatably to the ME.
(ii) High flexibility.
(iii) High electrical insulation resistance.
(iv) Very good thermal conductivity.
(v) Low mechanical stiffness.
(vi) Good adhesion to the substrate.

2.2 Strain gauge materials

Ideally, strain gauge materials are required for the measurement of steady strain. Most common resistance alloys before Bertodo[6] were based on binary or ternary alloys of the transition elements of groups 8, 9 & 10 of the 4th period of the periodic table, with each other, or with elements from group 6. Bertodo considered other alloys consisting of the elements shown in table 2.01. Elements of the fourth period having atomic numbers lower than chromium would not be suitable from a workability point of view. Those with atomic numbers higher than Ni have inadequate oxidation resistance. Alloys containing Mg are extremely complex. Group 11 alloys containing Au & Ag were studied but these had poor resistance to oxidation. Bertodo used the premise that alloys from the same periods had similar characteristics and so concentrated on period 5 and 6 alloys.

	6	7	8	9	10	11
4	Cr	Mn	Fe	Co	Ni	Cu
5	Mo	Tc	Ru	Rh	Pd	Ag
6	W	Re	Os	Ir	Pt	Au

Table 2.01: Relevant portion of periodic table of elements (Bertodo [6])

The criteria used to study these stemmed from the equation:

$$\Delta\varepsilon = \left(\frac{\alpha}{S_t} - \beta_w\right)\frac{I^2\rho}{Kd^3} + \left(\frac{\alpha}{S_t} - \beta_w + \beta_m\right)\Delta T + \frac{\gamma t}{S_t}\Delta T \quad \text{.....Equation 2.}$$

Where:

$\Delta\varepsilon$ = Apparent strain, α = temperature coefficient of resistance, β_w = temperature coefficient of expansion of gauge element, β_m = temperature coefficient of expansion of substrate, S_t = gauge sensitivity, I = gauge excitation current, ρ = gauge resistivity, d= gauge diameter, ΔT = temperature change, t = time at temperature, γ = rate of change of resistance due to oxidation and K = heat dissipation factor

The first part of the equation represents the effect due to gauge self-heating, the middle bracket due to temperature dependent effects and the last part due to time dependent resistance drift.

If the alloy satisfies the relationship:

$$\frac{\alpha}{S_t} = \beta_w \quad \text{.....Equation 3.}$$

Then equation 2 reduces to:

$$\Delta \varepsilon = \left(\beta_m + \frac{\gamma t}{S_t} \right) \Delta T \quad \text{.....Equation 4.}$$

Here the short-term change in apparent strain would be governed by the thermal expansion of the substrate, which is predictable. The long-term drift will be a function of time dependent variables only. Thus the search for suitable alloys has concentrated on those materials that satisfy equation 3.

Of the 48 alloys studied by Bertodo[6] only 3 satisfied equation 3, namely Cu-Ni, Pd-Ag & Ni-Cr. None of these are suitable for high temperatures. Indeed, it was found that equation 2 was not compatible with high temperature alloys. As the sensitivity increases it becomes increasingly difficult to obtain a satisfactory alloy for the measurement of steady strains at high temperatures. Instead strain gauges are mainly used for the measurement of dynamic strain at high temperatures.

Bertodo[6] reported that the most satisfactory alloys for high temperature use appeared to be those containing Pt and highlighted the benefits of PtW. However, it was shown that it could exist in two states, a solid solution or duplex state. This depended on the temperature history of the material. Bertodo[6] recommended that a 45% Pt-45% Pd-10% Mo alloy be investigated in future. This exhibited a temperature coefficient of

resistance (α) of 100$\mu\Omega/\Omega/°C$ and a strain sensitivity of 4. Resistivity measurements gave values of (ρ) in the range 78-79$\mu\Omega$cm.

More recently in the 1980s, the NASA Lewis research centre has studied 34 PdCr alloys. These alloys form an adherent, self-protective scale of Cr_2O_3, which resists additional oxidation of the remaining Cr[7]. The alloy containing 13% Cr was found to be the optimum composition. Alloys containing more than 13 % Cr have poorer resistance to oxidation[8]. For fine drawn wires, Pd-Cr has exhibited a step change in resistance at 800°C but NASA Lewis have claimed that in thin film form the resistance change is linear to 1000°C[9]. This has been confirmed by Ishikawajima-Harima Heavy Industries (IHI) and the results presented to Rolls-Royce as part of a collaborative venture[10]. The resistance to oxidation of this alloy can be improved by the addition of Y or Zr to the aluminium oxide overcoat layer. More recently, further work by NASA Lewis has shown that the addition of a Cr overcoat can produce a self-protective scale. Best results were obtained by oxidising the Cr overcoat in oxygen at 600°C. With this overcoat, dynamic strain gauge operation was demonstrated to over 1000°C[11].

Work performed by the Institute of Precious Metals (IPM) in China has tried to improve the resistance to oxidation of strain gauges by alloying Pt with elements close to it in the periodic table [12,13]. Resistance to oxidation was best for the alloy PtWReNiCrY but this still has a high temperature coefficient of resistance. An alternative was a AuPtCr alloy. An optimum seven component alloy: AuPdCrPtFeAlY has a higher resistivity than Pt. The temperature coefficient of resistance is lower than PtW and can be adjusted from positive to negative by altering the content of Fe.

Alloy	Electrical Resistivity μΩ cm	Temperature Coefficient of Resistance, x10^{-6} /°C	Strain Sensitivity S_t
Pt-8%W	58	225	3.7-4.2
Pt-8.5%W	62	191	3.7-4.2
Pt-9%W	76	170	3.5

Table 2.02: Effect of variation of composition on electrical properties of PtW strain gauges[12].

The use of this gauge material for measuring static strains must be approached with caution. A PtW gauge will have an elastic limit of 5000με[14]. The gauge factors often quoted are only valid within the elastic region. PtW has a temperature coefficient of expansion (β_w) of 7.2 x10^{-6} /°C. For a gauge bonded to a stainless steel substrate which has a temperature coefficient of expansion of 18x10^{-6} /°C, there will be an induced strain of 10.8 x10^{-6} /°C [15]. Thus, for a temperature rise from 20 to 800°C there will be an induced strain of 7770με, well beyond the elastic limit of PtW. Above the elastic limit, the gauge factor of PtW approaches 2.

Bethe and Schon [16] have shown that the sensor properties such as temperature coefficient of resistance, creep and strain sensitivity are; highly dependent on the sputtering conditions. Some important parameters are substrate temperature, argon pressure, residual gas (nitrogen, oxygen water vapour), deposition power and the geometry of the glow discharge. These can all affect the final sensor.

2.3 Rolls-Royce produced high temperature strain gauges

Low temperature sensors, for use in environments less than 250°C, are purchased from a proprietor such as Micro Measurements Ltd. The sensors consist of a foil of 'Karma' patterned onto an epoxy sheet and usually include a protection layer, contact tabs and integral leadout wires. Gauges on a Kapton sheet could be used continuously to 300°C. These are bonded to the component using a resin adhesive. If the necessary surface preparation and application techniques are used then the

bonded sensor will perform satisfactory during an engine test. This type of sensor is used in a number of industries and the technique is well established.

However, above 300°C, it is difficult to find a backing material and adhesive combination that is acceptable. Since this is higher than most industries would use, Rolls-Royce have historically developed and manufactured their own gauges.

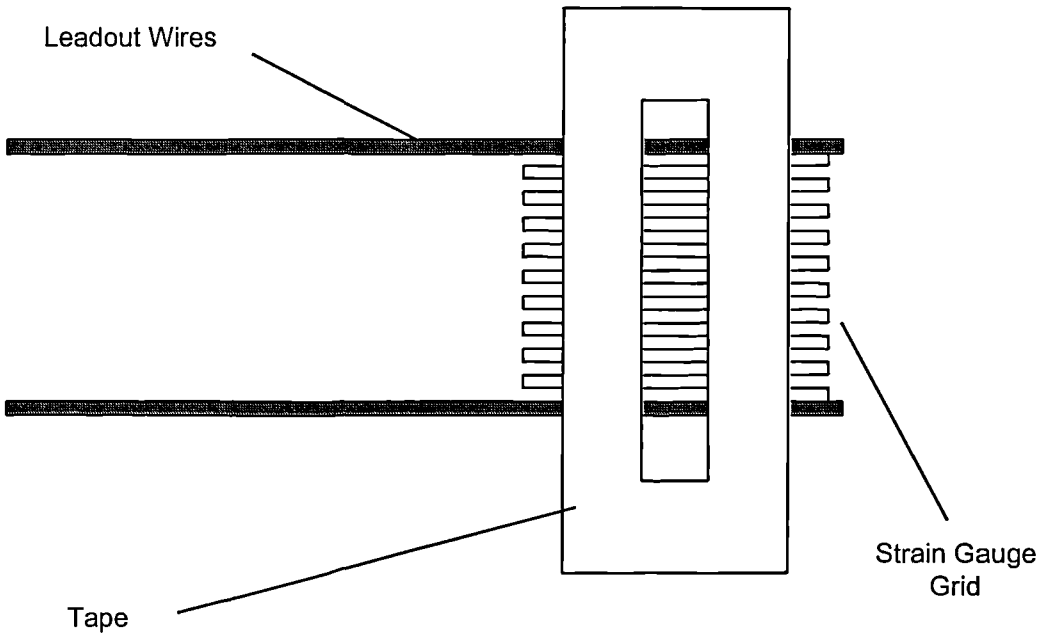

Figure 2.02: Conventional high temperature strain gauge

For tests above this temperature a Rolls-Royce produced gauge is used. This is made by wrapping 17 μm diameter Pt 8%W wire into a grid using a hand operated jig. To obtain the correct resistance the grid size is determined by the number of turns and cannot be reduced. The standard size gauge is 5 mm by 3 mm. Larger diameter 100μm Chromel leadout wires are welded to the grid and the whole assembly is held together until use by adhesive tape (see figure 2.02). Two specialist technicians are employed full time to manufacture the gauges. They can adjust the wire length used to make a gauge to obtain a resistance within ± 1Ω of the standard value. The gauges are stored until they applied to a component.

The blade surface is prepared by sand blasting. A number of thin layers of Rolls-Royce manufactured P354 ceramic cement are hand painted on. The gauge is applied to the component using the tape and further layers painted over the areas of exposed gauge. The tape is then removed and an overcoat of ceramic cement is applied over the whole gauge. Each layer must go through a curing cycle. The total thickness of the gauge is 300μm. The gauge has a sensitivity of approximately 4 at room temperature. This is routinely confirmed using a four point loaded bending beam at room temperature. The gauges can be applied 2.5 mm to the gauge centre from the aerofoil leading or trailing edge.

2.4 Limitations of conventional strain gauging

The uncertainty in low temperature dynamic strain gauge measurements is quite small and insignificant compared to the blade-to-blade variations in strain levels during a test. The uncertainty for high temperature applications becomes very large and is poorly quantified. The number and complexity of contributing error sources make an effective determination of the true error difficult[17,18,19].

Installed gauges have a thickness of 300μm and this has a detrimental effect on the testing of the component. The strain gauge can disrupt the airflow over the component altering the component performance. There is a minimum size the wire gauges can be produced to, so on very small compressor components the ceramic cement may cover the aerofoil surface. The effect of this is very difficult to quantify but is of concern to Rolls-Royce performance engineers. The size of the installation limits the number of gauges that can be fitted to the component. This makes the analysis more difficult because vibration engineers would ideally like to study all the vibration modes on the same component to eliminate the effect of blade-to-blade variations.

On small components the mass of the strain gauge can dampen the vibration modes leading to inconclusive results from very expensive tests. This has never been properly assessed. However, there is evidence that in several applications the

component would not vibrate in the mode of interest once the strain gauge had been applied[20]. In the past a trial has been made to assess the difference between gauged and ungauged components using an optical blade tip timing technique. Unfortunately this was on quite large components and any difference was hidden by blade-to-blade variations[21].

It is difficult to fit the sensors on complex components close to the blade leading and trailing edges and near the blade fillet radii. A normal design rule would be that the gauge centre cannot be specified less than 2.5 mm from a component edge or radius[22].

The conventional techniques have been developed over a period of approximately 25 years and are considered a mature technology. The quality of the gauges is very operator dependent and requires strict quality control. Specialist technicians are used for this work. This makes the process slow and expensive. For high temperature gauges one trained technician could fit one gauge in an 8-hour shift, including the leadout wires. On a low-pressure turbine component, where the component temperature will be less than 600°C, a 25% failure rate of the gauges is expected. As the temperature increases to over 1000°C on the high-pressure turbine component, 75-100% of the gauges are expected to fail over the length of an engine test[23]. At extreme surface metal temperatures (1000°C plus) on HP turbine blades, the poor bonding of ceramic cements to the blade alloy may limit the survivability of the conventional gauges[24]. The fatigue life of wire/ cement gauges is poor: in the order of 1/10 that of low temperature stick on resin type gauges[1].

2.4.1 Strain gauging on thermal barrier coated components

Increasingly TBCs are used on high-pressure turbine components. The strain gauging cannot be applied above or below this coating. Instead the component must be masked off during TBC application to leave an area of bare metal where the gauge is to be applied. The conventional wire gauge is then applied as per the previous section. The presence of the gauge will therefore alter the metal temperature because

of the differences on thermal conductivity between thermal barrier coating and ceramic cement. For extended temperature testing, gauges can be applied for initial vibration testing of the test vehicle. A build change is then required to replace the gauged components with ungauged components for the high temperature testing of the rig or engine. This increases the cost and timescales of the rig build and increases the risk of a failure of the component during the high temperature running[25]

Chapter 3: Review of temperature measurement techniques

3.1 Component temperature measurement methods

A review has been made of the various component temperature measurement methods available to Rolls-Royce[26,27]. These are shown in figure 3.01. The techniques can be divided into optical non-contacting and contacting techniques. Of the latter, thermal paints are used regularly on engine development programmes, and embedded thermocouples on specialist turbine and combustion research projects. Luminescence thermometry, thin film thermocouples and thermal melts are under development to complement or replace the existing techniques. Radiation pyrometry and thermal paints need further development to extend their high temperature capability to the higher turbine temperatures found in modern engines. Contacting techniques are preferred because they give a direct measurement of temperature. However, contacting techniques tend to be very expensive, requiring dedicated tests or expensive telemetry systems, and technically very challenging due to the harsh environment. Optical non-contacting techniques can give a cheaper alternative but access for these line-of-sight systems is often limited. Also, large errors can result from the reflection of radiation from the combustion chamber off the surface of interest.

This work will focus on thermocouple measurements. The other techniques are shown so that an overall view can be seen. This chapter will briefly describe the sensor theory and suitable materials. The conventional application method of embedding a mineral insulated thermocouple in a surface is shown. This technique has several sources of inaccuracy. These would not be applicable if a thin film sensor were used. An estimation of the expected inaccuracy of the conventional technique is made to show the benefit of using a thin film sensor.

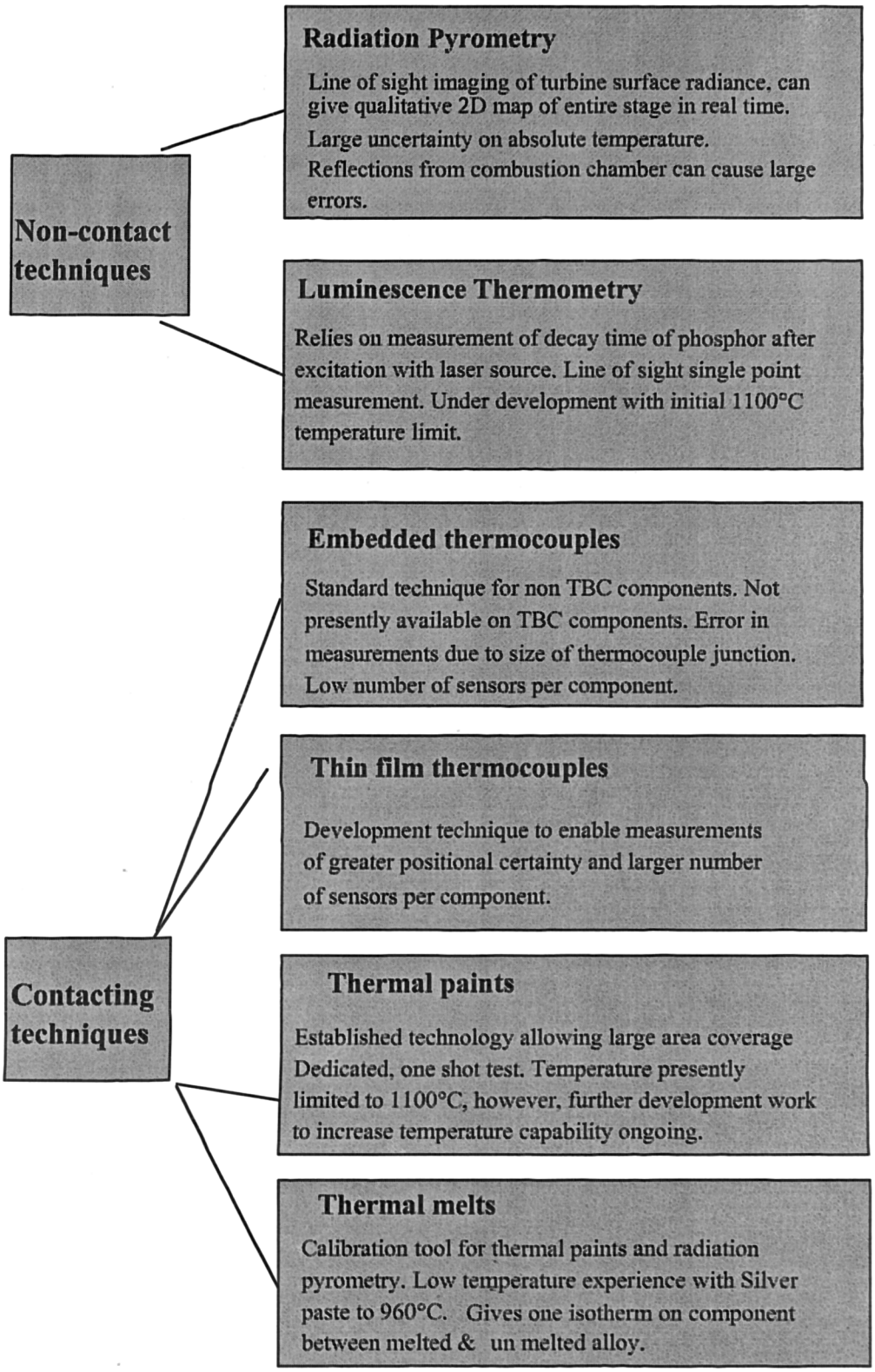

Figure 3.01 Turbine temperature measurement techniques

3.2 Thermocouple sensor theory

A metal consists of a lattice of positively charged atoms and a 'sea' of valence electrons, which dictate the electrical properties of the metal. The energy state of the electrons is a function of their temperature. When two ends of a metal conductor are at different temperatures, electrons will flow from the high-energy hot end to the lower-energy cool end thus generating an electromotive force (EMF). This is known as the Seebeck effect. The absolute thermoelectric power (ATP) for a material is expressed as the EMF generated per degree C of temperature difference. This has units of μV/°C.

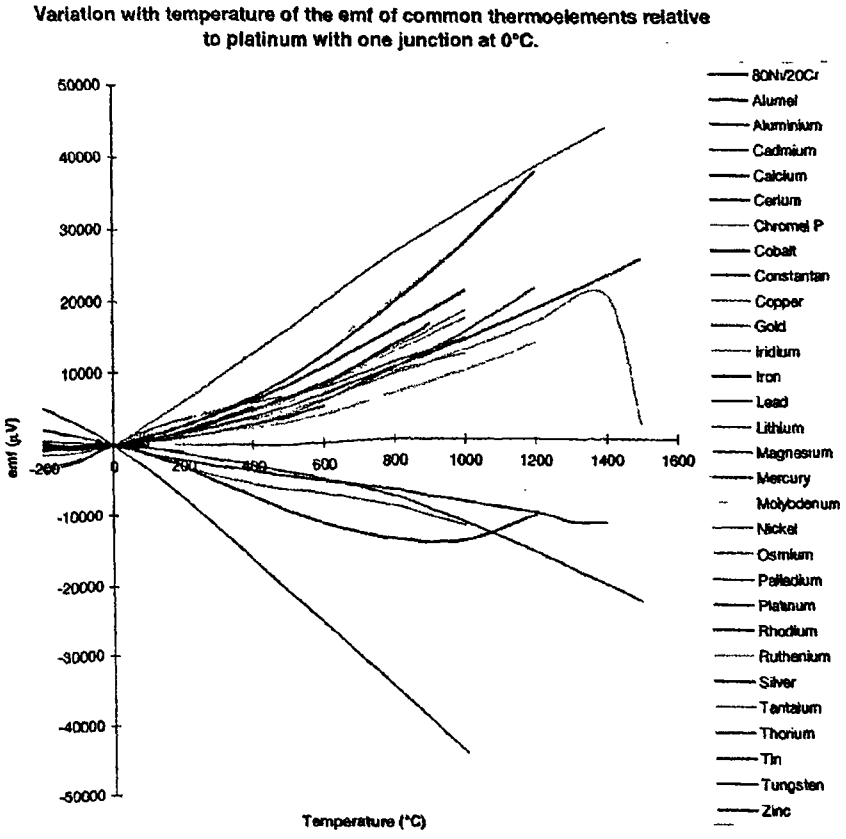

Figure 3.02: Variations in thermoelectric power of some elements and alloys relative to platinum with cold junction at 0°C (taken from Greenwood[32]) Other sources of this information: Kaye & Laby[28], Finch[29], Lide[30], Michalski[31]

The crystal lattice of the metal can be modified by the addition of impurities, such as Rh atoms, to a Pt metal lattice. This changes the behaviour of the metal as a function

of temperature. By utilising the thermoelectric power of two different metals or alloys into an electric circuit, we have the basis of a measurement system.

Materials can be classified in terms of their thermoelectric polarity. A positive material is one in which the EMF increases with temperature. Information on the EMF is available from many sources including suppliers' literature. The information is presented well in Greenwood[32]. Different materials are shown relative to pure Pt in figure 3.02;. This shows that a circuit comprising materials with different ATP's will give a net output.

Thermocouples can be categorised as noble metal, base metal, high temperature or refractory or non-metal[32,33]. The family of elements consisting of Au, Ag, Rh, Pd, Ir and Pt are commonly referred to as noble metals, which are relatively inert. Their use in thermocouples stems from their stability and absolute EMF. Certain base metals such as Cu, Fe, Ni, Al and Cr, as well as their alloys with additional impurities can be combined to produce thermo-elements with desirable properties. A simple thermocouple circuit and electrical equivalent are shown in figure 3.03.

3.4 Thermocouple materials

A review of different thermocouple alloys available in wire form has been undertaken. The results are shown in table 3.01. Of the thermocouple elements identified only types B and R have the temperature capability and stability for high temperature work. Type B is sometimes preferred because it has Rh in both legs and is therefore more stable than the type R where instability is most often due to contamination of the Pt leg[34]. This is particularly true at the hot junction where diffusion of rhodium can occur into the platinum leg[35]. This is less likely to occur if rhodium exists in both legs. The type B has a lower output. Type-R remains the most common cable type for use both as a standard in calibration laboratories and for high temperature applications furnaces and gas turbines. Pt is well known as a catalyst and this property can present a problem for temperature measurement in combusting or hydrocarbon laden flows. Here the exothermic reaction taking place at exposed

thermocouple hot junction may elevate the junction temperature above the surroundings[35].

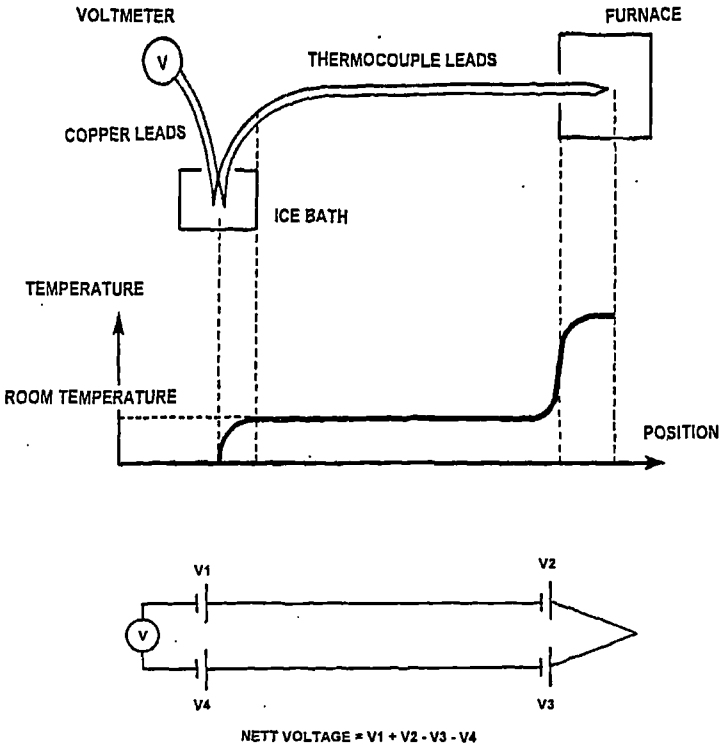

Figure 3.03: A simple thermocouple circuit and electrical equivalent (taken from Bedwell[36])

Common Names of Alloys	Temperature Range (short term)	Output (μV/°C)	Cost	Stability	Cable Spec
Copper/Constantan	-180 to + 300°C	46	low	low	Type-T
Iron /Constantan	+20 to 700°C	46	low	low	Type-J
Chromel/Constantan	0 to +800°C	68	low	low-mid	Type-E
Chromel/Alumel	0 to 1100°C	42	low	low	Type-K
Nicrosil/Nisil	0 to 1200°C	38	low	mid-high	Type-N
Platinum-Rhodium/ Platinum-Rhodium	100 to 1500°C	5	high	high	Type-B
Platinum-Rhodium/ Platinum	0 to 1400°C	10	high	high	Type-R

Table 3.01: Comparison of various thermocouple types (taken from Bedwell[36]), Original source: Kinzie[37]

3.4 Embedded thermocouples

The measurement of surface temperatures using surface thermocouple sensors is not a standard technique used on most engine development programmes. This technique is mainly used on research programmes to validate advanced combustion and turbine cooling designs. The conventional method for surface thermocouple measurements would be to embed a small diameter NiCr/NiAl (Type-K) mineral insulated cable in an Electro Discharge Machining (EDM) produced groove as shown in figure 3.04[38]. The cable would be 0.25 mm diameter and the slot 0.35 deep and wide.

The slot would be filled with a Ni based vacuum furnace braze if possible or with a NiAl alloy flame spray. The excess would then be ground off to produce a smooth surface finish. The number of thermocouples that can be fitted to a blade and the locations of the sensors are limited because the grooves can weaken the blade. Several research blade designs have also had thin section walls where the application of embedded thermocouples would be impossible.

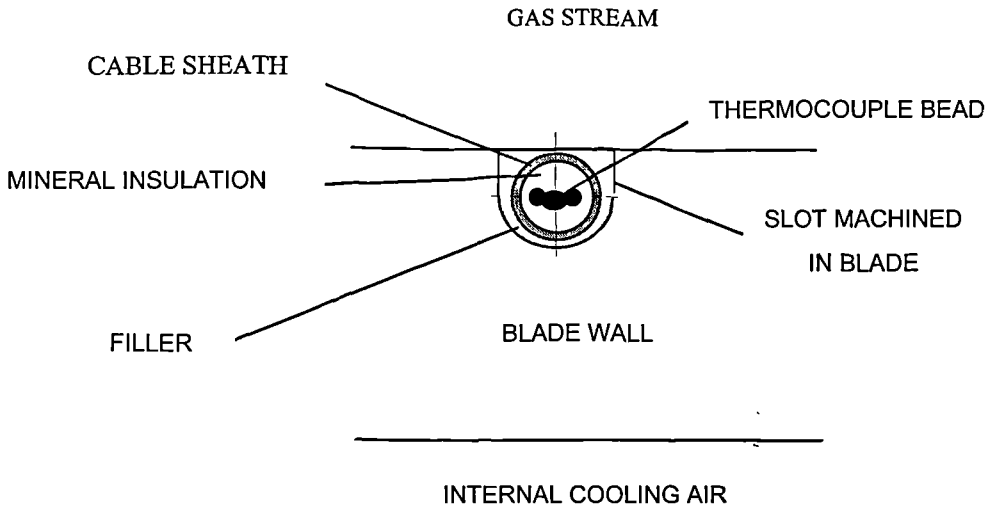

Figure 3.04: Embedded thermocouple (taken from Stringfellow[38])

This technique has been less successful on components to be thermal barrier coated. Here the NiCoCrAlY bond coat is removed, the embedded thermocouple installed and the TBC applied. A recent application trial resulted in only 2 out of twenty thermocouples working after the TBC process. The problem appears to be due to oxidation of the type K wires by the high temperature (1000°C) and high oxygen content of the TBC process. Development work is ongoing with type R platinum-platinum/rhodium thermocouple cables to prevent this. This has shown some promise and several successful installations have been produced.

3.5 Uncertainty analysis of embedded thermocouple sensors

The technique has several sources of error, which have been reviewed by Parrish[39] and reported below. For this it is assumed that the component is a turbine blade with 1 mm thick metal wall thickness between blade surface and air cooling passage. The two main error sources are due to positional uncertainty of the thermocouple bead and effect on the component from the installed thermocouple.

There is some uncertainty of the position of the thermocouple bead in the metal layer due to the slot being machined deep to bury the cable. There is also the uncertainty of position of the thermocouple bead in the mineral insulated cable. Because the metal layer will have a large temperature drop across it both these give a positional uncertainty of where the measurement is being made.

There will be an effect on the component temperature due to the installation of the thermocouple. The thermocouple will have a different thermal conductivity to the blade material as will the filler used to restore the surface. There may exist an air gap beneath the thermocouple bead and mineral insulated cable that will give a very large thermal conductivity difference from the blade material.

The magnitude of these effects has been assessed. The error summary must be quoted as a fraction of the temperature drop, ΔT, across the metal layer since this drop varies

from several hundreds of degrees Celsius to virtually nothing depending on the position on the surface of the component.

Correction for position of thermocouple	$-\Delta T/8$
Uncertainty due to installation of thermocouple	$\pm\Delta T/8$
Uncertainty in thermocouple measurement	$\pm 5°C$

Chapter 4: Literature review-Thin film sensors and processes

4.1 Thin film sensors

"The conclusion you reach by watching the world literature, is that resistance strain gauges of the future will be made by the adherent deposition of thin metal films on non-conducting layers which are in turn deposited on the base material. The amount of literature is pitifully small. A number of organisations, notably aircraft companies, have pursued this field, but their reports are not always readily available to the public"[40]. This was written in 1962. Thin film sensors have not gained the widespread use suggested here because of the complexity of the manufacturing technique. The main user of this technology is still the aerospace industry.

A thin film sensor is electrically equivalent to the conventional sensors described earlier. Its fabrication is different in that it is made of thin coatings of insulator, sensor and protective overcoat layer. A typical sensor, for example, is a dynamic strain gauge. This consists of 10μm of aluminium oxide deposited onto a polished blade surface followed by a nickel-20% chromium gauge matrix and leadout track, which is 1 μm thick. The leadout track is overcoated with 1 μm of gold to reduce unwanted resistance. The sensor grid and leadout track is overcoated with 1-2 μm of aluminium oxide, which acts as a mechanical protective coating. The coatings are applied by a vacuum sputtering process as described in section 4.2. The patterning of the sensor grid and leadout tracks is performed using a photolithographic process (section 4.4).

Over the past several decades, thin film sensor techniques have been the subject of increased interest and research. The driving force behind the research into thin film sensors is their considerable advantages over conventional methods. The main application of this technology has been for the study of compressor blade strain, turbine blade temperature measurements and study of boundary layer states.

Thin film strain gauges have an overall thickness no greater than 12 μm, compared with that of conventional ceramic cement gauges, which are up to 300 μm. This is illustrated in figure 4.01, which is a photograph of the two strain gauge types. The thickness of the conventional gauges is sufficient to cause disturbance to the airflow over the component. However, this has proved difficult to quantify, whereas for the thin film gauge, it is negligible[9]. It has also been shown that the mass of the conventional gauges has, on occasion, altered the mechanical behaviour of the component under test[41]. This is more significant for smaller components. For applications where high gradients of both stress and temperature would be present and require minimal aerodynamic effects, a thin film strain gauge is preferred. Thin film gauges allow strain readings that are truly characteristic of the blade under investigation. Their shapes and sizes are more easily adapted to individual applications and their production less sensitive to operator skill than conventional techniques.

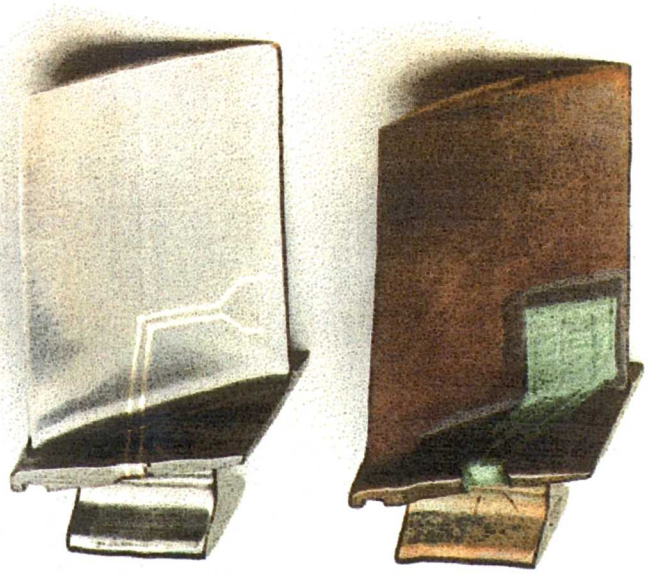

(a) Thin Film dynamic strain gauge (12 μm overall thickness)

(b) Wire in ceramic cement. (300 μm overall)

Figure 4.01: Thin film and conventional ceramic cement strain gauges mounted on the surface of compressor blades.

At extreme surface metal temperatures (1000°C plus) on HP turbine blades, the poor bonding of ceramic cements to the blade alloy may limit the survivability of the conventional gauges. The fatigue life of wire/ cement gauges is in the order of 1/10 of that of low temperature stick on resin type gauges[1]. The thin film sensors have excellent fatigue lives, and can approach that of the blade on which they are mounted.

For low temperature instrumentation (less than 500°C), this method complements the conventional techniques. However, above 500°C this technology offers a new approach for sensor production, particularly where these layers can be deposited on top of each other to form more sophisticated sensor types.

4.1.1 Strain gauge measurements

A review has been performed on the limited reports of thin film sensor applications. The application process is described in a General Electric (GE) patent[42], which describes the limitations of conventional gauges, such as the alteration of mass, shape and other natural mechanical characteristics of the competent under test. GE started working on the technique in 1970's and now has a production facility. GE has established routine production of some basic sensor types in less hostile environments[43].

When Rolls-Royce-produced thin film dynamic strain gauges have been used on aero-thermal rig tests, the limited data obtained compared well with that acquired from conventional gauges in similar locations[44].

Grant[45], Grey[46], Grey[47] and Aona[48] report other applications of thin film gauges on compressor blades. The former describes the nickel-chromium fabrication process of strain gauges on a deposited layer of silica.

Lei[8] reported the use of a welded strain gauge, consisting of a sputtered steady strain gauge, fabricated on a metal shim. The installation consisted of a Pd-Cr strain gauge

with a Pt temperature compensation leg. This allowed the application of improved sensors to components that were too large to fit into a vacuum chamber for direct deposition. The mechanical response of the weldable gauge was similar to that of a directly deposited gauge.

The potential application of thin film sensors to strain measurements on gas turbine rotor blades is discussed by Dennis[49] and Kayser[50]. Bethe[51] describes the use of thin film deposited strain gauges in transducers for the measurement of pressure, acceleration and torque and gives the method of fabrication.

An alternative sensor material of multilayered Cu-Cr is reported in Whiting[52].

4.1.2 Temperature Measurements

The increasing trend towards high temperature, fuel-efficient jet engines has led to the development of complex cooling schemes for the turbine blades. The measurement of temperature during operation, which is accomplished in conventional blade designs by embedding wire thermocouples in the blade wall, causes serious structural and aerodynamic problems in the case of cooled turbines. Budhani[53] reviews the current state of the art for this measurement, which is to deposit thin film thermocouples on a NiCoCrAlY base. A European collaborative programme[54] demonstrated thin film thermocouples of PtRh/Pt types on Ni based super alloys to 1000°C using a NiCoCrAlY plus thermally grown oxide system. Rolls-Royce was a partner in this programme with the deposition and patterning of the sensors performed by sub-contractors. Kreider[55] and Dils[56] have also used this system.

For high temperature thin film thermocouples, the need to machine a slot in the component is eliminated, allowing more scope for placement of the sensors and less positional uncertainty (see section 3.4).

A number of other reported applications of thin film thermocouple sensors have been found. Richardson[57] and Stowell[58] report the use of thin film thermocouples on turbine blades using a sputtered insulation layer.

Rimai[59] reports a method to deposit thin film thermocouples on a flexible substrate using evaporation techniques. This device allows the temperature of processes to be determined accurately without affecting the process. An example of this could be the measurement of temperature between heated rollers during a production process.

Most of the reported thin film work has been with Pt-Rh alloys. Godefroy[60] recommends a Platinel alloy thermocouple consisting of Pd-Pt-Au and Au-Pd legs. Yoshida[61] has followed this approach. It was found that the thermocouples have lower than bulk sensitivities. This may be due to the structure of the deposits but also due to contamination. It was found that the sensitivity approaches the bulk value when the thermocouple is annealed in a neutral gas. Kuo[62] describes the fabrication and calibration of Cu-Cr thermocouples.

Thin film sensors have a very low thermal mass and thus a fast response rate. This makes them ideal for fast response measurements. A number of applications are described in internal combustion engines[63,64,65,66,67].

In a description of current capabilities in 1985, GE[68] expressed an interest in applying thin film sensors under TBCs. The author could find no further information on this.

There are many other reported applications for the thin film sensor techniques. These include the application of hot film anemometer sensors and heat flux gauges on gas turbine components and the fabrication of pressure sensors. Rolls-Royce has already used thin film processes for the fabrication of hot film anemometer gauges[69,70]. Indeed, Barker[71] showed that the use of thin film deposited insulators may offer an improvement to the technique in terms of frequency response. However, there is insufficient demand or funding for this technique at present to develop it further.

4.2 Sputter deposition processes

4.2.1 Diode sputtering

Sputtering is a high vacuum process in which material is ejected from a solid surface, by a momentum exchange process, due to high-energy bombardment of the surface. The high-energy particles are ions of an inert gas, and the most common method of realisation is by forming an abnormal glow discharge in argon[72]. Here, the potential difference across the gas is increased until it breaks down to form a plasma. The plasma consists of neutral atoms and charged species consisting of ions (for example an argon atom where an electron has acquired sufficient energy to escape leaving the resultant positively charged). The argon ions so produced, strike the cathode and release material from the cathode, usually in atomic form. The sputter yield, (i.e., the number of atoms sputtered per incident ion) increases almost linearly with ion energy up to about 500eV[73]. Because of the momentum transfer process, the yield depends on the relative masses of atom and ion. Thus, the sputter yield and hence, the deposition rate is material and plasma dependent Table 4.01 gives a list of some materials likely to be used in this project and their sputter yield relative to aluminium for dc diode sputtering with argon.

Material	Yield relative to aluminium
Chromium	1.04
Gold	2.20
Nickel	1.20
Palladium	1.24
Platinum	1.16
Tungsten	0.50

Table 4.01: Sputter yields of various materials relative to aluminium (taken from CVC information bulletin[74])

As well as removing an atom, the collision also ejects a secondary electron. This is accelerated towards the anode causing further ionisation, and thus the plasma

becomes self-sustaining. Positive ions are the most convenient source for sputtering since varying the potential on the target can control their momentum[75]. Over 95% of the incident ion's energy remain in the target, so sputtering targets must be cooled.

Any surface placed near to the cathode will intercept atoms from the cathode and be coated. The atoms will leave the target in all directions and undergo further collisional scattering with argon atoms. The amount, energy and angle of atoms reaching the substrate are highly dependent on the working pressure of argon[76]. The electrons produced have a mean free path greater than the dimensions of the sputtering system. These are of interest because they can reach the anode and cause heating of the substrate.

4.3.1 Magnetron sputtering

Diode sputtering suffers from very low deposition rates. An improvement to the technique is to magnetically enhance the process and is known as magnetron sputtering. The magnetron uses the principle of applying a specially shaped magnetic field to a diode cathode.

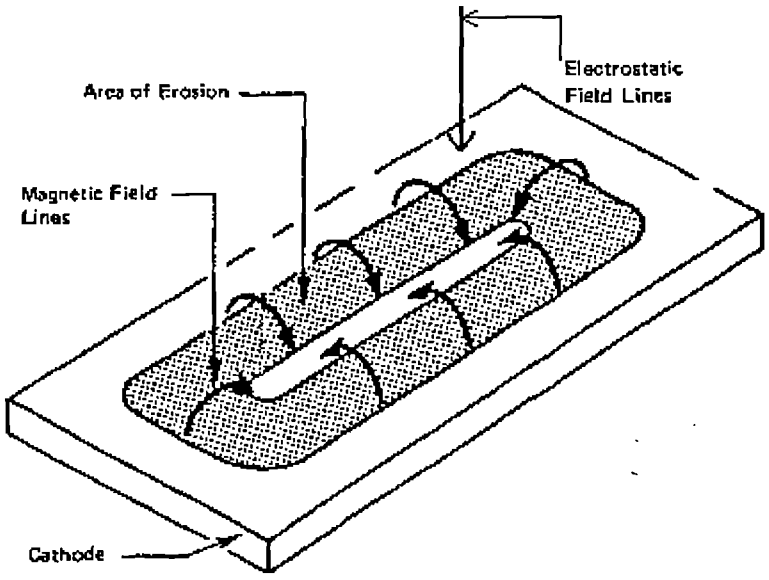

Figure 4.02: Magnetic field line arrangement in magnetron sputtering (taken from CVC training material[76])

The negative potential on the target establishes an electric field that is everywhere normal to the target, while the cathode surface is immersed in a magnetic field (see figure 4.02). The combined effect of these orthogonal fields is to confine secondary electrons, a product of the ion bombardment of the target, in cycloidal paths around the target, while they are free to move parallel to the target in an endless 'racetrack' pattern[77]. This increases the likelihood of an ionising collision with an argon atom. With a potential –V on the target and a magnetic field B, the radius of the electron orbit is

$$r = \left(2m/e\right)^{1/2} V^{1/2} B^{-1} \qquad \text{Equation 5.}$$

Where m is the electron mass in kg, e the electron charge in Coulomb, V is the target potential in volts and B the magnetic flux density in Tesla. The secondary electrons generate further ions by collision with the sputtering gas. The ions are accelerated by the electric field to the target across a distance of a few millimetres. The magnetron design causes the plasma impedance to drop so that the source operates at much lower voltages (500-600 V as compared to several kV for diode sputtering). This greater ionisation efficiency leads to an increase in ion current density, which is proportional to the erosion rate of the target. Magnetron processes are significantly cooler than diode processes because of their more efficient design. Ions, whose masses are greater than electrons, less affected by the magnetic field.

4.2.3 Film purity

The purity and fabrication process of the target and the effect of residual gas in the vacuum chamber can effect the purity of the deposited film. Outgassing of water during deposition from the chamber wall may be important during film growth. In the case of bias sputtering, a negative voltage is deliberately applied to the substrate. The ions (from impurity atoms), produced near the anode, may reach the film with substantial energies[78]. Another concern is that impurities may enter the system from contamination in the supply lines between the bottled gas and the system. The sputtering target itself may be a source of impurities in the discharge. The method of

fabricating the target is an important consideration. Those formed by compacting or hot pressing powder are porous and entrap gas, which is then continuously released during sputtering[79].

4.2.4 Film structure

The growth of the film is influenced by the conditions at the substrate. The nucleation and growth of thin films is reviewed in Reichelt[80]. This gives a representation of the mathematical theories of the growth of thin films in the initial stages. A model of film structure by Thornton[81] is shown in figure 4.03. The numbers refer to Movchan-Demchishin zones. Zone I of the model has a columnar structure, consisting of tapered units defined by voided growth boundaries. This structure is created by atomic shadowing and promoted by surface irregularities or step features that cause oblique angles of the deposited flux. Zone I coatings have higher resistivity, and increased oxidation due to exposure of the open grain boundaries during growth or after exposure to the atmosphere. A zone I structure contains little trapped gas from the deposition process and has residual tensile stresses.

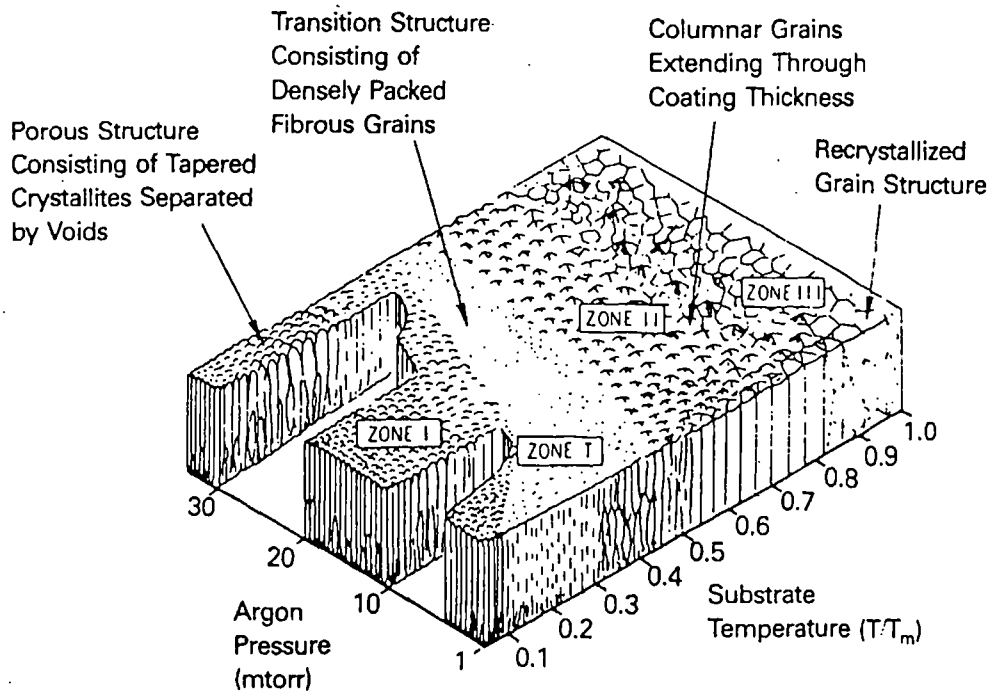

Figure 4.03: Influence of substrate temperature and argon pressure on microstructure of sputtered metallic coatings (taken from Thornton[81])

Zone II consists of columnar grains defined by metallurgical boundaries. The grains increase in width according to the activation energy of surface diffusion. Zone III is a high temperature structure where bulk diffusion processes are dominant. Zone T is a transition between zones II & I. Zone T structures are associated with high reflectance mirror like surface finishes, low resistivity, high compressive stresses and entrapped working gas. In a practical sense, zone T is a zone I structure with crystal sizes that are difficult to resolve and appear fibrous, with boundaries that are sufficiently dense to yield respectable material properties.

The working gas pressure can affect the structure because collisional scattering enhances the oblique component in the deposition flux. The zone I/zone T boundary results from competition between the effects of energetic particle bombardment, which produces dense micro structure (zone T), and oblique deposition, which produces open structure (zone I). In the case of sputtering, an increase in pressure tends to promote zone I by reducing the discharge voltage and scattering energetic reflected species and incident sputtered flux. Surface roughness or irregularities that increase the atomic shadowing during deposition also promote zone I structures. The structure and orientation of columnar growth is influenced by oblique incidence deposition[82]. This is significant for the deposition onto complex 3-D shaped gas turbine components.

4.2.5 Deposition of multi-component alloys

Sputtering can be used to deposit multi-component alloys. The element with the greater sputter yield is initially sputtered at a greater rate from the target, and as long as the target is cooled so that diffusion cannot occur, this depletes the surface of that element so that its rate falls. Equilibrium is reached only when the sputtered flux leaving the alloy target is the same as that of the bulk alloy (Westwood[83]). The generation of a sputtered flux with the correct elemental concentration does not ensure that this ratio will be maintained in the deposited film. The composition of the deposited film depends on the difference between the arrival and removal rates of

that element from the substrate. The film can be re-sputtered either by reflected neutral atoms of the sputtering gas or ions accelerated to the substrate by bias sputtering. The plasma must always be the most positive potential in the whole system. Even if the substrate is grounded it is at a negative potential relative to the plasma and thus will be bombarded by argon ions. If these argon ions have enough energy for sputtering the alloy composition will differ from the bulk target.

This project includes the deposition of a NiCoCrAlY alloy. Previously reported work with this alloy has been reviewed. A sputtered NiCoCrAlY layer has been used as an intermediate layer between the blade material and the insulating layer for a thin film sensor application[84]. The alternative Vacuum Plasma Spray (VPS) process was not selected for this coating because of the excessive porosity of this coating even after heat treatment. Office National d'Etudes et de Recherches Aerspatiales (ONERA) have deposited coatings, which have exhibited a homogenous microcrystalline structure. This structure, when heated, evolved towards an increase in the grain size, with the appearance of βNi-Al and nickel-solid-solution phases[54]. This phenomenon was accompanied by variations in the volume, which reduced the adhesion of the coating. This was prevented by pre-heating the substrate prior to deposition. Motoren-und Turbinen-Union (MTU) has sputtered NiCoCrAlY on turbine blades. The crystallographic orientation, microstructure and surface roughness on the aerofoil and other flat surfaces depend on the deposition parameters and initial state of the substrate surface. Around the platform, the homogeneity, with regards to the thickness and morphology, was poor. The orientation of the structure observed, was caused by the direction of flow of particles from the target to the substrate and many columnar defects resulted[54].

4.3 Insulator coatings

4.3.1 Choice of material

The electrical insulation of high temperature sensors is problematic. The deterioration of electrical insulation with temperature shorts the sensor to the substrate and across

the leadout tracks, causing inaccuracies in the measurement. For most high temperature insulator materials, the electrical resistivity drops off approximately an order of magnitude for every hundred degrees Celsius[85]. Thus, for even the best insulator materials with typically 10 microns coating thickness, the insulation resistance will be in the order of $10^3\Omega$ at 1000°C. A thicker coating thickness is not practical because of the slow deposition time and because residual stresses in the coating will increase with thickness and cause spalling of the coating. Other requirements for the insulation layer are that they transmit the strain to the sensor (strain gauges) and have high thermal conductivity (thermocouple sensors).

A summary of the electrical conductivity of high temperature insulation materials is shown in figure 4.04. In the range 500-1200°C, the best materials are BN, MgO and Al_2O_3. Of these, aluminium oxide is most widely used as an electrical insulator for high temperature sensors.

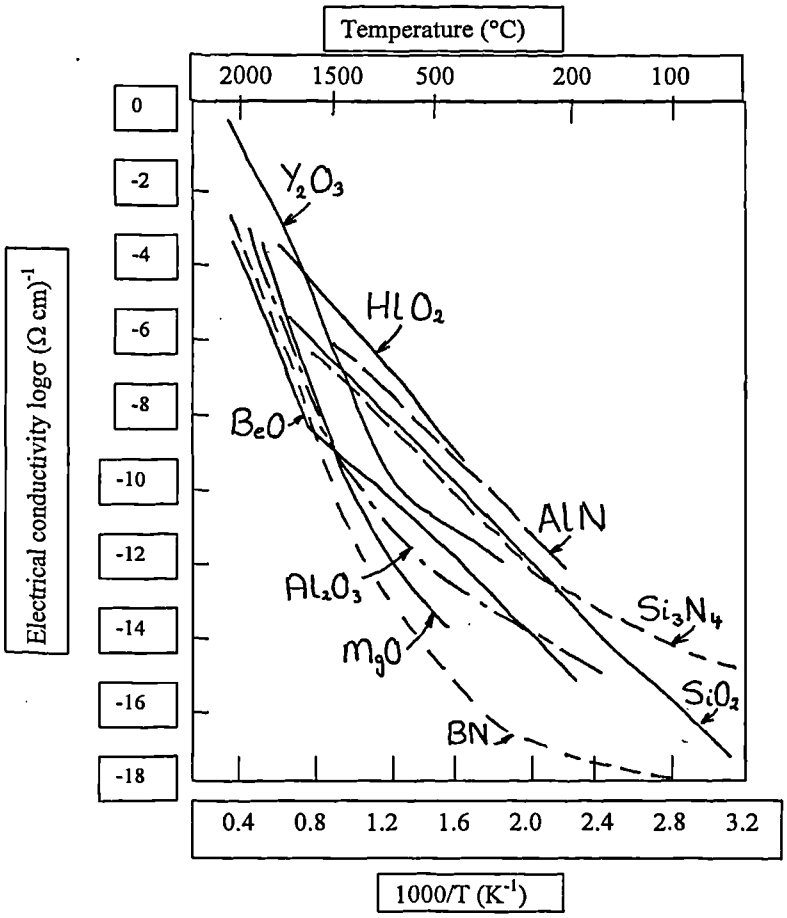

Figure 4.04: Variation of electrical conductivity for insulation materials (Information from Bauer[86])

Boron nitride would appear to offer the best electrical insulation properties and has been reviewed as a thin film sputter deposited coating. Boron nitride has been deposited by radio frequency magnetron sputtering usually for the purpose of mechanical protective coatings. Several authors deposited hexagonal BN films[87,88]. Most work reports a mixed phase of hexagonal and cubic boron nitride[89]. Those coatings, which were mainly cubic boron nitride, had high compressive stresses and peeled off easily from the substrate[90,91]. The film structure would appear to be highly influenced by the sputtering process[92], target[93] and substrate. It is presently considered too risky to use this coating for this project.

Silicon Nitride has previously been used as an insulator coating in thin film thermocouple applications. Rolls-Royce has previously collaborated in a research effort to develop multilayer insulator coatings using silicon nitride and aluminium oxide. The resistivity of the multilayer was greater than the same thickness of a single material because of the ability of the multilayer to suppress defect growth[94]. A single non-reactively sputtered silicon nitride layer has previously been successfully used for the fabrication of thin film thermocouple and resistance temperature sensors to above 1000°C[95].

The use of aluminium oxide may also be problematic at high temperatures. Concern has been raised about a phase change from γ-Al_2O_3 to α-Al_2O_3[54]. However, as the change is very slow just above 1000°C, this may not cause problems. Godefroy recommends the use of substrate heating to 800-900°C during deposition, to fabricate a dense and thick aluminium oxide layer that is useful up to 1040°C[96]. Goranchev[97] has studied the influence of deposition conditions on the structure of dc reactively sputtered aluminium oxide and found that the substrate temperature influenced the structure. Kuwahara[98] has studied the internal stresses in deposited films and found that aluminium oxide films exhibited compressive stresses.

Kreider[99] has reported the use of thermally grown aluminium oxide coatings for high temperature insulation. The coating was grown onto NiCoCrAlY and FeCrAlY coatings at temperatures between 1027 and 1127°C. These coatings had defects and

impurities that limited their insulating properties. The insulating quality of the coating was greatly improved by the addition of a reactively sputtered layer of aluminium oxide over the thermal oxide.

4.3.2 Reactive sputtering

The mechanism of using two or more gases is known as reactive sputtering and is normally used in one of two ways, namely:

1. The formation of a particular alloy film from a pure metal target, for example the production of a thin film of aluminium oxide in a partial pressure of argon and oxygen from an aluminium target.
2. In situations where dissociation of an alloy target may occur, for example during the deposition of Si_3N_4. If during the process, nitrogen were lost, then the correct stoichiometry would not be obtained[100]. The addition of nitrogen here would ensure that the film deposited had the correct stoichiometry.

The benefits of using the former for the production of thin film sensor insulator coatings are the increase in deposition rate obtained over sputtering from a compound target. This technique also gives the possibility of depositing graded coatings by varying the oxygen content of the film during its deposition. The effect of oxygen partial pressure on the deposition rate is shown in figure 4.05.

Because of the affinity of aluminium for oxygen at low partial pressures, it is gettered so effectively, by the sputtered coating on the substrate and chamber walls, that none is available for sputtering. When the sputtered material has gettered all the oxygen that it can, aluminium oxide begins to form on the target surface. This causes a reduction in the sputtering rate from the target and hence a reduction in the amount of gettering. Thus the situation runs away until a new equilibrium is established when Al_2O_3 covers the whole target surface. In order to increase the deposition rate, the amount of oxygen partial pressure must be reduced until the oxide on the target face is removed by sputtering and the target face becomes mostly metallic. Increases in

the current due to the addition of oxygen to an argon discharge have been attributed to increases in secondary electron emission from the target[101].

Thus, a reactive sputtering process is dynamic. However, the vertical portion of the graph contains the areas of interest, i.e., the ability to control composition at higher deposition rates than are achievable with a compound target. This is achieved, in the Rolls-Royce system, by monitoring the intensity of the aluminium spectral line in the plasma[102] and controlling the addition of oxygen to the chamber dynamically to maintain the required set point.

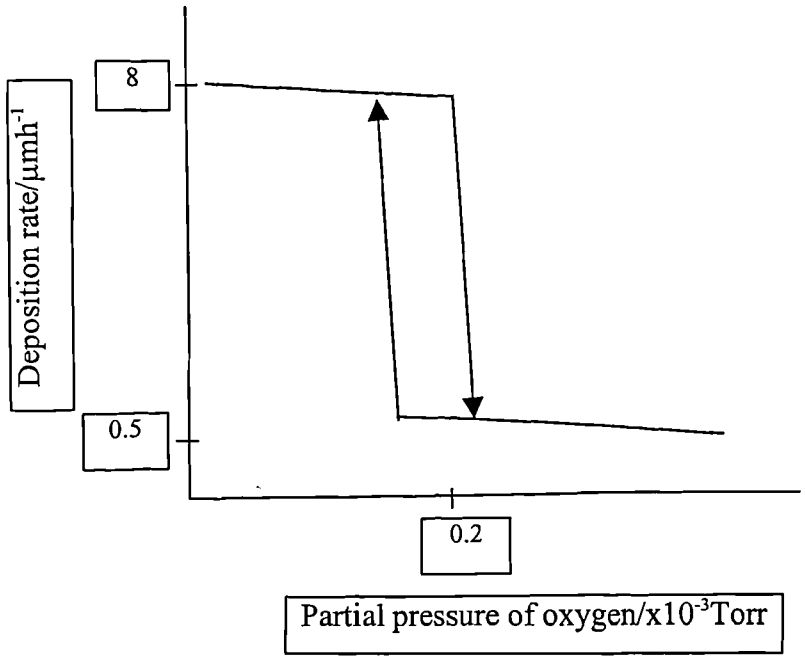

Figure 4.05: Effect on deposition rate of oxygen partial pressure. Values shown are from previous work at Rolls-Royce.

4.3.3 Arcing during reactive sputtering

Most references found indicate the use of dc power supplies for the reactive sputtering of aluminium oxide. The ion bombardment removes aluminium from the target. However, the re-deposited insulating film on the target face behaves in a very different manner. As the film forms it tends to collect low energy ions on its surface, charging the surface of the film towards the applied voltage as a parasitic capacitor.

As the capacitor voltage climbs, it reduces the available energy with which the ions can strike the insulator, thus reducing the likelihood of the film being sputtered off (see figure 4.06). This process can result in the electric breakdown of the film.

Strauder[103] has shown that the introduction of a medium frequency power supply reduces the arcing by several orders of magnitude. Rolls-Royce and its subcontractors have used radio frequency sputtering to reduce the formation of oxide. This has been only partially successful and particulates of aluminium have been incorporated in the deposited film from the ejection of material during arcing on the target face. This has been reported by Mallins[104] and Dunker[54]. Mallins analysed the composition of one such defect and found it had higher aluminium content than that of the surrounding deposited film.

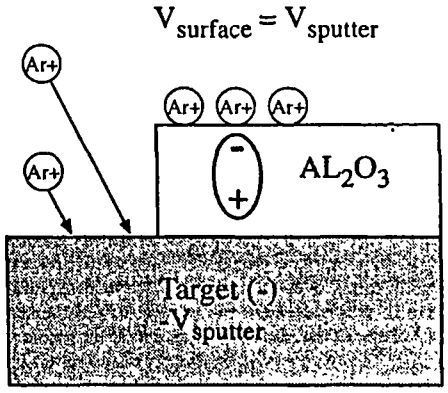

Figure 4.06: Charging of oxide on target face during dc sputtering

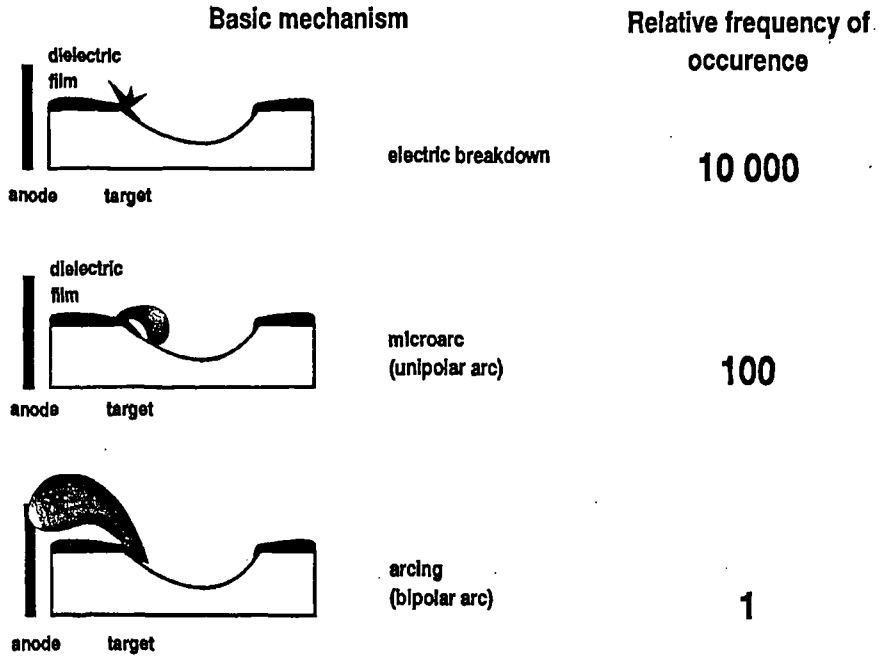

Figure 4.07: Simple model of arcing formation during a reactive sputter process (taken from Schiller[105])

Arcing in a magnetron discharge means the occurrence of unipolar microarcs, and bipolar arcs. The unipolar arcs are plasma-energised arcs, the onset and termination of which occurs on the same electrode. The event starts with an electric breakdown of thin dielectric layers on the target surface (see figure 4.07). The electric breakdown can trigger a cascade of unipolar arcs. The arcs can cause craters where material has been removed and can be deposited on the target face or get incorporated into the depositing film. Here, the rapid recognition of an arc with subsequent disconnection of the voltage supply alone proves to be inadequate since such a device detects already fired arcs only. This reduces the problem but does not remove the source. The unipolar arcing can also initiate bipolar arcing where arcing occurs from the cathode to the anode.

4.3.4 Pulsed dc power supplies

Schiller[106] describes the technique of pulsed dc magnetron sputtering. This may take two forms, bipolar sputtering, where the power supply is connected to two adjacent

cathodes and unipolar sputtering where only a single cathode is used. For this project, unipolar sputtering is considered.

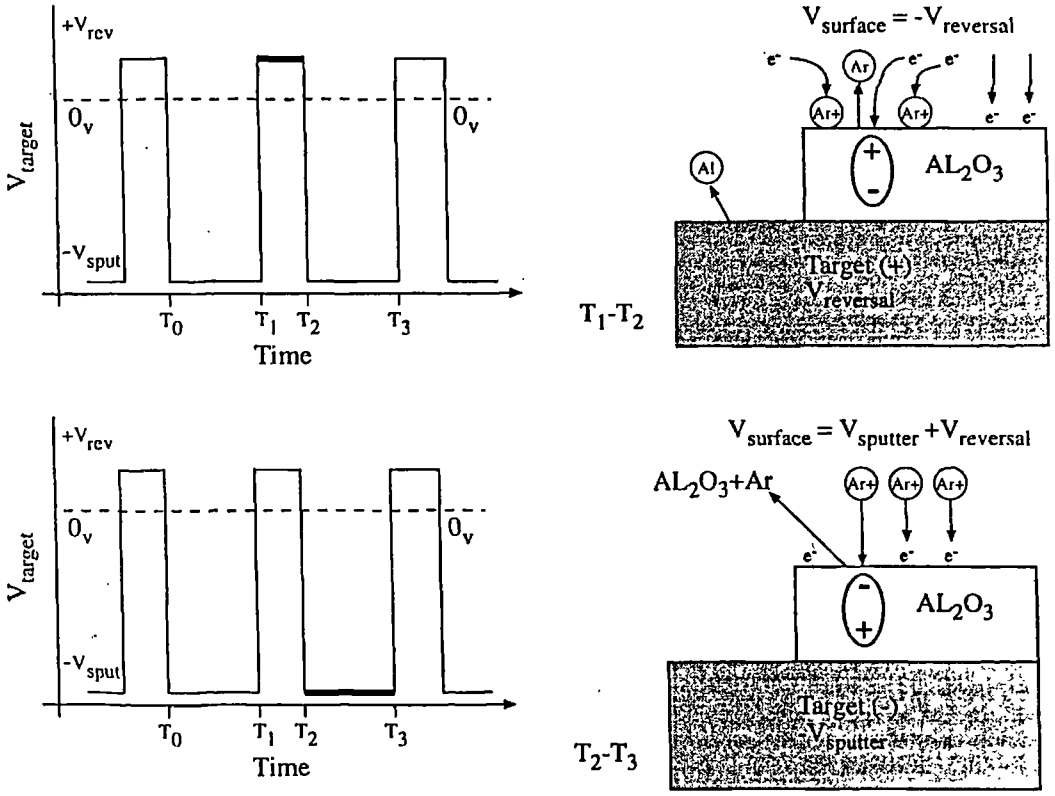

Figure 4.08: Principle of pulsed dc sputtering to prevent arcing on target face. Upper (charging of insulating film to positive potential). Lower (preferential sputtering of insulating film). Taken from ENI Technical note[107]

Here, an asymmetric waveform is applied to the target (see figure 4.08). The positive voltage level is factory set. The frequency, pulse width and power level can be set by the operator. During the positive voltage part of the waveform the capacitor, consisting of the insulating film, is charged to the opposite polarity from the normal sputtering mode, by electron bombardment. Preferential sputtering is initiated on the negative going edge when the ions are attracted towards the insulating film in preference to the target. Thus, by the careful adjustment of the asymmetric waveform, the potential build up of oxide may be limited to values where breakdowns do not occur.

4.4 Thin film sensor patterning process

The standard Rolls-Royce low temperature thin film dynamic strain gauge process is shown in figure 4.09 and described in this section. The metal substrate (blade or test sample) is prepared by polishing. This reduces the number of defects in the insulating and sensor films. The substrates are ultrasonically cleaned in isopropyl alcohol prior to loading into the deposition chamber. The components are dried using a filtered nitrogen gun. Coatings are applied sequentially in the chamber without breaking the vacuum to minimise interface contamination between each layer.

The component is removed and a photoresist spinner is used to apply a uniform coating over the area to be instrumented. Shipley Microposit S1813 photoresist is drawn into a syringe and applied over the test sample using a Nalgene 0.2 μm solvent resistant filter until the whole surface is covered[108]. The spinner is then activated and the component spun at 4000 rpm for 25 seconds. The acceleration time from stationary to spin speed is adjustable. It is set to 1 second so that the excess photoresist is thrown off and a uniform layer is achieved before the resist starts to dry.

The photoresist layer is cured to remove solvents, and exposed to ultra-violet light through a mask that defines the sensor grid (stage 2). This had been defined on a CAD system. Serat Ltd. then printed the patterns 40 times size on large transparent sheets and photographically reduced them to the correct size. This process ensures that the sensor grid has the correct definition, since a printer would not be able to produce this scale of detail. The photoresist is developed using Shipley Microposit MF319 developer, washed with de-ionised water and dried with nitrogen (stage 3). The unwanted films are then removed by chemical etching, with each coating material having a specific chemical etch.

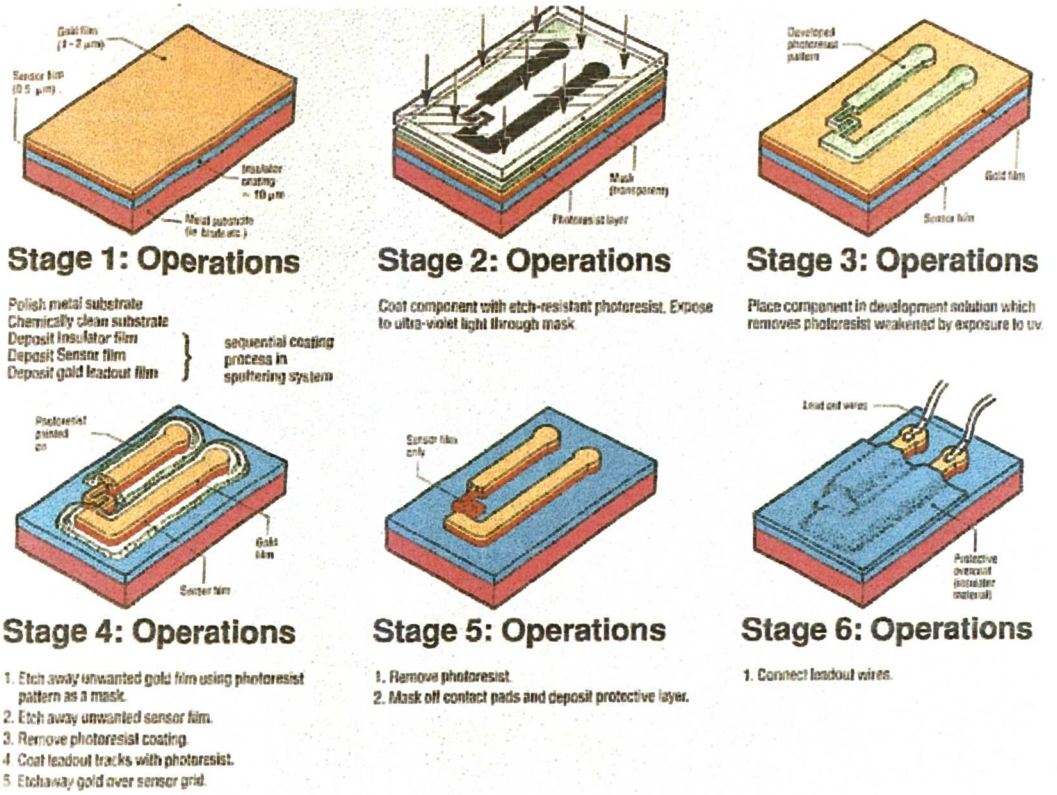

Figure 4.09: Processing route for low temperature dynamic strain gauge patterning

The gold etch is 5g iodine (I_2) + 15g potassium iodine (KI) + 200ml water. Shipley Microposit chrome etch 18 is used to etch the NiCr.

The photoresist is removed using Shipley 1165 remover. The component is dried then photoresist is hand painted over the leadoff tracks and the gold coating over the sensor etched away. The sensor resistance can be trimmed during this operation to within 1Ω of the required value. This is achieved by only exposing part of the sensor grid to the chemical etch. By gradually increasing the exposed grid area the sensor resistance can be increased in a number of steps (stage 4). The sensor is then overcoated with a protective layer of aluminium oxide and then fine nickel wires are attached using a parallel gap welding technique.

Chapter 5: Project proposal

5.1 Introduction

A requirement for a new application technique for high temperature strain and thermocouple sensors has been established in the preceding chapters. In particular there was an urgent requirement for the application of sensors on TBC components. Here, conventional techniques have proven unreliable and inaccurate. Whilst there was work underway on temperature measurement techniques to provide TBC surface temperatures and improve the embedded thermocouple measurement technique, all of these had limitations (see chapter 3). Although the driving force and main funding source for this work was on military engine development programmes, there was also significant demand for this measurement technique on civilian aero-engine applications such as the Trent 500.

A new technique of applying thin dielectric and metallic films to the test component and using a patterning technique to define the sensor and leadout positions has been used for low temperature applications up to 500°C. It was possible that these techniques could be extended for high temperature applications.

The applicability of thin film sensor techniques is considered in this chapter for the application of sensors on TBC components. The areas where development work was necessary and the originality of this work are discussed.

5.2 Feasibility study

Before work could start on the sensor project, the author performed a feasibility study. This was the first of a number of project review stages, including risk assessment and risk management meetings. These involved support from a number of technical specialists from relevant disciplines across the company. None of the specialists had direct experience of thin film sensors, their background being in other

measurement or vacuum coating techniques. This was one of the requirements of the Ministry of Defence who partially funded this work. It was also a requirement of Rolls-Royce that project review meetings, project planning and financial project management activities be performed.

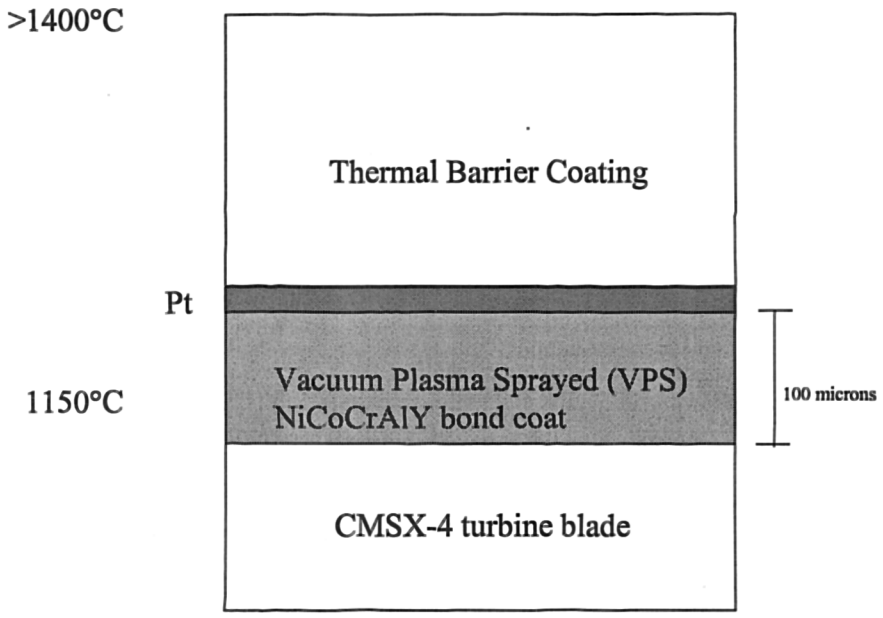

Figure 5.01: Thermal barrier coat arrangement

The Author's proposed solution to the customer's requirement was discussed. The following is a summary of the results of the discussions. The contributions of the individual specialists are referenced.

The aero-thermal engineer would ideally like the measurement of strain and temperature at the surface of the CMSX-4 substrate[109], see figure 5.01. This would allow the determination of the blade behaviour and temperature to be directly compared to the computational fluid dynamic and stress models of the component. Since this has previously proven difficult using the conventional techniques, other options for the placement of thin film sensors were discussed in order to eliminate them.

Optical techniques, see section 3.1, measured the surface temperature of the TBC coating and from this, inferred the CMSX-4 temperature. A sensor placed on top of the TBC would calibrate these techniques, which would be very beneficial. However, there are several reasons why this was not practical. First, the TBC has a columnar structure[110], which would cause difficulties in the sensor patterning process. Also the partially yttrium stabilised zirconia TBC is not a sufficient electrical insulator for the sensors[111], so additional insulation would be required. This would also prove difficult on the columnar TBC. Secondly, the sensor would experience the full gas stream temperature. At these temperatures the errors in measurement become very large and the survival rate poor. Rolls-Royce has little experience of successfully applying strain gauge sensors above 1100°C[112]. Thirdly, the sensor would also be exposed to the unburned hydrocarbons from the combustion chamber that is immediately upstream of the intended component position.

Thermal melt techniques are being developed for higher temperatures to help calibrate the optical measurement methods to fulfil this requirement. One option being pursued is the application of the thermal melt alloys by magnetron sputtering.

The TBC processing route is shown in table 5.01. The sensor cannot be located at the metal-ceramic interface, since it would not survive the TBC application directly onto it. This is because of the high oxygen content and temperature of the process. This has already been seen on buried type K mineral insulated thermocouples where only 5% of the thermocouples were working after TBC application[113]. The sensor needs protection from the TBC application process. It was proposed that thin film techniques be used to construct a sensor package between two layers of the NiCoCrAlY bond coat. This is shown in figure 5.02. The NiCoCrAlY upper layer should protect the sensor from the TBC process while the lower layer would be used as a base for the sensor. This includes the formation of a thermally grown oxide layer to form part of the electrical insulation of the sensor.

Thus, the bond coat application process was critical to the survivability of the sensor. If the sensor survived the bond coat process and heat treatment, then there was a high probability that it would survive the TBC application process and rig running.

Stage 1	Stage 2: Bond Coat Layer (100 μm thick) MSRR 9537/1	Stage 3: TBC Layer (250 μm thick) Partially Yttrium stabilised Zirconia MSRR 9515/104
Gritting	Vacuum Plasma Spray (VPS) (Currently the preferred option) Process: Deposit @ 700-800°C Heat treat for 1 hour @ 1100°C Surface finish peen then Apply Pt coating 8-10 μm thick by electroplating	Gritting 15 minutes pre-heated to 1000°C PVD Coat in 90% Oxygen 10% Argon atmosphere Deposition time < 1 hour @ 1000°C Final heat treatment 1 hour @ 1100°C 1 hour @ 700°C 1 hour @ 875°C

Table 5.01: Thermal Barrier Coat processing route[114,115]

The Vacuum Plasma Spray (VPS) bond coat process needed shot peening then polishing to produce a dense smooth coating. This would have put large stresses into any sensor package located below it almost certainly damaging the sensor. Thus a less aggressive bond coat process had to be developed for the instrumented components. This could have been achieved by modifying the VPS process. This would have been acceptable because the coatings only needed to survive the length of the test and not the component life in service. Alternatively, a physical vapour deposition process could have been used which, if suitable deposition conditions were found, would have needed little further treatment. The sputtering of a NiCoCrAlY coating in a low rate process appeared to be the most suitable although the thermal spray process could not be ruled out. The long process time was

acceptable because only a limited number of components were required for instrumentation.

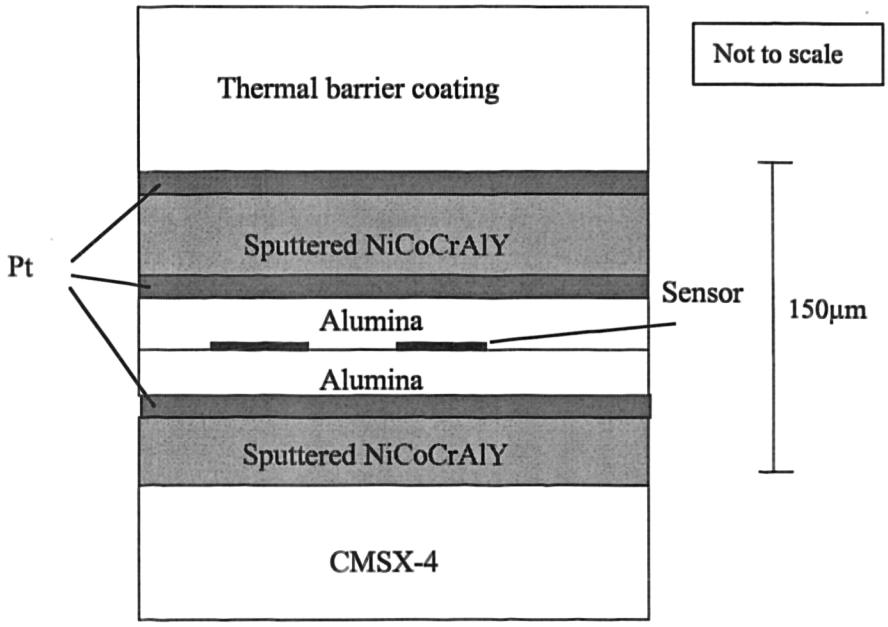

Figure 5.02: Proposed sensor package

The sensor package needed to be protected from diffusion from the TBC and CMSX-4 substrate. The platinum aluminium layer currently used on the TBC process could be utilised to protect the sensor from diffusion[116].

The sensor would therefore be separated from the CMSX-4 substrate by a layer of NiCoCrAlY. The effects of this needed to be understood. There would be a small but possibly significant temperature drop across the NiCoCrAlY. This might need to be modelled for compensation of the temperature measurements. The NiCoCrAlY bond coat material becomes soft as it approaches its temperature limit of 1150°C. This may be problematic for strain measurements[117] and would require investigation. The best way to understand this would be to construct a sensor package on a tensile test component and investigate the strain sensitivity of the sensor package at temperature.

The electrical insulation of the sensor would be very challenging. A graph of the insulation resistance of aluminium oxide against temperature is shown in figure 5.03. The resistivity of aluminium oxide at elevated temperatures has been obtained from

Morell[118]. The insulation resistance values have been calculated assuming a coating thickness of 8 μm and a contact area of a 3 mm-diameter circle. This was compared to the value previously obtained for a reactively sputter deposited thin film aluminium oxide coating measured to 800°C. The resistance of the thin film coating has been extrapolated to higher temperatures. It was seen that the insulation resistance would reduce to a few kilohms at 1100°C. This would cause large errors in the amplitude of dynamic strain measurements.

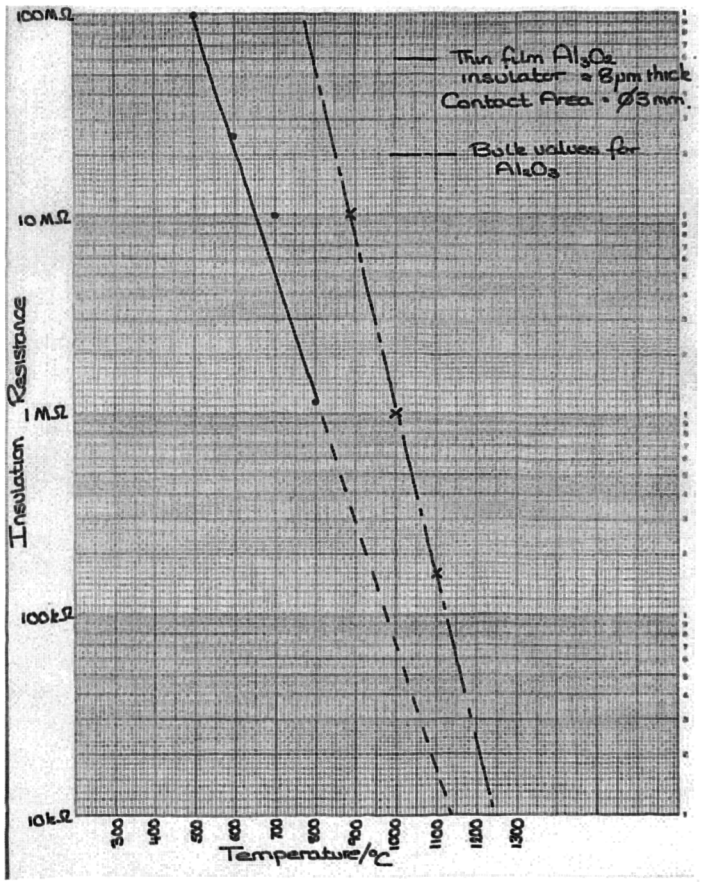

Figure 5.03: Variation of insulation resistance of aluminium oxide with temperature

The slip ring system used on the intended application employed a constant current potentiometric circuit for gauge polarisation which was significantly more tolerant of low insulation resistance to ground than a Wheatstone bridge circuit. So for a insulation resistance of 1 kilohm, a loss of between 10 and 20% of signal voltage was expected for a 120 ohm strain gauge (see figure 5.04). For insulation resistances this

low, it was also necessary to consider the capacitance through the insulator film since the 'leaky' circuit acts as a low pass filter.

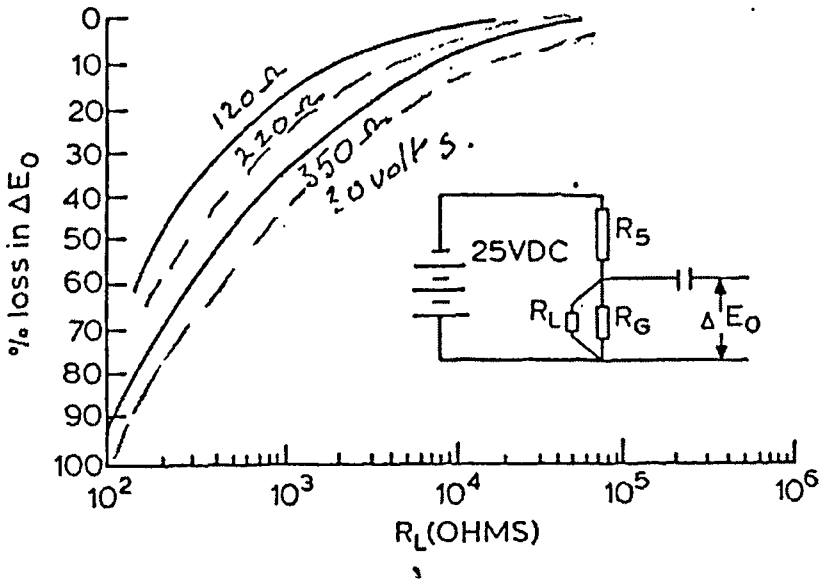

Figure 5.04: Effect of leakage resistance on potentiometric circuits[119]

Thermocouples are less sensitive to earth leakage than strain gauges. In a study performed by ONERA[54], a thickness of 8 μm of aluminium oxide was used for high temperature electrical insulation. This had a resistivity (ρ) of 2-5 MΩcm at 1100°C. Their model showed a loss of 1 to 2 % of EMF. This was for a very small sensor area. In practice the sensor area and hence the loss will be greater. This demonstrates the necessity to keep the sensor contact area small.

The insulation resistance can be reduced further by defects in the film, due to a number of causes. The overall thickness of the coating must be limited to prevent failure due to residual and thermally induced stresses. It was considered likely that initially, the sensor package would only be usable to a lower temperature than the requirement. Since even a reduced sensor temperature will increase the measurement capability significantly, this was acceptable to the customer.

The lower temperature seen below the TBC would also be an advantage in terms of sensor performance. The several hundred degrees temperature drop across the TBC

equates to several orders of magnitude of insulation resistance. Thus, a thin film gauge in this location is potentially more accurate than the conventional wire gauge installation.

5.3 Feasibility study trial

A test sample was produced using the currently available techniques to test the proposed sensor package. This would give some confidence that a working sensor was feasible and also highlight the areas where development work was needed. The sensor package was produced on an INCO 718 substrate that was readily available.

First, the substrate was sand blasted and a layer of NiCoCrAlY bond coat VPS applied by a sub-contractor to the standard Rolls-Royce process. A buff polishing method was used to produce a good surface finish. Later, trials showed that a much better mirror-like surface finish could be achieved by a further buff polishing operation. It is probable that this further operation would be needed to improve the insulation resistance of the sensor.

A layer of platinum was deposited onto the bond coat layer through a physical mask. Because a platinum target was not available, a piece of platinum foil was clamped to the cathode. The physical mask defined four sensor package areas on the substrate. It was fashioned from stainless steel shim and held against the substrate using paper clips. A different size mask was produced for each coating layer. A reactive sputtering process was used to deposit a layer of aluminium oxide onto the platinum through a smaller mask. Successive layers of platinum, aluminium oxide and platinum were applied through the masks to define the sensor strip, top insulator and top Pt layer.

The sub-contractor applied a final coating of VPS NiCoCrAlY. The substrate was cut up to produce four test samples, each piece having a sensor package. One such test piece is shown in figures 5.05.

Three of the samples were heat treated at 1100°C in vacuum for 1 hour, vacuum for 25 hours and air for 1 hour, respectively. The samples survived the NiCoCrAlY and heat treatment processes remarkably well. In all cases there are varying degrees of spalling of the NiCoCrAlY coating over the sensor package. For an actual sensor, the package width would be significantly narrower, which may reduce this effect.

The sensor strips were electrically shorted to the substrate. This may be due to defects in the coating, the surface roughness of the NiCoCrAlY coating or the large electrode area. After heat treatment in air, the insulation resistance improved to several Megohm, but this may be due to the separation of the coatings.

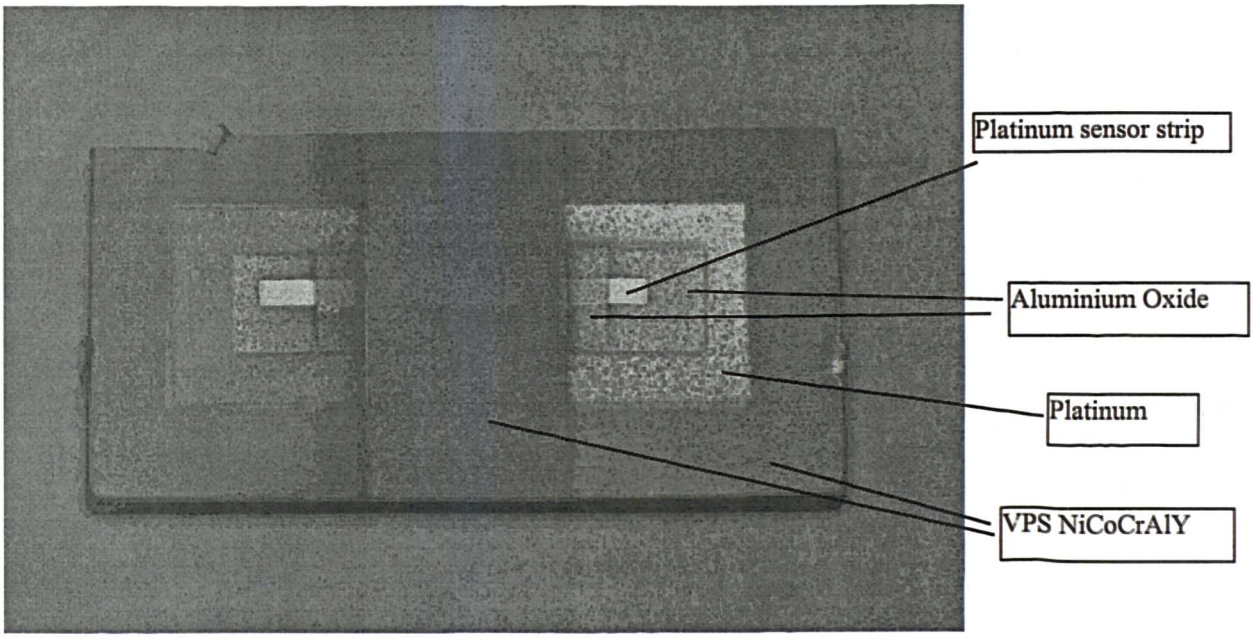

Figure 5.05: Feasibility study sample heated to 1100°C for 1 h in vacuum[120]

Because of the poor electrical insulation resistance, only limited electrical tests could be performed and further temperature evaluation were not considered beneficial.

5.4 Statement of originality

The application of thin film strain and temperature sensors has been documented on compressor and turbine blades using a single insulating layer of thin film dielectric, normally aluminium oxide or silicon nitride. Sputtered NiCoCrAlY layers have been used as a base layer for insulator coatings or with layers of aluminium oxide

thermally grown onto the NiCoCrAlY. High temperature thin film sensor materials have been evaluated on ceramic substrates or on single sputtered insulating layers.

The novel aspect of this work lies in the development of a complex multilayer structure consisting of up to nine sputter deposited layers to fabricate a sensor package able to make measurements of temperature and strain below a PVD applied thermal barrier coating. No previously reported work could be found on this type of installation. This consisted of the development of patterning techniques for high temperature sensor materials on complex three-dimensional components. Here, previously reported work is vague as to the methods used and the sensor patterns appear poorly defined on complex components.

A new type of sputtering power supply was evaluated for the deposition by reactive sputtering of aluminium oxide coatings. There is only limited reported work on the applicability of this type of power supply for thick (>several micron) aluminium oxide coatings. Finally, sputtered layers of NiCoCrAlY were applied on rough and highly polished surfaces with dense structure and the correct composition.

5.5 Conclusions

A novel application for thin film sensor techniques was proposed. A thin film sensor would be sandwiched between two layers of a sputtered NiCoCrAlY bond coat. The TBC would be applied onto this package. This would give a direct measurement of the CMSX-4 blade temperature and strain after a small compensation was made for the effect of the lower layer of bond coat. This had significant advantages over the conventional strain gauge and buried thermocouple methods described in chapters 2 and 3 respectively.

The sensor assembly formed a very complicated multilayer package where the adhesion and interface effects are very important. Poor adhesion of any of the coatings would cause the failure of the sensor package or the removal of the TBC from the blade. The application process of the bond coat was critical to the

survivability of the sensor. The preferred option was to develop a sputter coating that requires minimal shot peening so that the sensor package is not damaged by the application of the bond coat on top of it. This increased the risk that the failure of this coating could cause the TBC to separate from the blade. Whilst this would have a significant effect on the sensor package it was an acceptable risk since the instrumented component needed only survive a 30-hour test compared to the standard TBC process that was designed for engines in service. The blade would survive with the TBC missing over this period of time.

A trial has been performed using the techniques that are currently available. This gave confidence that a solution was feasible. The poor electrical insulation achieved meant that only limited evaluation of the sensor package could be made. This has highlighted that the polishing of the NiCoCrAlY layer and deposition of the insulation layer need development. Even with excellent coatings the sensor would have inaccuracies due to the deterioration of the insulation resistance with temperature. It was considered probable that this would limit the temperature to which useable results could be gained. If the insulation resistance was known this error could be compensated for and other corrections could be made for other temperature effects to improve the high temperature sensor accuracy.

New sensor materials and patterning processes needed evaluating for this work since the current NiCr sensor process was unsuitable for applications above 500°C. The work done would also benefit the low temperature applications and would allow the application of simple sensor packages consisting of a single insulator layer to turbine components without TBC's.

Chapter 6: Facilities used and project management activities

6.1 Introduction

A project proposal has been outlined in chapter 5. The thin film sensor deposition and evaluation was performed in a purpose built facility on the Sinfin-A site at Derby. Initially, another deposition facility located on the Elton Road site at Derby was used for the deposition and evaluation of the NiCoCrAlY coating. This was because of the long elapsed time coating runs required for this work and the need to perform this activity in parallel with the sensor development. The work was then to be transferred to the Sinfin-A site facility later in the project. This was so that all of the coatings could be applied in the same facility, minimising contamination between layers and handling damage. This chapter gives a description of the deposition, patterning and analytical facilities available for use and the project planning performed for this project.

6.2 Deposition facilities

Equipment was specified to be able to apply the low temperature application process as suggested by a sub-contractor. This was the sequential deposition of aluminium oxide, nickel-chromium and gold. The vacuum chamber and chemical workstation components were specified so that they would accept the largest component for which coating was envisaged. This was a single turbine low-pressure guide vane.

The deposition system is a CVC custom-built model denoted 703S. It incorporates features from across the CVC range of systems. The basic configuration is a U-shaped box process chamber, nominally 610 mm in diameter and 510 mm in height, with a 305 mm by 125 mm sideways sputtering magnetron cathode on each of its four walls. The process chamber is cooled by externally mounted water pipes. These are fed from a re-circulating water cooler located outside the clean room. It has a hinged front loading door on which one of the water-cooled cathodes is located. The

chamber is shown in figure 6.01. The NiCr cathode can be seen in the door and one of the planets inside.

System pumping is achieved by an Edwards 32 m^3 two stage rotary roughing pump and then a Cryo-Torr-10 high speed cryo pump capable of pumping 9000 litre/second water vapour and 3000 litre/second air. The system is fitted with a Leda Mass residual gas analyser. This can scan the base vacuum pressure for contaminants showing the presence of air leaks or rotary pump oil and also allows leak checking of the vacuum chamber with helium. The ultimate vacuum and working gas pressures are displayed on ion and Pirani gauges respectively. The deposition processes are not started until the chamber pressure falls below 5×10^{-6} Torr. This typically takes two hours pumping time. If continued overnight, the pressure will fall to 10^{-7} Torr. A Polycold unit has been acquired to reduce these pumping times to increase the throughput of the system. So far there has been insufficient time to do the engineering work necessary to fit this to the system. The control of the vacuum values is automated to ease the use of the system and provide system protection.

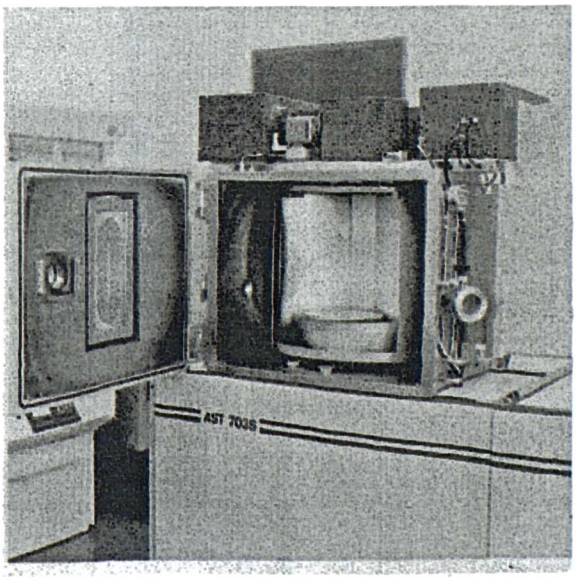

Figure 6.01: Sinfin-A site CVC 703S deposition chamber

The unit has a water-cooled rotary substrate table, on whose periphery is located, at 90-degree intervals, four rotating planets of 229 mm diameter. Full height quadrant shielding is incorporated to isolate each planet from its neighbour, thus preventing

cross-contamination. Each quadrant of the system is fitted with a view port for positioning of the components during deposition. Substrate components may be positioned vertically or horizontally on the planets for maximum flexibility in coating substrates of complex shape. Angular adjustment of the component by rotating the planet may be made to improve material deposition coverage over edges and undersides of components

Radio frequency bias etching of substrates is provided and incorporates a 1kW CVC RF generator and autotune-matching network with digital DC bias voltage monitoring. The bias power is supplied to the four planets via a central glass shielded copper rod from the matching network located on top of the chamber.

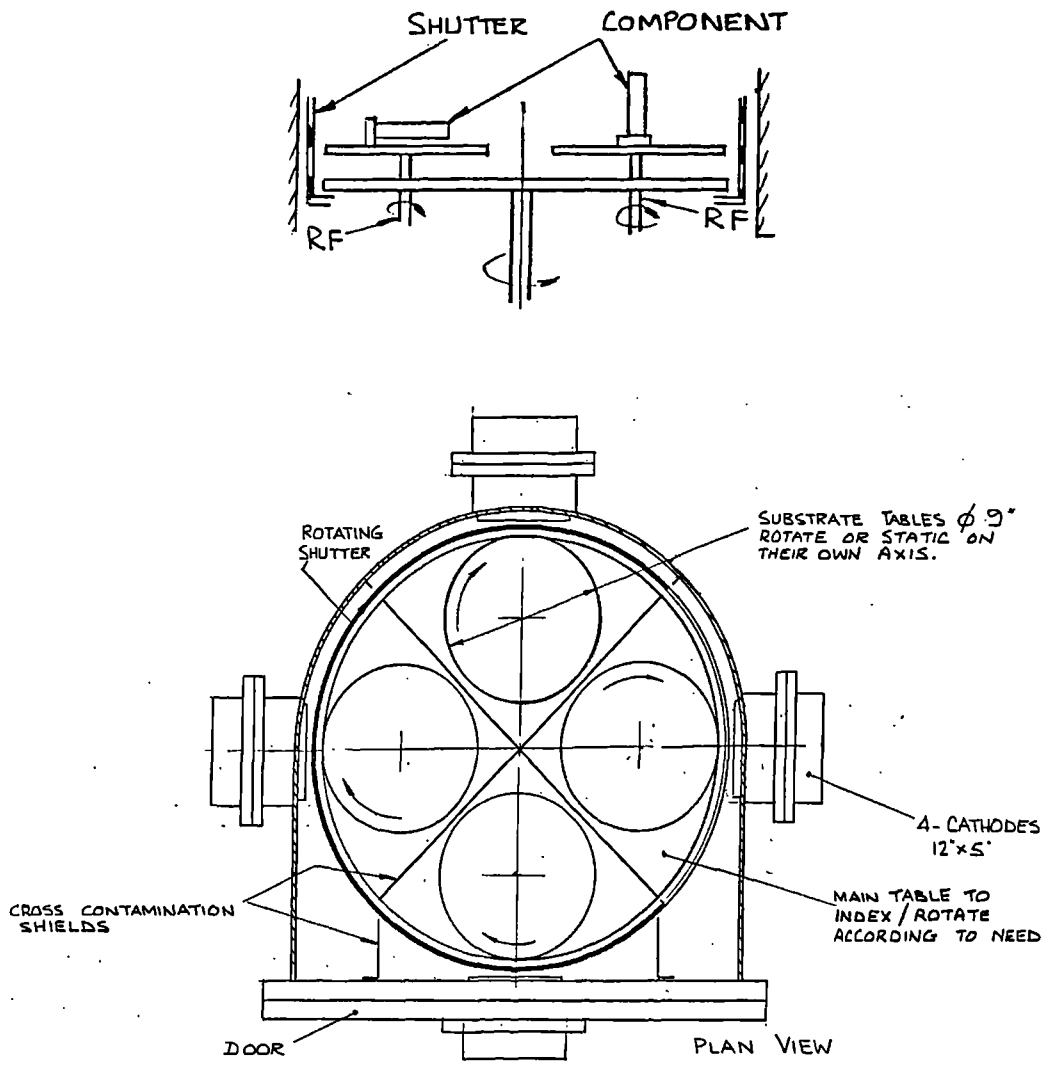

Figure 6.02: Substrate geometry of the CVC system (taken from CVC operating manual[121])

A motorised drum type shutter is provided which effectively encloses the substrate holder and isolates substrates from sputter cathodes during pre-deposition and substrate etch/clean (see figure 6.02).

Two of the four cathodes were configured to operate in DC magnetron mode with power switched from a common 4.5 kW CVC DC power supply for the sputtering of Au and NiCr. The two remaining cathodes were configured to operate in RF magnetron mode for reactive/non-reactive sputtering of Al_2O_3 and RF diode mode for Ni deposition respectively. These were powered by a 3kW CVC RF generator with programmable autotune matching network.

An optical sighting tube is located through the process chamber bottom plate, in a position below the reactive sputtering cathode, such that the cathode face can be seen. This has shielding to prevent loss of signal through deposition onto the optics. A fibre optic coupler links the sighting tube to a monochromator for signal analysis. The monochromator is tuned to 394.4 nm[122], the wavelength of one of the aluminium emission lines. The output is fed back to the gas control loop to maintain optimum gas flow conditions for reactive sputtering. This consists of a Megatech Reactaflo unit which controls a separate fast response mass flow valve based on the intensity of the monochromator signal. This allows the mixing of the reactive gas with the main gas prior to entry into the process chamber.

6.3 Patterning facilities

The equipment is housed within a refurbished class 10,000 clean room. In order to maintain the standards of the clean room, special clothing has been purchased-including lab coats, overshoes and hats. The room is fitted with a radio alarm system based on a belt carried transmitter. This was fitted to protect lone workers because of poor visibility into the room from the outside.

The American standard classification of the air quality denotes the number of particles per cubic metre of air and set limits on the particle size. The air quality was

achieved by a series of filtration stages. The clean room was run at an over pressure so that there would be an outflow of air when doors were open. The windows, room and workstation lights and the bench lighting were fitted with ultra violet filters to remove wavelengths in the range 450-520 nanometres. The photoresist is sensitive in this range and the only source should be the UV exposure box.

The main patterning processes are performed within a custom-built workstation. The workstation has class-100 filtration laminar flow air onto the working surface to minimise dust contamination of the process. This air is taken from outside the clean room and passes through several filtration stages. The nature of the chemicals to be used is such that fume extraction is provided through a perforated work surface. The airflow within the workspace was adjusted so that there is a negative pressure differential between the workstation and the room. This prevents fumes reaching the operator. This is inspected every year. The workstation is shown in figure 6.03.

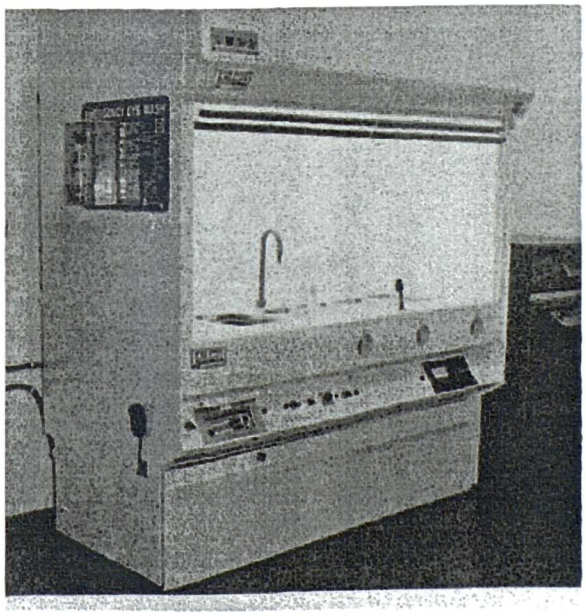

Figure 6.03: Class 100 laminar flow chemical workstation

The workstation houses a heated ultrasonic cleaning tank for cleaning components. An Elga Prima 3 deionised unit supplied filtered water at a rate of 75 litres per hour into a tank located outside the clean room. The water was then passed through a final filtration stage to achieve 18MΩ resistivity quality water on demand for washing

components. The water was blown off the components using a filtered nitrogen gun. Photoresist was applied using a Headway Research Inc. spinner. This consists of a spinner bowl, drive motor, substrate vacuum clamp, vacuum pump and controller. The workstation is fitted with three etching tanks large enough to take turbine components. However, for most of the compressor application work and development trials, glass beakers were used.

The photoresist layer is cured to remove solvents in an Autoveyor fan oven capable of 425°C with fume extraction, air circulation and nitrogen purge. Natgraph Ltd manufactured a custom-built ultra violet exposure box. This has a light meter so that the exposure time is increased as the bulb fades, which ensures a repeatable exposure process.

6.4 Analysis Techniques to be used

The following techniques were used to analyse the coatings produced for this project

Auger Electron Spectroscopy
Energy Dispersive Spectroscopy
Talysurf Profiler
Optical Microscopy
Scanning Electron Microscopy

6.4.1 Auger Electron Spectroscopy (AES)

When an electron beam bombards a small area, a number of interactions occur. The electrons undergo elastic and inelastic collisions before they come to rest a certain distance below the surface. This gives rise to a number of particles being produced. These include back-scattered, secondary and Auger electrons. The Auger electron is named after its discoverer, Pierre Auger. It is released as the parent atom relaxes after excitation by the electron beam of energy in the range 3-20keV[123]. The energy of the electron is characteristic of the energy level in the parent atom. It can be used to

identify the atom from which it came. The distance the Auger electrons travel in solids before losing their energy is approximately 1-2 nm, which gives the technique its surface sensitivity. In combination with ion bombardment, using argon or xenon, to remove atomic layers by sputtering, AES can give elemental concentration as a function of depth. However, at depths beyond a few microns the process becomes very time consuming and depth resolution is reduced[124].

Mechanical methods of sample preparation, such as sectioning or cratering may be used to speed up the depth profiling. In the cratering method, a rotating ball impregnated with abrasive grind is used to form a crater in the sample. Ion bombardment can be used to clean off any contamination resulting from the cratering process. Because the geometry of the crater is well defined, scans across the crater may be translated to depth profiles[125].

Quantification of AES spectra is relatively straightforward, but the accuracy of results relies on a suitable standard being available for comparison. AES is sensitive to all elements except hydrogen and helium.

The Institute of Surface Science and Technology (ISST) at Loughborough University carried out this work.

6.4.2 Energy Dispersive Spectroscopy (EDS)

The technique of EDS has been reviewed by studying the books of Elliot[126] and Scott[127]. During the electron bombardment, described above, characteristic X-rays are also produced. These are superimposed on a continuous background of Bremsstrahlung radiation. The X-ray's energy and wavelength are related by Planck's equation.

$$\lambda=hc/E \qquad \text{Equation 6.}$$

Where λ is the wavelength of the X-ray, c is the speed of light, h is Planck's constant and E is the energy of the X-ray. The X-ray can therefore be characterised either by wavelength or energy. For this work, the energy has been used to study the X-ray emissions by a technique known as Energy Dispersive Spectroscopy

The Bremsstrahlung or 'braking radiation' is produced by the deceleration of the electrons by inelastic collisions with the atoms in the sample. These X-rays have energies ranging from zero to the energy of the incoming electrons. The characteristic X-rays are a result of interactions of high-energy electrons with the inner core of an atom resulting in ejection of an electron from a particular orbit. The atom returns to its ground state releasing the excess energy as a X-ray photon. The energy of the X-ray is therefore related to the difference in energy between two energy levels. The X-ray lines are named according to the shell from which the vacancy occurred and the shell from which the electron falls to fill the vacancy. As the atomic number of the element increases, so does the number of possible transitions and hence the complexity of the X-ray spectrum.

Since each element emits a unique pattern of X-ray energies, the elements in the sample can be identified. From the intensity of the X-rays, the composition of the sample can be determined. The X-rays are collected by a solid state resolving spectrometer. This sorts them electronically to produce a simultaneous recording of the whole X-ray energy spectrum emitted from the sample. The intensities of the emitted X-rays are strongly affected by the operating conditions of the microscope and the composition of the sample. For quantitative analysis, the concentrations of elements in the sample are calculated from the measured intensities of the characteristic X-ray lines. This is usually performed by comparison with a standard of the pure element or of known composition under identical conditions.

The detector is a solid state silicon device. Incident X-rays are absorbed by silicon atoms by the photoelectric effect. The X-ray photon energy is transferred which results in raising valence band electrons into the conduction band. These electrons can move freely through the lattice causing electrical conductivity.

One problem with this technique is the spectral resolution of the detector, which leads to overlapping of the emission lines. A wavelength dispersive technique has better spectral resolution and so avoids this problem.

The EDS facility is available on the scanning electron microscopes at the Elton Road site.

6.4.3 Choice of analysis technique

The choice of EDS or AES techniques was as much to do with convenience of use as the differences in the techniques. The probability of whether a characteristic x-ray or an Auger electron is emitted from the sample is dependent primarily on the atomic number of the excited atom. This is referred to as the fluorescent yield. Elements with low atomic numbers have a low fluorescent yield and the emission of Auger electrons is favoured, whereas at higher atomic numbers the emission of characteristic x-rays is preferred. EDS has a limited elemental range compared to AES. The assessment of composition of the metal alloys used in this project is possible with both techniques. During busy periods it was often difficult to gain access to the Elton-Road facility, so work was sent to Loughborough University. AES was preferred for the analysis of the aluminium oxide coatings and for the measurement of interface contamination.

6.4.4 Talysurf Profiler

There are two modes of use of the Rank Taylor-Hobson Talysurf 10. Firstly with a skid in place and the traverse shaft hinged, the Talysurf can be used for average surface roughness measurements. A pick-up was driven slowly across the surface and a sharply pointed stylus followed the profile of the surface irregularities. The pick-up has an optical transducer and the vertical movements of the stylus are sensed photo-electrically. The signal was processed for display on a R_a meter. The roughness average, R_a, is defined as the arithmetical average of the departure of the profile

above and below the reference line (centre or electrical mean line) throughout the prescribed sampling length. The stylus was traversed over the area of interest. The cut-off length must be set with care. The choice of selection is shown in the Talysurf operation manual[128].

The device was calibrated against a standard before use. The stylus was traversed across a ruling having nominal R_a of 0.89μm (tolerance 4%). The value obtained on the R_a meter must be within 4% of the value shown on the standard.

Secondly, with the skid removed and the traverse shaft locked, the Talysurf was used to profile across steps such as the edge of a film to determine the film thickness. The profile was printed on paper. The recorder sensitivity was checked against a calibration before use. This was done on the x10,000 setting. The stylus was traversed across three lines scratched on a glass surface. The lines are nominally 2.5μm deep. The profile of the lines was produced on the recorder paper. The height of the central line was measured with an accurate graduated rule. It was compared against the value marked on the standard. The measurement should be within 2% of the standard. If it was outside this tolerance, a potentiometer on the unit was adjusted to bring the height within tolerance.

The procedure for using the Talysurf was similar for both measurements. Firstly, the traverse arm must be levelled against the sample surface. This was done with the amplifier set on low magnification. The stylus was traversed across the sample and the movement of the recorder pen noted. The traverse unit level adjustment was altered until there was no movement of the pen. The sample was then moved so that the stylus traversed the area of interest. The step profile was produced on the recorder paper and measured with an accurate rule, or a R_a value was displayed on the meter.

6.5 Facilities upgraded for this project

The feasibility study identified the activities that needed to be performed for this project. The equipment currently used in the facility was acceptable for the low

temperature sensor work but needed to be upgraded for this work. The changes made are summarised in this section.

The CVC power supplies were problematic. The 3kW radio frequency supply had no arc suppression system, which resulted in aluminium particles being incorporated into the growing film. The reliability of the power supply was also of concern. It failed during several important sensor production jobs, holding up a rig build in one case. The 4.5kW dc power supply also had no arc suppression and had a number of wiring problems. It was finally considered a health and safety risk. These two power supplies were replaced with a single ENI RPG 5kW power supply capable of operating in dc mode or as a pulsed dc power supply.

Six new materials were required to be coated for this project. The samples would be small test pieces. The cost of large rectangular targets in these materials would have been prohibitively expensive. A financial justification could be made for the £12,000 cost of two new 3-inch diameter cathodes. For example, the cost of a new rectangular gold target was approximately £15,000. A 3-inch diameter target in this material would be under £2500. Two AJA A330 3-inch diameter-sputtering cathodes were purchased. These were fitted on stainless steel flanges so they could be bolted to the vacuum chamber in place of the rectangular cathodes.

A substrate temperature measuring system was designed and built. This allowed the monitoring of the test sample during deposition. This was particularly important during the deposition of coatings onto the photoresist in the lift-off patterning technique. The details of this system are given in Appendix 1.

An ISI 100 scanning electron microscope was acquired from Loughborough University and installed inside the clean room. This allowed quicker inspection of the samples. The photographic facility on the microscope was poor. When permanent records of the sample were required, they were taken to the Elton Road facility or to Loughborough University.

A 1000°C temperature capability Lloyd Instruments MX-100 tensile test machine was purchased to allow the determination of gauge sensitivity on high temperature strain gauge sensors. Originally, this gave large inaccuracies in the strain seen on adjacent faces of a test sample due to the misalignment of the sample, support rods and machine alignment. Other tensile machines within Rolls-Royce are being improved to give 5% accuracy on applied strain to a component. At the time of writing this thesis, the work was still on-going to align this machine.

Finally, the clean room was air conditioned to improve the working conditions.

6.6 Project plan

Project planning activities are a requirement of Rolls-Royce and the Ministry of Defence. There would be no funding for this work without regular reporting stages and financial accountability. The work was planned as a series of milestones, each with a deliverable. These were drawn up after the feasibility study and risk assessment activities. The duration of each was based on an estimation of the technical work involved. This, of course, needed regular updating due to technical problems encountered during the work and other delays, some out of the control of the author. These included equipment failure, late delivery of equipment and target materials, loss of technician support to other projects and the use of the facility to support the low temperature thin film sensor work. Failure to meet a milestone would result in non-payment of contribution from the Ministry of Defence.

It was a necessity that the facility be used regularly for routine sensor production to support rig and engine tests. These paid for the upkeep of the facility but were also of political importance. The short turn-around time, required to meet engine assembly timescales, meant that other work ceased during these activities. The turbine test was also delayed from 1998 to 2000, causing a change in the spend profile during the project. The project plan had to be updated at each of these changes. The plan was reviewed regularly with the customer. Because of the number of tasks and changes

made it is not practical to show anything other than a summary of the activities performed. This is shown in figure 6.04.

Responsibility for financial accountability rests at a number of levels in the organisation. The Approved Technical Package (ATP) owner controls a particular piece of work. He/She reports to a Work Package owner, typically an engine owner or department manager. The engine owner will report to the engine development project owner, the Costed Technical Package (CTP) owner.

The ATP is set out as a spend profile for each year. Each milestone of planned work is broken down into technical time, manufacturing and bought out items. Many task doers can book to each ATP to perform technical work, manufacturing or provide services and for the purchase of bought out items. The ATP owner has the responsibility for control of these activities.

Thin film sensor techniques for the instrumentation of ceramic/metal interfaces in next generation aero gas turbines

ID	Task Name
1	**Literature review stage**
2	Feasibility study
3	Risk assesment
4	Literature review
5	Upgrade of facility for project
6	**Bond Coat process**
7	Experiment deisgn
8	Preparation of targets
9	Deposition & analysis of results
10	**Optimisation of NiCoCrAlY process**
11	Heat treatment and sample preparation
12	Improvement of Aluminium content
13	Deposition problems associated with target wear
14	**Evaluation of Pulsed DC power supply**
15	Purchase of ENI power supply
16	Purchase of Gencoa cathode
17	**Sensor development**
18	Development of patterning techniques
19	Purchase of targets
20	PtW deposition & evaluation
21	PdCr deposition & evaluation
22	PtRh deposition & evaluation
23	Purchase of tensile test machine

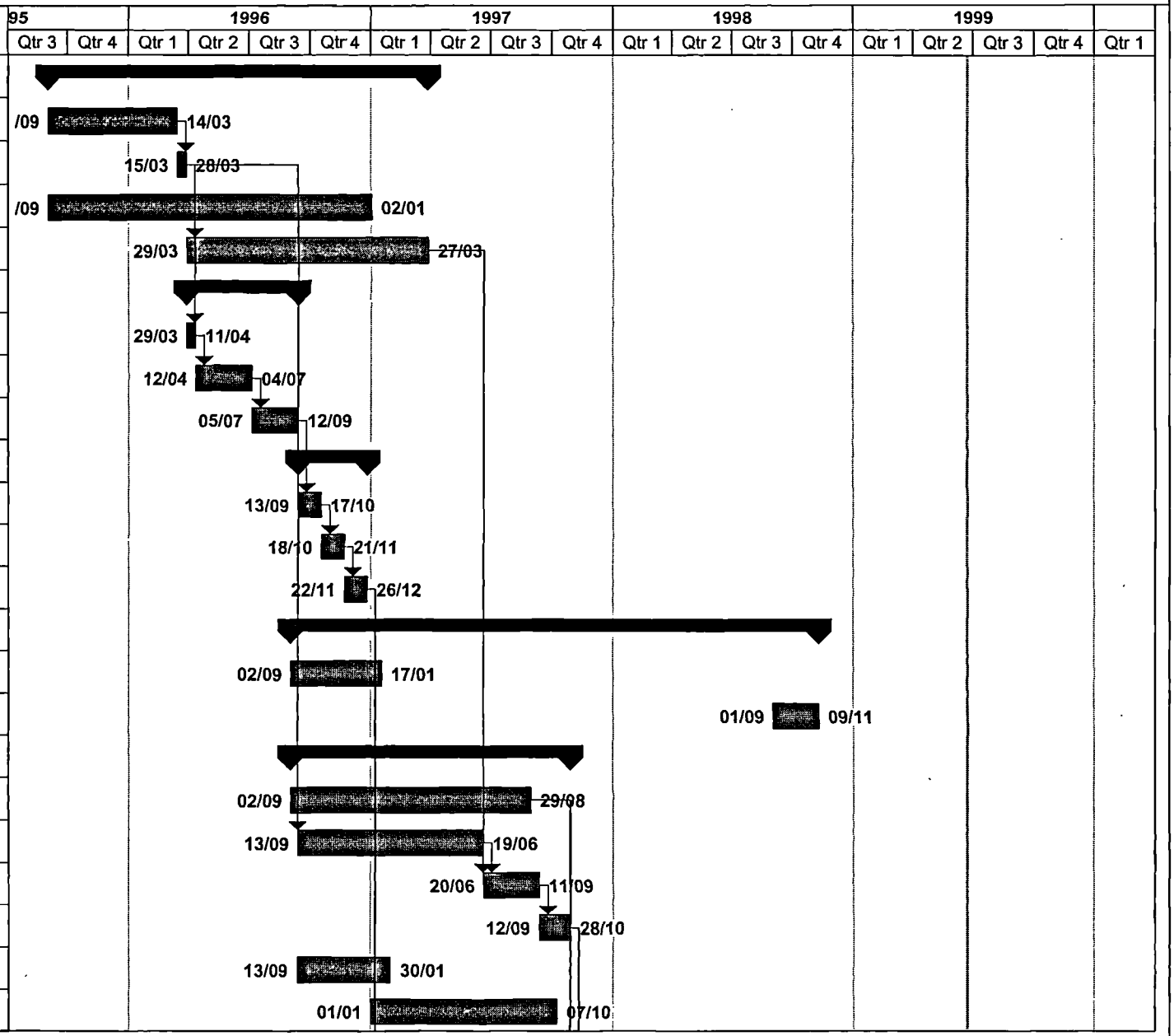

Thin film sensor techniques for the instrumentation of ceramic/metal interfaces in next generation aero gas turbines

ID	Task Name
24	**Integration of processes into sensor package**
25	Batch 1
26	Batch 2
27	Batch 3
28	**Report writing**

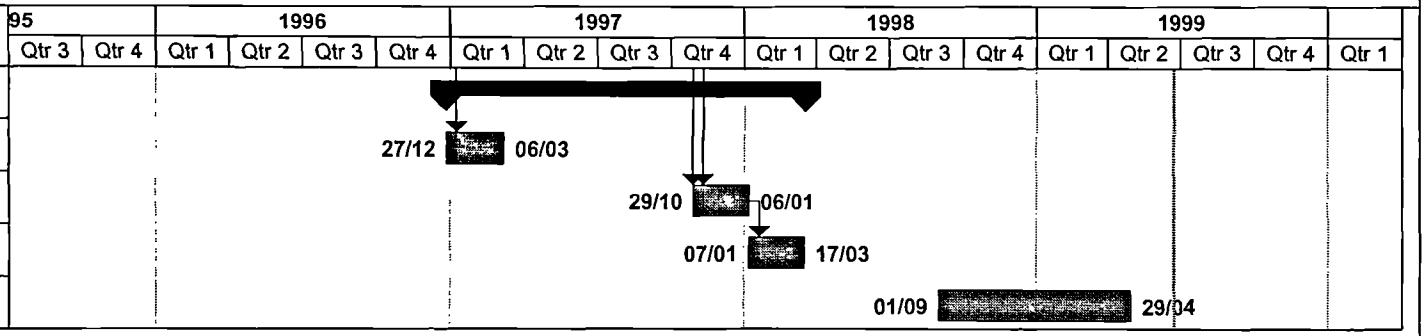

6.7 Risk Management

Any package of work is normally required to meet particular targets, usually in terms of time to complete the work, the cost and the specification of deliverables. However, due to increasingly tight time-scales, the drive to reduce costs and the introduction of new technologies, there will be uncertainty in achieving the customer's targets. This uncertainty is due to hazards or problems, which may occur during the programme of work, some of which may be anticipated before the start of the project. Typical examples could be equipment failure when a project relies upon a dedicated piece of equipment, poor adhesion of coatings or unsuitable material selection. These hazards pose risks to the programme, which can be expressed as[129]:

RISK posed by a hazard occurring	=	LIKELIHOOD of the hazard occurring	*	CONSEQUENCE of the hazard occurring

Risk management will provide the greatest benefit if applied early in the programme. The level of effort that should be dedicated to risk management will obviously vary from project to project. The factors that will dictate the level of commitment include:

The stage of project.
The size, cost and time-scales of the project.
The perceived level of uncertainty of the technique
How challenging is the specification.
The customer's requirements, i.e., for MOD funded work.
The consequence of failure.

The feasibility study has shown that the specification for this project was very challenging. There was no published work on this type of sensor package. This justified a large amount of effort being put into the risk management of the project. It was also a requirement of the Ministry of Defence, who partly funded this work.

6.7.1 Risk Assessment

In order to be of greatest benefit, it was important that all the contributions of perceived risk and assessment of significance are made by a selected group of people. This group included the customer and other specialists working in related fields. This was done in the form of a brainstorming session. The risks identified by the brainstorming session were sorted to remove repetitions and then assessed. Two assessments were made for each risk. The first was the likelihood of the event happening. The second was the consequence, to the final deliverable, of the risk happening. A special likelihood and consequence chart was drawn up for this project, in terms of the specification i.e. time scales, cost, accuracy & survivability of the sensor package during engine testing.

	LIKELIHOOD	CONSEQUENCE
LOW	<1 in 10	Time: Up to 1 week slip to project milestone Cost: Up to £5,000 overspend Spec.: Up to 5% shortfall on accuracy or bandwidth Survivability: Temperature achieved or life achieved
MEDIUM	>1 in 10 but < 1 in 3	Time: 1 month slip to project milestone Cost: Between £ 5,000 & £15,000 overspend Spec.: Between 5% & 10% shortfall on bandwidth Survivability: Up to 100°C shortfall on temperature Up to 10 hours shortfall on gauge life
HIGH	>1 in 3	TBC loss on blade Time: Up to 3 months slip to project milestones Cost: More than £15,000 overspend Spec.: More than 10% shortfall of bandwidth More than 100°C shortfall on temperature More than 10 hours shortfall on gauge life

Table 6.01: Likelihood & consequence chart for the project

As an example of this a selection of the high and medium risks are given in table 6.02.

Likelihood/Consequence	Risk
High/High	**PVD TBC process may cause sensor failure due to 90% oxygen content at 1100°C** **Main messages** i) Design of sensor package has been made to prevent this ii) Will not be able to test for this until the sensor package is constructed at the end of the project
Unassessed	**Sensor leadout system not currently defined**
Medium/High	**Aluminium oxide insulating layer does not have adequate insulation properties at temperature** **Main messages** i) Reliant on reactive sputtering process that has particulate defects. ii) Need information on leadout routing. iii) Assessment of insulation resistance above 900°C difficult
Medium/Medium	**Potential failure of deposition equipment may delay work and mean sensor batch re-work (currently 10% down time)** **Main messages** Not predictable and difficult to plan contingency Failure of a critical component would result in one month down-time **Actions**: Continue logging and build contingency in time scales for sensor production
Medium/Medium	**Flat plate testing of aluminium oxide and other coatings are not representative of curved turbine blades** **Main messages** i) Additional variable which will complicate sensor development ii) Turbine blade required for this experiment **Actions**: Rig owner to provide scrap blades for trials

Table 6.02: Selected risks from the project

Risk mitigation actions were assigned to all high consequence or likelihood hazards. A new project plan was then drawn up including the mitigating actions.

6.7.2 Risk Monitoring

The hazards were reviewed at 6 monthly intervals. The progress made is shown in figure 6.05.

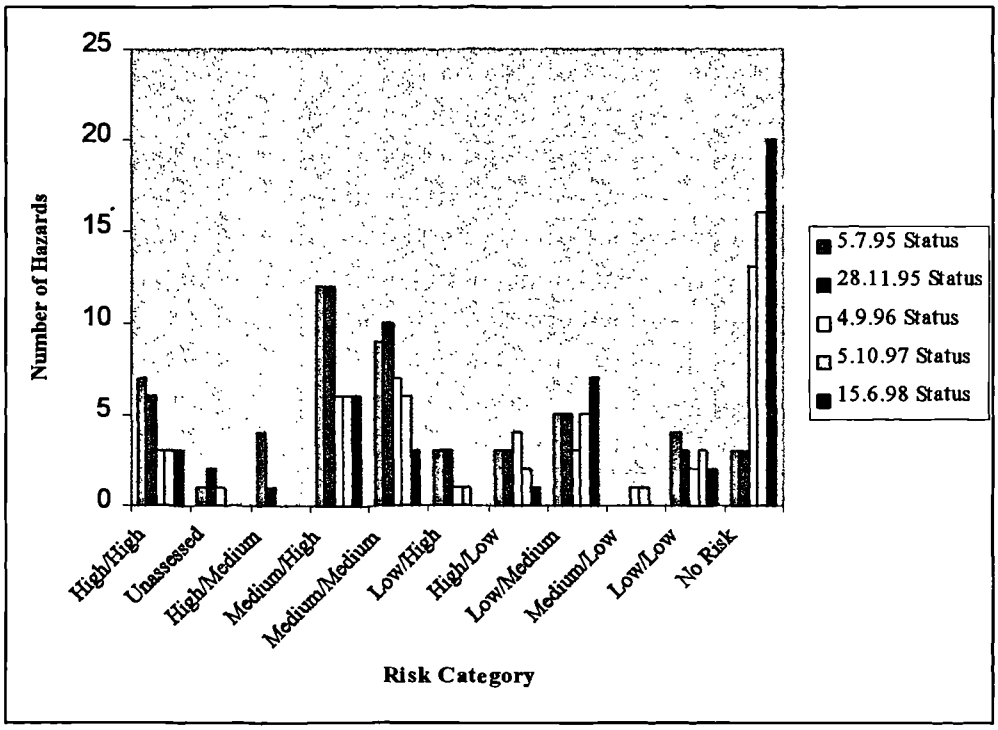

Figure 6.05: Risk monitoring during the project

The project risks were reassessed at regular intervals. Many of the earlier risks are due to a lack of definition in the proposal. These reduced during the first six months of the work. Unassessed risks were considered the same status as high/high. Mitigation actions were assigned for all high risks and increased the work to be performed. Some risks had to be accepted, because no mitigation actions could be identified to reduce the likelihood of the risk happening or its consequence. This risk management activity gave greater visibility to the customer of the progress of the project and the potential risk of not achieving the required goal. This information was incorporated into the customer's management activity, which was sent to the Ministry of Defence.

Chapter 7: Magnetron sputtering of NiCoCrAlY

7.1: Introduction

A requirement has been established to deposit a magnetron sputtered layer of NiCoCrAlY, to replace the VPS process, as a bond coating in the TBC application process. If suitable deposition parameters were chosen, less surface treatment of the applied layer would be required to produce a dense coating Two layers of NiCoCrAlY were deposited (see figure 7.01), to sandwich the sensor package. The structures of both layers were important. The lower layer formed the base for the sensor package and any surface features might have caused problems with the sensor patterning or electrical insulation. The upper layer must protect the sensor when the PVD TBC layer is applied and must act as a suitable base for the TBC.

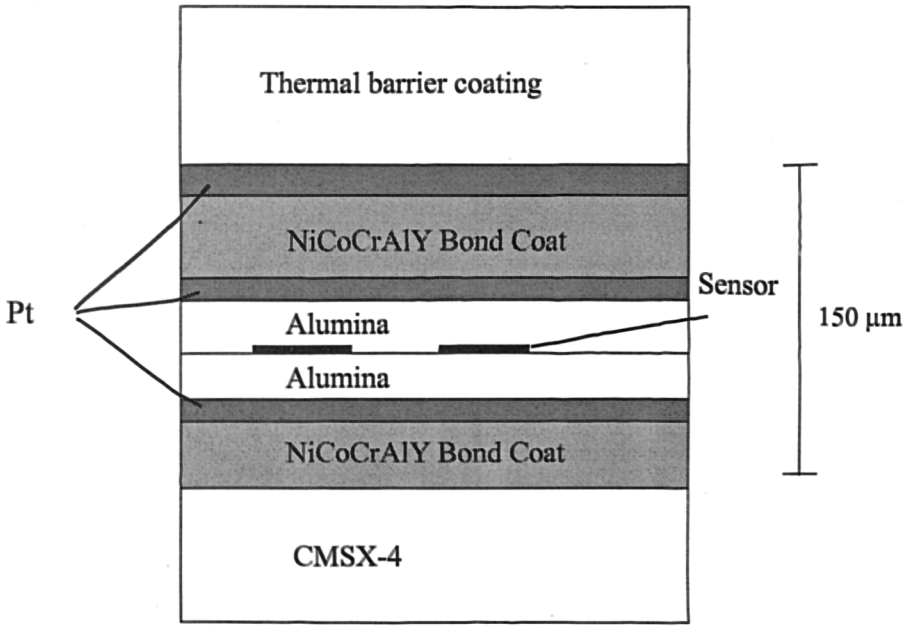

Figure 7.01: Proposed sensor package

The effects of the parameters on the structure and composition of the deposited metallic coatings were reviewed in chapter 4. The aim of this chapter was to investigate how the deposition parameters affect the coating structure and composition of NiCoCrAlY using the Rolls-Royce facilities. Magnetron sputtering is

very sensitive to small changes in deposition parameters making the deposition unreliable. The coating process is also very slow. The deposition and analysis of each deposited film takes 3-4 days work. Thus a conventional approach to experiment trials where one variable was varied at a time would have been very expensive. An experiment design process has been used to sort the important process parameters and optimise these. This is similar to a Taguchi methodology[130]. For this project the course notes and book by Davies[131] have been extensively used and his experiment design rules followed.

7.2: Design of experiment

A list was made of all the parameters that could affect the coating composition, structure and deposition rate. This is given in table 7.01:

Parameters	
1	Deposition power
2	Substrate to target distance
3	Argon pressure
4	Ultimate vacuum pressure
5	Substrate temperature
6	Substrate to target orientation
7	Bias power
8	Surface roughness
9	Ion cleaning times and power
10	Equipment operator

Table 7.01: Process parameters that could be varied during the deposition of metallic coatings

It was estimated that it would take 3-4 days work to perform the preparation, deposition and assessment of each coating. Even with an efficient fractional factorial

experiment it would be prohibitively expensive to sort this number of parameters. The parameters were sorted using an engineering judgement based on previous experience of depositing metallic coating. Those that could be fixed for all the work could be ignored. For example, the sample temperature could not be fixed but depended on the deposition conditions. Neither could it be monitored. Design work was started on a temperature monitoring system, but for this trial, the substrate temperature was ignored.

This reduced the list of parameters down to four. These were confirmed with a limited trial. This was to ensure that each sample of the experiment would produce a measurable coating. For example, it was found that the coatings spalled off highly polished substrates, making the evaluation of their properties difficult. A set of parameter levels was found that resulted in an well-adhered coating. For the main experiment, levels were set either side of those used on the trial. Again care was taken to choose the levels. If one parameter was dominant, a large variation in its value may have swamped the effect of the other variables. The parameters chosen are shown in table 7.02.

Parameter	High Level (+)	Low level (-)
Parameter A : Deposition setting	800mA	500mA
Parameter B : Argon Pressure	30 x10^{-3}Torr	15 x10^{-3}Torr
Parameter C : Bias Power	100W	Floating
Parameter D : Surface Roughness	Vapour blast	Dry blast

Table 7.02: Experiment parameters with high and low level values

This is described as a 2^4 experiment, i.e., four parameters at two levels, with 16 possible treatment combinations for a full factorial experiment. Because of the time and cost involved with preparing and analysing the samples, this number of coating trials was impractical. Therefore, the treatment combinations have been divided into 2 blocks, i.e., a fractional factorial experiment, in such a way that there was little information lost by just performing 8 coating trials instead of 16.

When dividing the experiment into two blocks, the loss of one degree of freedom will produce an error source. This was confined to one unwanted interaction[131], i.e. the effect ABCD, which is the effect of varying the parameter A on the interaction of B, C & D.

From a Yates table this can be expressed in terms of the required parameters and interactions by:

$Effect_{ABCD}$ = abcd+cd+bd+ad+bc+ac+ab+1-bcd-acd-abd-d-abc-c-b-a

The lower case letters represent a trial where the parameter has been set high and the trial represented by 1 where all the parameters are low. By putting all the positive terms into the principal block and the entire negative terms into the second block we get:

Experimental trials	Principal block	Second block
1	1	a
2	ab	b
3	ac	c
4	bc	d
5	ad	acd
6	bd	bcd
7	cd	abc
8	abcd	abd

Table 7.03: The 16 treatment combinations divided into two blocks for a fractional factorial experiment

The principal block was expanded to show the eight experiment trials and the levels of each parameter. The trials have been arranged in a random order to prevent systematic error affecting the results.

The letters represent the high (+) values for each parameter. For block 1 this gives

Experiment No.	Random Order	A	B	C	D
1	1	-	-	-	-
2	4	-	+	+	-
3	7	-	-	+	+
4	5	+	-	-	+
5	6	-	+	-	+
6	3	+	-	+	-
7	2	+	+	-	-
8	8	+	+	+	+

Table 7.04: Experiment design showing the levels of each parameter for the eight coating runs

Expanding the Yates table for this particular design took several days of work of calculations and checking. Since this work was performed, a computer software package has been made available to quickly design the experiment based, on the number of parameters and levels entered.

7.3 Experimental Detail

7.3.1 Preparation of targets

A target was produced from powder of Rolls-Royce specification MSRR.9537/1. The composition of the powder is given in table 7.05. The powder was pressed into a 3-inch diameter bar by HIP Ltd using a hot isostatic pressing method and then sectioned to form a number of one-quarter inch thick sputtering target discs. Several segments of the target were removed and analysed to confirm the correct target composition, and that the powder was evenly mixed throughout the pressed bar.

Element	Minimum %	Maximum %
Nickel	31	33
Chromium	20	22
Aluminium	7	9
Yttrium	0.35	0.65
Carbon	-	0.015
Oxygen	-	0.05
Other elements (total)		0.5
Cobalt	Remainder	Remainder

Table 7.05: Composition of NiCoCrAlY powder, (Rolls-Royce specification MSRR 9537/1), used to form sputtering target[132]

7.3.2 Coating details

Samples were machined from a bar of Cannon-Muskegon single crystal no 4 turbine blade material (Rolls-Royce specification MSRR 7248). The composition of this material is given in table 7.06. The samples were then prepared for deposition of the NiCoCrAlY coating using a dryblast process using 120/220 SiC grit or a vapour blast process using the same grit size.

Element	Nominal %
Chromium	6.5
Cobalt	9.6
Tantalum	6.5
Tungsten	6.4
Nickel	remainder

Table 7.06: Composition of CMSX-4 single crystal turbine blade alloy (MSRR 7248)[133]

The coating runs were performed in the order given with the same person performing all the operations to eliminate the effect of operator dependence. The coatings were first deposited on glass slides for several hours to establish the deposition rate. The ends of the glass slide were masked off with other slides. This gave a step edge, which was profiled using a Talysurf 10 instrument (see section 6.4). The coating thickness was determined for each set of parameters. The deposition times were then scaled to give a thickness of 25 μm for each coating and the coatings repeated on the prepared samples. A total of four components were coated for each deposition, two prepared using a dryblast process and two using a vapour blast process.

The Sinfin-A site deposition system is described in section 6.2. The initial deposition trial was performed in the Elton Road CVC deposition system with later deposition and optimisation work transferred to the Sinfin-A site system. The Elton road system is very similar except that this system has only two cathodes and limited substrate rotation. The coating was deposited from an AJA 3inch diameter magnetron cathode, purchased for this project.

Process	Parameters
Chemical clean	Ultrasonically clean in Isopropyl alcohol
Substrate cleaning	100W bias ion clean for 20 minutes
Target cleaning	800/500mA deposition onto shield for 60 minutes
Deposition	800/500mA DC magnetron deposition at 30/15x10^{-3} Torr argon pressure with 0/100 W bias sputtering of substrate

Table 7.07: Coating details of NiCoCrAlY trials

7.3.3 Measurement of deposition rate

Because of the surface roughness produced by the dryblast or vapour blast process, step profiling was not practical. The samples were cut into two pieces. One half was encased in a bakelite mould and polished on an automated polishing machine. The

thickness of each film was measured by optical microscopy for each sample. Knowing the deposition time, the deposition rate was calculated. Inaccuracies in the original calculation of deposition rate from the glass slide or non-repeatability in the process caused the films to vary in thickness between 17 and 30 μm.

7.3.4 Assessment of structure

No quantitative value could be obtained to describe the structure of the coating. Instead the films were judged qualitatively. The surface and sectioned edge of the eight samples were viewed using a scanning electron microscope. Photographs of the coatings are shown in the results section. However, it was found easier to perform the judgement by looking at a number of areas of the coating. These were then arranged in order from the most favourable for this work to the least favourable. Zone T structures would get a high value out of a maximum score of 10, whereas a zone 1 structure would get a low value.

7.3.5 Measurement of film composition

The composition of the films was measured by energy dispersive spectroscopy (EDS). This is described in section 6.4. Here, quantitative values can be measured for the percentages of Al and Y in the film. The composition was measured in 3 μm intervals throughout the thickness of the coating. The values obtained from the middle of the coating were averaged.

7.3.6 Analysis of results from experiment design trial

By examination of the results for each of the eight experiments some determination could be made of the effect of each of the parameters on the measurands. One method to achieve this was to add the results where the parameters are high and taking away the results where the parameters are low. Parameters that significantly effect the measurand will have high positive or negative values. Those that have little effect will have values closer to zero.

The benefit of the statistical design approach was that information could also be gained on the effect of the parameters and their interactions.

The first column represents the results expressed in terms of the coating parameters from the experiment design. This was expanded by the summation and subtraction of rows. A fuller description and explanation is given in Davies[131] and is not necessary here.

Response	1st column of analysis	2nd column of analysis	3rd column of analysis
1	1+ab	1+ab+ac+bc	1+ab+ac+bc+ad+bd+cd+abcd=Total
ab	ac+bc	ad+bd+cd+abcd	ab+bc+bd+abcd-1-ac-ad-cd=2effB
ac	ad+bd	ab-1+bc-ac	ac+bc+cd+abcd-1-ab-ad-bd=2effC
bc	cd+abcd	bd-ad+abcd-cd	bc+1+abcd+ad-ac-ab-cd-bd=2effBC
ad	ab-1	ac+bc-1-ab	ad+bd+cd+abcd-1-ab-ac-bc=2effD
bd	bc-ac	cd+abcd-ad-bd	bd+1+ac+abcd-ad-cd-ab-bc=2effBD
cd	bd-ad	bc-ac-ab+1	cd+abcd+1+ab-ad-bd-ac-bc=2effCD
abcd	abcd-cd	abcd-cd-bd+ad	abcd+ad+ac+ab-cd-bd-bc-1=2effA

Table 7.08: Expanded Yates table gives values for interactions of variables in terms of experiment results

The third column of analysis gives the effect of each parameter and chosen interactions in terms of the experiment results.

To help examine which were significant, the effects were plotted on normal probability paper. If results from an experiment where only randomness played a part were plotted on probability paper, then a curve would be produced. The effect of using normal probability paper is to make the points lie on a straight line. If the experiments were repeated with one of the variables having a significant effect, this would lie off the line.

The effects were arranged in order of increasing magnitude and plotted on the horizontal linear scale of the normal probability paper. Each parameter was given a probability value from the equation:

$$p_i = \left(i - 0.5 / n - 1\right) \times 100 \qquad \text{Equation 7.}$$

Where i is the number of the point in its ascending order and (n-1) is the total number of parameters or interactions. Points that are due to randomness only will lie on a straight line close to zero value. Points that lie off this line may be significant and deserve further attention.

7.4 Results

The results from the eight coating runs are given below

Experiment No.	Random Order	Run No	A	B	C	D	Target Voltage (Volts)	Thickness (μm)	Deposition Time (hours)	Deposition Rate (μm/h)	Relative % of Y to Target composition	Relative % of Al to Target composition	Qualitative assessment of film structure
1	1	368	-	-	-	-	415	24	4.5	5.3	77.8	105.2	5
2	4	373	-	+	+	-	505	21	5	4.2	88.9	100	4
3	7	374	-	-	+	+	563	30	7	4.3	33.8	33.7	9
4	5	370	+	-	-	+	500	25	3	8.3	100	115.6	7
5	6	375	-	+	-	+	526	22	4.5	4.89	100	89.6	2
6	3	371	+	-	+	-	450	24	4	6	55.6	79.2	10
7	2	369	+	+	-	-	426	17	2	8.5	100	103.9	1
8	8	376	+	+	+	+	524	29	4	7.25	100	106.5	6

Table 7.09: Table of results showing the deposition rate, qualitative assessment of structure and composition of coatings

7.4.1 Analysis of Deposition Rate

The levels of the effects of parameters and interactions on the deposition rate are given in table 7.10.

Parameter or interaction	A	B	C	D	BC	CD	AC
Effect level	5.68	0.48	-2.62	0.38	0.68	0.98	-0.92

Table 7.10: Effect factors of parameters on deposition rate

The effect of the variables on the deposition rate is shown in figure 7.02. For this, measurement D was a dummy parameter, since it was anticipated that the surface roughness would have no effect on the deposition rate of the coating. The effect level of parameter D should be close to zero, as should its interaction with other variables. This allowed a line to be drawn between D and CD. Any other points lying on this line should also be insignificant. The graph clearly showed that the deposition pressure was also insignificant. The two significant variables were the deposition current, which increased the deposition rate, and the bias power that reduced the deposition rate. There was a significant interaction between the deposition current and bias power. This result was expected, based on previous experience with metallic coatings, and gave confidence in the statistical experiment design process.

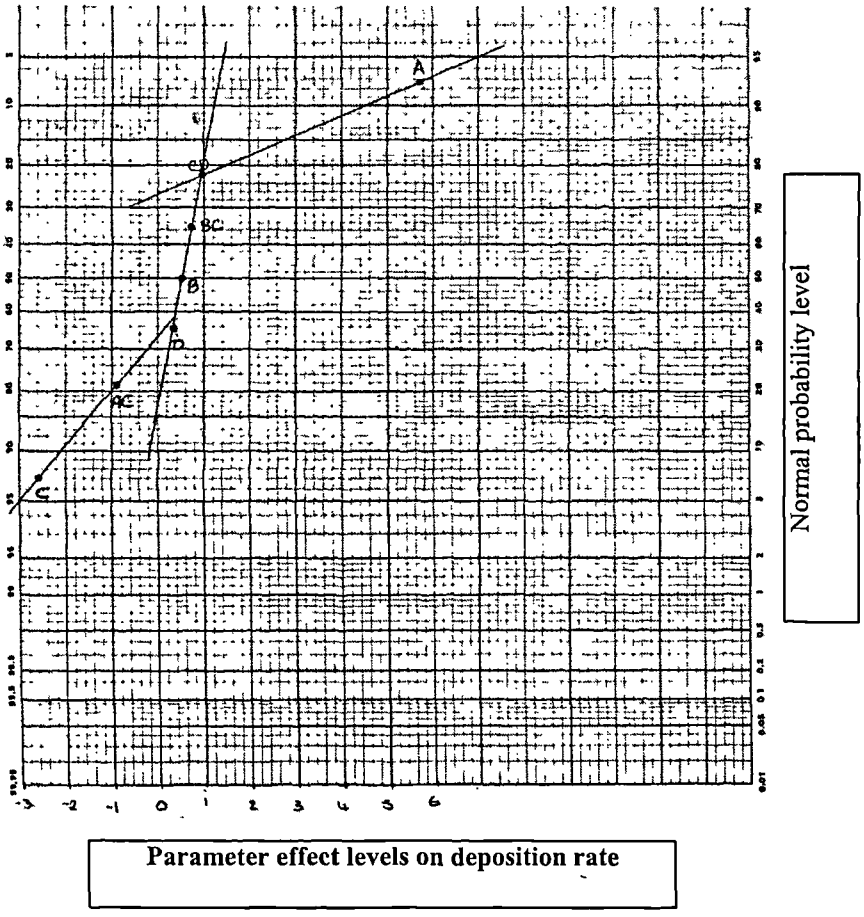

Figure 7.02: Effect of parameters on deposition rate of NiCoCrAlY

7.4.2 Analysis of film structure

Scanning electron microscope photographs for the 8 samples are shown in figures 7.03 (a-h). A range of structures existed from highly voided to dense coating showing that the initial choice of parameter levels produced both zone 1 and zone T structures. The effect factors for the coating structure could be calculated from the result table and is shown in table 7.11.

Parameter or interaction	A	B	C	D	BC	CD	BD	AC
Effect level	2	-9	7	2	0	-1	1	1

Table 7.11: Effect factors of parameters on film structure

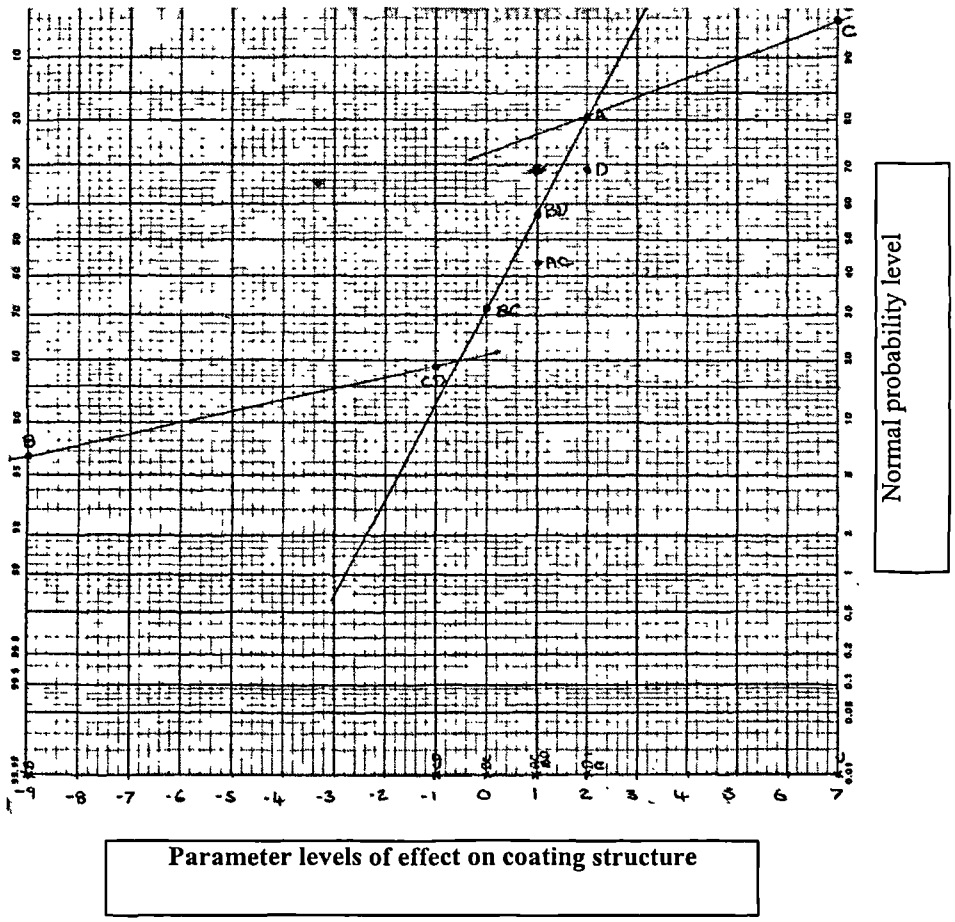

Figure 7.04: Effect of parameters on NiCoCrAlY structure

The melting points of the alloy components have been examined and with the exception of aluminium at 660°C, all have a melting point (T_m) above 1450°C[134]. Thus, the melting point of the alloy was expected to be greater than 1200°C. The sample temperature (T) during deposition has been measured during a later coating run (see Appendix 1). The sample temperature did not exceed 250°C. Thus, the deposition process had a T/T_m value less than 0.2 (see section 4.2.4). This ruled out the diffusion processes that could cause zone 3 structures. Only low T/T_m processes affected the film structure.

The analysis of the effects of the variables on the film structure is given in figure 7.04. The analysis of this graph was more difficult. The argon pressure (B) and the bias power (C) were obviously significant. The other parameters and interactions had effect values closer to zero. The parameters A and D need further investigation to determine if they have a significant effect on the film structure. It was possible that these were significant but have been dwarfed by the effects of B and C. The analysis would have been easier had several dummy parameters been used.

The lack of effect of the substrate finish (D) was somewhat surprising as voided growth could be initiated by shadowing caused by surface roughness. It is believed that there was insufficient difference between the dryblast and vapour blast levels. A smoother surface finish was not used in the trial because it may have resulted in poor adhesion of the coatings and may have been difficult to achieve repeatably.

Figure 7.03(a): Scanning electron microscope image of NiCoCrAlY coating for qualitative assessment of coating structure: Run 371, graded 10/10

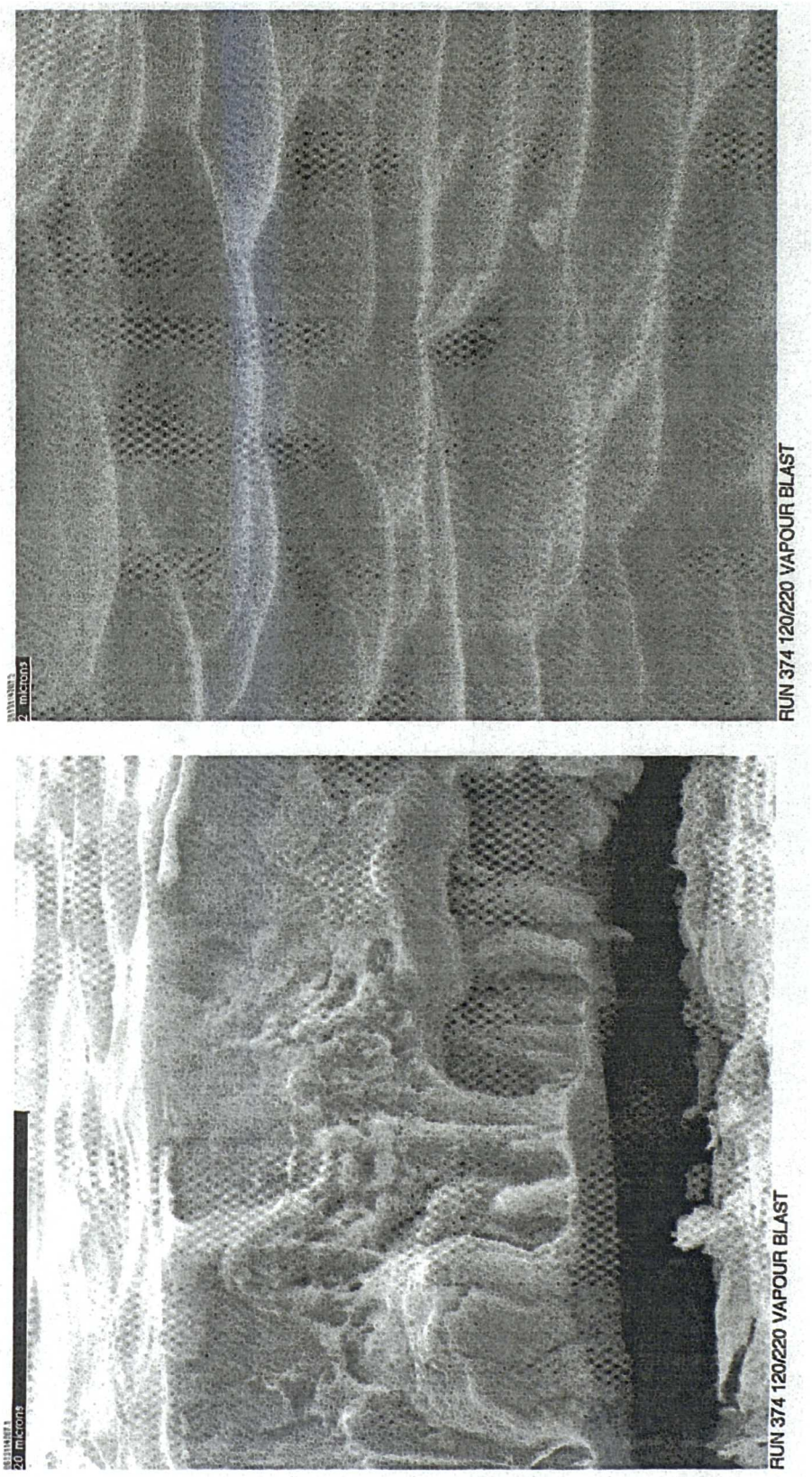

Figure 7.03(b): Scanning electron microscope image of NiCoCrAlY coating for qualitative assessment of coating structure: Run 374, graded 9/10

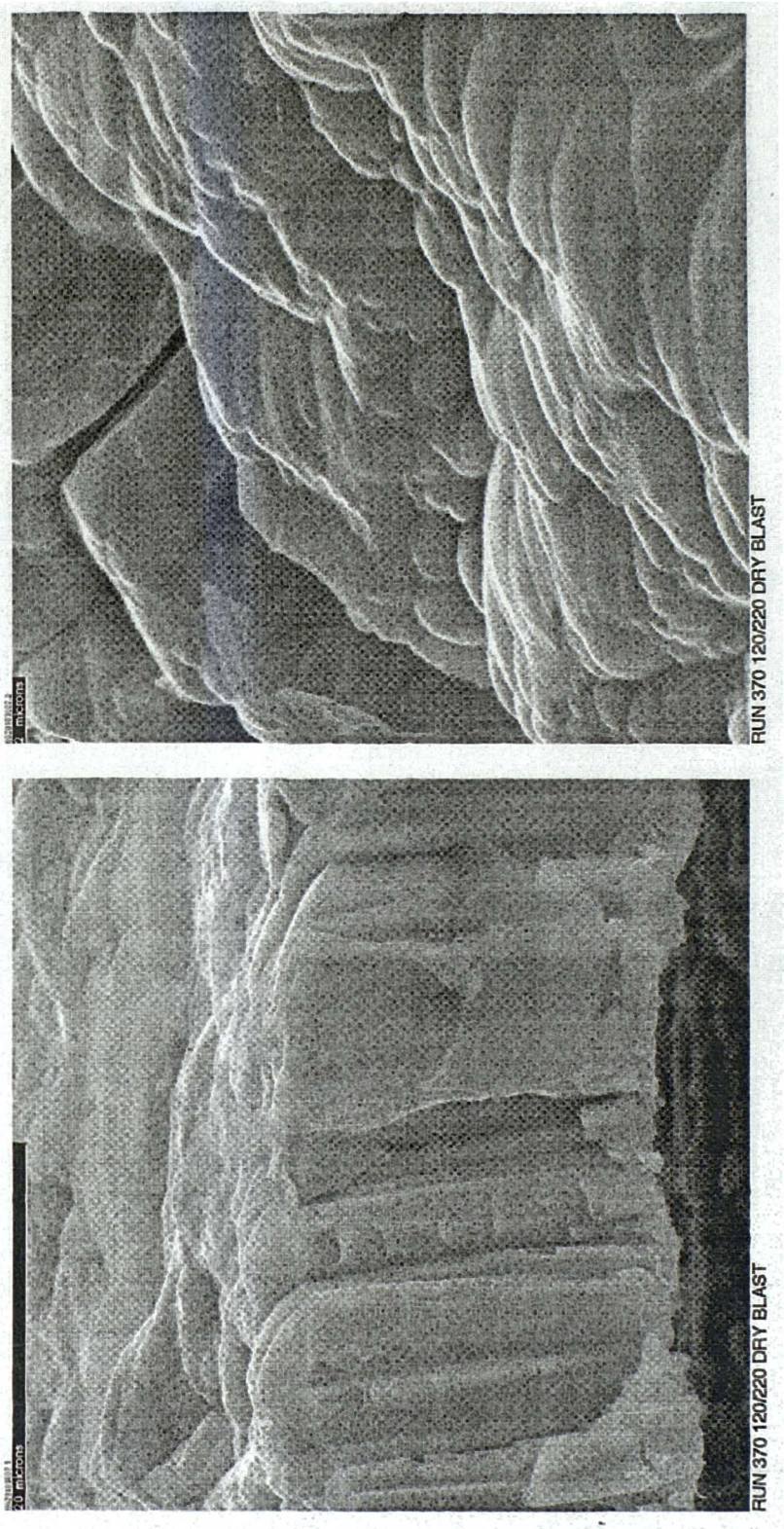

Figure 7.03(c): Scanning electron microscope image of NiCoCrAlY coating for qualitative assessment of coating structure: Run 370, graded 7/10

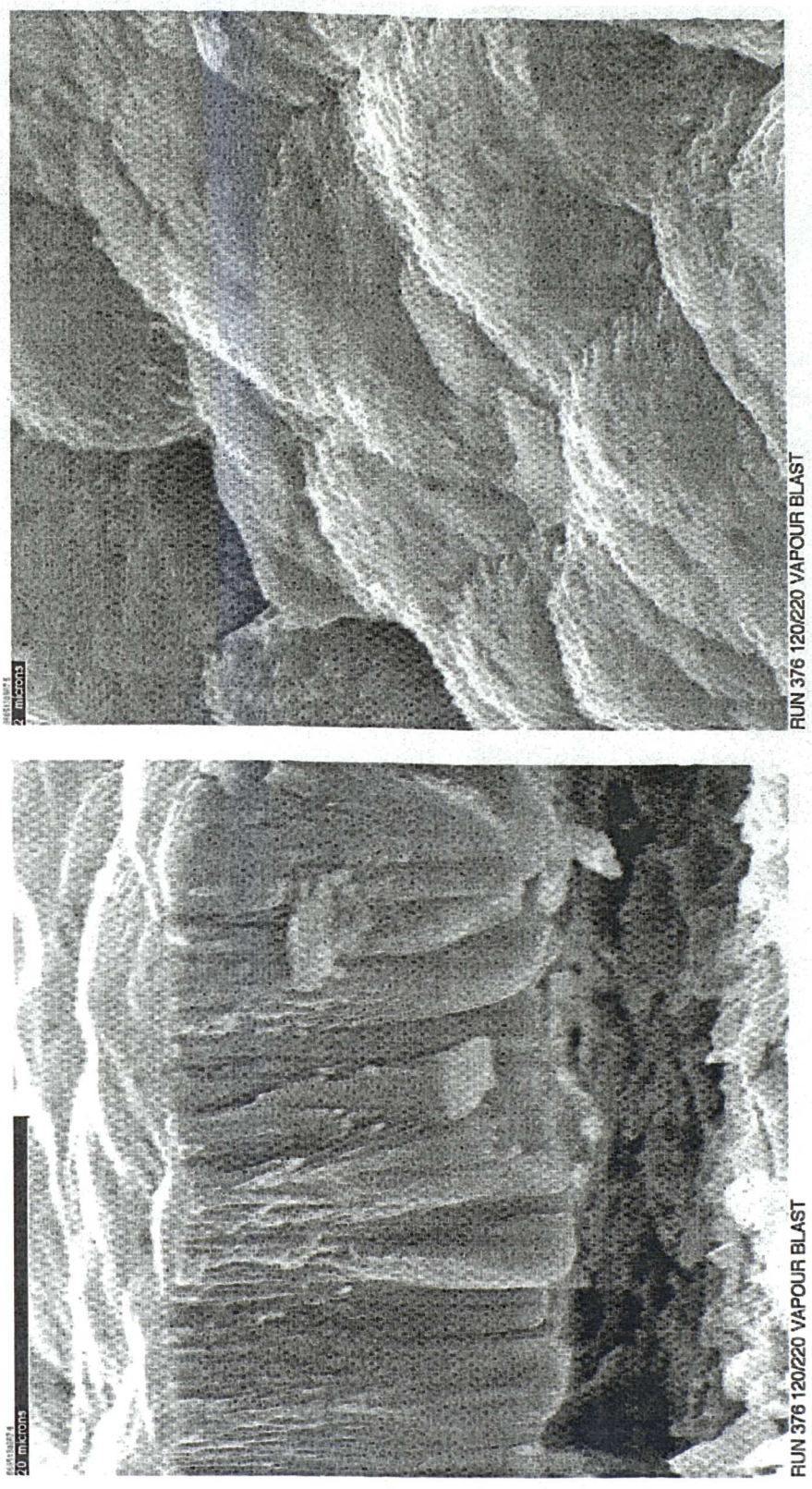

Figure 7.03(d): Scanning electron microscope image of NiCoCrAlY coating for qualitative assessment of coating structure: Run 376, graded 6/10

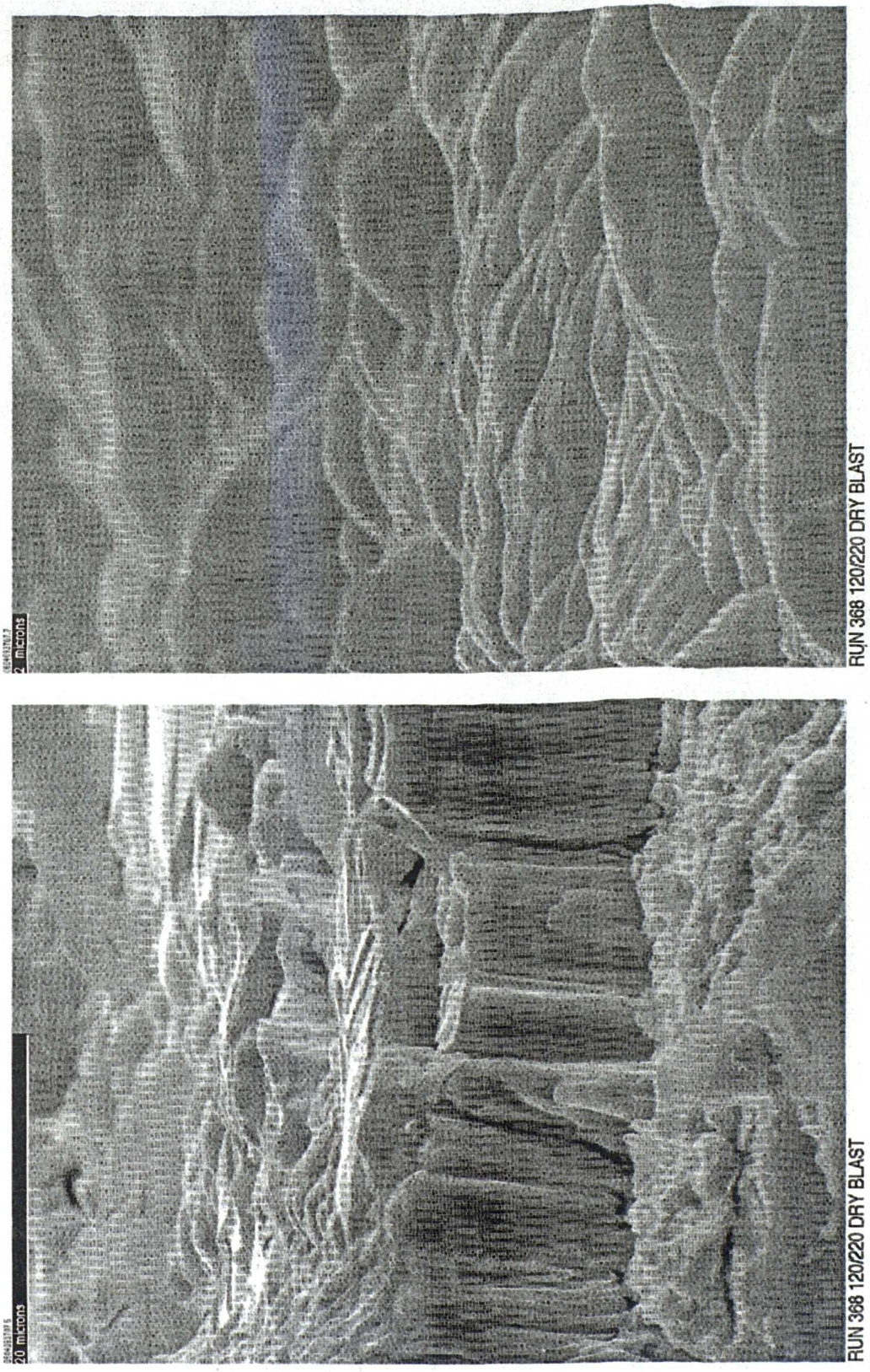

Figure 7.03(e): Scanning electron microscope image of NiCoCrAlY coating for qualitative assessment of coating structure: Run 368, graded 5/10

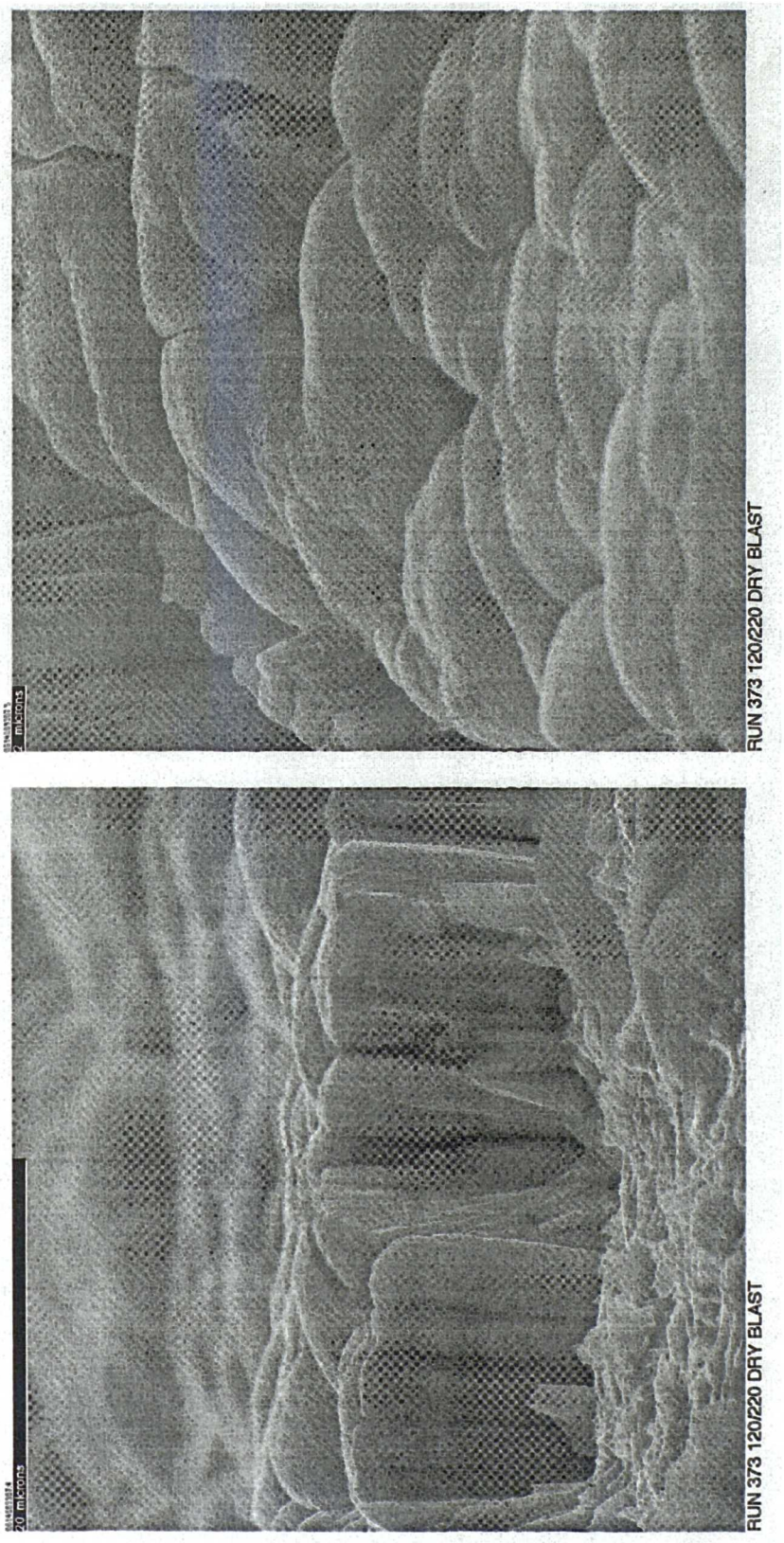

Figure 7.03(f): Scanning electron microscope image of NiCoCrAlY coating for qualitative assessment of coating structure: Run 373, graded 4/10

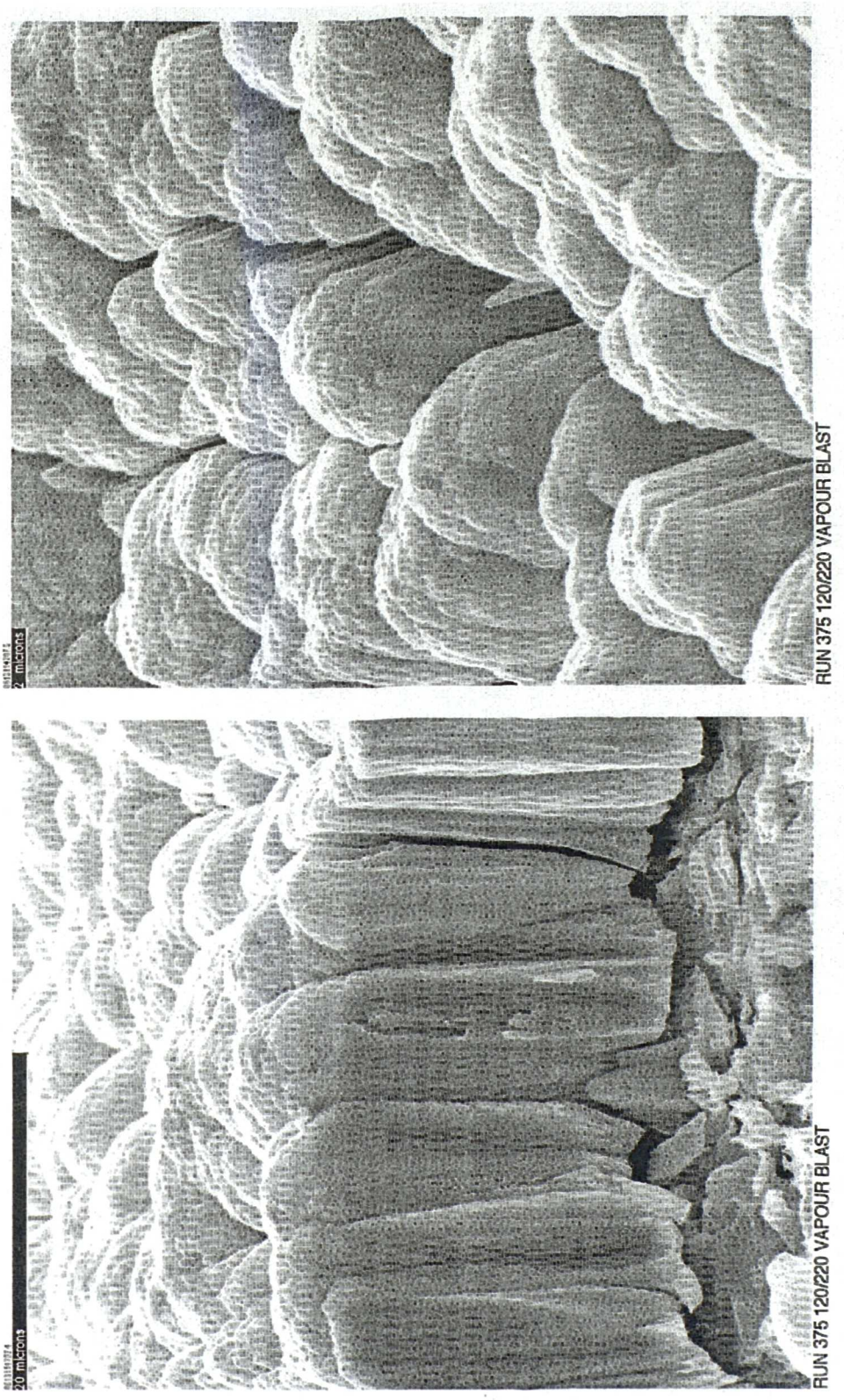

Figure 7.03(g): Scanning electron microscope image of NiCoCrAlY coating for qualitative assessment of coating structure: Run 375, graded 2/10

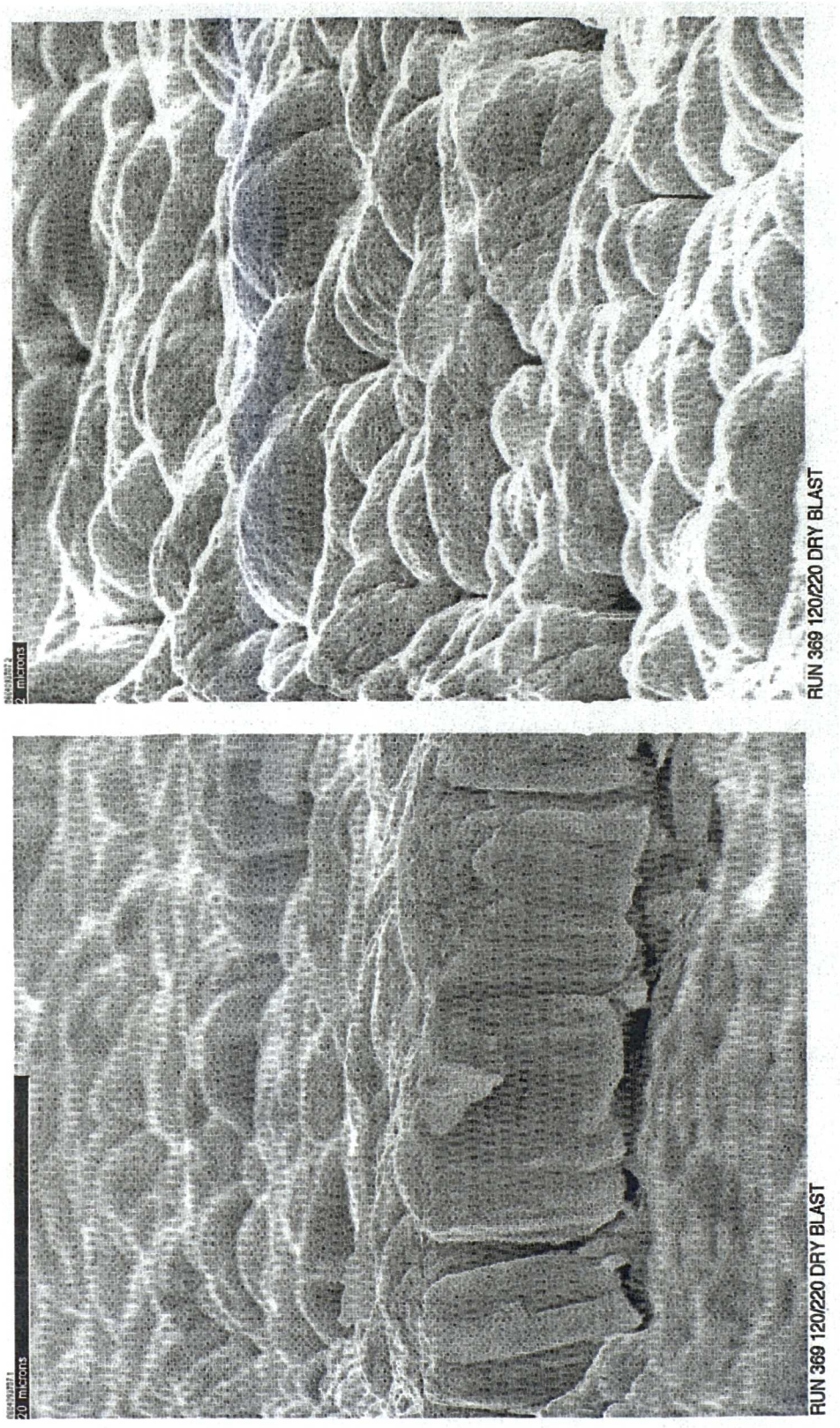

Figure 7.03(h): Scanning electron microscope image of NiCoCrAlY coating for qualitative assessment of coating structure: Run 369, graded 1/10

7.4.3 Analysis of composition

The effect factors for the composition of the coatings is given in table 7.12. The factors are shown on the graph in figure 7.05.

Parameter or interaction	A	B	C	D	AB	BD	AC
Effect on Al percentage	19.18	16.57	-23.73	-10.73	-8.78	6.83	-4.55
Effect on Y percentage	13.77	30.42	-24.87	2.87	-8.23	2.68	2.68

Table 7.12: Effect factors of parameters on film composition

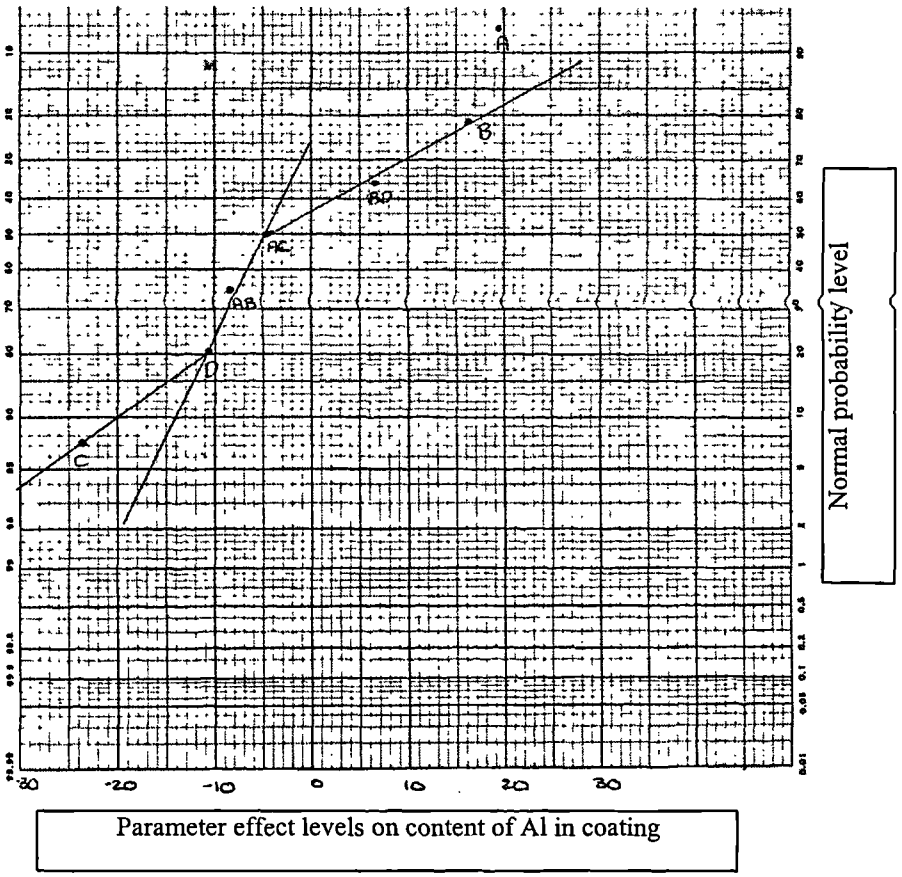

Figure 7.05(a): Effect of parameters on Al content of NiCoCrAlY coating

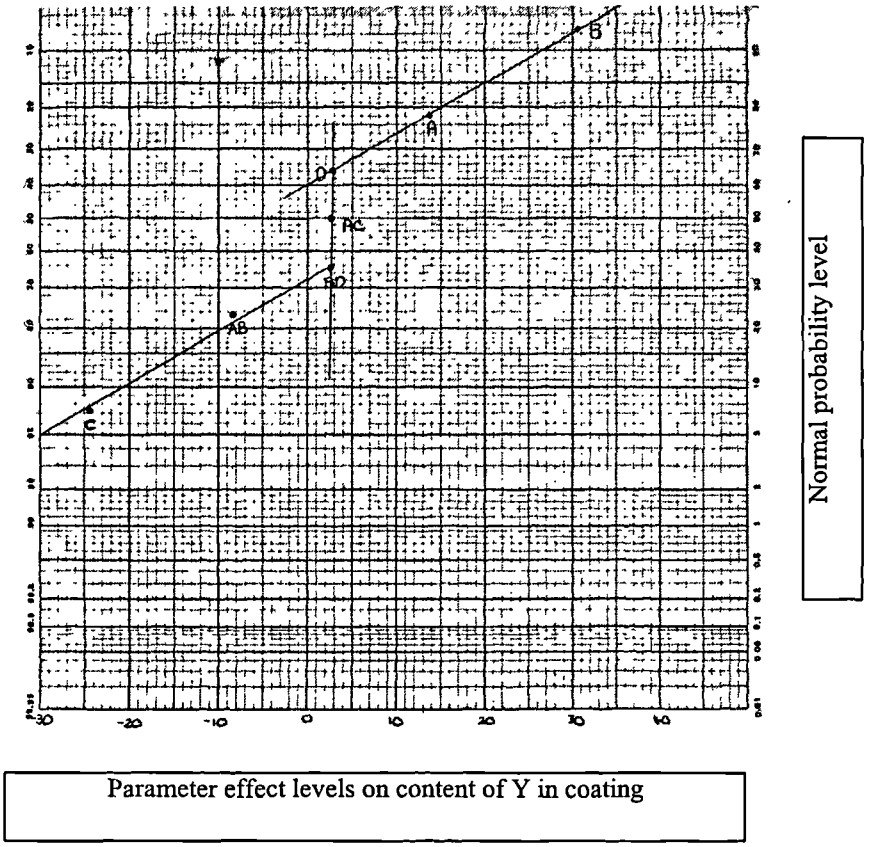

Figure 7.05(b): Effect of parameters on Y content of NiCoCrAlY coating

As long as the sputtering target was cooled so that diffusion processes could not take place within it, the sputtered flux was the same as the average bulk composition. If the deposition parameters were altered, a depleted state would exist at the surface of the target and equilibrium re-established so that the bulk composition was sputtered. The processes that affected the composition of the coating occurred at the substrate. The amount of an element in the coating depended on the difference between its arrival and removal rate at the substrate. Depending on their chemical state, Al and Y may have been preferentially removed by the bias sputtering (parameter C) compared to the other elements in the alloy. Therefore, an increase in bias power depleted the coating further. If the deposition current (A) increased, the arrival rate of the element would increase, causing the percentage of the element in the coating to increase. The deposition pressure (B) has previously been shown not to alter the film growth rate, but altered the energy of incident ions at the substrate and thus the removal rate of the lighter elements.

7.5 Discussion of results

A fractional factorial experiment has been designed. This allowed the assessment of the effect of four parameters and several interactions to be made on the magnetron sputtering of NiCoCrAlY with only eight coating runs. The full factorial experiment was divided into two blocks, only one of which needed to be performed. The division of the full factorial was performed in such a way so that the error caused by this division was in the least significant interaction. This was the effect of parameter A on the interactions of BC and D. In practice the reduction of the parameters used to just four made the analysis difficult because all four had an effect on the coatings. It would have been useful to include several dummy parameters into the experiment design. These would have had no effect on the coatings but would have made the analysis of the graphs easier.

The coatings have exhibited both zone 1 and zone T structures, which have shown that the careful selection of the parameter levels has given the trial some useful results. The voided boundary columnar structure of zone 1 was undesirable for this work. Some densification of the coating would have been required, which would be acceptable for the lower coating but not for the upper layer. An open grain structure would have allowed preferential oxidation of the NiCoCrAlY during the TBC process. This structure would be a poor base for the application of the insulator and sensor coatings. Sputtering is a low temperature process so the zone III structure will be unobtainable. The aim of this work was to achieve a zone T structure. The most suitable parameters were those used for run 371, i.e., high deposition current and bias power and low working pressure.

The composition of the coatings was also important to the formation of good adhesion of the TBC coating. This is discussed further in the next chapter. For the NiCoCrAlY coating the parameters that would be used to obtain a good structure will also reduce the Al content of the coating, resulting in a trade-off between composition and structure. However, the deposition current was also a significant parameter for the Al content of the deposited film. It altered the ratio of arrival to removal rate of that element at the substrate. It had an insignificant effect on the structure over the limited levels of the trial. Hence, there is scope for using the working pressure and bias power to obtain the correct

structure, then independently increasing the deposition current to improve the aluminium content. This will change the deposition rate of the coatings. Alternatively a higher aluminium content target could be used to gain better compositions whilst maintaining the structure seen in run 371. From the deposition rate analysis, it was clear that there was also an interaction between the deposition current and bias power level. There was no significant effect on the films of altering the sample preparation from dryblasting to vapour blasting.

Chapter 8: Optimisation of NiCoCrAlY process

8.1 Introduction

A statistical experiment design has previously been performed to determine the deposition parameters that affect the film structure, composition and deposition rate. This showed that one particular set of parameters gave a dense coating suitable for this work. The next step should have been the optimisation of the parameters and to determine the sensitivity of the coating to small variations about the optimum[131]. This would have allowed a decision to be made on the level of equipment calibration. Further, the coating should have been characterised for adhesion to the substrate, residual stress and interfacial contamination.

However, before this could take place, several large alterations to the process had to be made. These would have invalidated the optimisation work. Firstly, the deposition condition voltage and current have been seen to significantly alter with target wear. This could cause poor repeatability of the coating structure and composition.

Secondly, the Al content of the coating was lower than that of the target. The next coating to be applied on top of the NiCoCrAlY layer was a coating of Pt. This was heat treated to form a Pt-Al alloy. Exposure to an oxygen atmosphere at 1000°C immediately prior to the TBC application (see section 5.2) formed a layer of Al-O on the Pt-Al layer. This was used to form a good bond with the TBC coating. The source of the Al for the thermally grown oxide was the NiCoCrAlY layer[135]. Thus, a low Al coating content may result in poor TBC adhesion.

Finally, the Elton Road system was required for higher priority work before the logical completion of the experimental work. The coating trials were transferred to the similar Sinfin-A site CVC deposition system. It was anticipated that even the small differences in system designs would have an effect on the deposition conditions obtained.

8.2 Further coating assessment work

8.2.1 Heat treatment of samples

It was possible that heat treatment of the samples may alter the structure and adhesion of the coatings described in chapter 7. A vapour blast sample from each coating run was heat treated for one hour at 1100°C in a vacuum furnace. The samples were cut into two pieces, encased in a bakelite mould and polished using different grades of SiC abrasive paper. These were examined using an optical microscope. Images of the samples are shown in figures 8.01(a-c), along with the qualitative grades given to the coating runs in chapter 7. The adhesion of the coatings to the substrate appeared satisfactory. With the exception of the interface voids, the coating produced with the run 371 parameters looked satisfactory as a base for the sensor package.

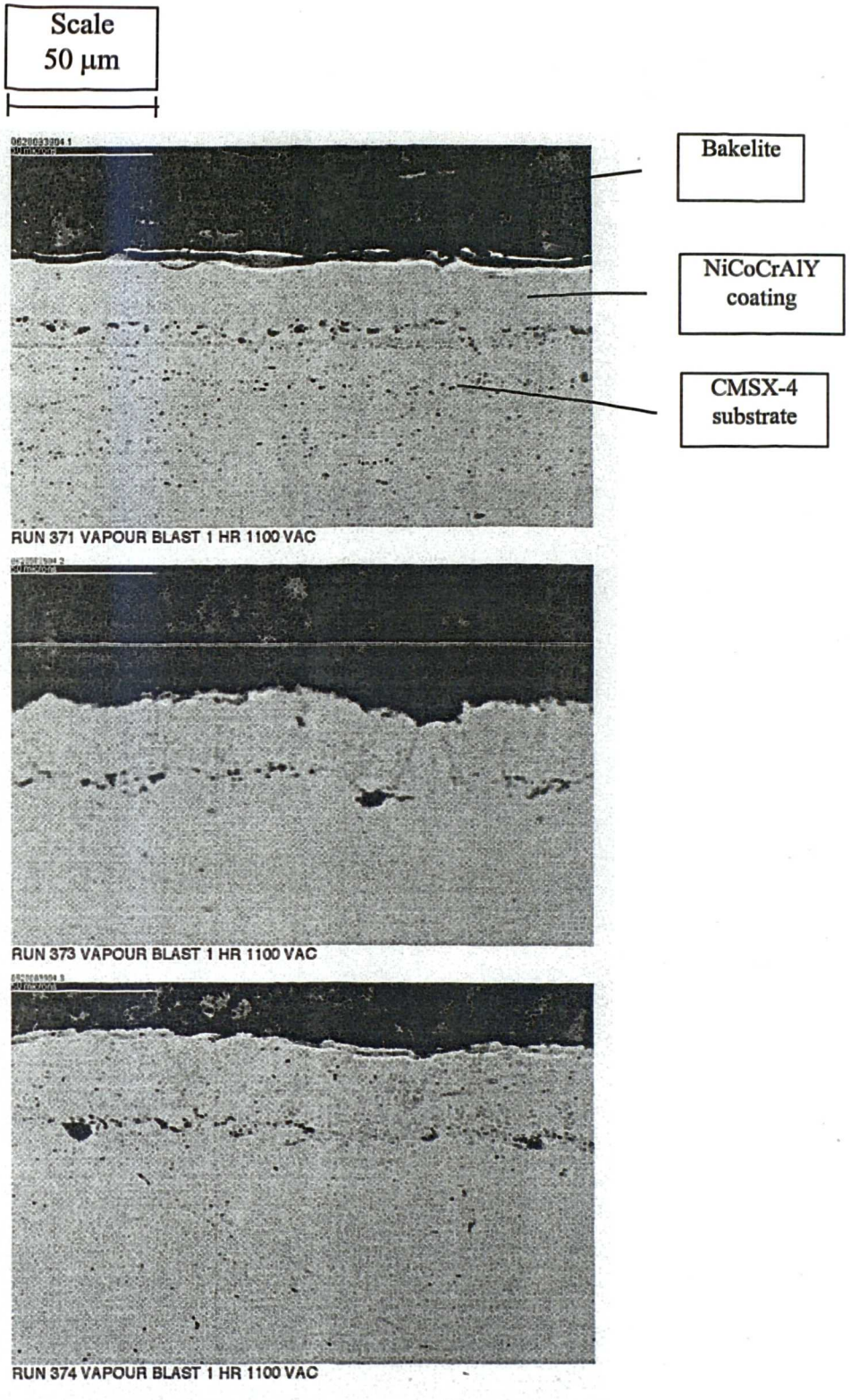

Figure 8.01(a): Heat-treated NiCoCrAlY coatings on vapour blasted substrates. Upper (run 371 graded 10/10), middle (run 373 graded 4/10) and lower (run 374 graded 9/10)

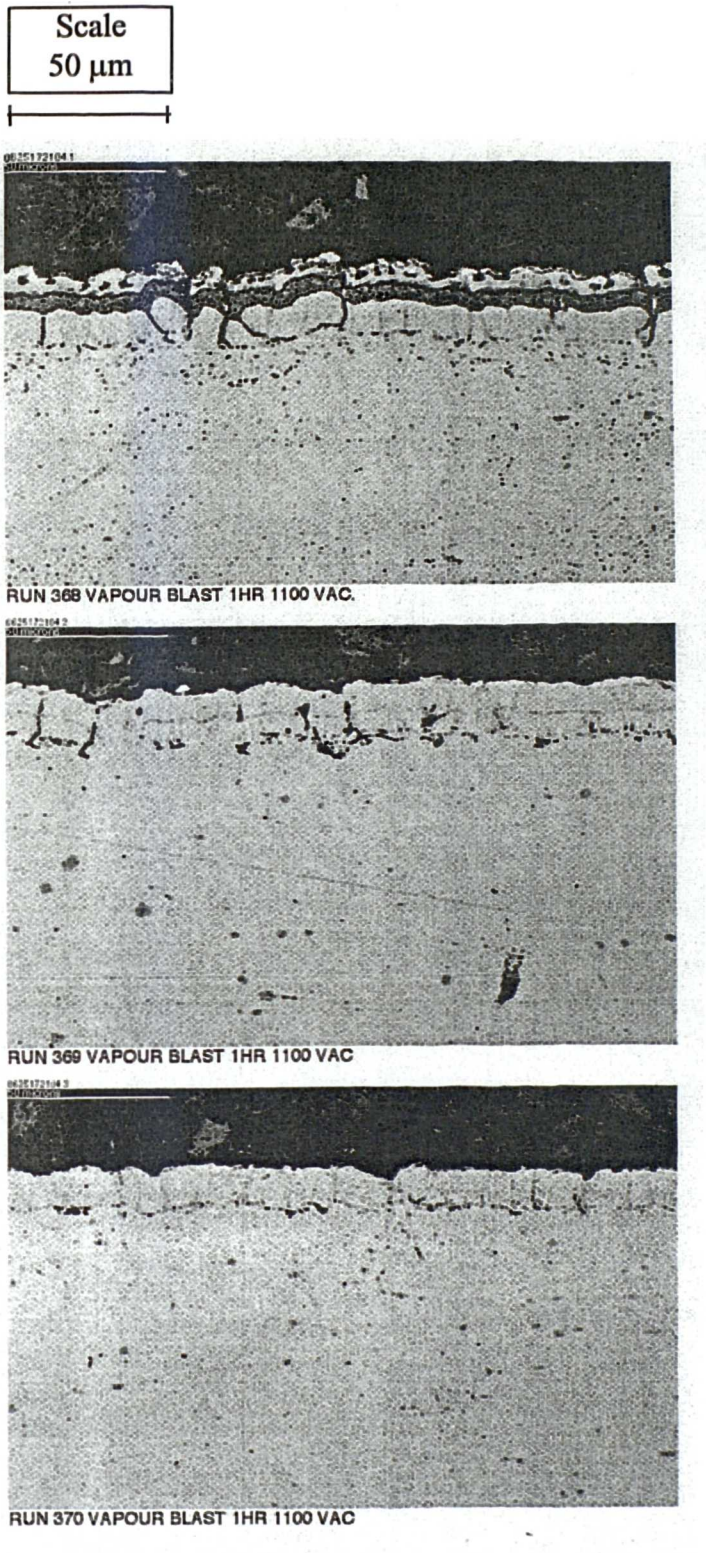

Figure 8.01(b): Heat-treated NiCoCrAlY coatings on vapour blasted substrates. Upper (run 368 graded 5/10), middle (run 369 graded 1/10) and lower (run 370 graded 7/10)

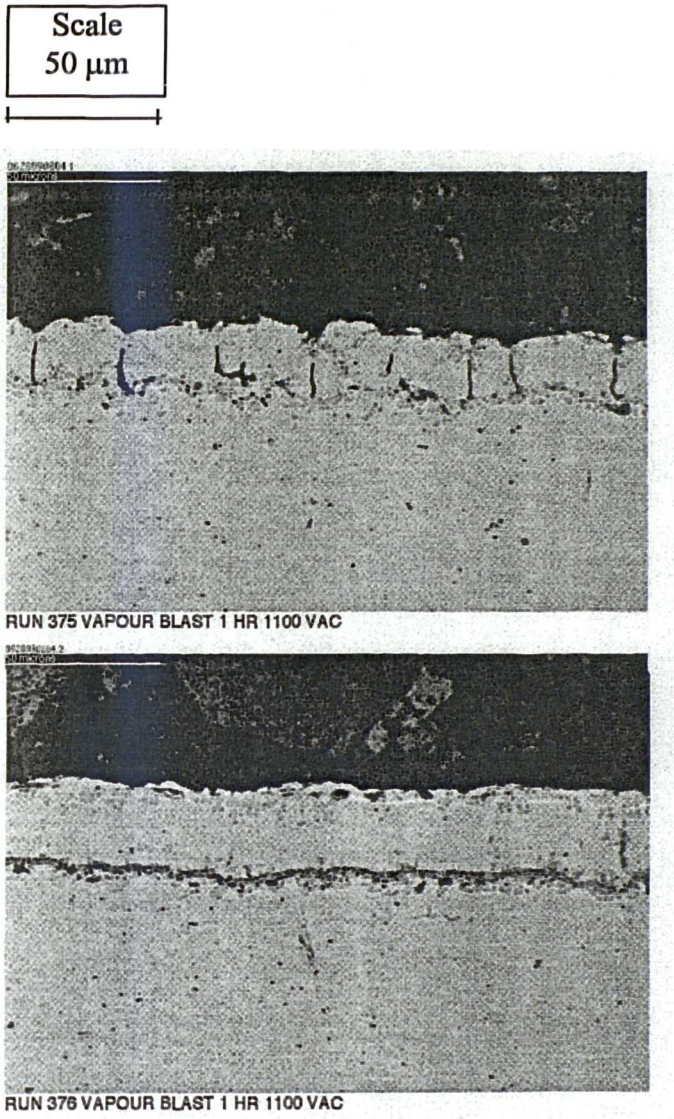

Figure 8.01(c): Heat-treated NiCoCrAlY coatings on vapour blasted substrates. Upper (run 375 graded 2/10) and lower (run 376 graded 6/10)

8.2.2 Evaluation of substrate preparation

The work described in chapter 7 showed that the difference between vapour blast and dryblast prepared samples had no significant effect on the film structure. The voids at the interface, however, are a result of shadowing during the early stages of deposition and may be affected by the sample preparation method. Because both types of sample had been coated in the previous trial, a direct comparison could be made on the run 371 parameters. This is shown in figure 8.02.

The vapour blast sample has the lowest number of voids. Thus, there was the possibility that producing a smoother surface finish would reduce the voids further. This could have been achieved by using finer grit in the vapour blast operation or by polishing the sample. However, a previous trial, prior to the experiment design, showed that the adhesion of the coating to highly polished substrates was poor.

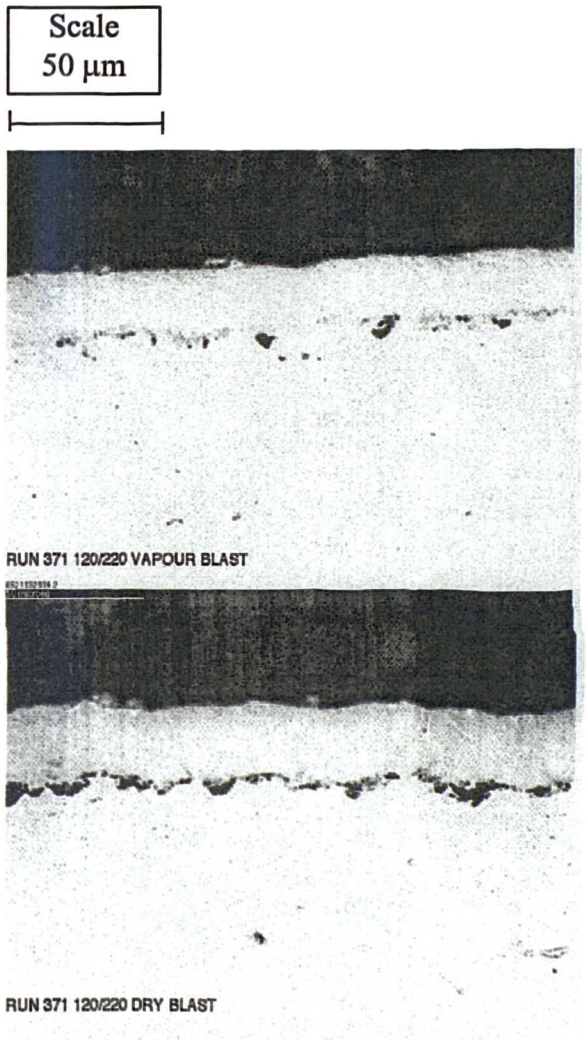

Figure 8.02: Comparison of interface voids from run 371 with vapour blast (top) and dryblast (lower) prepared substrates

Instead, a trial was performed to determine whether a longer ion clean prior to NiCoCrAlY deposition would reduce the voids, i.e., if the voids were initiated by contamination on the substrate surface or if bias etching could remove peaks on the ough surface vapour blasted surface. Temperature measurements later in the

programme (see appendix 1) showed that the sample temperature becomes constant after 30 minutes ion cleaning. Thus, this work did not affect the deposition due to raised sample temperatures. Substrate ion cleaning times of 30, 60 and 90 minutes were performed prior to an eight-hour coating of NiCoCrAlY numbered run 380,381 and 382 respectively The coating parameters used for run 371 were repeated. The power supply was controlled in current mode and set to a value of 800mA. The argon pressure was $15x10^{-3}$ Torr and 100 Watts of radio frequency bias were applied to the sample during deposition. The samples were then heat-treated, sectioned and polished. The optical microscope images in figure 8.03 reveal that there is little difference between the three samples. Therefore there is no advantage in using ion clean times longer than 30 minutes. These samples were used later in the batch 1 trial in section 11.2.

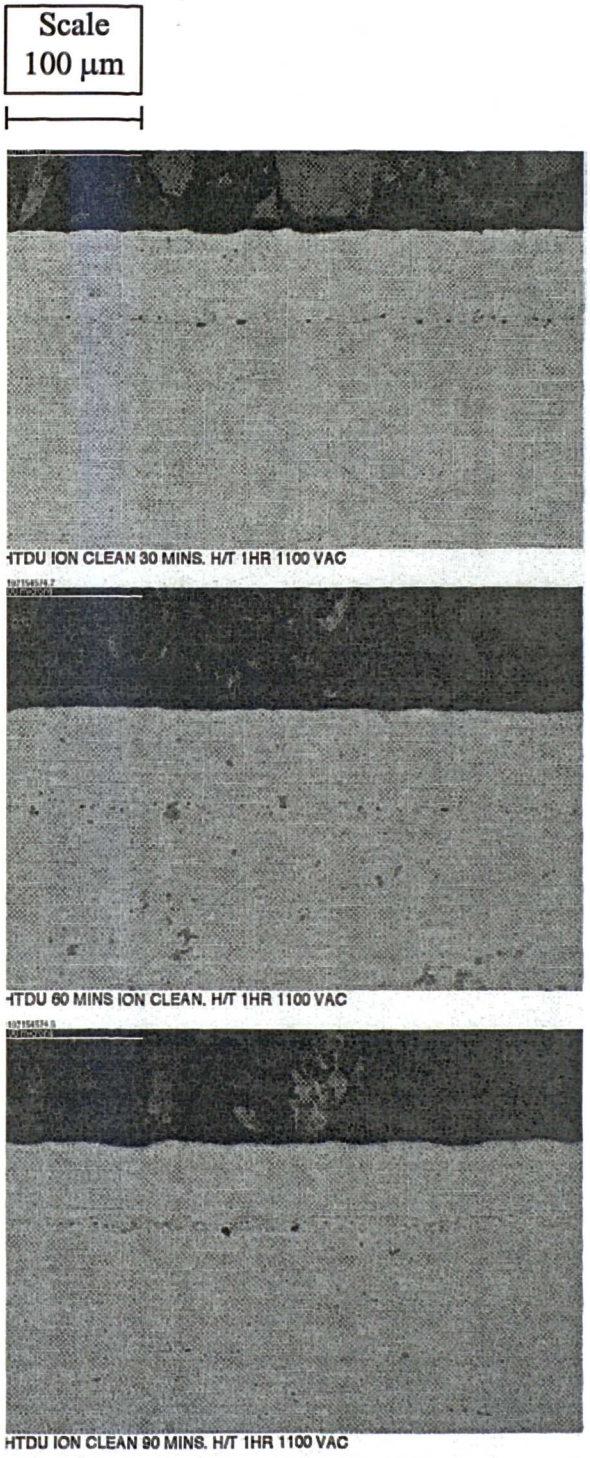

Figure 8.03: Comparison of number of voids after heat treatment at CMSX-4-NiCoCrAlY interface from different ion cleaning times prior to deposition of NiCoCrAlY coating. 30 minutes (top), 60 minutes (middle) and 90 minutes (lower)

8.3 Transfer of process to Sinfin-A site deposition system

The Elton Road CVC system was required for other higher priority coating work and the transfer of the coating work to the Sinfin-A site system had to be completed sooner than planned.

The two deposition systems have very different types of substrate clamping geometry. It was considered likely that the deposition parameters would need to be altered to obtain similar coatings. Problems were also found with radio frequency biasing on the Sinfin-A site system. The Sinfin-A site system had four 'planet' sample holders, shown in figure 6.02. The applied power was distributed between these. The load seen by the radio frequency generator depended on the number of samples or plasma condition of each of the planets. The voltage seen by the sample under investigation was seen to vary from run to run. This would have made the analysis of the effect of bias power difficult. The system was modified by removing three of the planets and power feed arms. The matching of the system had to be altered to compensate for this change in load on the RF generator. Also it was decided to control the bias sputtering to the indicated target voltage instead of the applied power.

Sample number	Coating run number	Sample preparation method	Deposition voltage	Bias voltage
1	470	Polished to 400 grade paper	371	0
2	470	Polished to 240 grade paper	371	0
3	470	120/220 dryblast	371	0
4	471	Polished to 400 grade paper	500	100
5	471	Polished to 240 grade paper	500	100
6	471	120/220 dryblast	500	100

Table 8.01: Investigation of the effect of 100 volts of bias on NiCoCrAlY coatings deposited on differently prepared CMSX-4 substrates

Several samples were produced using different bias voltages on substrates prepared to different surface finishes. First the CMSX-4 samples were dressed back to remove machining marks. The samples then had one of the following preparation levels: polishing with 240-grit paper, polishing to 400-grit paper or dryblasting with 120/220 grit. Two eight-hour coating runs of NiCoCrAlY were performed, one with 100 volts RF bias and one without. One of each of the prepared samples was coated for each run. This is shown in table 8.01.

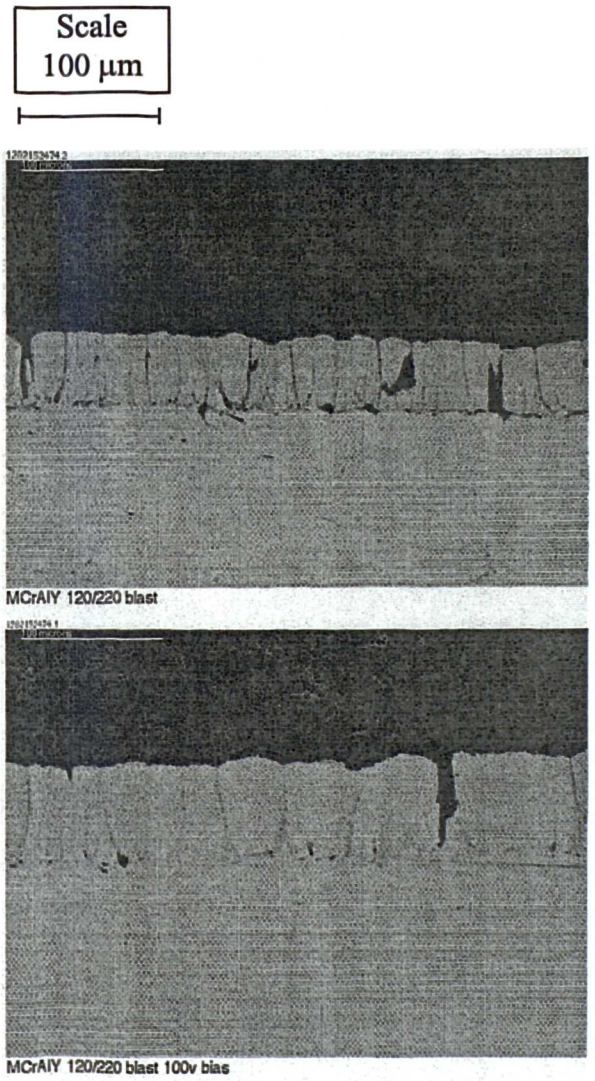

Figure 8.04: NiCoCrAlY coatings deposited on 120/220 grit dryblast substrate without bias (upper) and with 100V bias (lower) during deposition.

Samples 1 to 3 were deposited from a heavily eroded target. It was intended to use this target for the coating with bias. However, the target appeared to be too heavily eroded. Therefore, a new target was used which introduces an additional variable into

the trial. Despite two eight-hour target conditioning runs, the deposition voltage on run 471 was 500V as compared with 371V in run 470 (see table 8.01). This is discussed further in section 8.5. After deposition the coatings were sectioned and polished. They were then examined using an optical microscope.

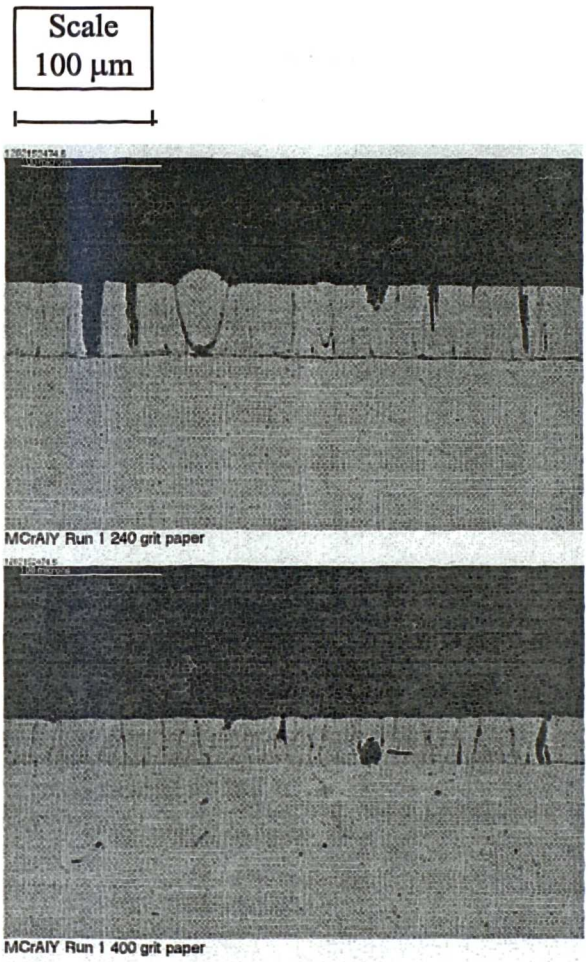

Figure 8.05: NiCoCrAlY deposited onto CMSX-4 substrate prepared to 240 (upper) and 400-grade abrasive paper (lower)

The coating deposited onto the 120/220 gritted surface (samples 3 and 6, shown in figure 8.04) have a columnar structure. The application of 100 volts of radio frequency bias to the substrate during deposition is insufficient to recreate the structure seen for the Elton-Road run 371 parameters. Thus, a higher level must be used.

If the substrate had a smoother surface finish then less bias would be needed to achieve a zone T type structure. This would leave the coating with a higher Al content (see section 8.4).

The cross-sections of the NiCoCrAlY coatings deposited without bias, on 240 and 400 grade surfaces, are shown in figure 8.05. These coatings also have a columnar structure. Sample 2 exhibits a good example of a nodular defect.

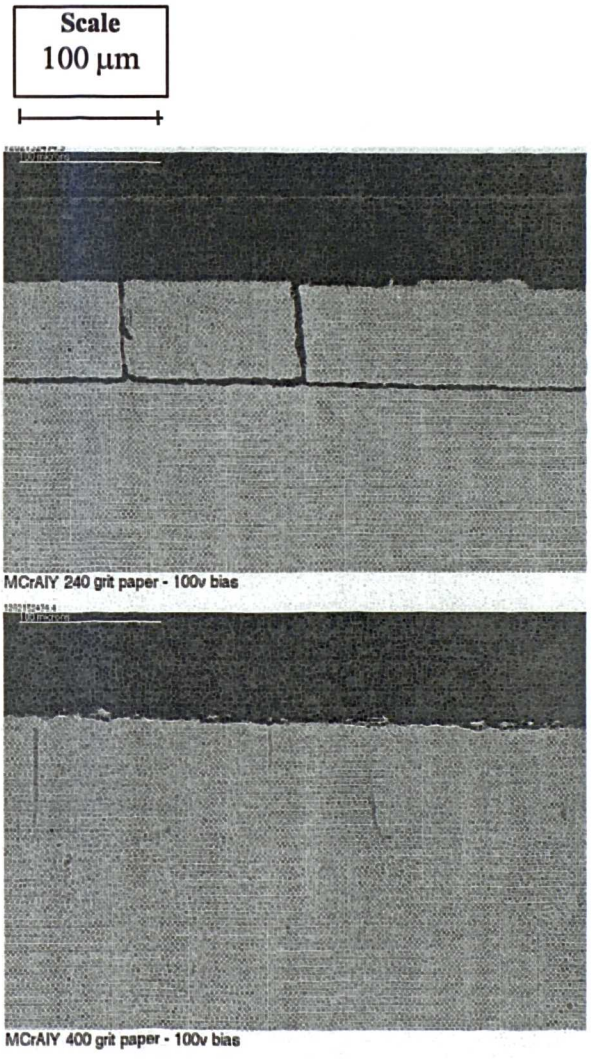

Figure 8.06: NiCoCrAlY coating deposited onto CMSX-4 substrate prepared to 240 grade abrasive paper (upper) and 400 grade abrasive paper with 100V bias during deposition (lower)

Figure 8.06 shows a sample prepared to the same standard but with the coating applied with 100 volts of bias. Here a dense coating has been produced but the

coating has delaminated on the 240-grit (sample 5) substrate. It is surprising that the adhesion on the 240-grit paper sample is worse than that on the 400 grit (sample 4) sample.

It is clear that the substrate needs to be vapour blasted to ensure good adhesion of the coating when bias is applied. Further bias voltages greater than 100 volts are necessary to produce a zone T type structure.

8.4 Improvement of Al content

Measurement of the composition of the samples shown in figure 8.03 gave the Al content to be 79% of the level in the target or 6.3 % of the film composition. The next coating to be applied on top of the NiCoCrAlY layer is a coating of platinum. This is heat treated to form a Pt-Al alloy. Exposure to an oxygen atmosphere at 1000°C immediately prior to the TBC application (see section 5.2) grows a layer of Al-O on the Pt-Al layer. This is used to form a good bond with the TBC coating. The source of the Al for the thermally grown oxide is the NiCoCrAlY layer. Thus, a low Al coating content may result in poor TBC adhesion. Although the formation of this layer is not going to be studied in any detail in this work, examination of the Batch 1 trial of chapter 11 show the Pt–Al layer to be weakly defined compared to the VPS applied NiCoCrAlY used in the conventional TBC application. Low Al content may have resulted in the poor adhesion of the TBC layer.

The experiment design trial showed that the coating structure was not significantly affected by the deposition power. However, the deposition power had a significant effect on the Al and Y content by increasing the arrival rate of these elements at the substrate compared to the removal rate from the substrate. Ideally a trial would be performed to improve the Al content of the coating by increased deposition current, keeping the bias and working pressure the same. This is a direct conclusion of performing the statistical experiment design process in the previous chapter. However the ENI RPG power supply used on the Sinfin-A site system is voltage limited. This prevents higher power deposition runs being performed.

Test sample	% Al content
Batch 1 lower coat (biased with 200V)	6.3
Batch 1 overcoat (unbiased)	7.8
Batch 2 (unbiased)	8.1
Al studded target (biased with 100V)	10.2

Table 8.02: Percentages of Al in NiCoCrAlY coating for various runs

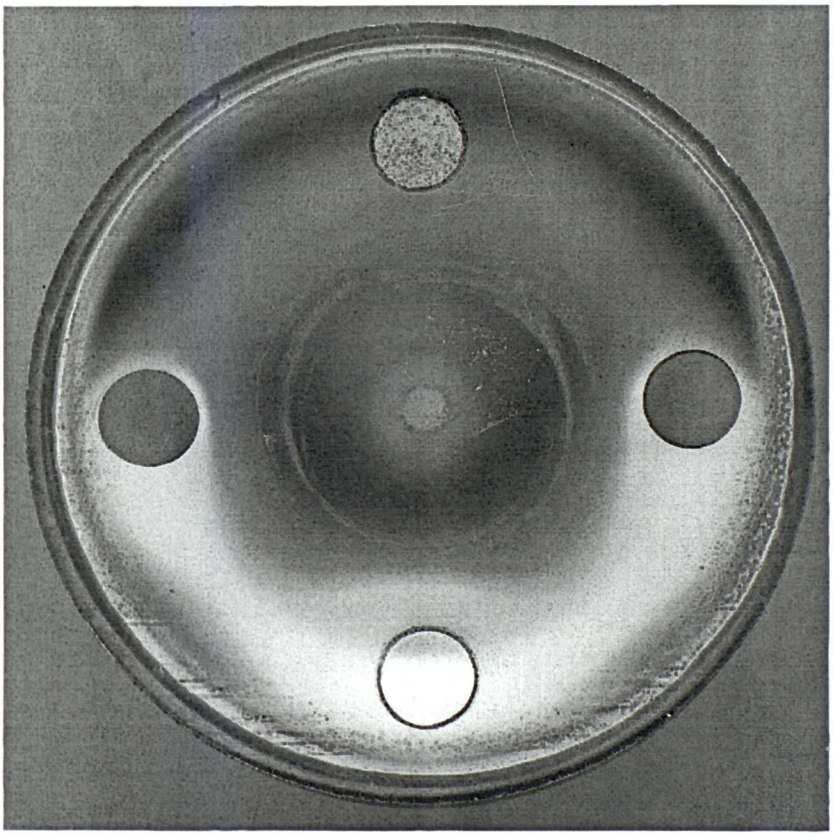

Figure 8.07: NiCoCrAlY target of composition MSRR 9537/1 with Al studs to improve composition of deposited coatings

Instead, a trial was performed to use a higher Al content target to get a better coating composition. The effect of having a higher bulk composition will be to increase the ratio of the arrival rate to removal rate of Al at the substrate. A ready mixed NiCoCrAlY powder with higher Al content was not commercially available[136]. Instead holes were drilled through the NiCoCrAlY target and Al plugs inserted at regular intervals around the racetrack. One such target is shown in figure 8.07. Table

8.02 shows a comparison of NiCoCrAlY compositions using the old and new targets. A further improvement of this technique was to taper the hole and plugs so that when inserted from the rear of the target the plugs could not be dislodged during deposition and required no bonding. The samples were analysed by AES at Loughborough University and using EDS at Rolls-Royce.

8.5 Deposition problems associated with target wear

The conditions used to deposit the NiCoCrAlY in the experiment design could not be recreated and different target voltage levels were observed during coating runs with new targets. This is particularly problematic for the Sinfin-A site system which has a power supply voltage limit of 600V, which is lower than the voltages seen during the Elton Road work. It was noted that when the target was heavily eroded the target voltages produced were similar to the previous Elton Road work. The experimental design trial was performed with a worn target. The target wear changed the deposition conditions so that the results of run 371 in the deposition trial were not reproduced. However it took two days of sputtering to reach this condition for each new target and wasted a lot of the target material.

It was originally considered that this was due to the target material. This may have interfered with the permanent magnetic field lines in the cathode but would have less effect using a heavily eroded target. A reduced magnetic field would have increased the plasma impedance causing higher target voltages to be seen.

Several options were available. Firstly, live with the long conditioning time to erode the target to the favourable deposition conditions. The second option was to use a diode arrangement by removing the magnets from the cathode. This would maintain the same parameters as the target wears however, a consequence of this would be much higher target and substrate temperatures and a much slower deposition rate. The final option was to use a thinner target. This would require new clamps and dark space shield manufactured for the cathode.

Batch 1 of the sensor assembly (see chapter 11) used the NiCoCrAlY deposited during the bias etch trials, whilst in order to expedite batch 2 it was decided to continuously run the target until heavily worn so that more favourable conditions could be obtained. In parallel with this the magnetic field strength of the cathode was measured to determine the effect of the target wear.

8.5.1 Test of Magnetic field strength, H of AJA A-330 3-inch diameter cathodes

A tufnol pattern was manufactured to fit over the target as shown in figure 8.08. Position datum holes were drilled through the tufnol to achieve repeatable probe positioning. The measurement of magnetic field strength was made with an Institute Dr.Forster Magnetoscope 1.580 using an axial probe 1.599-045-100-034 and a transverse probe 1.599-085-097. In each case the probe was placed in contact with the target surface, so, for example, for the worn target the probe was in contact with the bottom of the racetrack. Measurements were made for a 6mm copper blank, a new 6mm thick NiCoCrAlY and heavily eroded 6mm NiCoCrAlY target, and a 3mm thick NiCoCrAlY target. Only a qualitative assessment could be made because the instrument was out of calibration.

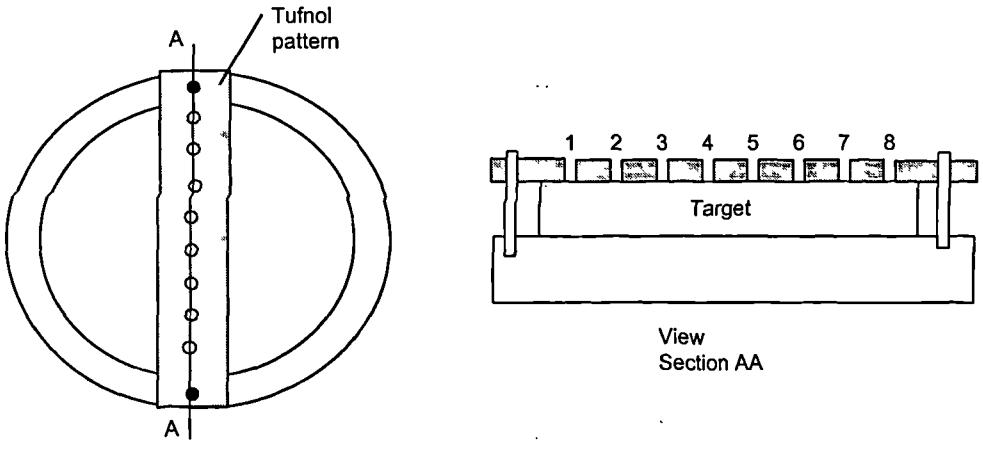

Figure 8.08: Probe positions for magnetic field strength measurements on AJA cathode with various targets

The results are shown in table 8.03 and figure 8.09. No difference could be detected between the copper and the NiCoCrAlY target. Therefore, the alteration in deposition

conditions was not due to the target material. The probe positions of interest on the other targets are positions 2 and 7 that correspond to the centre of the racetrack. Here, both the worn target and 3mm target have higher values than the 6mm target. The field strengths are similar to each other. The 3mm target has higher field strengths in the other positions since, for the worn target, the measurement points are further from the cathode. From these results it was seen that it would be beneficial to use a 3mm target to recreate the conditions used in the earlier trial. Because the target is thinner it would have to be replaced more regularly, but the variation between a new and exhausted target would be less.

Target	6mm Copper		6 mm NiCoCrAlY		Used 6mm NiCoCrAlY		3mm NiCoCrAlY	
position number	Axial kA/m	Transverse kA/m	Axial kA/m	Transverse kA/m	Axial kA/m	Transverse kA/m	Axial kA/m	Transverse kA/m
1	-27.5	6	-28.5	6	-29	4	-37	9
2	0	14.5	-1	13.5	-7	22.5	4	18.5
3	12.5	13	11	13	13	14	15	17
4	35	9	33	10	30	8.5	50	17
5	35	-10	34	-11	34	-9	55	-15
6	11	-13.5	10	-12	10	-15	13	-17
7	-3	-14.5	-2	-13.5	7	-22.5	2	-19
8	-28.5	2	-27	-3	-27.5	5	-38	-5

Table 8.03: Results from measurement of magnetic field strength of AJA cathode

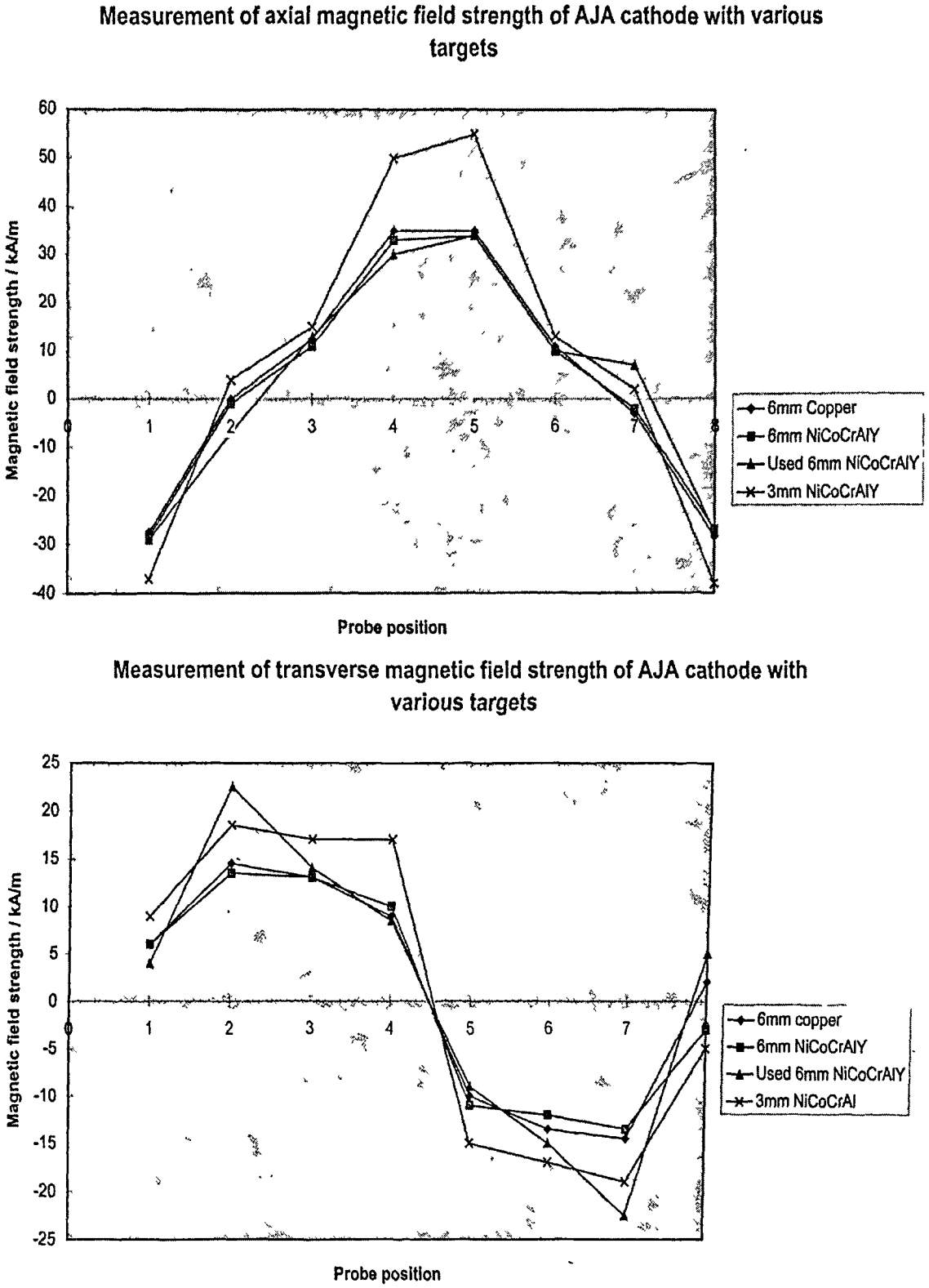

Figure 8.09: Magnetic field strength of AJA cathode with various targets

8.6 Conclusions

Further analysis of the coatings described in chapter 7 has been performed. The coatings have been heat-treated with no adhesion problems seen. The parameters used in run 371 look favourable with minimal densification needed. Voids exist at the interface with the CMSX-4 substrate. These are worse on the dryblasted sample and so are related to the roughness of the substrate. Little improvement in the reduction of interface voids is noted beyond 30 minutes ion cleaning of the substrate prior to deposition.

The deposition of the NiCoCrAlY has been moved to the Sinfin-A site facility. This necessitated trials to repeat the coatings seen using the run 371 parameters. The same voltage levels seen in the previous work could not be recreated because of the limitations of the power supply used on the Sinfin-A site deposition system. Also the bias proved to be unrepeatable because the bias power is distributed between four planets. Initially the target voltage seen on the planet varied between coating runs. Three of the planets were removed and the bias process was set to a voltage level rather than power.

Trials have been performed using different levels of surface finish. A zone T type structure can be obtained using lower bias levels on polished substrates. However, the adhesion of the coating to the substrate is adversely affected. This has confirmed that the best method of sample preparation is a vapour blast process.

The Al content of the films deposited with run 371 parameters is approximately 6.3%. A higher Al content is preferred to ensure TBC adhesion. A direct conclusion from the experiment design trial used in chapter 7 would be to increase the deposition power to improve the Al content without affecting the structure of the coating. However, this is not possible with the power supply used presently. Instead, Al studs have been inserted into the target racetrack area. This has been shown to increase the Al content of the biased coatings deposited with this target from 8 to 10% of film content.

The deposition conditions for the NiCoCrAlY are dependent on the amount of target wear. The trial described in chapter 7 was with a worn target. It takes several days of deposition to achieve these parameters. This is expensive and wasteful of target material. The target voltages may be several hundred volts higher on a new target. A trial has been performed to determine if the target material is responsible for the unfavourable conditions obtained with a new target. The work has shown that the problem is due to the target thickness. Favourable conditions can be obtained with a thinner target without the need to erode the target.

Chapter 9: Deposition of insulator coating

9.1 Introduction

The electrical insulation of thin film sensors has previously been problematic. The deposition of aluminium oxide from a ceramic target was low (0.5 μm/h). This was because power must be limited to prevent shattering of the brittle target. For this project, coatings must be applied on complex shaped components. This necessitates the rotation of the component to achieve a uniform coating, so the deposition of a 10 μm coating may take many tens of hours. Although this may be acceptable for trials, such a long process time would make the application of thin film sensors unacceptable for engine applications. Reactive sputtering has been used to speed up the deposition process. Using this process deposition rates of 5 μm/h have been obtained. One problem inherent to this technique was the build up of oxide on the target face, which can cause electrical breakdown and arcing. For this reason Rolls-Royce have used a radio frequency power supply, which because of its waveform should allow the sputtering of the oxide. This should prevent oxide build up on the target and minimise the arcing compared to a DC power supply used in other references.

One consequence of using an old model of power supply such as the CVC 3kW device, with no arc suppression system, was that arcing was allowed to take place. This can result in Al particulate being incorporated in the growing film. These can cause pinholes in the sensor device by acting as preferential etching sites. The pinholes are also thought to reduce the electrical resistivity of the coating.

Because of other electrical problems with the CVC radio frequency power supply, it was necessary to upgrade to a new power supply. This presented the opportunity to purchase a pulsed DC power supply instead of a replacement RF supply. These have been shown to reduce arcing compared to DC processes and have modern arc suppression systems

An ENI RPG-50 pulsed DC power supply was purchased. This experience of use of the new power supply is described in this chapter. In particular, the ability of the new power

supply to reduce target arcing and the quality of the deposited films by reactive sputtering was assessed and is reported here. This work has found the existence of nodular defect growths in the deposited coating. It will be shown that these are due to surface imperfections on the substrate. The solution to reducing their formation and growth lies in the biasing of the substrate during deposition of the coating. The theory behind the use of pulsed DC power supply to reduce arcing is given in chapter 4.

9.2 Setting up of power supply and system

A 5kW ENI power supply was connected to the DC cathode as shown in figure 9.01. The power lead could be connected straight onto the DC cathodes. However, the old radio frequency cathode had to be modified with a new N type connector to accept the power supply cable.

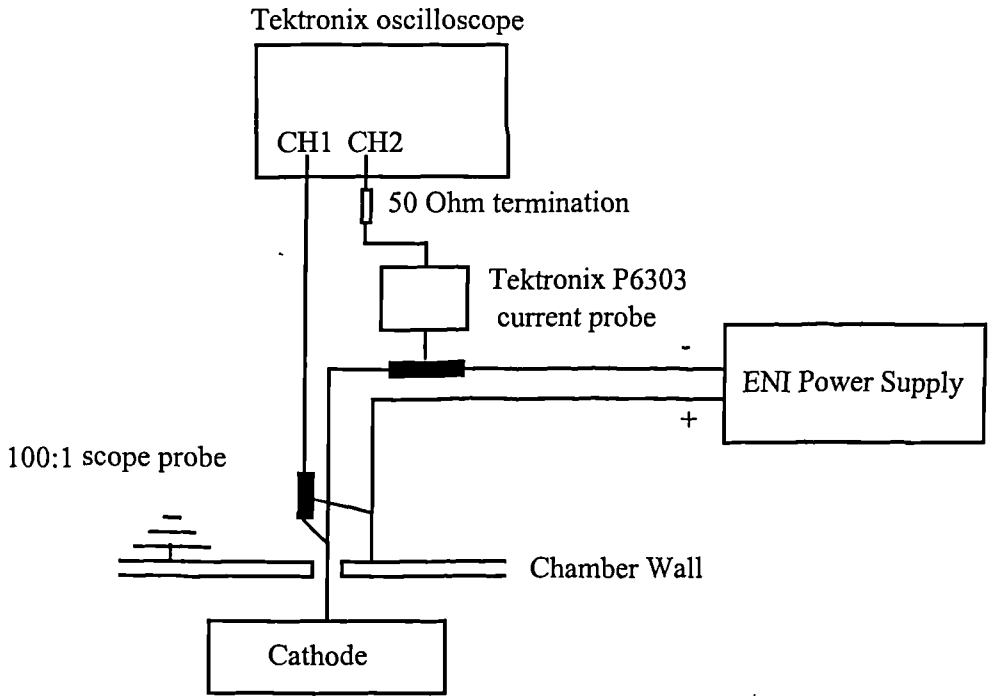

Figure 9.01: ENI RPG-50 power supply connection diagram

A 100:1 voltage probe was connected across the input of the cathode. The resultant voltage waveform was then examined on an oscilloscope. This revealed the system ringing in response to the square wave pulses. The ringing frequency was different for the positive and negative portions of the waveform. The positive pulse width was increased until the

ringing had died down (see figure 9.02). This ensured that any poisoned areas of the target surface are fully charged to the positive potential. From this it was deduced that the minimum pulse width acceptable was 3240ns at 5 x10^{-3} Torr argon pressure.

A Tektronix P6303 current probe was used to examine the current waveform for evidence of back sputtering during the positive pulse caused by excessive positive voltage. The current waveform is displayed in figure 9.02. This was compared to the manufacturers operating manual and from this it was determined that no back sputtering was occurring.

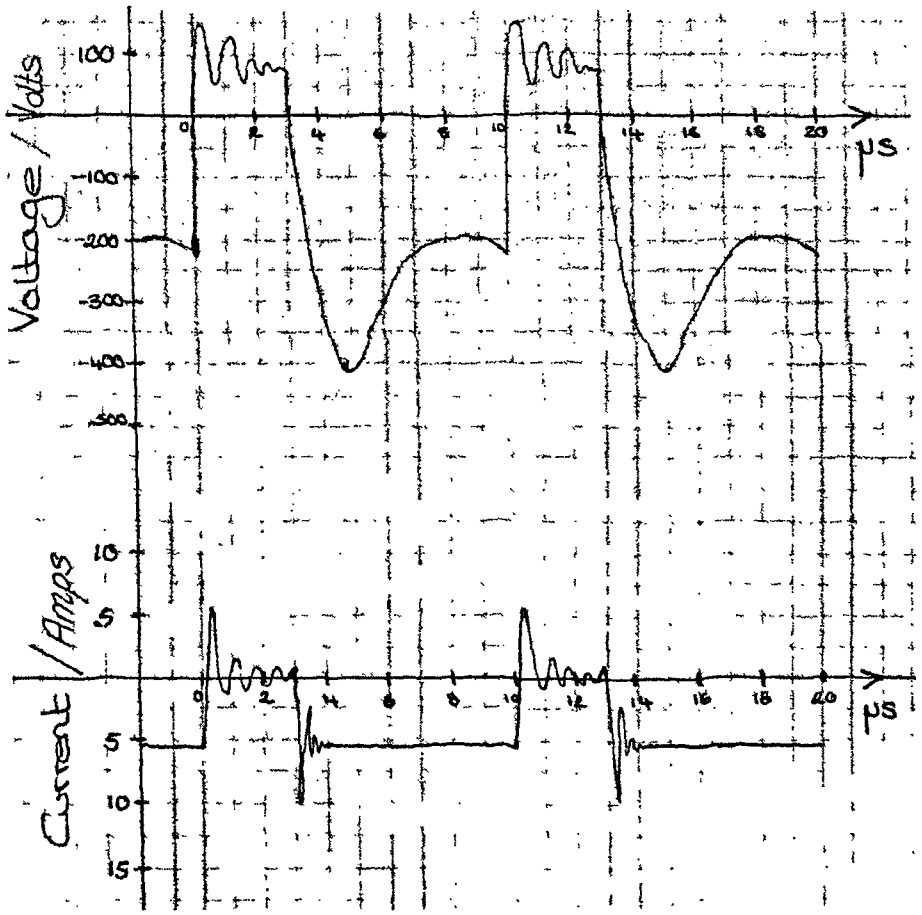

Figure 9.02: Voltage and current waveforms of ENI RPG-50 power supply at 100kHz

The target was pre-sputtered for 30 minutes with the power supply in pulse mode and set to 100kHz. During this time the power supply suppressed arcing by cutting power to the target each time the current exceeded the arc threshold. The power was only applied to the target again after an operator set delay. For this project 400 μs has been used as the delay.

9.2.1 Arcing problems encountered during process

At powers over 1500W, the arcing was observed to be so severe that it became continuous, and the required setting could not be obtained. Operation at high powers required a compromise where the arc threshold was set to maximum, which resulted in arcing.

The cable and power supplies were eliminated as causes of arcing by running the power supply into a dummy load. The power supply could be run at 2000W even in minimum arc threshold level. Therefore the arcing was real and occurring within the chamber.

The base pressure and argon were checked for contamination that could cause arcing on the target face using the system's residual gas analyser. The Leda Mass residual gas analyser will only operate at very low pressure($<1x10^{-5}$ Torr). The system was operated with the throttle valve open to maintain a very low argon pressure. No significant contamination was detected in either the base pressure or argon supply.

A mirror was placed in the chamber so that the target face could be observed during the target clean process. Arcing was seen at the edge of the racetrack between the metallic area and the surrounding region where oxide had previously been allowed to build up. A dark oxide region exists on the target as shown in figure 9.03. The photograph also shows the sites of arcing near the target clamps and nodular growths within the racetrack region.

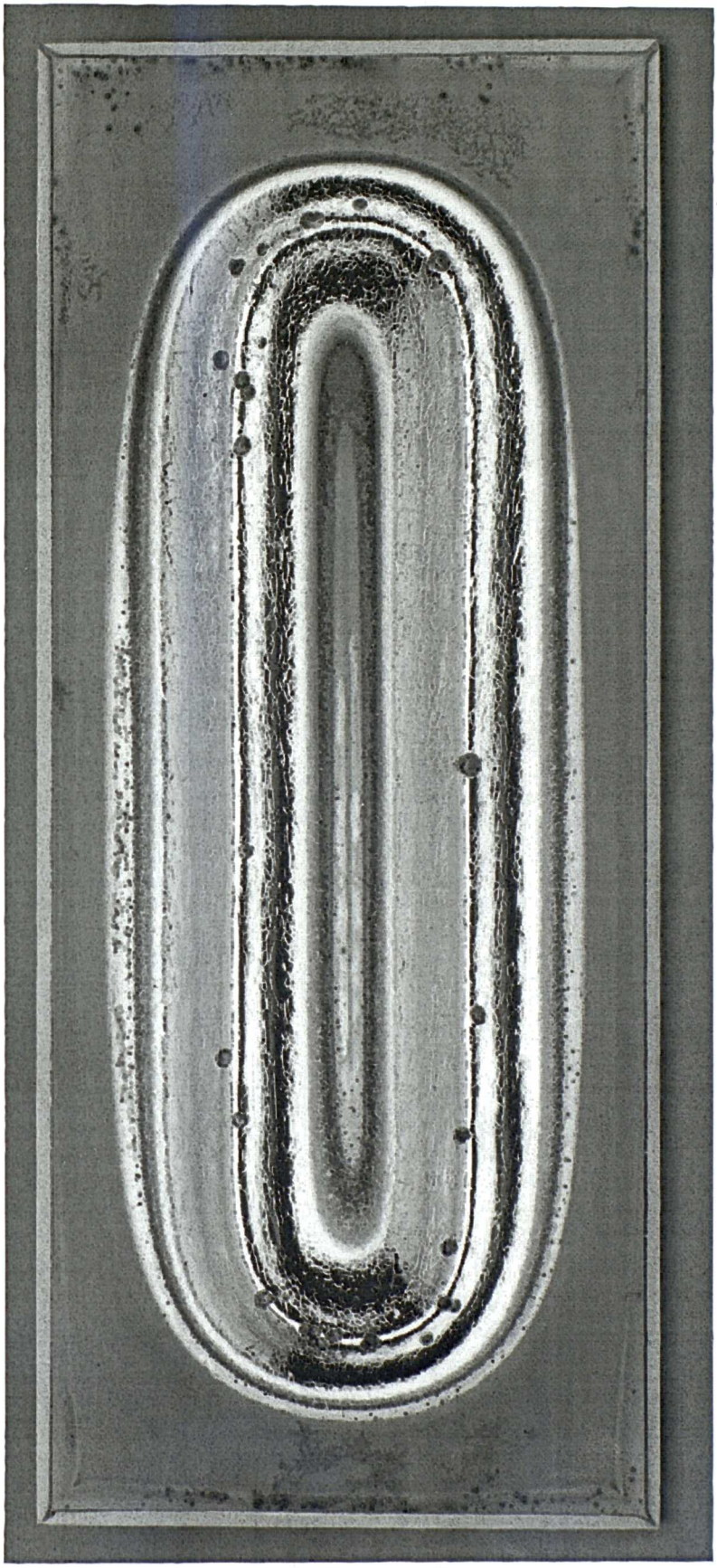

Figure 9.03: Al target showing arcing sites and oxide band

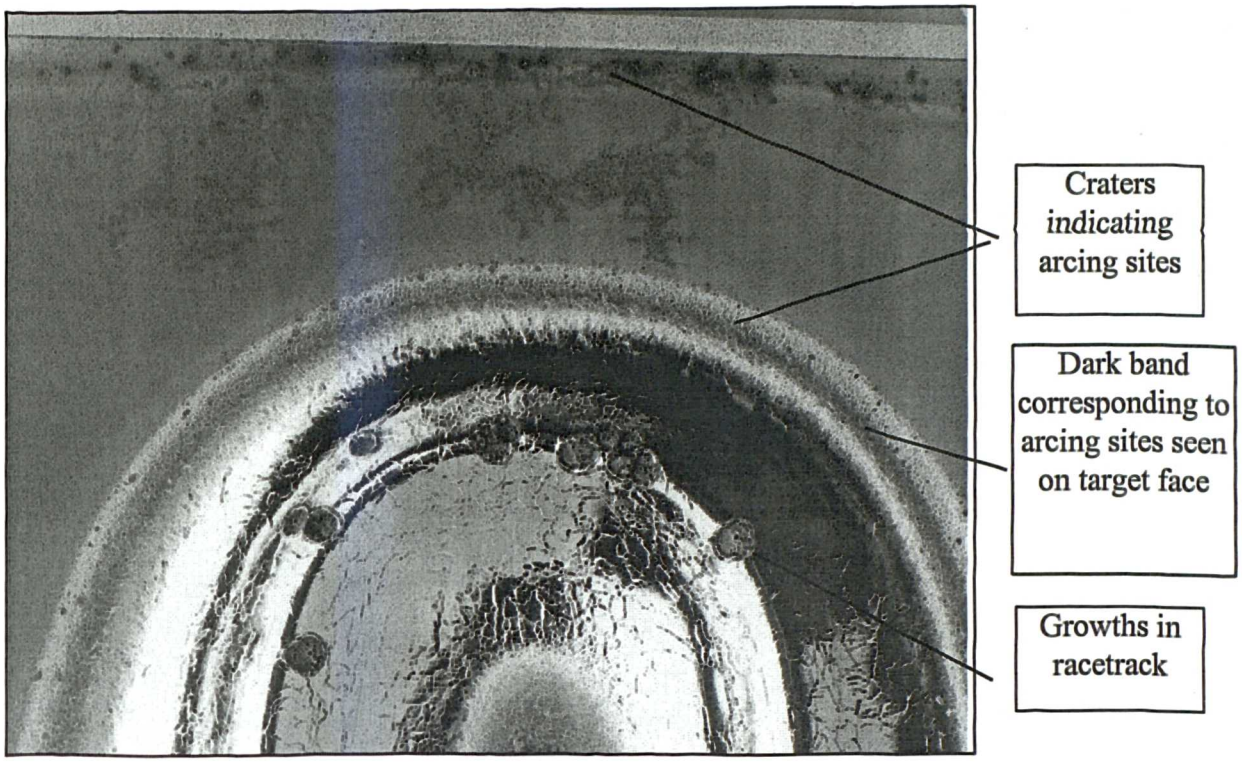

Figure 9.04: Photograph of arc sites and racetrack defects on Al target

The cathode was removed from the system. The spacing between the cathode clamps and anode housing was checked with feeler gauges. The gap was not uniform around the cathode because the target has been positioned with the cathode vertical on the system. In places the spacing was less than 0,90 mm. The cathode assembly was stripped. There was some evidence of arcing on the outside edge of the target clamps. This arcing increases as oxide builds up on the target and shields. It can be reduced by regularly cleaning the clamps and shields to remove the build up of coating. The surfaces were then polished using 500 grade abrasive paper to remove peaks that may encourage arcing.

The cathode was then reassembled and an equal spacing set around the target clamps. The gap achievable was 1,00 mm. This was considered too small. There was little information available for these cathodes, however the AJA operation manual for the 3 inch diameter cathodes recommended 1-2 mm for working pressures less than 10 $x10^{-3}$ Torr. The clamps were machined to remove material to increase the gap by 0.5 mm. This was the same spacing as the copper cathode block from the housing. This reduced the arcing so that 2000W was achievable even with MIN arcing detection threshold. Subsequent coating runs

showed that the arcing became a problem as the target, clamps and shields became coated with oxide. This problem could not be resolved, the level of arcing being dependant on the build up of oxide and cleaning intervals.

It was thought that the cathode design needed to be improved. Figure 9.03 shows how little of the target surface was eroded, leaving large areas for oxide to build up. Modern cathode designs allow the race track to cover virtually the entire target surface. It is intended to install a new Gencoa PP125305 magnetron cathode for this work. The shielding will also be improved to prevent the arcing around the clamps.

9.3 Evaluation of coatings produced by reactive sputtering process

9.3.1 Experimental detail

The Al target was cleaned at the deposition power. The sensitivity of the monochromator was adjusted to give a datum level of 1000 on the Megatech reactaflo unit. This was the intensity of the emission from the plasma at 394.4 nm, the wavelength corresponding to the Al spectral line. The set point on the controller was adjusted to 325 so that oxygen would be added until the output of the monochromator reduced to 32.5 % of the intensity obtained from the Al target in a 100% argon atmosphere. This had previously been determined to give stoichiometric aluminium oxide for radio frequency reactive sputtering. When the oxygen was added the arcing started so that control could only be maintained with power supply in maximum arcing detection threshold. The current increased to 9.96 Amps, which was very close to the power supply limit. During reactive sputtering plasma was seen under the substrate planet. The plasma impedance was also seen to increase resulting in a slight drop in the current level.

A number of 3 hour coating runs were performed at different levels of argon pressure at 2000W power onto glass slides. The ends of the slides were masked off to leave a step edge in the film. A Talysurf 10 step profiler was then used to determine the coating thickness at several points at each end of the slides. The results were averaged to give a

coating thickness. Knowing the deposition time, the deposition rate was calculated. The composition of the coatings was determined at a number of depths using AES.

9.3.2 Results

The results from several coating runs are shown in table 9.01. As the deposition pressure was decreased the Al target voltage increases. The deposition rate reduces with reducing deposition pressure.

Run No	Argon Pressure x10^{-3} Torr	Al target voltage /Volts	Al-O target voltage /Volts	Deposition current /Amps	Total pressure x10^{-3} Torr	Deposition rate/ μm/h
490	4	356	204	9.80	4.5	3.42
491	3	384.5	223	8.96	3.4	2.87
492	2	455	214	9.34	2.4	2.23

Table 9.01: Summary of coating parameters

Compositional analysis of the coatings is given in table 9.02. For all the coatings, stoichiometric aluminium oxide has been produced and the coating composition was uniform over a depth of 1.5 μm. No significant levels of contaminants have been found. Relatively low levels of C were observed in all three films, with the highest level of surface contamination on sample run 491 at ~17%.

Run No	Depth nm	O %	Al(O) %	Al(e) %	O/Al ratio
490	120	60.5	39.5	0	1.53
	360	61	39	0	1.56
	720	61.5	38.5	0	1.59
	1100	58.3	41.7	0	1.39
	1450	59.6	40.4		1.47
491	360	58.8	41.2	0	1.42
	720	59.8	40.2	0	1.48
	1450	61.3	38.7	0	1.58
492	360	61.8	38.3	0	1.61
	720	61.2	38.8	0	1.57
	1450	59.3	40.7	0	1.45

Table 9.02: Analysis of composition of aluminium oxide coatings by AES[137]

9.4 Evidence for nodular defect growth

A large number of defects exist in the coating. Mallins[104] has suggested that these are droplets of Al ejected from the target during arcing. Certainly when arcing was severe, spitting was seen from the target whilst depositing Al at 2000W. With the limited resolution of the analysis equipment available, the compositional analysis of these defects was not conclusive. Further examination of the defects obtained in this work suggested that a proportion of the defects seen were due to nodular defect growth. The surface features of the coatings were examined by SEM. Surfaces of Al_2O_3 were usually sputter deposited with a layer of gold a few nanometres thick to prevent them from charging in the SEM. The defect in figure 9.05 exhibits a low-density region surrounding the domed feature. This was consistent with the models of nodular defect growth given in other reported work[138].

Figure 9.05: Nodular defect in aluminium oxide coating

Figure 9.06 shows a view through a sectioned film. This exhibits the parabolic shape of a nodular defect common to a sputtering source. Interestingly this defect has formed from a point midway through the film, explaining why the defects are not all the same diameter. If the defects were initiated at the substrate then the size of the defect would be similar to the

film thickness. Nodular defect growths normally originate from substrate surface irregularities or preferential nucleation sites.

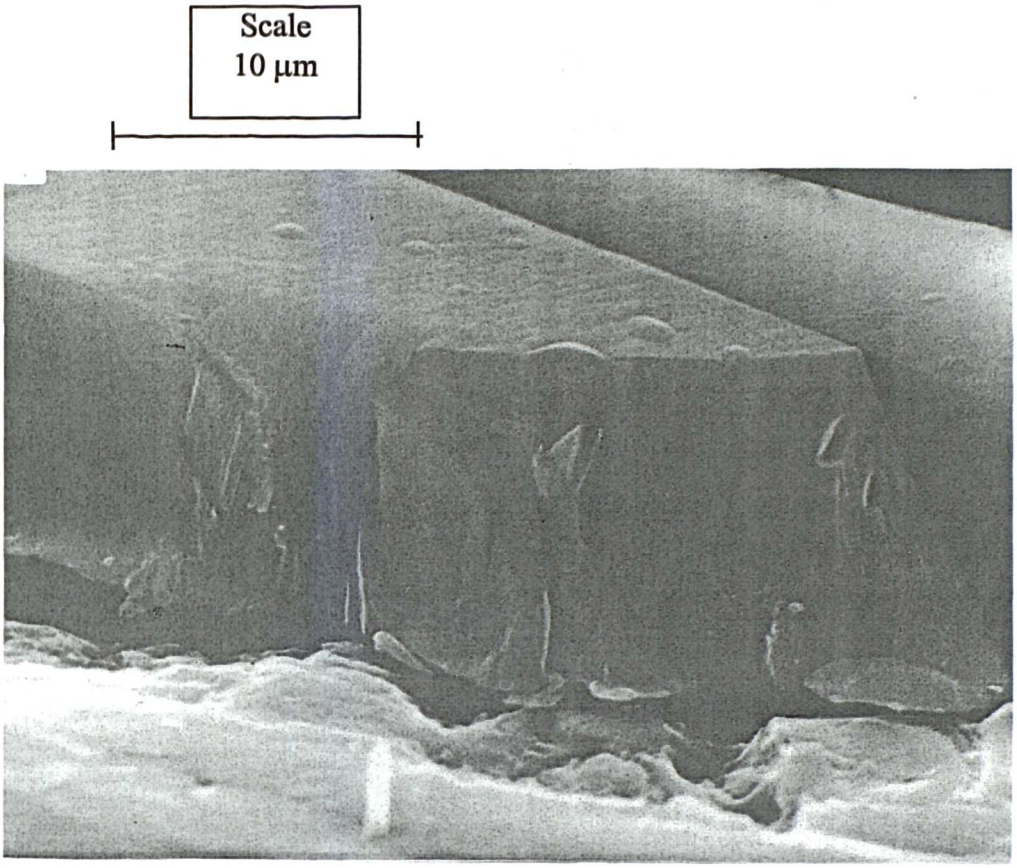

Figure 9.06: Scanning electron microscope image of aluminium oxide coating[104]

9.5 Effect of substrate roughness on nodular defect growth

To investigate the effect of surface roughness on defect growth, it was necessary to have samples prepared to two different standards of surface roughness. This was difficult to achieve using the current hand polishing method, which was not believed to be repeatable. Further, any measurements made gave an average roughness value, which may not have indicated a high level of local imperfection sites likely to cause the nodular growth. Instead a polished glass slide and a polished silicon wafer, acquired from Kulite Sensors Inc., were chosen as having different levels of imperfection sites. The average surface roughness of each was measured with a Talysurf 10 instrument. Both had an average surface roughness Ra value of 0.002 μm. Although giving the same values the polished silicon wafer was believed to have fewer surface irregularities. The samples were passed through an identical cleaning process, placed next to each other on the sample holder and given an identical

coating. The coating surfaces were examined at Loughborough University and are shown in figures 9.07. The image shows the only surface features found on the oxide coating on the silicon wafer. The rest of the coating was featureless. The defects seen on the glass slide were representative of the whole component.

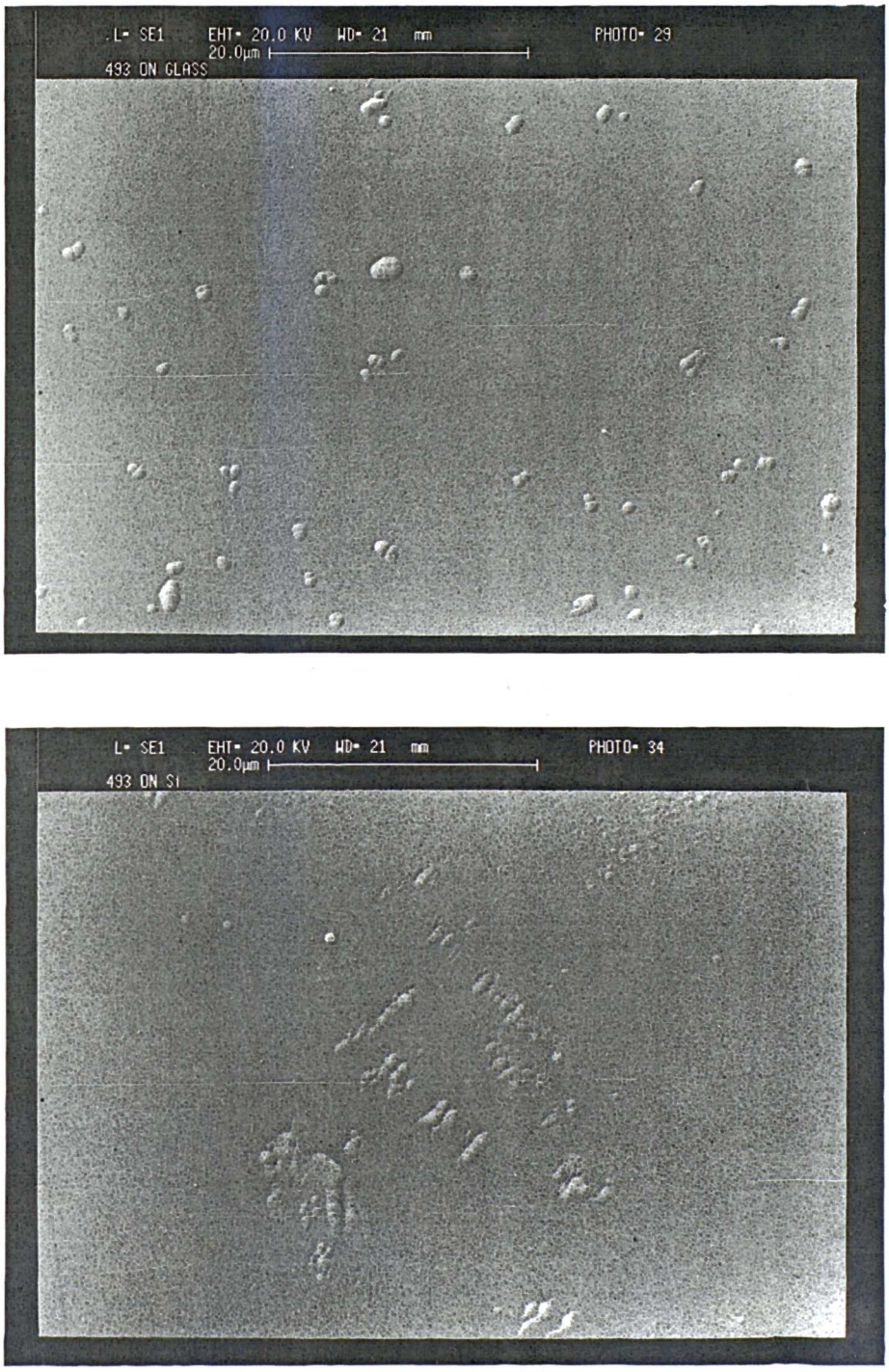

Figure 9.07: Aluminium oxide coating deposited onto glass slide (upper) and silicon wafer (lower)

9.6 Effect of bias voltage on nodular defect growth

9.6.1 Experimental detail

Given that it was difficult to achieve the levels of surface finish of a silicon wafer on a gas turbine component the next step was to investigate whether the growth of the defect can be suppressed by the use of bias etching during the deposition of the coating. Glass slides were used as the substrates because these produce a reasonable level of defects when unbiased coatings are applied. The bias voltages used and the coating parameters are given in table 9.03. The deposition rate of the coatings was measured using a Talysurf 10 step profiler. Scanning electron microscope photographs of the surface features were made at Loughborough University.

9.6.2 Results

Run	Al target voltage / Volts	Al-O target voltage / Volts	Deposition current /Amps	total pressure x10^{-3} Torr	Bias voltage /volts	Deposition rate / μm/h
501	348	217	9.21	4.6	60	3.42
502	350	206	9.7	4.6	100	3.42
503	350	205	9.75	4.6	140	3.42
504	352	198	10.10	4.6	180	3.67

Table 9.03: Results from bias trials on nodular defect growth

The deposition rate of the coatings was unaffected by the level of bias voltage over the range of voltages used. The voltage level used had a significant effect on the surface features of the coating. Scanning electron microscope photographs were obtained of the defects and are shown in figure 9.08-9.11. The 60V bias coating was not significantly different from unbiased coatings. The 180V biased coating, shown in figure 9.11, has few defects. Of the defects that remain the central region was of different appearance to the surrounding coating. Compositional analysis should be performed on this defect. It was thought that these might be Al particles resulting from arcing on the target face. The

coatings shown in figures 9.09 and 9.10 for 120 and 140V bias are more difficult to explain. The 120 V biased coating has a textured surface whilst the 140V sample has irregular shaped raised features. The later may be due to contamination of the sample.

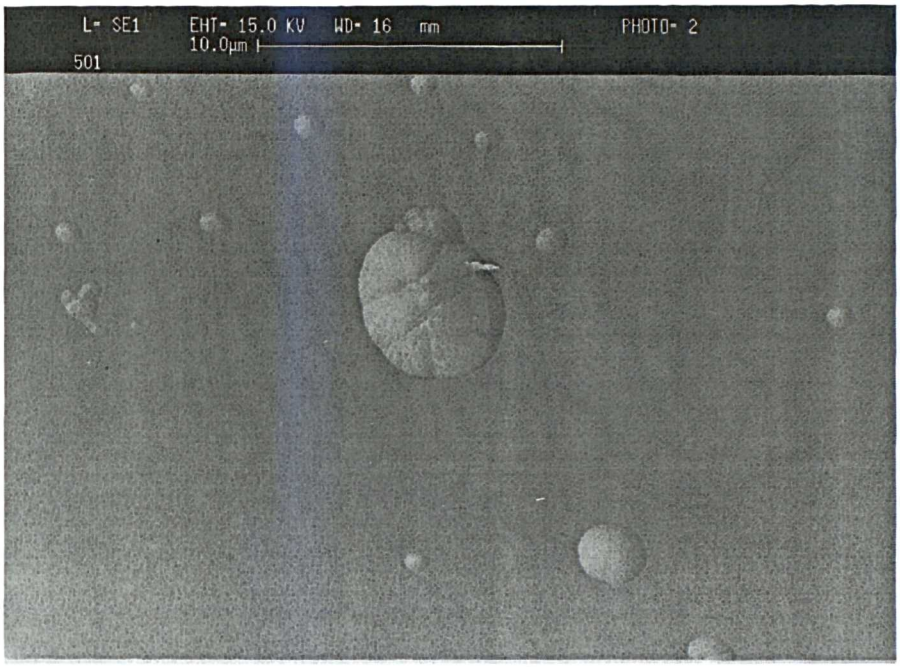

Figure 9.08: Aluminium oxide coating deposited onto glass slide with 60 volts radio frequency bias

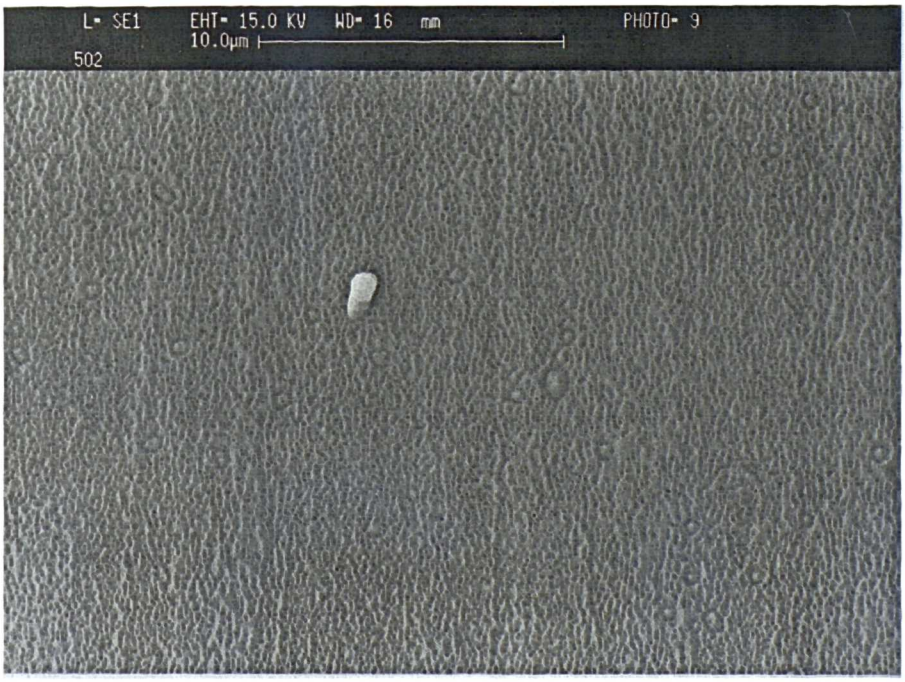

Figure 9.09: Aluminium oxide coating deposited onto glass slide with 100 volts radio frequency bias

Figure 9.10(a): Aluminium oxide coating deposited onto glass slide with 140 volts radio frequency bias

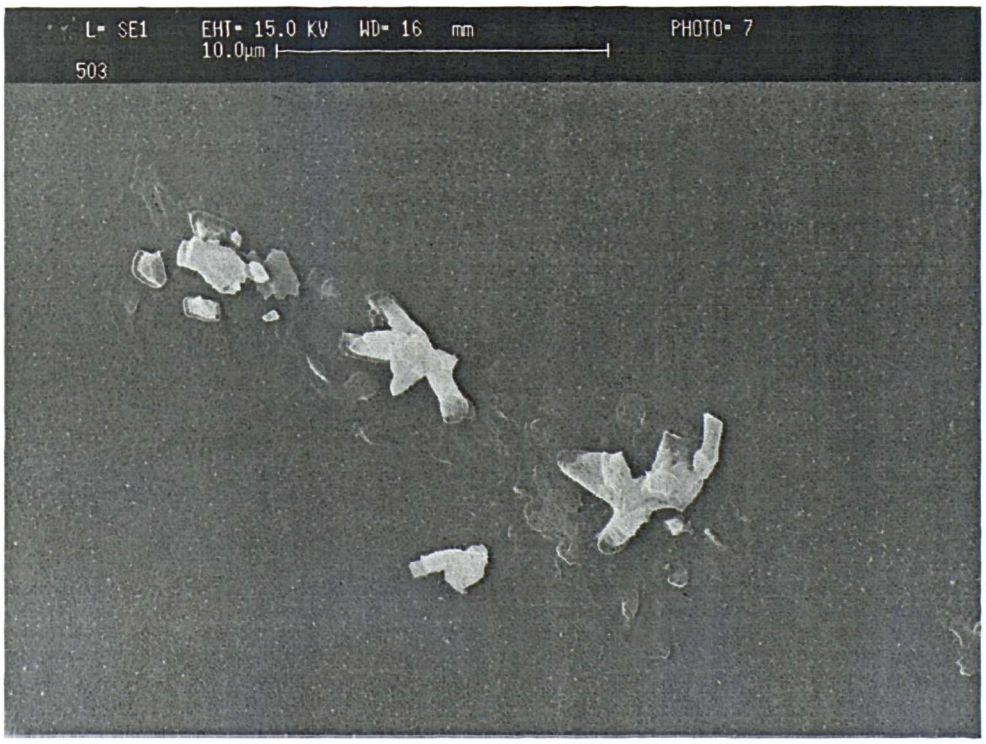

Figure 9.10(b): Aluminium oxide coating deposited onto glass slide with 140 volts radio frequency bias

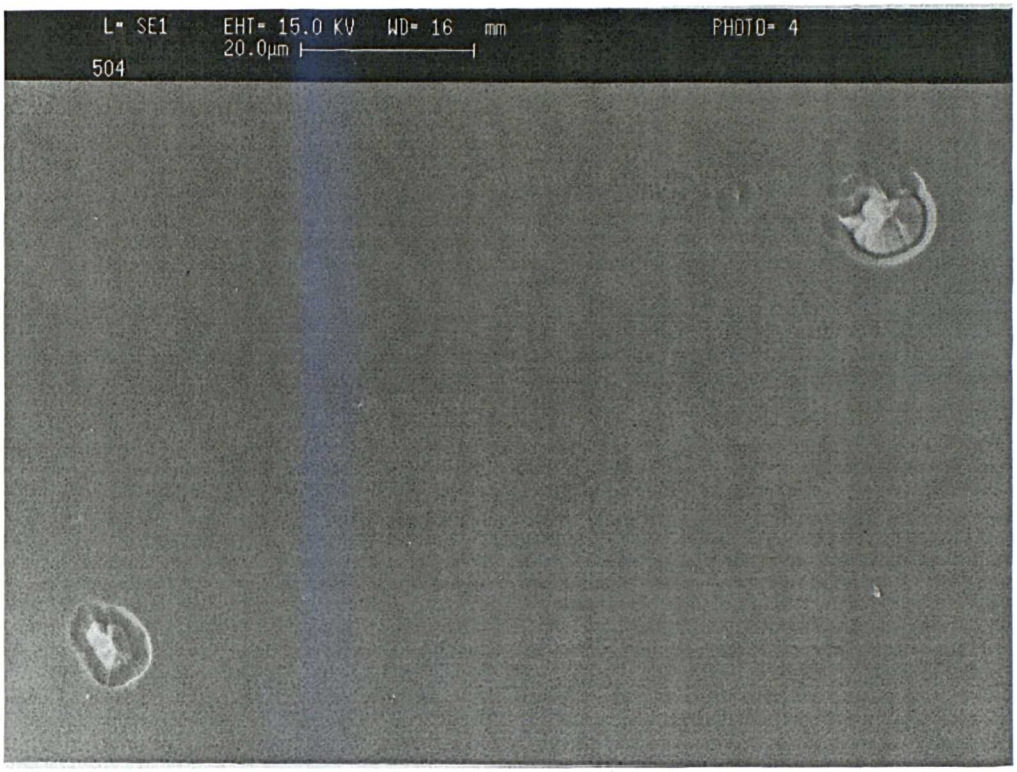

Figure 9.11(a): Aluminium oxide coating deposited onto glass slide with 180 volts radio frequency bias

Figure 9.11(b): Aluminium oxide coating deposited onto glass slide with 180 volts radio frequency bias

9.7 Conclusions

An ENI RPG-50 has been installed on the CVC deposition system replacing an old CVC 3kw radio frequency power supply. The power supply has been set up to have the optimum waveform in terms of pulse width to produce preferential sputtering of the oxide on the target face. The new power supply still has problems with arcing, and spitting can be seen when the arcing was severe. The arcing can only be reduced by regular cleaning of the target face, clamps and shielding. Thus the new power supply has not achieved its intended aim of producing defect free aluminium oxide coatings. However, from this study it is now believed that the arcing was due to a poor CVC cathode design. The CVC cathode utilised little of the target face for the racetrack, leaving a large area where oxide could be deposited. This can be seen on used targets and the arcing sites identified. Modern cathode designs remove material from the majority of the target face and this coupled with the preferential removal of the oxide coating using the ENI power supply should help to reduce the cause of the arcing. Gencoa Ltd has redesigned one of the cathodes. The new cathode was delivered during the write up of this work and should be evaluated as soon as possible.

The coatings produced by reactive sputtering using the ENI power supply and the CVC cathode have been analysed for deposition rate and composition. The coatings produced are stoichiometric aluminium oxide and are mainly free from contamination. A deposition rate of 3.42 μm/h has been obtained compared to a rate of 0.5 μm obtainable with an alternative non-reactively sputtered process. Higher deposition rates are prevented by the limitations of the power supply, which can only supply a current of 10 amps. This limits the power setting to 2000W during reactive sputtering. A higher output RPG-100 power supply has a current limit of 20 amps and may be preferable for this work.

The surface features of the oxide coatings have been studied by scanning electron microscope. A number of raised surface features have been seen. These were previously thought to be Al particulates incorporated in the growing film from arcing on the target face. It is the conclusion of this work that the majority of the defects seen are due to

nodular defect growth. These may cause problems in the patterning process and reduce the insulation resistance of a sensor deposited on top of them. A trial comparing a glass slide to a silicon wafer as substrates has demonstrated that these are likely to be caused by imperfections in the substrate. It is unlikely that the surface finish achieved on a silicon wafer can be reproduced on a turbine blade. Therefore the use of radio frequency bias sputtering of the substrate during deposition has been used to suppress their growth. It has been shown that the use of 180V bias level has prevented nodular defect growth formation without affecting the deposition rate. The remaining defects in the film may be due to the arcing on the target face. These defects need further investigation.

Chapter 10: Sensor development

10.1 Introduction

The aims of this work were to develop the sensor patterning processes for the new high temperature materials and evaluate the thin film sensor properties for use in a turbine environment. A review of high temperature materials is given in chapters 2 & 3 for dynamic strain gauges and thermocouples respectively. The NiCr sensor alloy used for dynamic strain gauge applications is limited to 500°C. The high temperatures seen in the HP turbine required that new sensor materials be evaluated. It was a conclusion of the risk assessment that the development of a high temperature strain gauge sensor would be very challenging. Therefore a recommendation was that two types of alloy should be developed in for strain gauge sensors. Although this increased the cost of the project and the amount of work involved, it reduced the technical risk to the customer.

Pd-12%Cr had been chosen as the preferred material because of the reports of excellent high temperature properties mainly from work done by the NASA Lewis research centre (see chapter 2). As a second choice, Pt-8%W was used. This material is used in wire form for high temperature gauging and although it has many sources of inaccuracies, these are understood. Also any results obtained could be compared to conventional gauges in the same position. The thermocouple sensor material choice was easier. The temperature necessitates a noble metal thermocouple be used and the most common is type R which is Pt / Pt13%Rh.

The sensor patterning technique needed improvement to reduce the patterning problems seen on the low temperature sensors, such as clamping of the mask on complex three dimensional components. The current technique would also not allow photoresist application to turbine components.

The selective etching process cannot be used on the high temperature sensor noble metal alloys so a lift-off process must be used. This was potentially more problematic since the process could result in poor adhesion of the sensor to the insulating layer.

The new sensor materials needed to be deposited and evaluated for their electrical properties. Because it was planned to buy at least five different material types for this project the purchase of 12 inch by 5 inch rectangular targets would be prohibitively expensive. Further, since only small test samples needed to be coated, much of the material deposited from a large rectangular target would be wasted. A financial case was made for the purchase of two new 3-inch diameter AJA cathodes for this deposition work. This allowed the purchase of smaller targets. The AJA cathodes were fitted to flange plates, which mounted onto the vacuum system in place of the 12-inch cathodes. When production-coating work is planned the larger 12-inch targets can be justified.

The work performed in this chapter will develop the sensor patterning techniques for noble metal alloys. The characterisation of Pt-Rh, Pt-W and Pd-Cr alloys are performed. Particular attention is placed on the adhesion of the sensor alloy to the aluminium oxide coating. The lift-off patterning process is of concern as it introduces contamination when the component is removed from the vacuum chamber.

10.2 Development of sensor patterning techniques

10.2.1 Selective etching and lift-off patterning techniques

For low temperature sensor alloys a selective etching patterning technique is appropriate. Here, the insulator and sensor coatings are deposited sequentially. A photoresist is then applied to the sample (see section 4.4). Because the film coatings are deposited sequentially without venting the vacuum chamber, contamination of the interfaces is minimised and adhesion between the layers excellent. This is therefore the preferred patterning method.

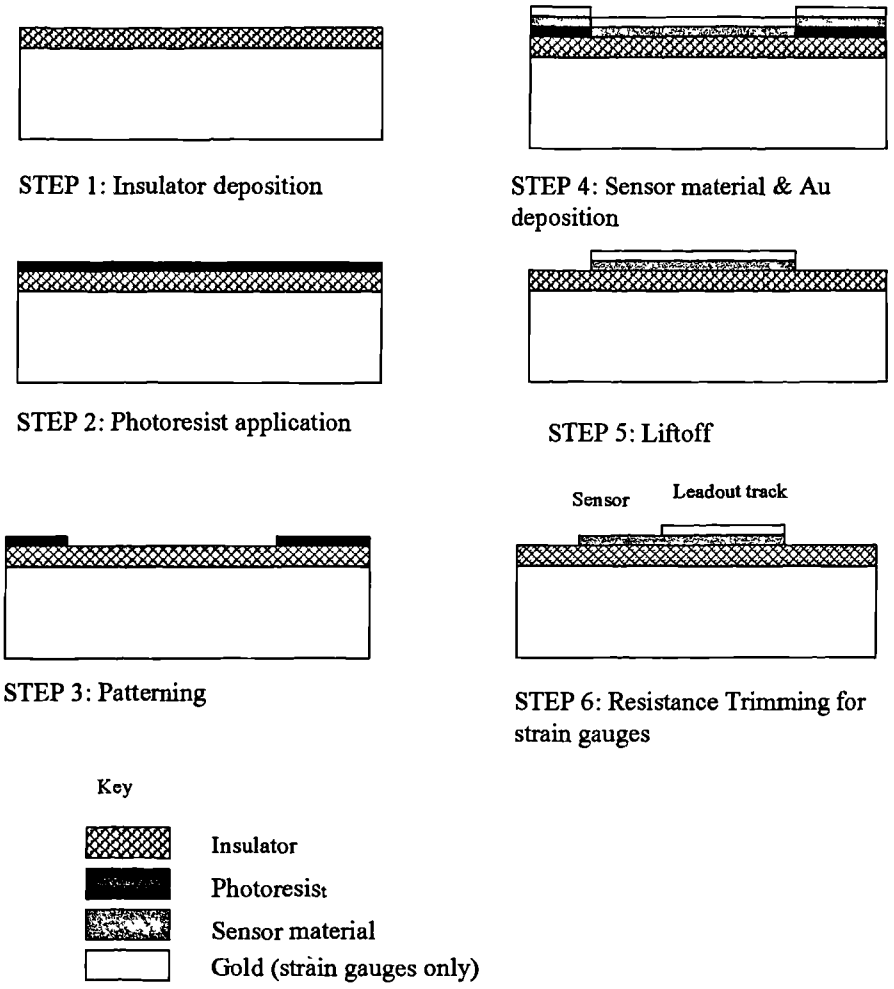

Figure 10.01: Liftoff patterning technique

However, for high temperature sensors, where noble metal alloys are used, this technique is no longer suitable. It is difficult to find a chemical etch that will remove the sensor film without damaging the other coatings and blade material. Instead a lift-off patterning technique must be employed. This is shown in figure 10.01. The insulator is deposited first, and then the sample must be removed from the vacuum chamber for photoresist application. The photoresist is patterned with a negative image; i.e. the photoresist is removed where the sensor tracks are required. The sensor material is then deposited onto the sample. When Shipley 1165 photoresist stripper removes the photoresist it "lifts-off" the unwanted sensor material to leave the required sensor pattern. One problem inherent to this technique is the risk of contamination of the samples at different stages of the process. Once the photoresist

has been applied, chemical cleaning of the sample is no longer possible and bias etching should be kept to a minimum to prevent out-gassing and damage to the photoresist layer.

10.2.2 Application of photoresist coating

For glass slides and other small flat components the photoresist is puddled over the component. A thin uniform layer is then achieved by spinning the component at 4000 rpm. The component is attached to the spinner by a vacuum clamp. For aero-engine components, a mechanical clamp is used. This was produced by spraying the component with a dry lubricant, placing it in a mould and pouring araldite around it. The araldite block was then cut in half to remove the component. After deposition of the coatings the component was inserted into the araldite block which was screwed to a brass plate. The component, araldite block and brass plate were then attached to the spinner. It was found that the whole clamp arrangement had to be balanced prior to spinning to prevent vibration and damage to the spinner motor. Balancing weights were added to the appropriate tapped holes beneath the brass plate. This arrangement is shown in figure 10.02.

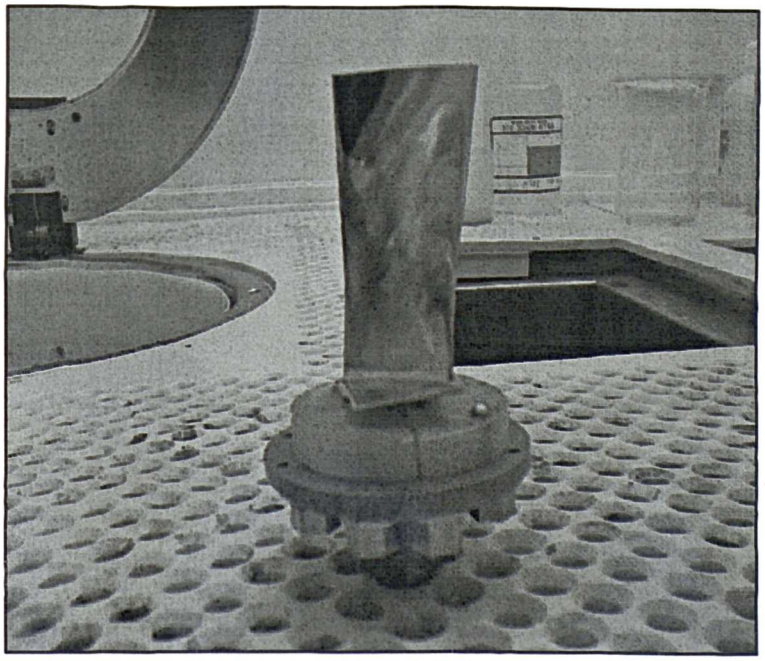

Figure 10.02: Photoresist spinner with mechanical clamp to hold small complex shaped components during photoresist application

With the development of high temperature sensors came the requirement to instrument shrouded turbine blades which were much heavier than the compressor blades. This made the spinning process impractical. The spinning process required a fast acceleration to the spinning speed to throw off the excess photoresist before it started to dry. The motor had insufficient torque to accelerate large components. Also the spinner would have had to be heavily shielded in case the component came loose whilst spinning. Instead a dipping process has been developed. A variable speed-dipping machine was designed and manufactured. This is shown in figure 10.03. This allowed the component to be lowered into a beaker of the photoresist solution and withdrawn at constant speed to leave a coating thickness dependent on the photoresist viscosity and withdrawal rate.

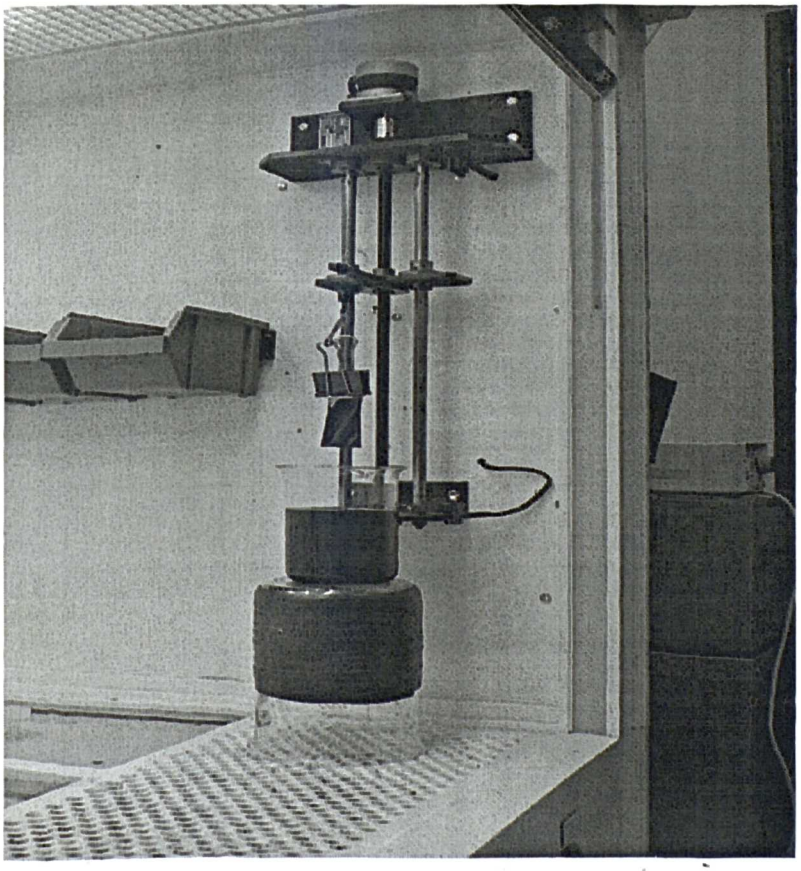

Figure 10.03: Dipping machine for the application of photoresist on large and heavy components

The S1400-25 photoresist, which is used with the spinning process, gave a thickness over 2 μm when dipped. A lower viscosity S1400-17 photoresist was purchased to

allow thinner coatings to be produced. A trial was performed using both photoresist types and varying the machine speed to obtain a range of different coating thickness. The coating thickness was measured at three positions along the centre of a glass slide (see figure 10.04). The thickness was measured by dipping a glass slide into the photoresist, curing the coating then producing a number of scratches in the coating with a scalpel. A Talysurf step profiler was then traversed across the scratches.

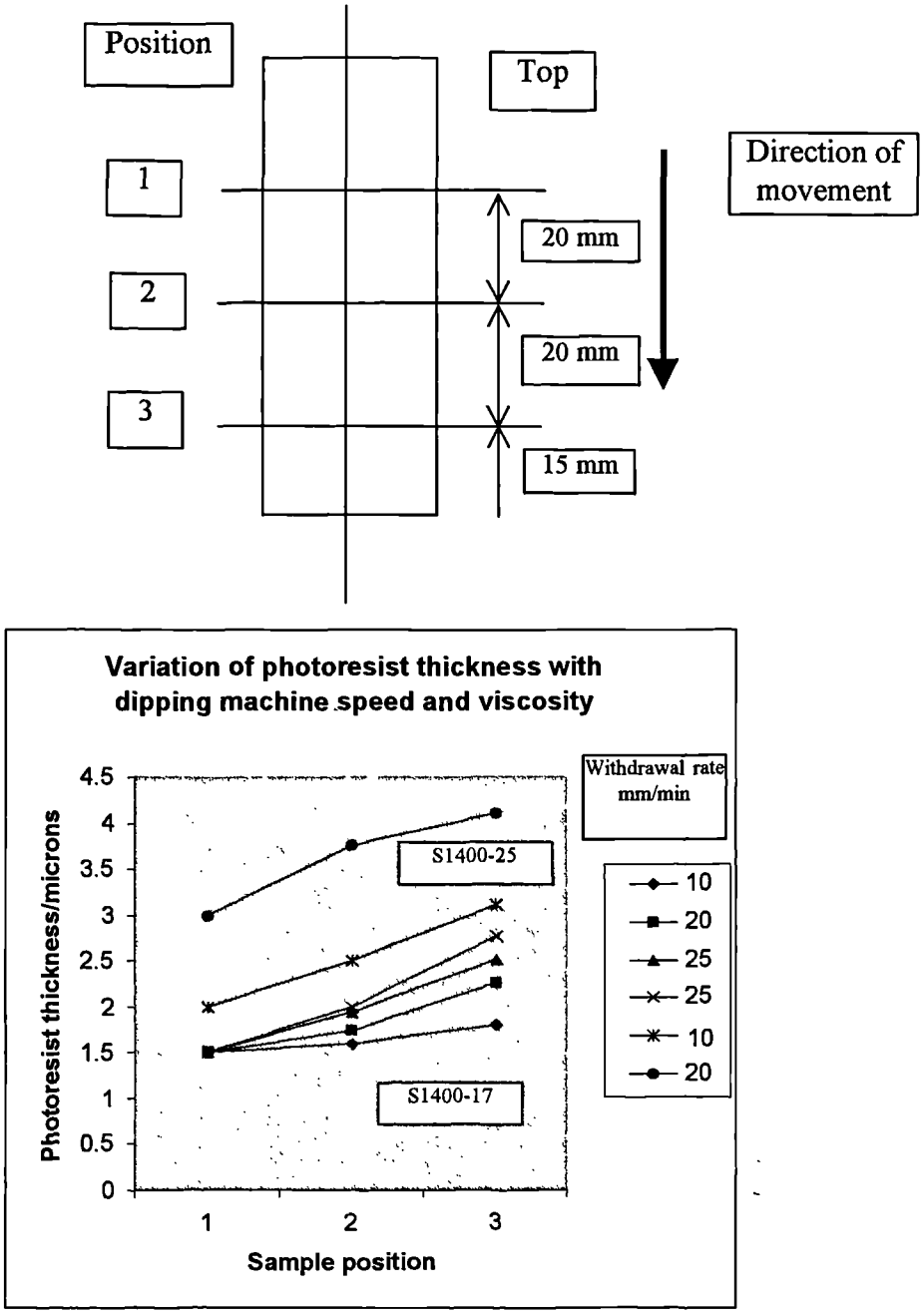

Figure 10. 04: Variation of photoresist thickness with dipping machine speed and photoresist viscosity

For selective etching a coating thickness of 1 μm is adequate. The lower viscosity photoresist gave a thickness of 1.5 μm in position 1, the coating becoming thicker towards the bottom of the sample. The best uniformity was achieved with the dipping machine at its slowest setting. For the lift-off process it was thought that a thicker coating would be beneficial. This would cause a large step at the edge of the sensor grid allowing the film to break easily during the removal of the photoresist.

A trial was performed to investigate the effect of the photoresist on film adhesion with dc magnetron sputtered PtW (see section 10.4). The dipping process was used to apply coatings of each photoresist on a glass slide. This gave coatings of 1.5 μm and 2-3 μm thick for the –17 and –25 photoresist respectively. The slides were then loaded next to each other in the vacuum chamber. A flash of nickel was applied prior to a coating of PtW. The slides were removed from the chamber and placed in a beaker of photoresist remover. The -25 photoresist resulted in worse adhesion than the thinner -17, possibly due to increased out-gassing during the deposition process.

It was found that the adhesion of the films could be improved by a second curing stage at 80°C after the patterning process to reduce the amount of solvent in the photoresist. The thinner resist still had the best adhesion but tended to leave a jagged edge for the gold film, which tears rather than snaps. This made the films difficult to remove especially around the sensor grid where the sensor element separation is 0.2 mm. The excess could be forced off but this often resulted in some damage to the sensor grid.

It was found that the samples should be removed from the chamber for the minimum amount of time possible and the photoresist dipping, curing, exposure, development, washing and post curing performed in quick succession with a minimum amount of handling. If the samples were left out overnight during the processing then poor sensor adhesion usually resulted.

10.2.3 Positioning of mask on component

For patterning on 3 dimensional aerofoil surfaces, it proved difficult to hold the mask in contact over its whole area. Usually the mask would be held at the edges with mylar adhesive tape, but would slightly separate from the component in the centre. This would be sufficient to allow UV under the sensor pattern reducing the width of the sensor tracks. One firm involved in this work has used the surface tension of a film of water to hold very thin flexible masks against the component. However, this does not work with the thicker photographically produced masks used for most of the routine work. After discussions with a number of companies, it was found that there was no equipment commercially available to hold the mask in place on this type of component.

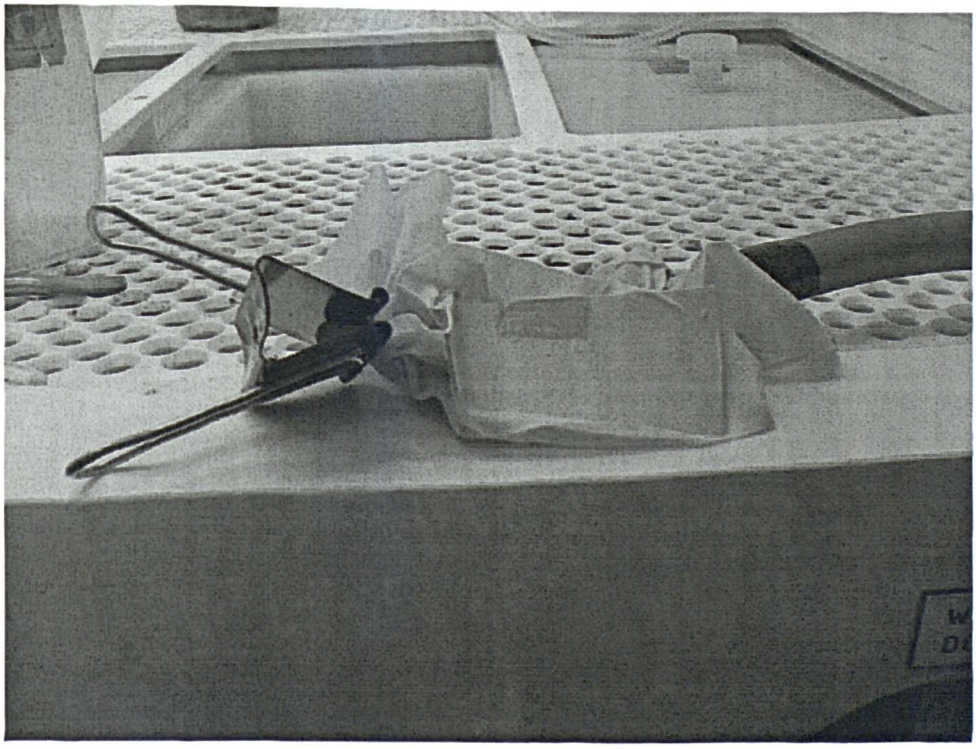

Figure 10.05: Latex glove vacuum clamp used to hold mask patterns against sample

Instead an improvised clamp was fashioned. A small vacuum pump was purchased. This was attached to one end of a flexible pipe. The other end was taped to a Pheonix Micro 100 (powder free) latex glove through a hole cut in one finger of the glove.

The mask was held at one edge only, placed inside the latex glove, which was sealed with a clip and evacuated (see figure 10.05). The component was then exposed through the thin latex. Using this method excellent sensor patterns could be obtained on complex components. Examples of the types of component patterned are shown later in this chapter.

10.2.4 Summary of patterning techniques

A number of techniques have been developed to allow patterning of films on complex 3-D components. Firstly, the design and manufacture of a dipping machine has improved the patterning capability to allow large components to be instrumented. A new photoresist was required to produce the correct coating thickness. Secondly, a novel vacuum clamp has improved the attachment of the mask pattern to the component. Finally, a lift-off patterning technique has been developed to produce sensor patterns when using noble-metal materials. The adhesion of the sensor film to the insulating layer is of concern. Initial trials used a flash of nickel between the insulating film and sensor material. This proved to be unsatisfactory. The adhesion of the coatings was improved by the replacement of the nickel with chromium.

10.3 Pt-Rh deposition & evaluation

10.3.1 Initial work

A 3-inch diameter Pt-13%Rh target of 99.999% purity was acquired. In order to reduce the initial costs, the target consisted of 3 mm thick Pt-Rh, bonded onto a 3 mm copper backing plate. A trial coating run was first made onto a glass slide using an AJA magnetron cathode. The deposition during run 510 was free from arcing. However, the adhesion of the Pt-Rh film to the glass slide was very poor. It was decided to use an adhesion promotion layer. A flash coating of metal was required between the aluminium oxide and the platinum-tungsten film. The metal chosen should oxidise easily so that it could form a strong bond with the aluminium oxide whilst forming a metallic bond with the platinum alloy. Ideally Cr should be used for

this as this was a well-known adhesion promotion layer. At the time this was not available, so nickel was used as alternative. Meanwhile a 3-inch diameter Cr target was ordered. A flash of nickel was deposited from a 12 by 5-inch rectangular radio frequency diode cathode prior to the platinum rhodium deposition. This improved the adhesion somewhat; however, there were intermittent adhesion problems during later work and the adhesion was not considered satisfactory until the Cr target was used.

A graduate trainee, working for the author, was asked to arrange for the measurement of composition at the failure interface (using the Ni adhesion promoter layer) and the effect of varying the deposition parameters on the composition of the coating. Since later work, performed by the author used these results, and the trainee was guided in this work by the author, it is reviewed here.

The composition profile across the failure interface was determined by AES. Adhesive tape was used to remove the weakly adhered coatings. The component surface and tape were then analysed to determine the failure interface and any contaminants present. The analysis was performed at Loughborough University.

A trial was then performed to measure the composition of the deposited films. For multi-element coatings it was known that the compositions of the coatings are dependent on the deposition parameters. This is due to preferential sputtering of the lighter element from the substrate. Work performed earlier on the NiCoCrAlY coatings has shown that the most significant parameters are the bias power, deposition power and argon pressure. A trial was performed to vary these parameters and measure the composition of each coating. This work would allow the optimisation of the coating parameters to achieve the correct composition and reduce variability of composition for future work. Small changes in composition would cause changes in the EMF produced by the thermocouple, which would lead to errors in temperature measurement.

The parameters are shown in table 10.01. A full factorial experiment of eight coating runs was used. The coating thickness was measured using a Talysurf 10 instrument.

Parameter	Variable	Low Value	High value
A	Argon Pressure	2 mTorr	4 mTorr
B	Bias Power	0W	40W
C	Deposition Power	200W	600W

Table 10.01: Study of parameters used to deposit PtRh by d.c. magnetron sputtering[139]

10.3.2 Results of initial work

The results of the compositional depth profile at the failure interface of PtRh deposited onto aluminium oxide with a nickel adhesion promotion layer is shown in figure 10.06. The height 0 represents the interface where there are two compositional values because the top layer of films on the component and sellotape were analysed. The AES analysis shows that the tape has removed the majority of the Ni layer and thus the film has failed at the aluminium oxide-nickel interface. The nickel was approximately 10 nm thick.

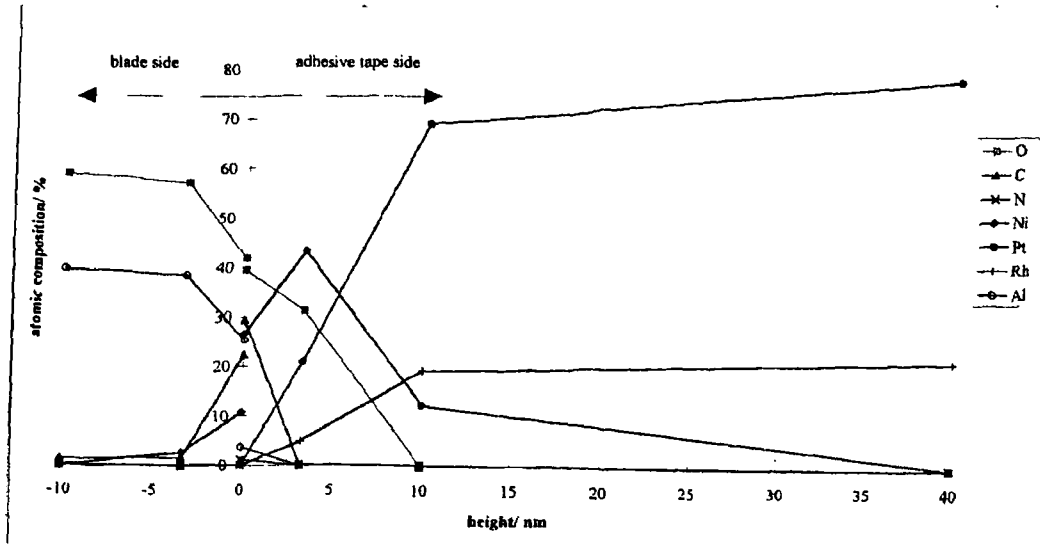

Figure 10.06: Composition depth profile of failure interface of PtRh to aluminium oxide using an adhesion promotion layer of nickel[139]

The results of the eight coating runs are shown in table 10.02. The rhodium content was found to vary from 11.00 to 11.90%, and fall short of the 13% composition of the target.

It was found that the deposition rate was most affected by the level of power applied to the target; an increase in deposition power resulted in an increase in deposition rate. The interaction between the deposition power and either the argon pressure or the bias power may also be important. The interaction between the deposition power and the bias power was by far the most important factor affecting the percentage of Rh in the PtRh film. Increasing the deposition power alone was also found to increase the proportion of Rh in the coating. The deposition power alone cannot be increased further as the power supply is limited to 600V.

Experiment no	A	B	C	Deposition Rate/μm/h	%Rh
1	-	-	-	2.22	11.00
2	+	-	-	1.85	11.55
3	-	+	-	1.50	11.20
4	+	+	-	2.01	11.05
5	-	-	+	5.83	11.75
6	+	-	+	5.68	11.90
7	-	+	+	5.90	11.25
8	+	+	+	5.87	11.10

Table 10.02: Results of compositional analysis of PtRh coatings deposited using different parameter levels[139]

Following this work, the author performed the development work and trials to fabricate and evaluate the films as thermocouple sensors. When a chromium target was delivered, the sellotape test was repeated. When chromium was used, the adhesion of the PtRh was excellent and could not be removed.

10.3.3 Calibration of Pt-Rh thin film thermocouple against wire thermocouple

The aim of this experiment was to determine the EMF of both the Pt and Pt/Rh legs relative to wires and the EMF of the thin film thermocouple relative to a conventional thermocouple. The experiment set-up shown in figure 10.07 was used. A long thin test plate, measuring 150 mm by 16 mm of INCO 718 was polished by hand, using progressively finer grades of silicon carbide abrasive paper. The component was ultrasonically cleaned in isopropyl alcohol and then bias etch cleaned in the vacuum chamber for 20 minutes at 200V RF. Aluminium oxide was deposited using a reactive sputtering process using a pulsed dc power supply. The deposition and patterning sequence for the platinum-rhodium leg is given in figure 10.08. The processes in the flow chart were then repeated, from the application of the photoresist, for the platinum leg. The photoresist was applied by dipping the component into a beaker of the S1400-17 photoresist.

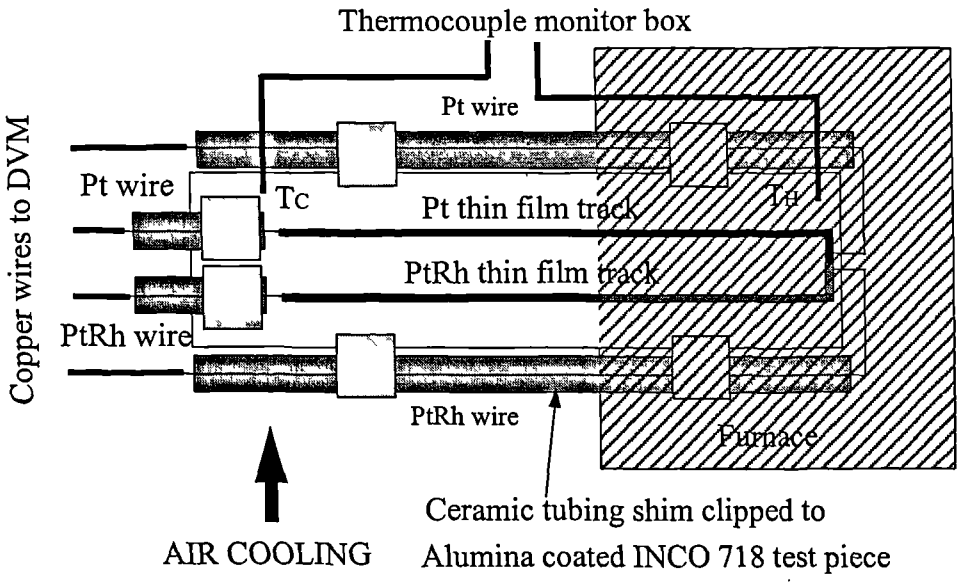

Figure 10.07: Experimental arrangement for calibration of thin film PtRh thermocouple against wire thermocouple.

Coating run number	Coating	Deposition Pressure	Deposition settingr	Deposition Time	Power supply mode
530	Al_2O_3	4 x10^{-3}Torr	2000W	3 hours	Pulsed DC
531	Cr	5 x10^{-3}Torr	1 Amp	2 minutes	DC
532	Pt	5 x10^{-3}Torr	1 Amp	12 minutes	DC
533	Cr	5 x10^{-3}Torr	1 Amp	2 minutes	DC
534	PtRh	4 x10^{-3}Torr	600W	15 minutes	DC

Table 10.03: Deposition parameters for Pt/PtRh thermocouple

The deposition parameters used in the production of the test sample are given in table 10.03. The PtRh deposition parameters were chosen so that they repeated experiment number 6 of the earlier trial, which gave the highest Rh content.

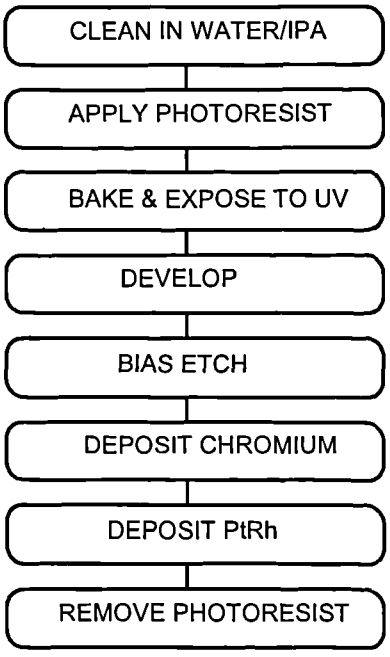

Figure 10.08: Flow chart for production of one leg of the thermocouple circuit

Ceramic tubing was clipped to the test piece to provide insulation for the leadout wires. Twenty-micron diameter Pt and PtRh wires were threaded through the ceramic tubing and parallel gap welded to the end of the thin film tracks and to the hot junction. The parallel gap welding technique is described in section 6.4.4. Thicker

silver plated copper wires were brazed to these and secured to the ceramic tubing. Reference K type thermocouples were attached to the sample to measure T_H and T_C, the hot and cold junction temperatures respectively. The test sample was inserted into a furnace so that 70 mm of the sample was inside the furnace. The gap around the sample was filled with thermal insulation. A temperature difference was achieved along the sample by blowing cold air over the exposed end of the test sample.

Measurements were made of the thin film thermocouple output, the output of the Pt-Pt/Rh wire thermocouple and of each film leg relative to the corresponding wire. It had been assumed that the temperature of the wire to film cold junction and the 20 micron to copper wire junction were at the same temperature so that no additional EMF were produced by this leg of the circuit if the film and wire properties were different. In practice, the cold junction warmed to 50°C when the furnace was at 750°C whilst the copper junction received more cooling as it was in the exposed air stream. This would have caused a source of error in the measurements. The temperature of the copper junction should have been measured so that this could have been allowed for.

The output of the wire and thin film thermocouples are shown in figure 10.09. The output of the wire Pt-Pt/Rh thermocouple has been compared to standard tables and exhibits the correct concave shape and voltage levels for this material. The thin film thermocouple output is very low in comparison to the reference. Examination of the individual legs of the film thermocouple relative to the corresponding wire shows that the PtRh leg is producing a sensible output. There is a difference between the film and wire amounting to 4% of wire thermocouple output. This is most likely due to a low Rh content in the film, measured at 11.0 to 11.90% compared to the 13% (type R) wire. From data of thermoelectric output relative to platinum for different compositions of Rh[140], it was seen that the lower Rh content of the film should only account for 1-2 % difference. Other reasons for the difference may be due to stress in the film track. This can be reduced by annealing, where a slow change occurs above 400°C and a complete anneal occurs above 1200°C[54].

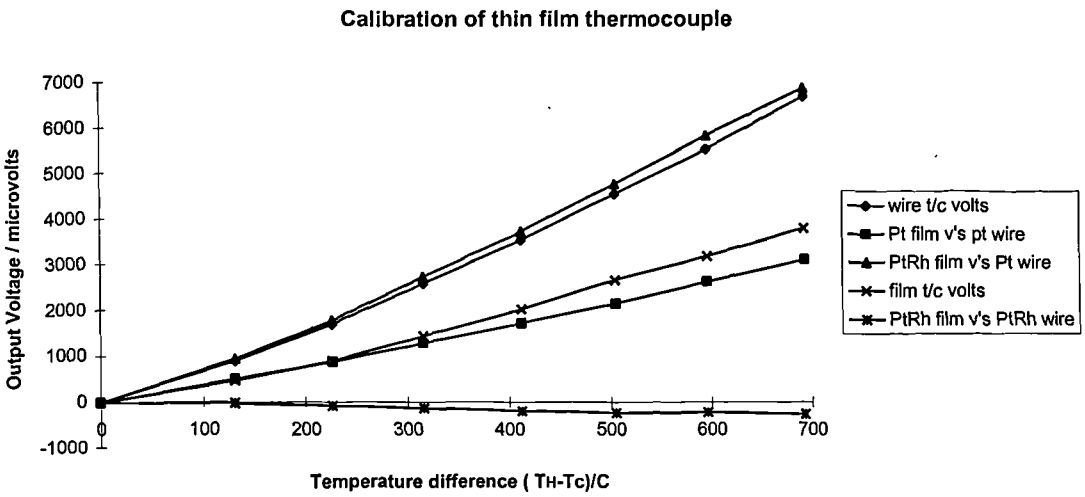

Figure 10.09: Thermoelectric output of thin film and conventional wire thermocouples

A large output is produced across the Pt film and Pt wire. This accounts for the low output of the thin film thermocouple. Platinum being the pure metal leg is most sensitive to contamination. Following this result the target was examined and it was found that the target has been exhausted and some of the solder bond between the platinum and the copper backing had been sputtered. The electrical insulation of the sensor to substrate decreased to 40kΩ at 750°C. This will not have affected the results, but may limit testing at higher temperatures. The film tracks are 1 mm wide. Producing narrower tracks will reduce the contact area and give a higher insulation resistance. However, to reach 1000°C several orders of magnitude of improvement needed to be seen. This can only be achieved by improving the aluminium oxide layer.

10.3.4 Conclusions

A thin film platinum rhodium thermocouple has been produced and calibrated against a type R wire thermocouple. The PtRh film leg compares well against the wire. The difference of 4% of output can be partially explained by the low composition of Rh in the PtRh leg (between 11.00 and 11.90% instead of 13%). The low output may also be due to the structure of the deposited film and may improve with annealing. The platinum leg has very low output compared to the Pt wire. This

gives the whole thermocouple a low output. The EMF of the platinum leg is very sensitive to contamination in the coating. In this case the coating was contaminated because the platinum target had been exhausted and the coating contained elements from the copper backing and bonding material. An order has been placed for a new target to repeat this work. The good results obtained with the PtRh leg have given confidence that an accurate thin film thermocouple can be fabricated.

10.4 Platinum Tungsten deposition & sensor evaluation.

10.4.1 Initial testing

A 3-inch diameter Pt-8%W target of 99.999% purity was acquired. In order to reduce the initial costs, the target consisted of a disk of 3 mm thick PtW, bonded onto a 3 mm copper backing plate. A trial coating run was made onto a glass slide using an AJA magnetron cathode. The deposition during run 550 was free from arcing. The ends of the slide were masked off with two other slides so that a film edge would be produced. The slide was ion cleaned for 5 minutes at 100Watts RF. The target was sputter cleaned for 20 minutes onto the chamber shield. The shield was then rotated and a ten-minute deposition at 367W made onto the slide at an argon deposition pressure of 5 $x10^{-3}$ Torr. The sample was biased at 100Watts RF during the deposition. A Talysurf 10 step profiler was used to traverse across the film step and a coating thickness averaged from a number of measurements at each end. This value was used to calculate the deposition rate of 4.35 μm/h. Several measurements of the composition of the coating were made by Auger. This gave averaged tungsten content of 7.95%. The adhesion of the film to the glass slide was poor, the coating could be easily pulled off using sellotape applied on top of the coating. It was also confirmed that the material could not be etched using any of the standard chemical etches.

The lift-off patterning technique was used to produce sensor patterns on a glass slide. The adhesion of the sensor film was very poor and many of the sensors produced on the slide were damaged in the lift-off process. The adhesion of PtW to the glass slide

was improved by the addition of a flash of Ni. The adhesion was not considered satisfactory until the nickel was replaced with chromium.

A trial was performed to determine a sensor thickness that gave a resistance (R) of 350Ω for a standard gauge pattern. Several coating runs of different deposition times were performed onto a patterned glass slide. The resistance of the patterned sensors was measured. The correct deposition time was 190 seconds, which corresponded to a thickness of 0.35 μm.

The gauge element will experience self-heating when polarised. Defects in the coating may have given high resistance locations. These would cause a deterioration of the gauge with time by causing local hot-spots when polarised. A standard polarising circuit applies 24V through a 1kΩ series resistor. For a gauge resistance of 350Ω this gives a polarising current (I) of 17 mA. Two gauges were produced on a scrap component. These were polarised at this current for 24 hours. The sensor resistance was measured before and after the 24-hour test. The sensor resistance did not change during the test. This was a good indication that there was no deterioration of the gauge.

10.4.2 Temperature testing of PtW thin film sensors

Eight sensor patterns (denoted A to H) were produced on an INCO 718 plate coated with 10 microns of non-reactively sputtered aluminium oxide. The plate was removed from the chamber, dipped with S1400-17 photoresist and patterned. Coatings of nickel, platinum-tungsten and gold were deposited sequentially. The photoresist was removed so that the sensor patterns were defined. The gauges were trimmed to 350Ω resistance by removal of the gold coating. Fifty-micron diameter nickel wires were parallel gap welded to the connection pads. The nickel wires were then brazed to mineral insulated leadout cables, which were shim clipped to the plate.

The insulation resistance of the sensors proved to be very low (< 2 MΩ). This was believed to be due to the mineral insulated cables, rather than the sensors. The

powder insulation is hydroscopic, and had absorbed moisture while being cut to size. The ends were then sealed which sealed the moisture in. This was confirmed during temperature testing, as the insulation resistance of the sensor circuit did not change with temperature. The test sample was heated in steps of 100°C to 600°C to calculate the temperature coefficient of resistance (α). The plate was then kept at 600°C for 400 hours to monitor the time dependant change of resistance of the sensor. This is particularly important for steady strain sensors but less so for dynamic sensors. For wire gauges, trials have shown that the wire must be heat treated for hundreds of hours for the resistance drift to stop. After this the material becomes very stable at temperatures below the heat treatment temperature.

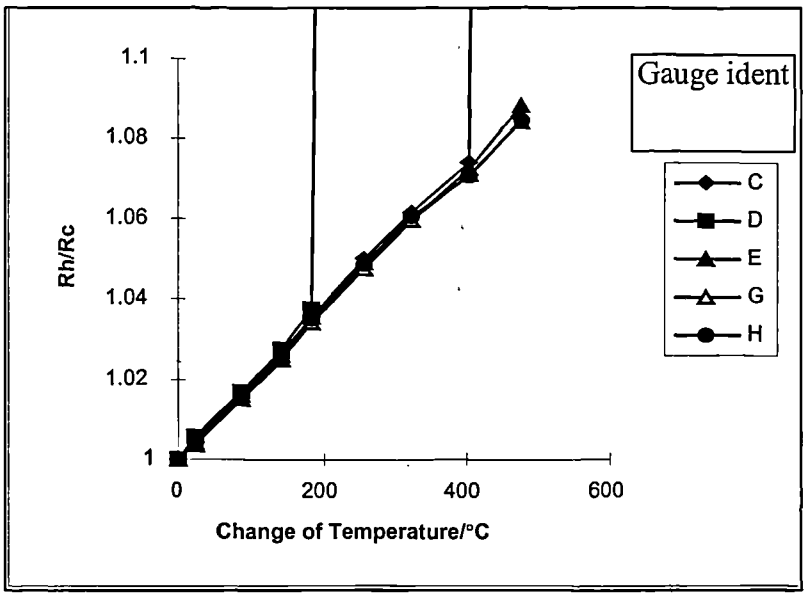

Figure 10.10: Temperature coefficient of resistance of PtW strain gauge. Where R_h=hot resistance and R_c =cold resistance

The graphs of resistance change with temperature and time dependent change of resistance at temperature are shown in figures 10.10 & 10.11 respectively. A number of gauges went open circuit due to the failure of the connections. This is seen as large increases in resistance in figure 10.10.

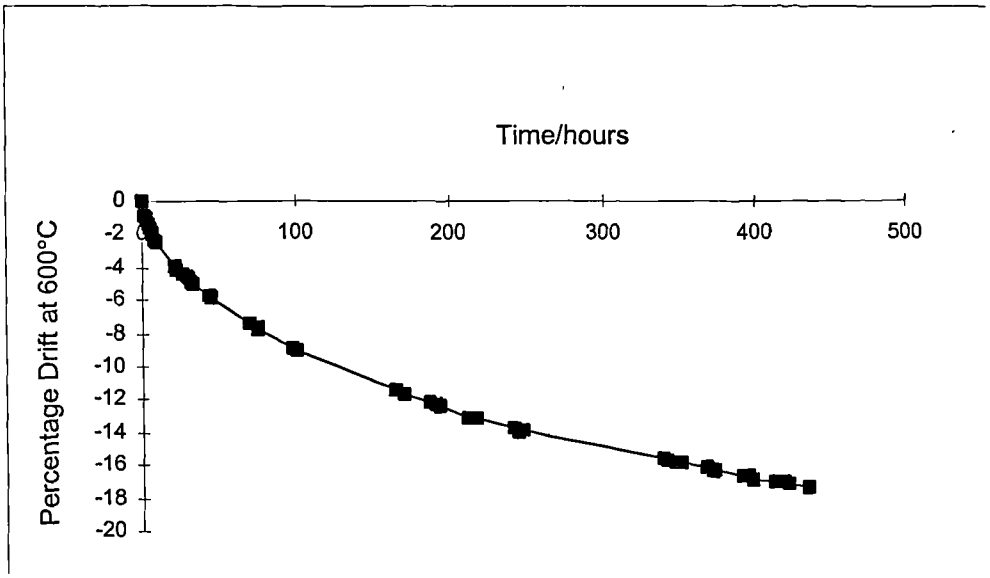

Figure 10.11: Time dependent change of resistance of PtW strain gauge at 600°C

The graph in figure 10.10 gives a temperature coefficient of resistance (α) for the platinum tungsten sensor of 171 $\mu\Omega/\Omega/°C$. This has been calculated from equation 8.

$$R_h=R_c(1+\alpha\Delta T). \quad \text{Equation 8.}$$

10.4.3 Calculation of gauge sensitivity of as-deposited PtW gauges

A Lloyd Instruments tensile test machine was purchased to evaluate the high temperature performance of the strain gauges. The machine initially produced large inaccuracies in strain applied to each face of a square cross-section tensile test specimen. This was due to misalignment of the sample, fixtures and machine. As a short-term measure to give an ambient temperature gauge sensitivity measurement, low temperature gauges were bonded to the test sample. The outputs of the thin film gauges were compared to conventional foil gauges bonded on the same face of the tensile test specimen. This gave the results given in table 10.04.

Face 1	
Foil gauge output /με GF=2.04 Resistance=350.2Ω	PtW thin film gauge output /με Resistance=625.4Ω
0	0
264	333
500	667
750	1016
1000	1377

Face 2	
PtW thin film gauge output /με Resistance=659.6Ω	Foil gauge output /με GF=2.04 Resistance=350.2Ω
0	0
320	288
676	535
1049	790
1407	1039

Table 10.04: Measurement of gauge factor of Pt 8%W thin film gauges

A calculation could be made of the gauge sensitivity of the thin film gauges by comparison with the conventional gauges. This gave a value of 2.80 for gauge 1 and 2.76 for gauge 2. These values are lower than the gauge sensitivity of PtW wire gauges, which would be 4.2 at room temperature.

10.4.4 Investigation of the effects of deposition parameters and gauge design on gauge sensitivity

The gauge sensitivity (S_f) was believed to be thickness sensitive. In very thin coatings the resistivity of the films are very dependent on surface defects. However, these are not strain sensitive and reduce the overall sensitivity compared to that of bulk. Once a certain thickness has been achieved the sensor would be insensitive to small changes in coating thickness. It was believed that the gauge sensitivity is also sensitive to alloy composition. The two most significant factors that may change the composition are the bias power and deposition pressure. These affect the arrival and removal rate of material from the substrate. It has been assumed that the deposition power will stay fixed during these trials.

Two of Rolls-Royce's competitors have used single-element strain gauges. They have claimed that this type of sensor exhibited better characteristics than the grid shown in figure 10.12. The single element gauge has a length to width ration of 50:1 and the

multi element gauge 156:1. Neither pattern has sharp corners, which would cause necking defects during the patterning process. Annealing can also be used to change the characteristics of the gauges.

The following are thus considered parameters, which could effect the gauge factor.

Parameter	Variable	Low Level	High Level
A	Deposition time	3 minutes	6 minutes
B	Bias Power	earthed	100W
C	Deposition Pressure	2 mTorr	5 mTorr
D	Gauge design (length to width ratio)	156:1	50:1
E	Annealing	none	400°C

Table 10.05: Study of parameters used to deposit PtW strain gauges

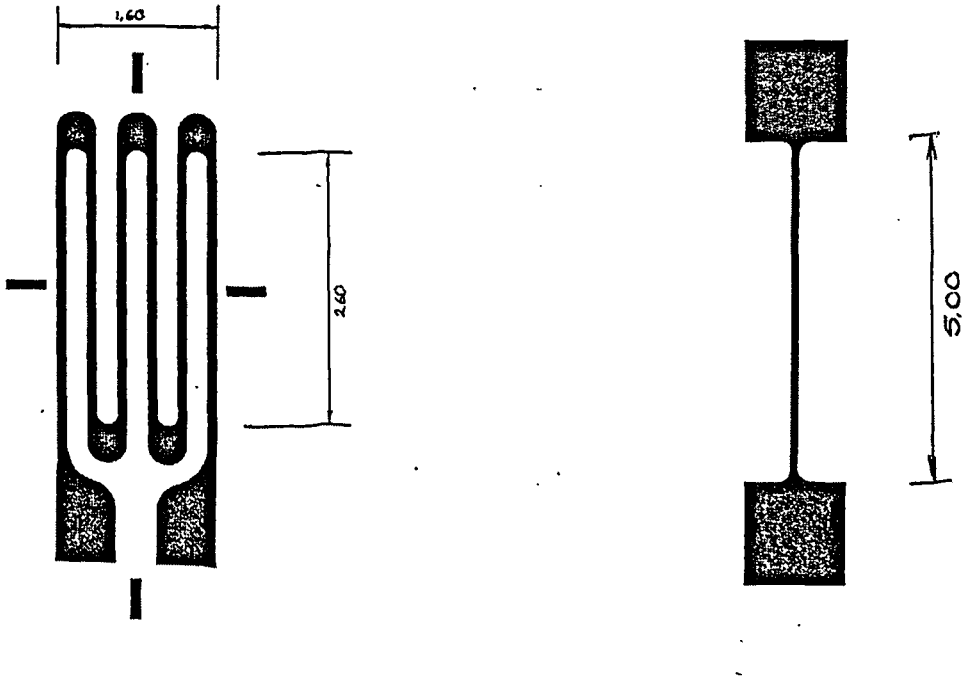

Figure 10.12: Comparison of different gauge designs used

This is a 2^5 experiment with 32 treatment combinations. It is estimated that it would take at least one week of work to produce each tensile test specimen. To produce a separate specimen for each treatment combination would therefore be prohibitively costly. Using a statistical design it was possible to divide this into a quarter fractional

factorial experiment design with a total of 8 separate experiments. This has been done following the rules shown in Davies[131] and is described further in chapter 7

Because each tensile test specimen has four separate faces, by masking off the other three faces for each coating it was possible to arrange for all 8 types of sensor experiment to be performed on two samples. This introduced errors since all the annealed coatings must be on the same specimen and the biased coatings must be performed first. This lost the randomness in which the experiments should have been arranged and introduced a source of systematic error. Thus the results must be treated with care.

The results from this experiment are given in table 10.06.

Coating Order	Coating run number	Experiment No	A	B	C	D	E	Resistance Ω	Gauge Factor
1	598	7	-	+	+	+	-	331	2.76
2	599	8	+	+	+	-	-	446	3.17
3	600	1	-	-	-	-	-	965	2.76
4	601	2	+	-	-	+	-	117	3.16
5	*	3	-	+	-	-	+		
6	*	4	+	+	-	+	+		
7	*	5	-	-	+	+	+		
8	*	6	+	-	+	-	+		

* These tests were not performed because the PtW target had been fully eroded

Table 10.06: Results of experiment design

Before completion of this work the target was used to produce sensors for an engine test. During this work the target was exhausted. A new target is needed before this work can be completed. However, the results obtained from the first sample have given a useful conclusion. The gauge sensitivity is dependent on the thickness. The sensitivity approached that of wire gauges as the thickness is increased.

10.4.5 Conclusions

Platinum tungsten has been deposited by magnetron sputtering. A bond coat layer of chromium was needed to ensure adhesion to glass slides and thin film aluminium oxide insulator layers. The coatings have been fabricated into a strain gauge using a lift-off patterning technique. The temperature coefficient of resistance up to 600°C and the time dependent change of resistance at 600°C have been measured. These gave similar values to conventional wire PtW strain gauges. The sensitivity of the strain gauge has been found to be dependent on the deposition conditions. In particular a thin coating gave a lower sensitivity because the majority of the resistance was due to surface defects. This did not contribute to the strain sensitivity. The sensitivity approaches that of wire gauges as the thickness was increased. This process has been used to instrument 21 components from an EJ200 high-pressure compressor for a strain gauge rig test. A stage six stator instrumented with a PtW thin film strain gauge is shown later in this chapter. The application process and the benefits of the thin film sensor technique are described for this application.

10.5 Palladium-Chromium deposition & evaluation

10.5.1 Experimental detail

A 3-inch diameter Palladium-12% Chromium target of 99.999% purity was acquired. In order to reduce the initial costs, the target consisted of 3 mm thick PdCr, bonded onto a 3 mm copper backing plate. The target was manufactured using a powder hot isostatic pressing method. The manufacturer claimed that this was the only method available with this material. The target when received had a loose powdery surface. A trial coating run was first made onto a glass slide using an AJA magnetron cathode, using the dc power supply. The process was very arcy, spitting particles from the target. This arcing did not reduce with time, as it would if the arcing were caused by surface contaminants. The arcing also made the process difficult to control. It is thought that the PdCr target contains trapped air and is outgassing

during the process as the target is eroded. This would cause contamination of the deposited film, which would alter the sensor properties.

A new target was acquired from an alternative manufacturer. This was produced using a metal melt method. The target had a much better appearance and when used in deposition was free from arcing. A coating was made on a glass slide and sent to Loughborough University for analysis of composition using AES. The chromium content of the coating was 11.5%. The oxygen content was 0.5% which was considered acceptable. A scanning electron microscope image of the coating showed that it contained a large number of particles, believed to be of the target material. This is shown in figure 10.13 and needs further investigation.

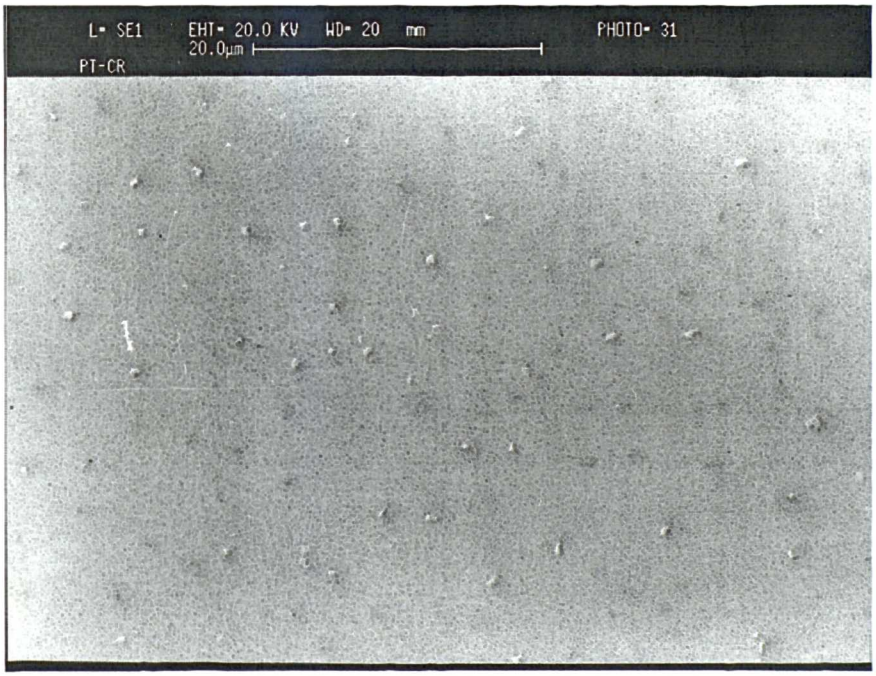

Figure 10.13: Surface defects on PdCr coating on glass slide

A trial was performed to pattern the coating using the selective etching process. The coating could not be etched by the Shipley Cr etch 18, which is the standard etch used for nickel-chromium films. The coating could be removed using Aqua Regia, which consists of 1 part nitric acid to 5 parts hydrochloric acid. However, the etching process left a uniform discoloration where the film had been removed. Analysis of this residue by AES revealed that it was chromium oxide. A further trial showed that

the thin layer of chromium oxide could be removed using the Shipley Cr etch. Thus a selective etching process is possible using a two-stage etching process. First Aqua Regia is used to remove the bulk of the coating, then Shipley Cr etch 18, to remove the chromium oxide residue. This is preferable to a lift-off process.

The need to replace the first pressed target resulted in a six-month delay to the coating work. The transfer of the NiCoCrAlY deposition work to the Sinfin-A site deposition system then made the arrangement of all the coating work difficult. Several engine sensor applications then cut further into the planned development work. A trial was started to produce Pd-Cr strain gauges on a CMSX-4 tensile test specimen for high temperature evaluation of the electrical properties of then material. This has not been completed and so no useful conclusions can be made.

10.6 Application of techniques on aeroengine components

Several examples of actual applications of thin film sensor technology incorporating the techniques developed in this work are shown in this section. The first is an application of the low temperature NiCr strain gauges using the selective etching pattering process. The aim was test to monitor strain levels on a hydraulic pipe elbow fitting on a Trent 700 flight test. The pipe elbow (Aeroquip no. AE 33459E) had failed in on flight test on a number of occasions. The elbow connects the pressure sensing pipe (SCD 2137) to the Trent 700 No. 1 hydraulic pump. The resultant loss in pressure caused the engine to shut down. The elbow had never failed on a static test bed. An investigation to monitor stress levels at the elbow during flight test was proposed. Conventional strain gauges were unsuitable due to the complicated shape of the component and the presence of the locking nut. The elbow had failed in the locking wire groove and the application of conventional strain gauges here would prevent fitting of the locking nut.

The application of thin film sensors was proposed as a solution. This work was performed for two separate flight tests. The first was used to investigate the problem and a solution was achieved by moving the clips that held the pipe to the engine. A

second test was performed several years later when an alteration was made to the hydraulic pump. A total of five components was produced with thin film sensors. One such component is shown in figure 10.14.

The elbow components were first dressed by hand on a polishing wheel. Surface imperfections were removed and sharp corners smoothed out. The outermost mating surface was protected by tape during this operation to ensure that the pipe elbow would fit correctly onto its mating part without leaking on build. The component was then hand polished with different grades of abrasive paper to give a mirror finish.

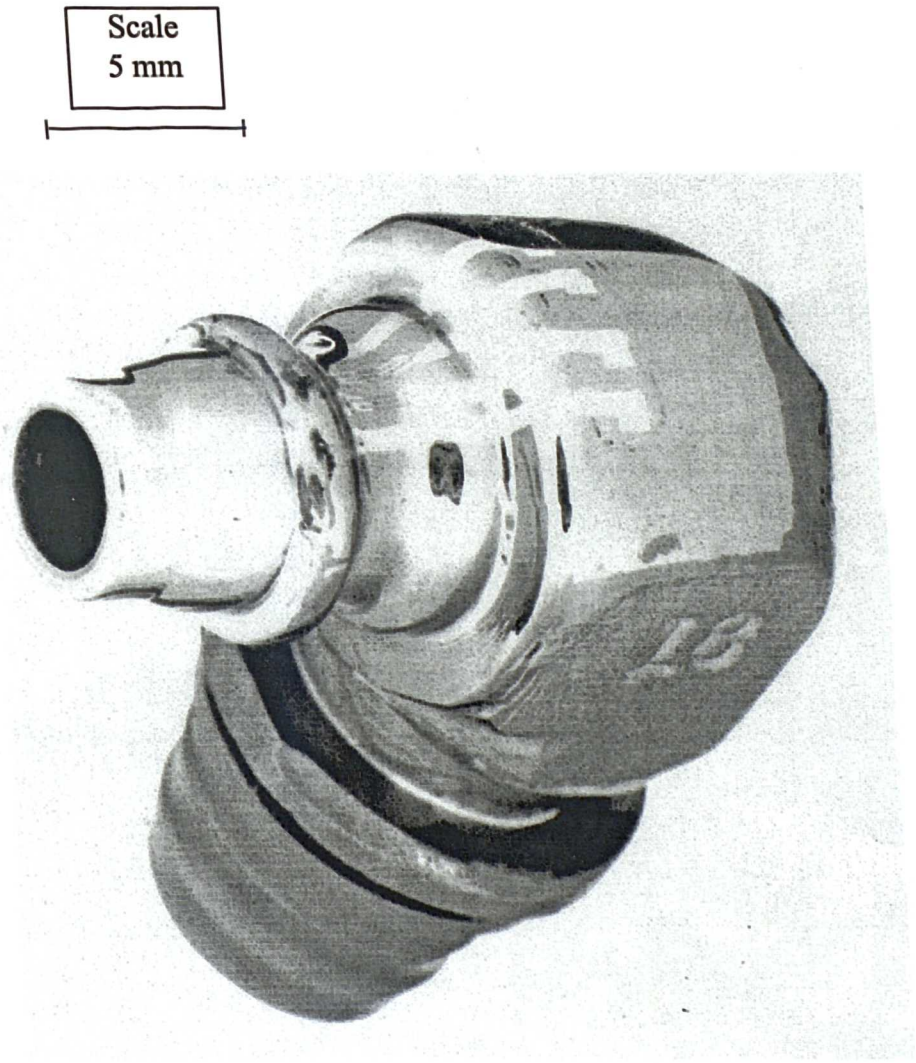

Figure 10.14: Hydraulic pipe fitting with NiCr strain gauges shown as an example of patterning on complex components.

Thin film coatings were then applied to the component in the sequence given in table 10.07. The component was removed from the vacuum chamber after the gold

coating. Dynamic strain gauges were fabricated using the selective etching patterning technique. Because of the complicated shape and number of radiuses, the photoresist was applied by spinning. An araldite clamp was made to hold the elbow on the spinner motor. This was balanced by the addition of weights to the brass plate. Shipley Microposit S1400-25 photoresist was puddled over the component on the area to be gauged. The component was then spun at 4000 rpm for 25 seconds.

Caoating run number	Material	Argon pressure	Deposition time	Deposition setting	Bias setting	Power supply mode
505	Al_2O_3	$5x10^{-3}$ Torr	3h	2000W		Pulsed DC
506	NiCr	$5x10^{-3}$ Torr	10m	1A	200V	DC
507	Au	$5x10^{-3}$ Torr	10m	1A		DC
Application of photoresist for selective etching and resistance trimming						
508	Al_2O_3	$5x10^{-3}$ Torr	1h	2000W		Pulsed DC

Table 10.07: Deposition condition for thin film coatings on hydraulic pipe-elbow.

A special flexible mask was manufactured to wrap around the radii on the component. A 25 μm thick mylar film was coated with 1μm of aluminium by pulsed dc deposition. The film was clamped against a glass slide so that the aluminium coating was face up. The glass slide was fitted on the photoresist spinner and a coating of photoresist applied onto the mylar film. After curing at 80°C, the mylar film was exposed to ultra-violet through the thicker photographically produced mask. The pattern was developed and the unwanted coating etched in Isoform aluminium etch to create a copy of the mask pattern on the mylar film. This was then cut to the size of the sensor. One edge of the mylar film was taped to the component in the correct position. The mylar film was then held in contact with the pipe fitting using the latex glove vacuum clamp. After development the component was patterned using the process described in section 4.4. The gold coating was removed over the contact area for later connection. An over coat of aluminium oxide was applied over the sensor grid. It was found that the first two components produced were damaged

during the application of the locking nut. The locking wire rubbed against the sensor when it was hammered into place. To prevent this, several layers of protective resin were applied over the gauge position. After the nut was applied and hydraulic pipe fitted, the gauges were checked electrically and wires were attached to the films using 60/40 solder.

The second example is an application of the lift-off patterning technique to produce PtW dynamic strain gauges on an compressor development rig test. The stage 6 stator has a 3-D shaped aerofoil. The application of a conventional wire gauge using ceramic cement would cover a large proportion of the aerofoil. The development project team chose a mixture of thin film and conventional gauges. PtW strain gauges were requested because of their greater sensitivity. A total of 6 stage 6 components and 15 other component from different stages of the rig were instrumented using a lift-off patterning technique.

The components were polished by hand using different grades of silicon carbide abrasive paper, from 400 to 4000 grit, to produce a mirror finish. Aluminium oxide was deposited by pulsed dc reactive sputtering onto the components. The components were removed from the chamber and S1400-17 photoresist was applied using the dipping method. This was cured at 80°C for 20 minutes. A mask was then placed in the correct location and angle. One edge of the mask was taped to the component using mylar tape. The mask was then held firmly against the component using the vacuum clamp. The photoresist was exposed to UV through the mask and then developed to leave the sensor grid defined. Leadout tracks were defined by hand painted photoresist. The component was cured and loaded into the vacuum chamber. Coatings were deposited in the sequence shown in table 10.08.

Coating run number	Material	Argon pressure	Deposition time	Deposition setting	Power supply mode
593	Al_2O_3	$5x10^{-3}$ Torr	3h	2000W	Pulsed DC
Application of photoresist					
594	Ni	$5x10^{-3}$ Torr	10m	500W	RF
595	PtW	$5x10^{-3}$ Torr	10m	1A	DC
596	Au	$5x10^{-3}$ Torr	10m	1A	DC
Lift-off of photoresist and resistance trimming					
597	Al_2O_3	$5x10^{-3}$ Torr	1h	2000W	Pulsed DC

Table 10.08: Deposition sequence for PtW dynamic strain gauges.

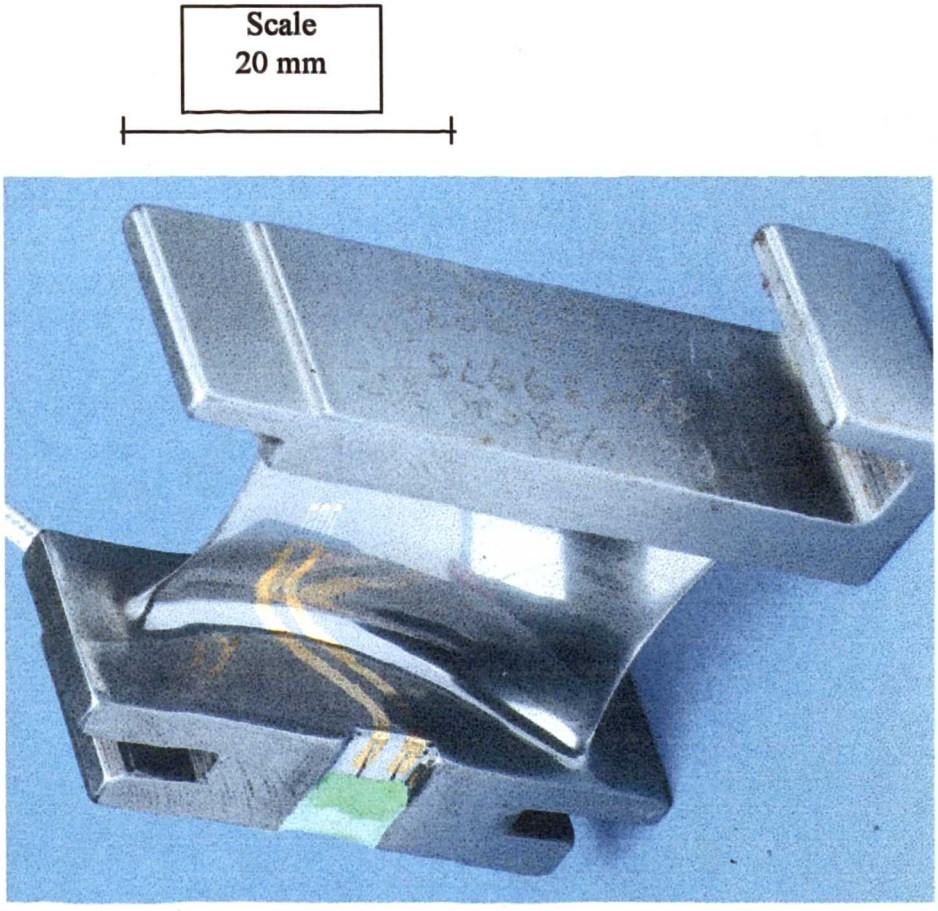

Figure 10.15: Compressor stator with PtW strain gauges as an example of patterning on a complex component

The work was performed before the delivery of the chromium target so nickel was used as a bond coat. The photoresist was removed and the strain gauge was trimmed

to the correct sensor resistance by etching the gold coating in a number of steps in a gold etch consisting of 5g Iodine + 25g potassium iodine +200 ml water. The connection area was masked off with hand painted photoresist and then the component was coated with 2μm of aluminium oxide to act as a mechanical protective layer. Fine nickel wires were parallel gap welded to the tracks in a slot machined in the stator platform. The fine wires were brazed to thicker leadout wire. The fine wires were held against the component using Rolls-Royce manufactured P354 ceramic cement.

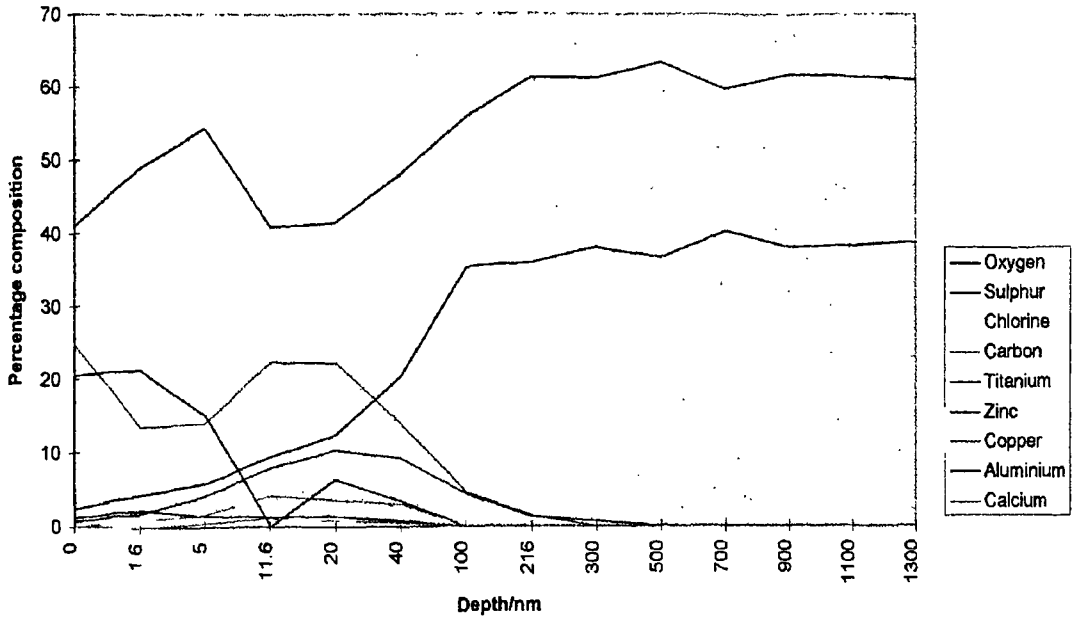

Figure 10.16: Auger depth profiling of component surface in area of sensor failure

A completed component is shown in figure 10.15. The instrumented components were successfully used on the rig for several hours before failure. On rig strip it was found that the sensor tracks had spalled off leaving a discoloured region where the sensor had been. In order to investigate the reason for the failure the area on the component was studied using an Auger depth profile to study for remains of the PtW or Ni layers. The depth profile is shown in figure 10.16. With the exception of surface contamination caused by rig running and exposure to the atmosphere no metallic coatings remain. The sensor has failed at the nickel-aluminium oxide

interface. The nickel layer will be replaced by chromium in all future work, which has been shown to improve the adhesion of noble metal alloys to aluminium oxide.

10.7 Conclusions

The processes to pattern thin film sensors for high temperature applications have been demonstrated. In particular a lift off patterning technique has been developed to pattern noble metal temperature and strain sensors. These can be applied to complex and heavy components due to the addition of a dipping process for the application of the photoresist coating and by an improvement in the attachment of the mask to the component during UV exposure

Four sensor materials have been deposited and successfully patterned. A high temperature thermocouple circuit has been produced using platinum and platinum-rhodium legs. This has been calibrated against a wire thermocouple. Despite the thermocouple output being low because of the contamination of the platinum film from an exhausted target, this has demonstrated the application process and the tests performed on the platinum–rhodium coating have demonstrated that an accurate thermocouple sensor is achievable. The patterning techniques and adhesion of the coatings is excellent. The noble metal coatings require a chromium adhesion promotion layer on glass slides of aluminium oxide coatings.

A platinum-tungsten coating and been patterned into a high temperature dynamic strain gauge. This has been successfully evaluated to 600°C and the properties have been similar to conventional wire strain gauges manufactured from this material. A trial has been started to investigate the dependence of gauge sensitivity on the deposition parameters and gauge design. This could not be completed because of the use of the sputtering target for routine sensor production work (also described in this chapter) which was outside of the control of the author. The target was exhausted and could not be replaced in the timescales of the project. Nevertheless valuable conclusions can be drawn from the partial result. The gauge sensitivity is very

sensitive to the coating thickness. For thin coatings the sensitivity is very low but approached that achieved by wire gauges as the thickness increases.

Palladium-chromium has been sputtered from pressed and melted alloy targets. The pressed target was found to be unsuitable for sputtering. The process was very arcy and difficult to control. This is believed to be due to trapped gas in the target, which is released as the target erodes causing oxidation of the deposited film. A new melt target was acquired and limited evaluation of the coating has been performed. The coating can be patterned using a selective etching technique using a two stage etching process. This avoids the need to remove the component from the chamber between coatings for photoresist application and thus improves the coating adhesion. The coating surface has been found to contain particulates. This needs further investigation.

The processes have been successfully demonstrated on a number of applications, two of which are reviewed here. The first is the application of dynamic strain gauges on a hydraulic pipe elbow for flight testing on the Trent 700 engine. This has shown the suitability of thin film sensors for application on small complex components. This measurement would not have been possible using the conventional techniques. The second application is the deposition of platinum tungsten dynamic strain gauges on a number of components from an EJ200 high-pressure compressor.

Chapter 11: Integration of processes into sensor package

11.1 Introduction

The experimental work aimed at developing the bond coat, insulating layer, sensor coatings and patterning techniques have been reported in the previous chapters. The formation of a sensor package required the integration of all these processes into a very complicated multilayer structure. The attempts at assembling the sensor structure were arranged in a series of batch trials with 3 to 4 samples produced in each batch. Because of the time scales of the project, the work in this chapter was performed in parallel with the development work of the individual coatings. The aim of the first batch was to gain confidence that a sensor package was achievable and reduce some of the risk items in the risk assessment work. The first batch therefore incorporated the established technology such as selective etching of NiCr sensor film and aluminium oxide deposited using RF reactive sputtering. The new sensor materials, patterning processes and the use of the pulsed dc power supply were incorporated into the later batches.

A summary of the coating processes used in each trial is given in figure 11.01. Throughout this work, the main assessment tools have been the examination of the coatings by optical and scanning electron microscopes.

11.2 Batch 1 trial

11.2.1 Experimental detail

The aim of the first sensor batch was to demonstrate the process and reduce a number of risk assessment items by showing satisfactory adhesion of the layers. A second aim was to highlight any problems so that further development work could have been incorporated into the project plan. A diagram of the batch 1 sensor package is shown in figure 11.02. In order to save time, several samples from the NiCoCrAlY coating development work were used as substrates for the sensor package. The samples

shown in figure 8.03 (30m ion clean and 60m ion clean) were denoted samples 1 and 2 respectively for the batch 1 trial.

BATCH 1

Initial investigation of sensor package integrity
NiCoCrAlY deposition on vapour blast substrate
Selective etching process of NiCr sensor used
Aluminium oxide deposited by reactive sputtering with RF power supply

BATCH 2

NiCoCrAlY deposited on polished substrate with no bias
Aluminium oxide deposited by pulsed dc reactive sputtering
NiCoCrAlY upper coat deposited at lower pressure

BATCH 3

Higher content NiCoCrAlY target used to deposit on vapour blast substrate
Improved polishing prior to Al_2O_3 deposition
Selective etching process of PdCr used
Cr adhesion promoter layer

Figure 11.01: Summary of the batch trials

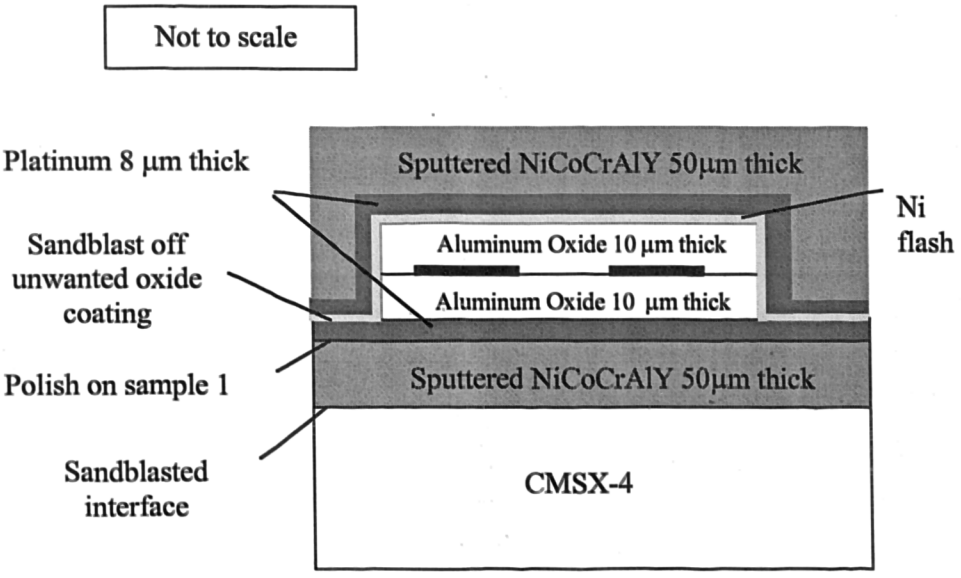

Figure 11.02: Summary of batch 1

The two NiCoCrAlY coated and heat treated samples then had different preparation routes so that the effect of polishing could be assessed. Sample 1 was polished using 1000, 2400 and 4000 grades of silicon carbide abrasive paper on a manual-polishing table. Sample 2 was not polished. The processing route for both samples, from the Pt deposition, is shown in figure 11.03

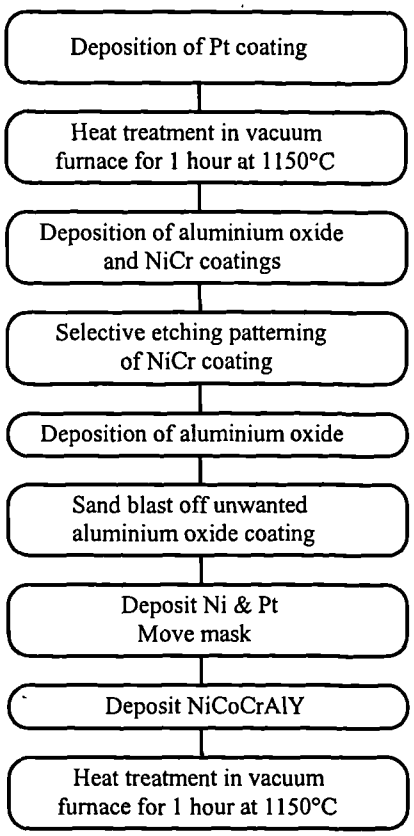

Figure 11.03: Processing route for the batch 1 samples. The NiCoCrAlY coated and heat-treated CMSX-4 substrates were taken from earlier work

The Pt coating was heat treated at 1150°C for 1 hour in a vacuum furnace to form a Pt Al layer. Aluminium oxide was deposited by reactive sputtering using a radio frequency power supply. The deposition was performed in two coating runs to minimise arcing on the target face. This may have resulted in particulates of Al being incorporated in the growing film, which would have reduced the electrical insulation of the sensor. The target was ion cleaned for 30 minutes between each run. A coating of NiCr was deposited directly onto the oxide coating without venting the vacuum chamber.

The patterning of the sensor film was performed using an established selective etching technique. Shipley S1400-25 was applied to the component through a Nalgene 0.2 μm solvent resistant filter. The component was then spun at 4000rpm to produce a layer 1 μm thick. This was cured at 80°C for 20 minutes. The photoresist was exposed to UV through a mask held against the component with a vacuum clamp, followed by development in Shipley MF-319 developer. The strain gauge pattern was the multi-element design shown in figure 10.10. Shipley Cr Etch 18 was used to etch the NiCr coating. The photoresist was removed with Shipley 1165 and the component washed in de-ionised water. The component was loaded into the vacuum chamber with a glass slide masking off the contact area, for the deposition of the Al_2O_3 top insulation layer.

This left the component coated with two layers of oxide. It had been decided to remove this back to the metallic coatings, except for a narrow strip that was several millimetres wider than the sensor grid and tracks. This would reduce the likelihood of spalling of the top layers due to a weak metal-oxide bond over a large area of the sample. The sensor was masked off with a PVC tape patch. Exposed coatings were removed down to the NiCoCrAlY layer by dryblasting with 120/220 SiC grit. The samples were inspected visually during the dryblast process to ensure all the oxide had been removed. The PVC tape was subsequently removed with Rosin solvent.

The electrical resistance of the sensor and its insulation resistance from the substrate were measured at each step of the operation after the sensor patterning. The main instrument used for this was a calibrated Fluke multimeter, which was limited to measurements up to 40MΩ because of battery voltage. For accurate high resistance measurement, a Comark Megohm meter was used. Due to a number of deposition system problems at Elton Road, the deposition of the top NiCoCrAlY layer for batch 1 was performed in the Sinfin-A site system. At the time, faults with the radio frequency bias power supply prevented the biasing of this coating during deposition. The coating was also deposited in two runs because the initial run had to be terminated due to a water cooler fault. After heat treatment the component was sectioned across the sensor grid. One half was encased in a bakelite mould and

polished on an automated polishing table. This was then studied by optical microscope. The section edge of the other half was examined under a scanning electron microscope.

The deposition parameters used for the batch 1 coatings are shown in table 11.01. The deposition parameters for the lower NiCoCrAlY coating are given section 8.2.

Material	Power supply mode/ setting	Time/ minutes	Target voltage	Pressure /10^{-3} Torr	Bias power	Comments
Pt	500mA DC	55	376	15	60W RF	
Al_2O_3	1500W RF	360	280*	5		Coating performed in two parts
NiCr	1.2 A DC	15	370	5	100W RF	
Al_2O_3	1500W RF	360	260*	5		Coating performed in two parts
Ni	500W RF	3	1030	5		
Pt	500mA DC	55	410	15	60W RF	
NiCoCrAlY	800mA DC	480	386	15		Coating performed in two parts.

*deposition voltage after addition of oxygen to the chamber

Table 11.01: Process parameters for batch 1 samples

11.2.2 Batch 1 results.

The two completed samples from batch 1 are shown in figure 11.04. The adhesion of the coatings appeared to be excellent. This was an improvement over the samples produced in the feasibility study trial in chapter 5.

Both samples were patterned using a selective etching process. The unpolished No.2 sample had an open circuit sensor due to defects in the patterning process caused by surface roughness. The polished No.1 sample had a continuous circuit and a sensor

resistance of 377Ω. This was higher than expected with the deposition current and time used for the NiCr coating. The electrical insulation of the sensor before the overcoat layers were applied was in excess of 40 Megohm. However, after the Ni, Pt and NiCoCrAlY coatings were applied, the insulation resistance dropped to a few ohms. Since both oxide-coating runs were identical, the reduction in insulation was due to defects in the top insulator coating. The defects were either from arcing in the RF reactive sputtering process or due to the imperfections in the NiCoCrAlY and Pt coating surfaces. These could cause nodular defect growths in both alumina layers. The nodular defects from the lower layer would continue to grow in size through the top layer and thus have a greater effect.

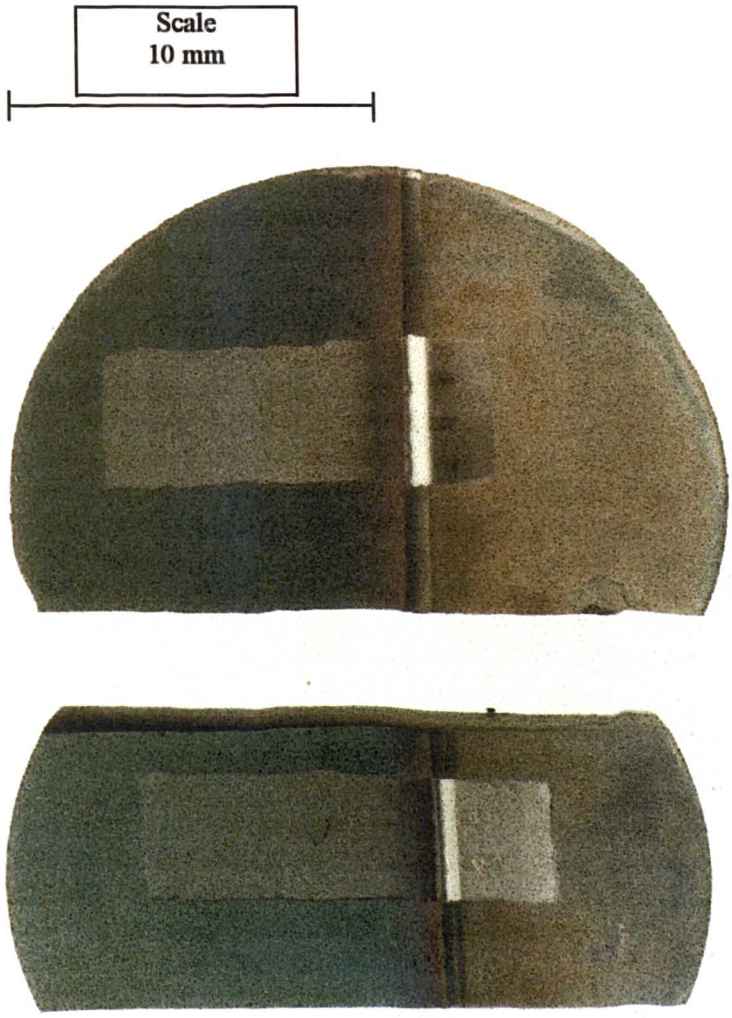

Figure 11.04: Heat-treated batch 1 samples; sample 2 (upper) and sample 1 (lower)

The optical microscope images have been examined. A cross section through the sensor package is shown in figure 11.05 where the seven coatings are identified. The

biased lower coating of NiCoCrAlY was dense and had excellent adhesion to the vapour blasted substrate (as seen before in section 8.2). The upper unbiased layer has a voided columnar structure. This was of concern since it would allow preferential oxidation of the NiCoCrAlY during the TBC application process. It is possible to see where this layer has been restarted.

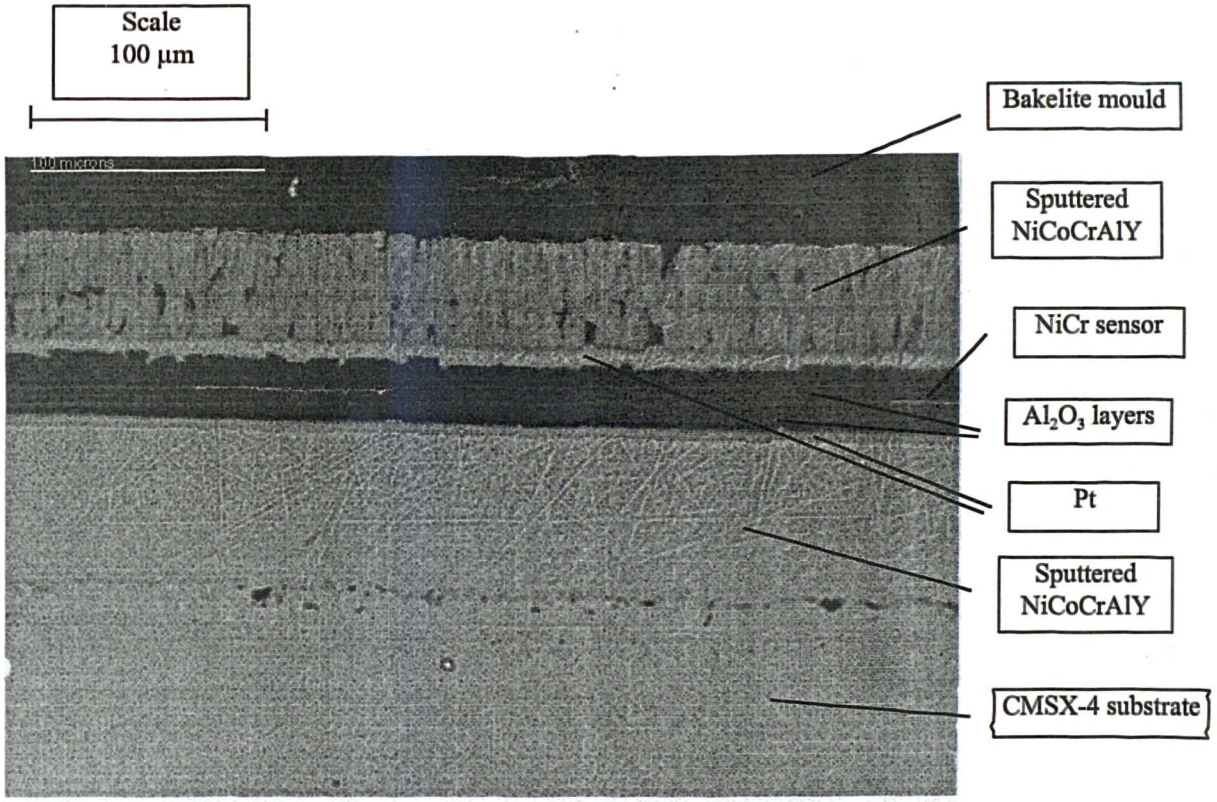

Figure 11.05: Optical microscope photograph of cross-section through sample 1 of the batch 1 sensor package

The composition of both NiCoCrAlY layers is shown in table 11.02. This analysis was made by EDS. The unbiased upper coating has a higher Al content than the biased lower NiCoCrAlY layer. With no bias being used, the compressive residual stress in the upper NiCoCrAlY coating will be low.

Closer examination of the cross-section shown in figure 11.06 reveals a rough surface layer for the deposition of the aluminium oxide layer. This may have been the cause of the poor electrical insulation of the sensor. The use of a dryblast process to remove the unwanted areas of insulator coating has been successful, as can be seen in figure 11.07.

Coating	% Al content
Batch 1 lower biased NiCoCrAlY coating	6.3
Batch 1 upper unbiased NiCoCrAlY coating	7.8

Table 11.02: Comparison of Al content in NiCoCrAlY coating runs on sample 1 of batch 1

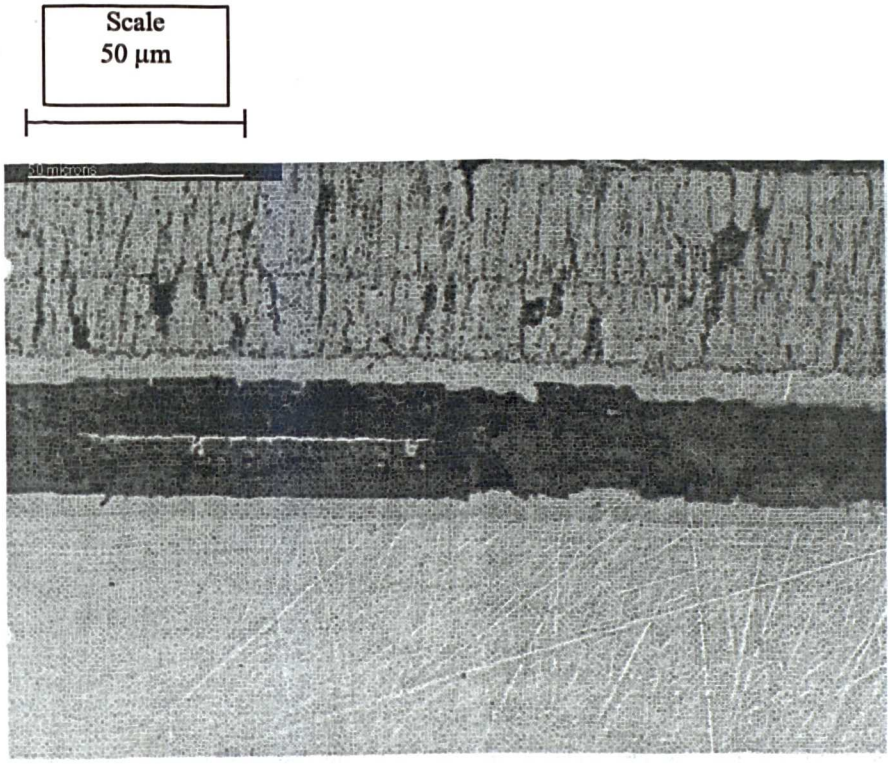

Figure 11.06: Cross section through sensor package of sample 1 in batch 1

Examination of the scanning electron microscope photographs of the surface topography, near a sectioned edge reveals that machining marks from the production of the CMSX-4 sample are still present. These have been reproduced in all the coatings. Figure 11.08 shows individual coatings spalled off near the sectioned edge. The machining marks on the CMSX-4 sample, NiCoCrAlY + Pt + lower oxide and upper oxide coatings are clearly visible. Figure 11.09 shows the machining marks in closer detail on the aluminium oxide layer. The polishing used on the NiCoCrAlY layer was insufficient to remove these defects. The CMSX-4 substrate needs to be 'dressed' back before vapour blasting.

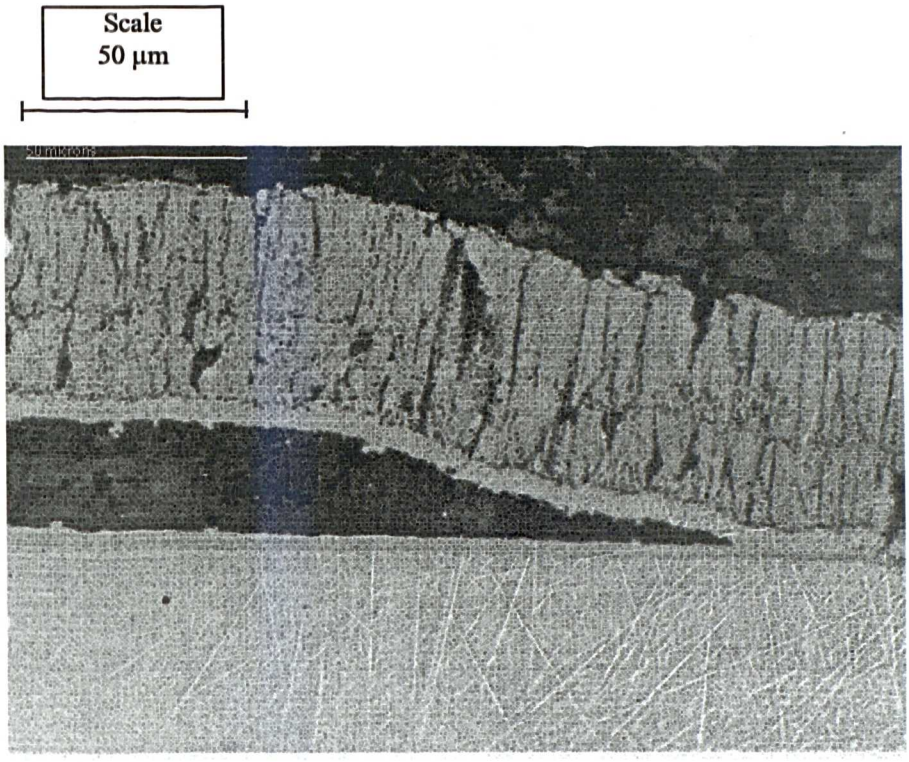

Figure 11.07: Cross-section through sensor package showing aluminium oxide removal

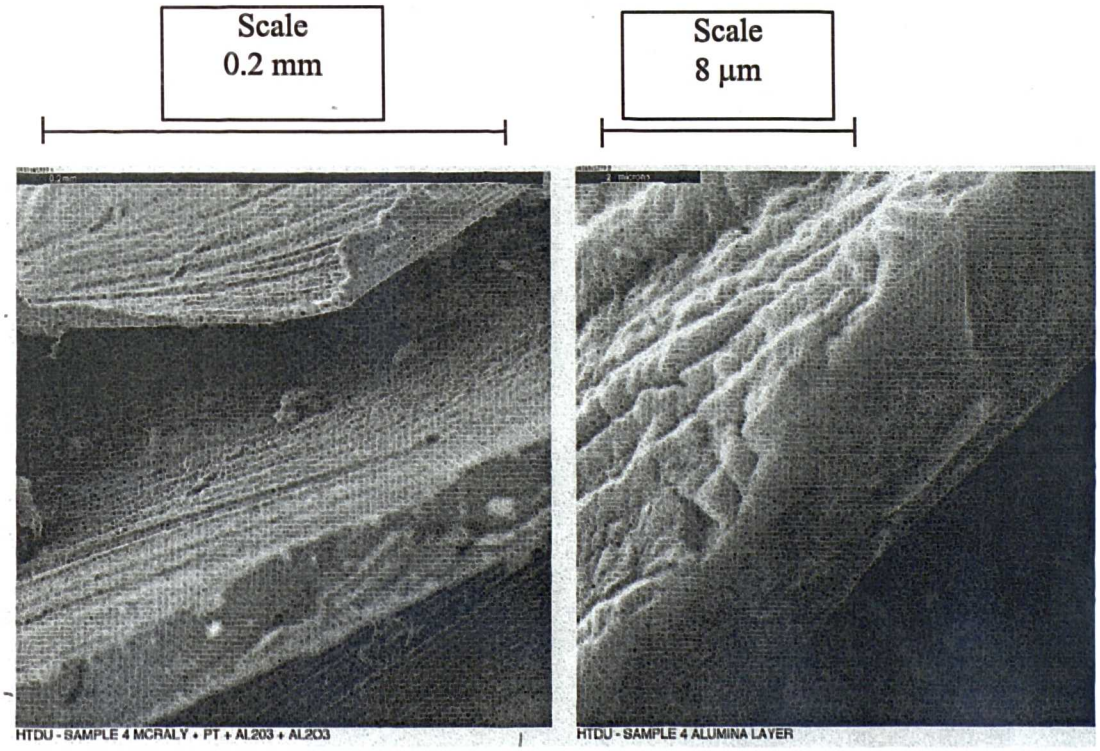

Figure 11.08: CMSX-4 substrate, NiCoCrAlY +Pt +oxide and upper oxide layers near a sectioned edge showing machining marks (left) and upper oxide film (right)

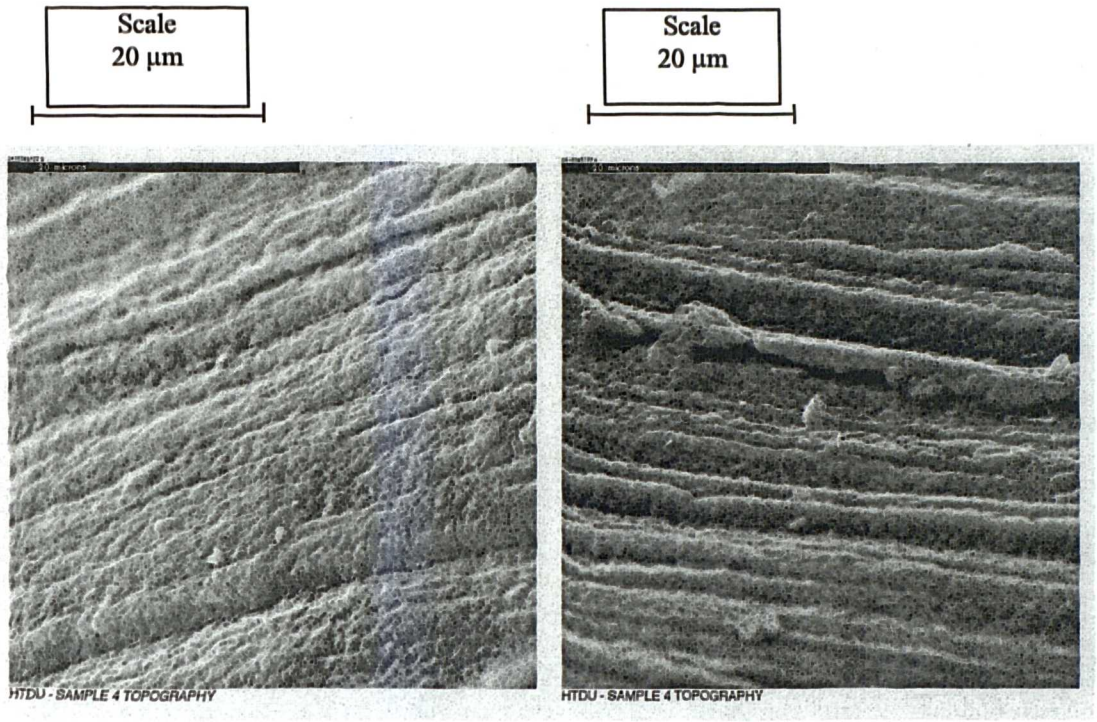

Figure 11.09: Scanning electron microscope image of machining marks as seen on surface of CMSX-4 (right) and aluminium oxide film (left).

11.3 Batch 2

11.3.1 Experimental detail

Earlier work has shown that the use of radio frequency biasing is necessary to produce a dense coating on vapour blasted substrates. The bias, however, reduces the Al and Y content of the coating, which has been shown to be important for the TBC adhesion with the VPS NiCoCrAlY application process. The vapour blasted substrate also produces a rough NiCoCrAlY surface, which must be polished to minimise defects in the aluminium oxide coating and patterned sensor. Earlier work was inconclusive to the effect of surface roughness on NiCoCrAlY adhesion (This batch was performed before the work in section 8.3).

During a risk assessment meeting, it was proposed that a polished substrate finish be used with little or no bias to achieve a dense, high-Al coating[141]. This would then

require less polishing. Further, the unbiased NiCoCrAlY top coating from batch 1 exhibited a columnar structure, which was unacceptable. From the NiCoCrAlY trial performed in chapter 7, it was clear that the deposition pressure had a significant effect on the film structure (although a reduction in pressure will also adversely affect the Al content). It was suggested that lower deposition pressures should be investigated to control the film structure of the upper NiCoCrAlY layer.

This was a different approach from the used in batch 1 and needed investigation to show its feasibility or eliminate it as a possibility.

In order to investigate this processing route, CMSX-4 samples were polished from 180 to 1000 grade abrasive paper. This removed the machining marks on the substrate. The NiCoCrAlY coating was then deposited with no bias during deposition. The NiCoCrAlY and Pt coatings were then polished to the best achievable finish. This would minimise the defects in the aluminium oxide coating. To further improve the insulation of the sensors, the pulsed dc power supply were used, which it was hoped would reduce the number of Al particulate defects in the coating. A summary of the batch 2 samples is shown in figure 10.10.

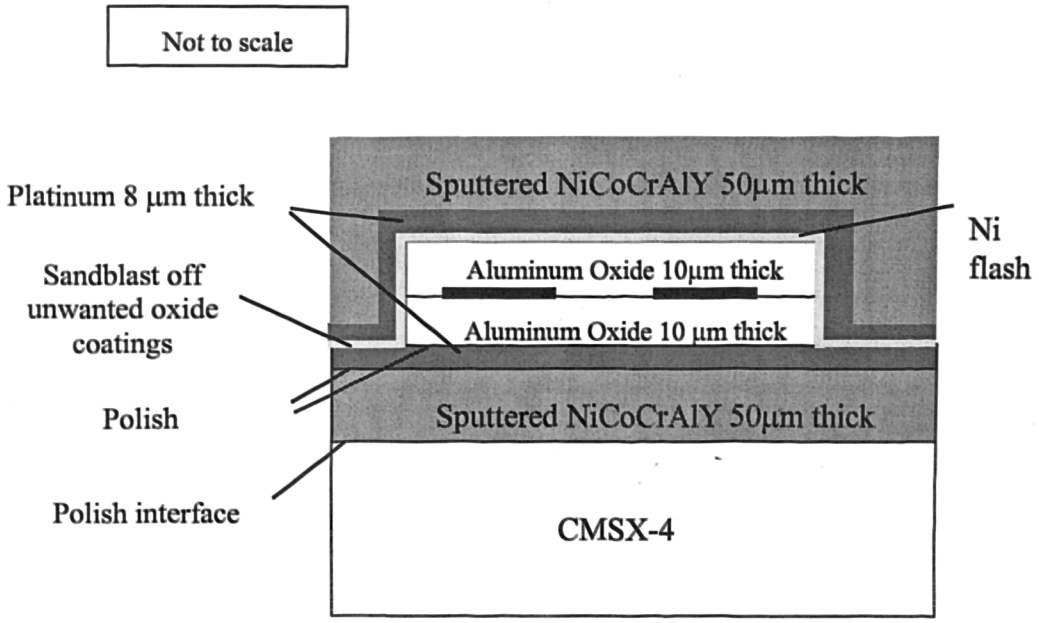

Figure 11.10: Summary of batch 2

The processing route for the batch 2 samples is shown in figure 11.11.

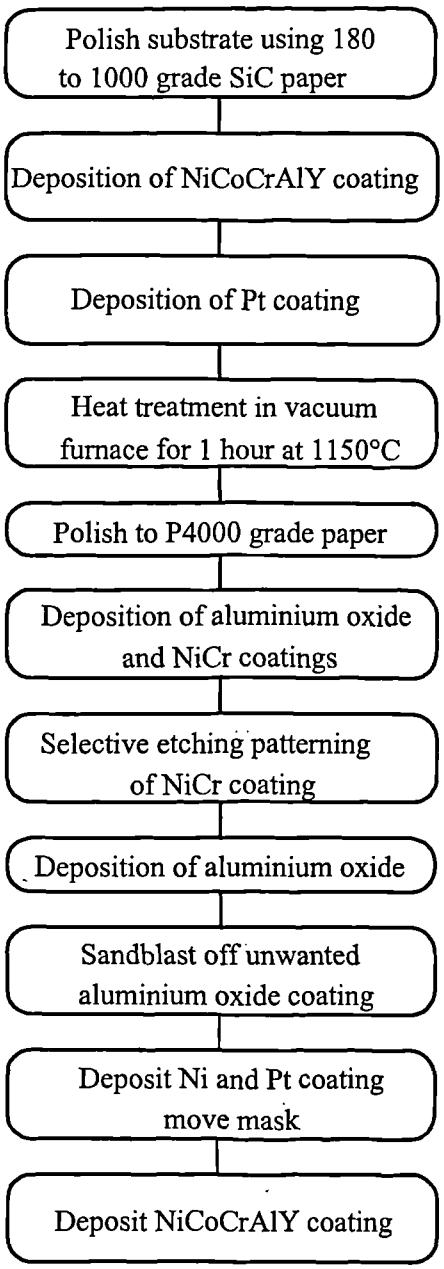

Figure 11.11: Processing route for batch 2 sample

The deposition conditions for all the batch 2 coatings are shown in table 11.03. The samples could not be heat treated as for the batch 1 because of spalling of some of the coatings after the NiCoCrAlY deposition. The sample was sectioned across the sensor grid, encased in an araldite mould and polished on an automated polishing machine. The cross-section of the coatings was examined by optical microscope.

Coating	Deposition Time	Deposition pressure	Bias voltage	Deposition regulation mode / setting
NiCoCrAlY	8 hours	15 x10^{-3}Torr	-	800 mA
Pt	80 minutes	15x10^{-3}Torr	60V	500 mA
Aluminium Oxide	180 minutes	4x10^{-3}Torr	-	2000W PDC
NiCr	15 minutes	5x10^{-3}Torr	-	450W
Aluminium Oxide	180 minutes	4x10^{-3}Torr	-	2000W PDC
Ni	180 seconds	5x10^{-3}Torr	-	500W RF
Pt	80 minutes	15x10^{-3}Torr	60V	500 mA
NiCoCrAlY	9 hours	7.5x10^{-3}Torr	-	800 mA

Table 11.03: Deposition parameters for batch 2 samples

11.3.2 Results

A batch 2 sample is shown in figure 11.12. The sample was not heat treated after the top NiCoCrAlY coating because the metallic coatings over the sensor package had separated. The sensor resistance was 627Ω, which was much higher than expected, indicating the presence of defects in the pattern. The insulation resistance was in excess of 40 Megohm prior to the metallic overcoat layers but dropped to 50Ω subsequently.

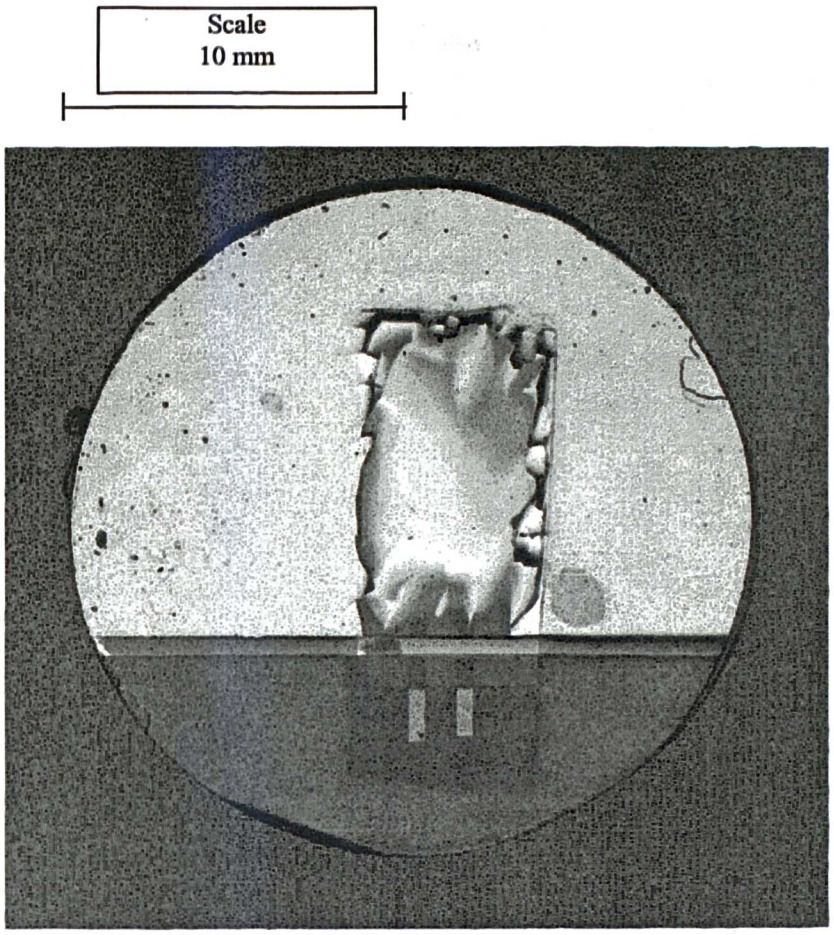

Figure 11.12: Photograph of a batch 2 sample

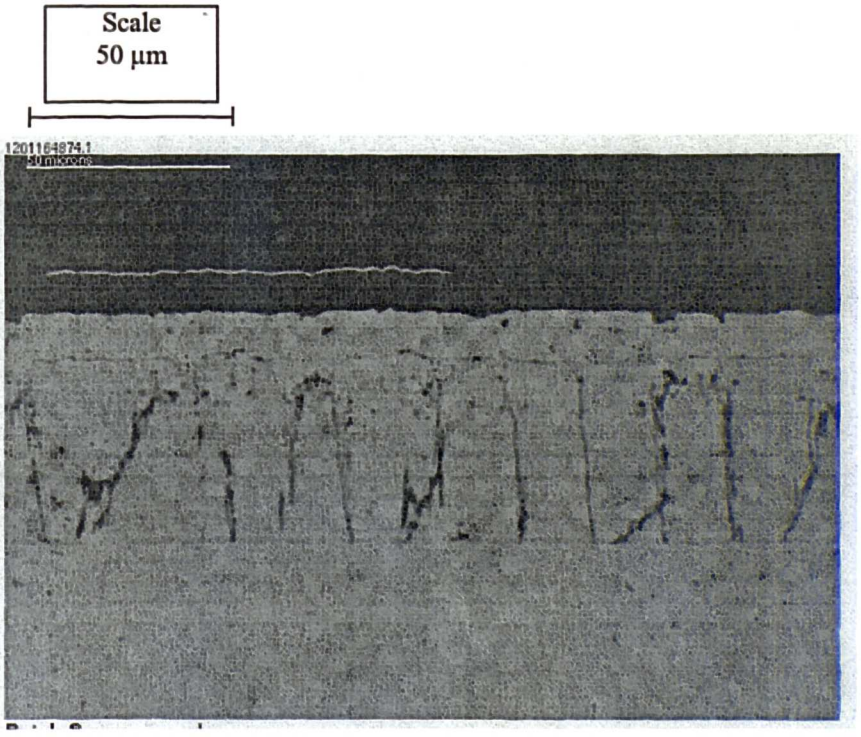

Figure 11.13: Optical microscope cross-section through the batch 2 sensor package

A cross-section of the sample is shown in figure 11.13. The lower unbiased NiCoCrAlY coating has a columnar structure. It appears to be well adhered to the CMSX-4 substrate. This was a poor base for the deposition of the aluminium oxide and sensor coatings. The surface contains voids from the columnar structure resulting in a rougher surface than the batch 1 samples. This is reflected in the sensor resistance, which is almost double the value reported in chapter 1. The upper metallic coatings can be seen in the cross-section of figure 11.14. The NiCoCrAlY appears dense and well adhered to the Pt coating. It was difficult to determine the failure point from this. However, figure 11.15 shows part of the Ni and Pt layer remaining on top of the aluminium oxide layer. The residual stress produced in the NiCoCrAlY coating due to the low deposition pressure has caused the coatings to fail at the weakest interface, in this case the aluminium oxide-Pt layer. The nickel layer was either insufficiently thick or was unsuitable as an adhesion promoter layer.

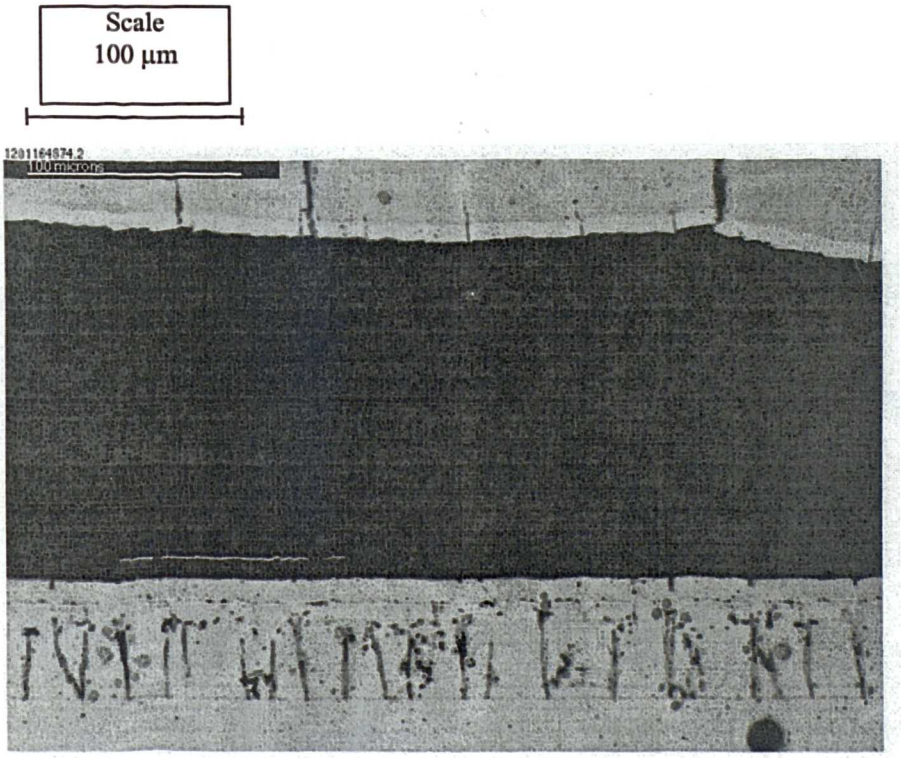

Figure 11.14: Optical microscope photograph of cross-section showing spalled off coating

The Al composition of the NiCoCrAlY layers has been analysed by EDS and was 8.1% of coating composition. The different deposition pressures have had no effect on the Al content of the coating.

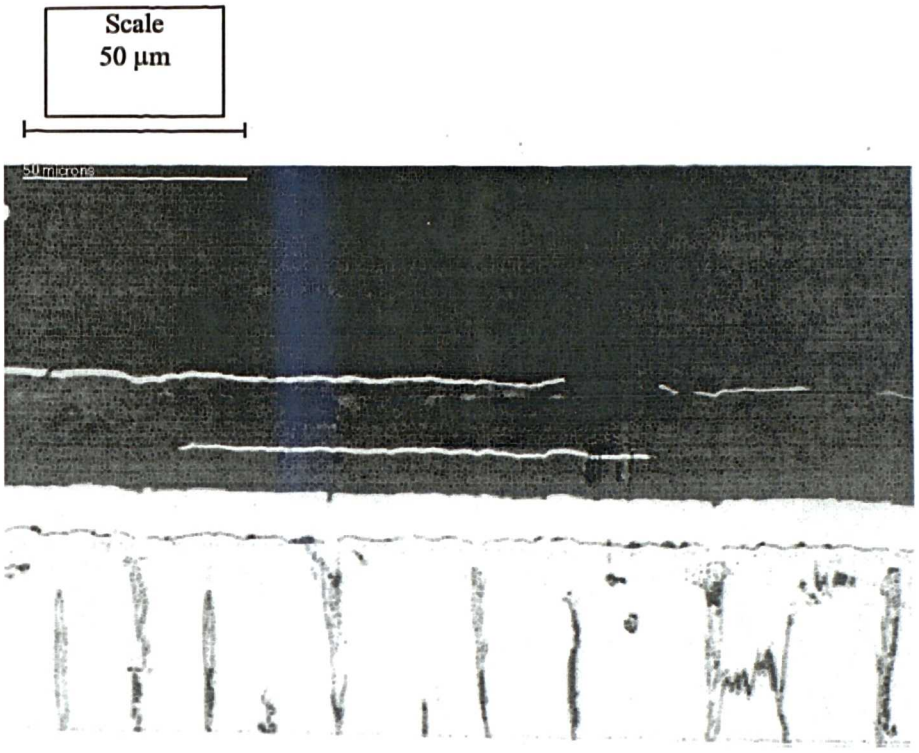

Figure 11.15: Cross-section through sensor showing metallic coating defining the top of the oxide layer

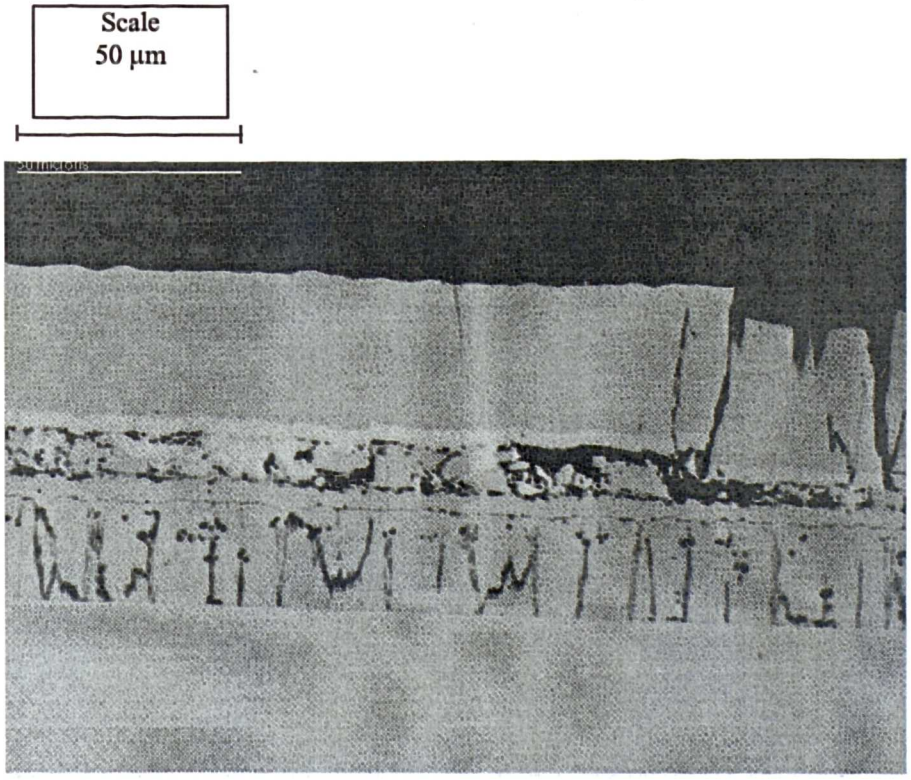

Figure 11.16: Cross-section of substrate showing insufficient removal of aluminium oxide coating

A cross-section showing the area of removed aluminium oxide is shown in figure 11.16. Here, the dryblast operation has not removed the aluminium oxide coating. The interface consists of two layers of Pt and a damaged oxide layer.

11.4 Batch 3

11.4.1 Experimental detail

The approach used in batch 1 was repeated for this batch of samples, with the developments of the proceeding chapters added. The main two areas where improvement were needed lay in the electrical insulation of the sensor package and the adhesion and structure of the upper NiCoCrAlY layer.

Firstly, the aluminium oxide layer was improved by the addition of 180 Volts RF bias to suppress nodular defect growth. The NiCoCrAlY and Pt coatings have been polished to the best achievable finish. The batch 3 sensor package is shown in figure 11.17.

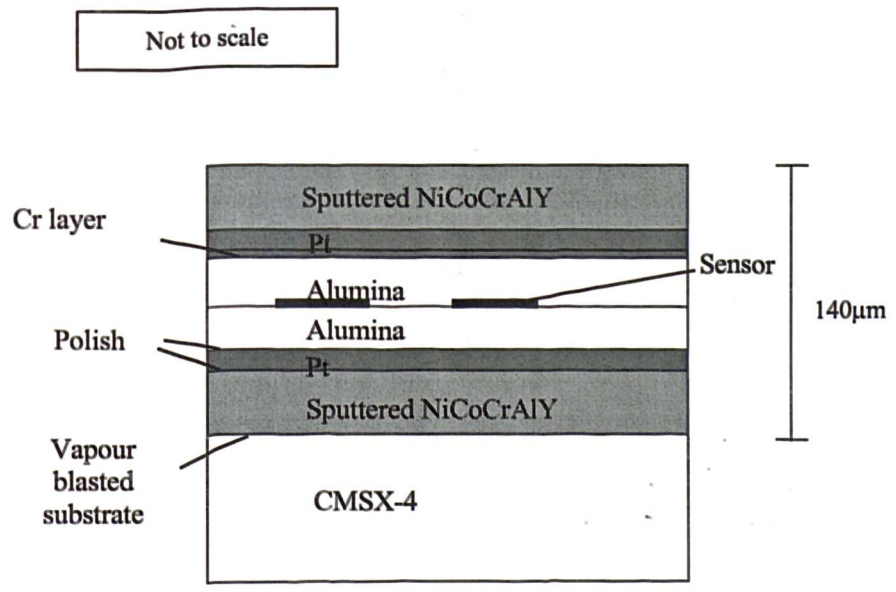

Figure 11.17: Summary of the batch 3 package

Secondly, the lower NiCoCrAlY coating must be free from voided columnar growth. Therefore, 200 volts of RF bias was applied during the deposition onto the vapour

blasted coating. For the upper coating, bias was required to prevent the open structure seen in batch 1. However, if the RF bias was too great then the compressive stress in the coating caused the spalling of the metallic coatings at the weakest interface as in batch 2 (addition of bias will have a similar effect as the lowering of deposition pressure on residual stress). For this batch a value of 100 volts was seen as a good compromise. Further, to improve the adhesion of the metallic coatings, a newly acquired chromium target was used to deposit an adhesion promoter layer. Herein lies another problem. The NiCoCrAlY, Pt and Cr films all require deposition from a 3-inch diameter target of which only two are possessed. Ideally, all 3 layers should be applied sequentially to minimise interface contamination. In practice, because of the limited number of cathodes, the chamber must be vented for a target change.

Another improvement made during this batch was the use of an Al-studded NiCoCrAlY target to improve the Al content of the upper layer. The coating has been deposited with 100 V bias during deposition. The work reported in section 8.3, (figure 8.06), has shown that this was sufficient to achieve a dense coating on a polished surface. Also, a selective etching technique was used to pattern a deposited PdCr sensor film, which was more suitable for high temperatures than the NiCr sensor used earlier.

Coating	Ion cleaning Voltage/time Volts/minutes	Deposition Time	Deposition pressure	Bias voltage	Deposition regulation mode & setting
NiCoCrAlY	200/120	9 hours	15 x10^{-3}Torr	200V	800mA DC
Pt	200/120	80 minutes	15x10^{-3}Torr	60V	500mA DC
Aluminium Oxide	200/60	4 hours	4x10^{-3}Torr	-	1800W PDC
PdCr		15 minutes	5x10^{-3}Torr	-	500mA DC
Aluminium Oxide	200/60	4 hours	4x10^{-3}Torr		1800W PDC
Chromium	200/30	10 minutes	5x10^{-3}Torr		500mA DC
Pt	200/30	60 minutes	15x10^{-3}Torr		500mA DC
NiCoCrAlY		9 hours	15x10^{-3}Torr	100V	800mA DC

Table 11.04: Deposition parameters for batch 3 coatings

The processing route for the batch 3 samples is shown in figure 11.18. The deposition conditions used for each coating run are shown in table 11.04.

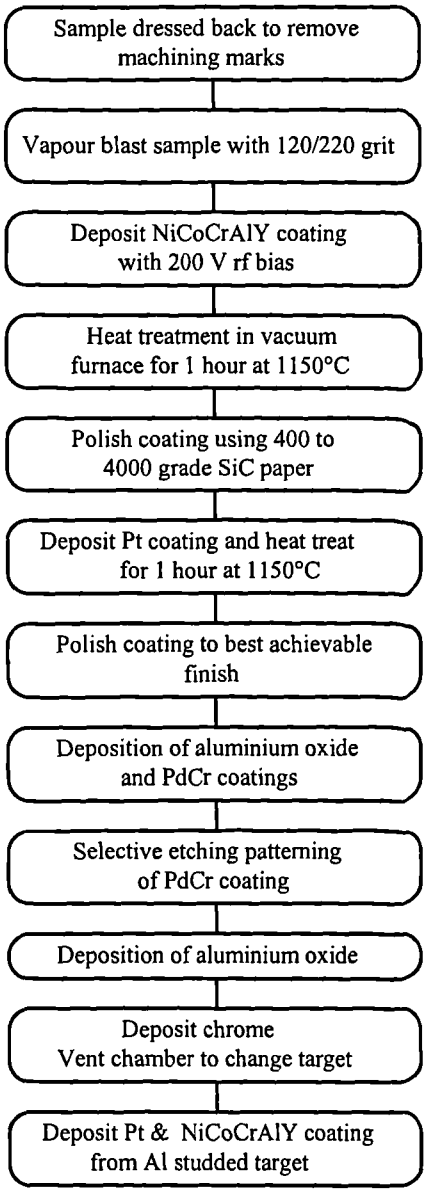

Figure 11.18: Processing route for batch 3 samples

11.4.2 Results

A sample from batch 3 is shown in figure 11.19. The sample was not heat treated after deposition of the upper NiCoCrAlY layer because of cracking in this layer. Examination under an optical microscope showed that the cracking was a result of compressive residual stress in the NiCoCrAlY coating. The coating was removed easily with sellotape leaving a metallic coating over the oxide. This layer was not

electrically conducting, and its thickness could not be detected using the Talysurf 10 step profiler. It is suggested that the package has failed at the interface between the Pt and Cr layers because of oxidation of the Cr layer when the vacuum chamber was opened.

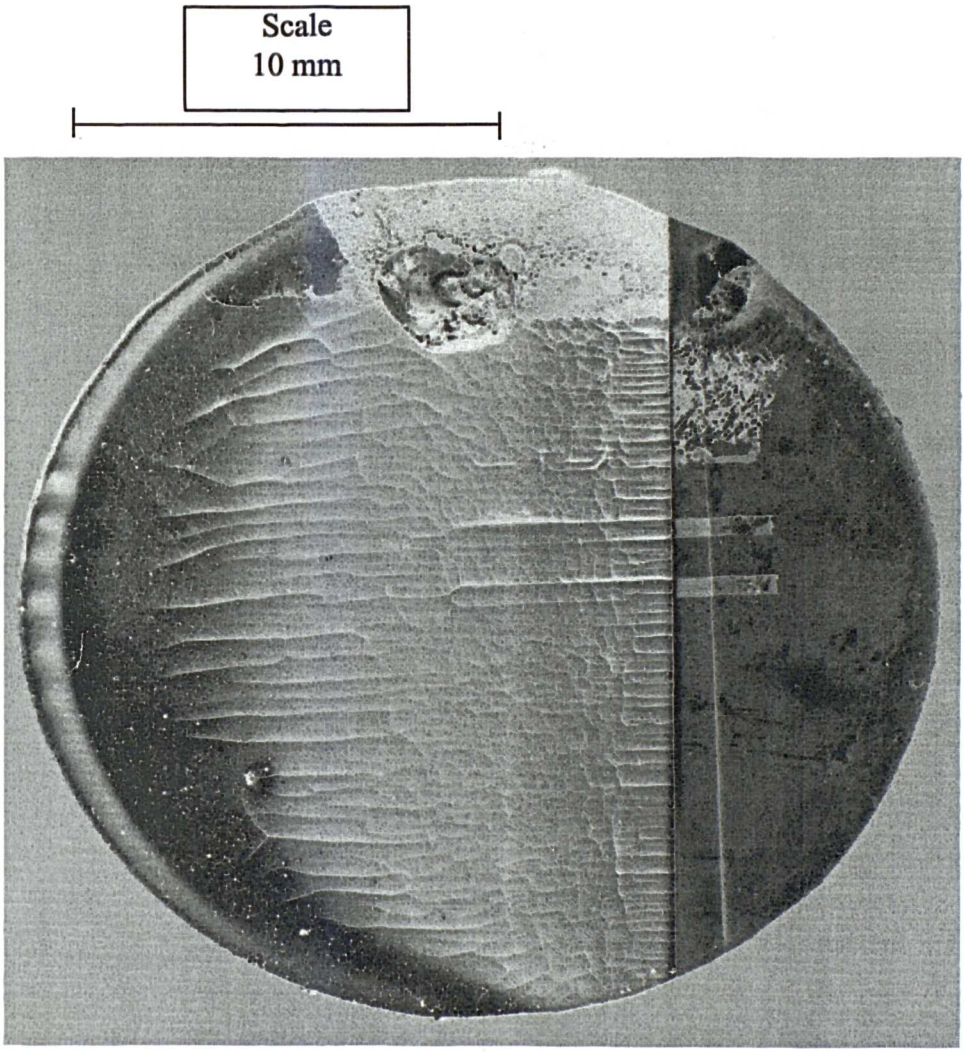

Figure 11.19: Photograph of a batch 3 sample

The batch 1 lower NiCoCrAlY process has been repeated for batch 2. The target was exhausted during the coating run and compositional analysis shows that there was a significant amount of copper contamination in the lower coating. The upper coating was performed with a new Al studded target, to increase the Al content in the coating. The work performed in section 8.4 shows that the Al composition increases to 10% using this method.

Polishing stages were added after the NiCoCrAlY and Pt deposition runs. The polishing stage had to be performed several times until a visually satisfactory finish could be obtained. The manual polishing method for the substrates, NiCoCrAlY and Pt coatings was not acceptable. The samples are polished by hand on a flat polishing table. The process was very time consuming and difficult to achieve a repeatable process. Because the samples are held by hand they can rock, causing particles from the edge of the sample to be broken off and buried in the polishing paper, where they are dragged over the sample face.

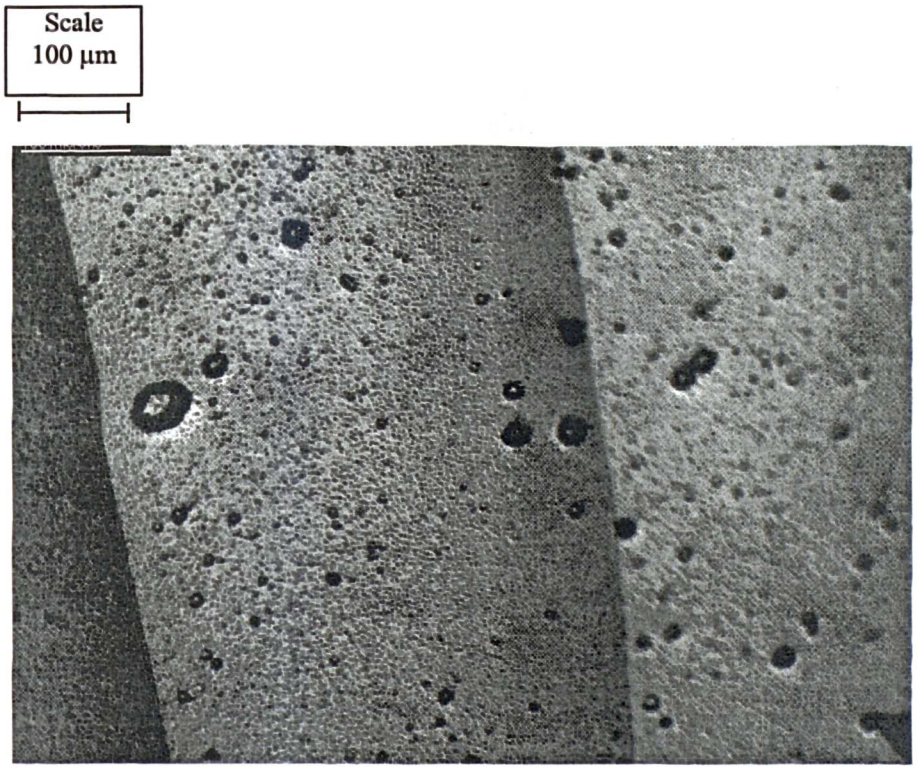

Figure 11.20: Surface features of NiCoCrAlY upper coating showing cracks and a large number of defects.

An electrical check was made of the sensor. The sensor resistance was unchanged but the electrical insulation resistance to the substrate had reduced to a few ohms. The insulation resistance prior to the upper aluminium oxide layer being deposited was in excess of 40 Megohms. Therefore, the upper coating, which was deposited under identical conditions to the lower, contains a number of defects. An optical microscope image of the sample surface, shown in figure 11.20, shows the impression of the sensor through the Pt and NiCoCrAlY layers, the cracks and ridges

of the NiCoCrAlY layer and a large number of particles or nodular defects. There are two sources of these; the first is nodular defect growth or particles of Al as discussed in chapter 9. The second is from the PdCr deposition (section 10.5).

11.5 Conclusions

The work performed in this chapter has demonstrated the feasibility of this type of sensor package. A total of three sensor batches have been produced, each consisting of several samples. Wherever possible the work has been performed using proven processes. The new high temperature processes developed in this project were only included, when there was confidence that their incorporation would not be detrimental to the sensor package. The first sensor batch consisted of seven layers. The next step would be to deposit and heat treat a layer of Pt on the top NiCoCrAlY layer then the deposition of the TBC layer. The following specific points were concluded from the first batch.

Firstly, the CMSX-4 substrate had machining marks on it. These were reproduced on the surface of all the subsequent coatings. The polishing used on the NiCoCrAlY coating was insufficient to remove the marks. These have caused a low insulation resistance and defects in the sensor pattern. The CMSX-4 substrate needs to be dressed back prior to preparation by vapour blasting. The NiCoCrAlY and Pt layer also needed further polishing steps to ensure good electrical insulation and sensor patterns.

Secondly, the upper NiCoCrAlY layer has been deposited without bias and has a resultant columnar structure. This was unacceptable for this project, as it would have allowed preferential oxidation of the coating during TBC application. The lower coating was deposited on a vapour blasted substrate using 200 volts of bias, which has produced a dense coating. The use of bias has left the lower coating low in Al content, compared to the unbiased upper coating.

The second batch has been produced on a polished substrate. The idea behind this was that this would require less biasing, and thus have higher Al content. Also less polishing of the coating would be required. The lower NiCoCrAlY coating was deposited with no bias. It had voided columnar structure. This was a poor base for the aluminium oxide and sensor films. The voided growth boundary produced surface irregularities, causing defect growth in the oxide coating and a very high sensor resistance. Following this batch, a trial was performed on the Sinfin-A site system to evaluate the structure on polished surfaces. This is reported in section 8.3. Another possibility was to use the deposition pressure to produce a dense coating. This was tried on the upper NiCoCrAlY. Here, the residual stress produced in the coating caused the failure of the coating package at the weakest interface. This was the interface of the metallic coatings to the aluminium oxide layer. Nickel had been used to improve the adhesion of the Pt coating to the oxide layer. This had been replaced with chromium for batch 3.

The original approach used in batch 1 has been repeated for batch 3. The NiCoCrAlY coating has been deposited onto a vapour blast substrate. The coating has been deposited with 200 volts bias to produce a dense coating. The NiCoCrAlY and Pt coatings have been polished to the best achievable finish subsequent to each run. This has highlighted the difficulty and the non-repeatability of the hand polishing method. Here, it was difficult to hold the sample and prevent it from rocking. This allowed particles from the edge of the sample to be pressed into the polishing paper and then dragged across the sample face causing scratches, which were difficult to remove in the later stages of polishing.

The upper NiCoCrAlY layer has been deposited with a reduced bias compared to batch 1. This was possible because the coating was deposited on a polished surface (see section 8.3). The target had Al studs inserted to improve the Al content. Here the aluminium oxide has not been removed around the sensor package. Again, the metallic-oxide interface failed with the failure point was between the Cr and Pt layer and was due to venting the vacuum chamber prior to the Pt coating. This was done so

that the Pt and NiCoCrAlY coatings could be deposited sequentially to minimise contamination that would prevent Pt–Al alloy forming during heat-treatment.

The main technical problems with the sensor package are the adhesion of the metal to oxide coatings and the electrical insulation of the sensor package. The former can be improved by addition of a third cathode to apply the three metallic layers sequentially, without venting the chamber. The bias can be reduced further to decrease the residual stress in the coating whilst maintaining the type T structure and the width of the sensor package can be kept to a minimum.

In order to improve the electrical insulation resistance, better polishing methods need developing. The aluminium oxide needs to be deposited with bias during deposition to suppress the formation of nodular defects, which could cause poor insulation. Finally, the new Gencoa cathode needs to be evaluated for the reduction in arcing that leads to Al particulate being incorporated in the deposited film.

Chapter 12: Project summary, conclusions and recommendations for future work

12.1 Project summary

In order to highlight the coating work performed in this study a summary is given in table 12.01.

Coating run number	Material	Deposition setting / mode	Deposition Pressure	Bias Setting / mode	Comments
368	NiCoCrAlY	500 mA DC	15 x10^{-3} Torr	Floating	Fractional factorial experiment to determine the effect of deposition parameters on the deposition rate, structure and composition of the coatings. This study has shown that the parameters 800 mA current, 15x10^{-3} Torr and 100W RF bias gave an acceptable coating structure for this project
369	NiCoCrAlY	800 mA DC	30 x10^{-3} Torr	Floating	
370	NiCoCrAlY	800 mA DC	15 x10^{-3} Torr	Floating	
371	NiCoCrAlY	800 mA DC	15 x10^{-3} Torr	100W RF	
373	NiCoCrAlY	500 mA DC	30 x10^{-3} Torr	100W RF	
374	NiCoCrAlY	500 mA DC	15 x10^{-3} Torr	100W RF	
375	NiCoCrAlY	500 mA DC	30 x10^{-3} Torr	Floating	
376	NiCoCrAlY	800 mA DC	30 x10^{-3} Torr	100W RF	
380	NiCoCrAlY	800 mA DC	15 x10^{-3} Torr	100W RF	Trial to reduce voids with different ion cleaning times prior to deposition. This trial showed that there was no benefit from ion cleaning the substrate longer than 30 minutes
381	NiCoCrAlY	800 mA DC	15 x10^{-3} Torr	100W RF	
382	NiCoCrAlY	800 mA DC	15 x10^{-3} Torr	100W RF	
470	NiCoCrAlY	800 mA DC	15 x10^{-3} Torr	Floating	Trial to investigate the effect of substrate preparation method and RF bias during deposition
471	NiCoCrAlY	800 mA DC	15 x10^{-3} Torr	100 V RF	
485	NiCoCrAlY	800 mA DC	15 x10^{-3} Torr	100 V RF	Evaluation of Al content using Al studded NiCoCrAlY target

Table 12.01 (a): Deposition parameters for coating runs in this study

Coating run number	Material	Deposition setting / mode	Deposition Pressure	Bias Setting / mode	Comments
490	Al_2O_3	2000 W PDC	4 x10^{-3} Torr	Floating	Coating runs 490, 491 and 492 show the variation in deposition rate with argon deposition pressure
491	Al_2O_3	2000 W PDC	3 x10^{-3} Torr	Floating	
492	Al_2O_3	2000 W PDC	2 x10^{-3} Torr	Floating	
493	Al_2O_3	2000 W PDC	4 x10^{-3} Torr	Floating	Comparison of nodular defects on glass slide and Si wafer
501	Al_2O_3	2000 W PDC	4 x10^{-3} Torr	60 V RF	Trial to investigate if the use of RF bias can suppress the formation of defects in oxide coatings.
502	Al_2O_3	2000 W PDC	4 x10^{-3} Torr	100 V RF	
503	Al_2O_3	2000 W PDC	4 x10^{-3} Torr	140 V RF	
504	Al_2O_3	2000 W PDC	4 x10^{-3} Torr	180 V RF	
510	PtRh	500 mA DC	5 x10^{-3} Torr	Floating	Initial investigation of deposition of PtRh onto glass slide
530	Al_2O_3	2000 W PDC	4 x10^{-3} Torr	Floating	Fabrication of a thin film thermocouple sensor for calibration against a wire thermocouple. This showed that accurate temperature measurements were feasible with this process. The PtRh leg agree with its wire equivalent to within 4%
531	Cr	1 A DC	5 x10^{-3} Torr	Floating	
532	Pt	1 A DC	5 x10^{-3} Torr	Floating	
533	Cr	1 A DC	5 x10^{-3} Torr	Floating	
534	PtRh	600 W DC	4 x10^{-3} Torr	Floating	
550	PtW	367 W DC	5 x10^{-3} Torr	100 W RF	Initial investigation of PtW
554	Al_2O_3	1500 W RF	5 x10^{-3} Torr	Floating	Deposition of PtW gauges onto INCO 718 plate for high temperature evaluation of electrical characteristics of strain gauges
555	Ni	500 W RF	5 x10^{-3} Torr	Floating	
556	PtW	367 W DC	5 x10^{-3} Torr	100 W RF	
557	Au	1.2 A DC	5 x10^{-3} Torr	Floating	

Table 12.01 (b): Deposition parameters for coating runs in this study

Coating run number	Material	Deposition setting / mode	Deposition Pressure	Bias Setting / mode	Comments
590	Al_2O_3	1500 W RF	5 x10^{-3} Torr	Floating	Deposition of PtW on tensile test component for investigation of ambient gauge sensitivity
591	Ni	500 W RF	5 x10^{-3} Torr	Floating	
592	PtW	367 W DC	5 x10^{-3} Torr	100 W RF	
598	PtW	367 W DC	5 x10^{-3} Torr	100 W RF	Investigation of effects of deposition parameters on gauge sensitivity. This showed that the coating thickness was significant
599	PtW	367 W DC	5 x10^{-3} Torr	100 W RF	
600	PtW	367 W DC	2 x10^{-3} Torr	Floating	
601	PtW	367 W DC	2 x10^{-3} Torr	Floating	
520	PdCr	500 mA DC	5 x10^{-3} Torr	Floating	Deposition of PdCr
580	PdCr	500 mA DC	5 x10^{-3} Torr	Floating	Deposition of PdCr
505	Al_2O_3	2000 W PDC	5 x10^{-3} Torr	Floating	Application of NiCr gauges on hydraulic pipe fitting for the acquisition of data on a flight test engine.
506	NiCr	1 A DC	5 x10^{-3} Torr	200 V RF	
507	Au	1 A DC	5 x10^{-3} Torr	Floating	
508	Al_2O_3	2000 W PDC	5 x10^{-3} Torr	Floating	
593	Al_2O_3	2000 W PDC	5 x10^{-3} Torr	Floating	Application of PtW gauges on compressor stator for the acquisition of data on an aerothermal rig test.
594	Ni	500 W RF	5 x10^{-3} Torr	Floating	
595	PtW	367 W DC	5 x10^{-3} Torr	Floating	
596	Au	1 A DC	5 x10^{-3} Torr	Floating	
597	Al_2O_3	2000 W PDC	5 x10^{-3} Torr	Floating	
494	Pt	500 mA DC	15 x10^{-3} Torr	60 V RF	Batch 1 samples
495	Al_2O_3	1500 W RF	5 x10^{-3} Torr	Floating	
496	NiCr	1.2 A DC	5 x10^{-3} Torr	100 W RF	
497	Al_2O_3	1500 W RF	5 x10^{-3} Torr	Floating	
498	Ni	500 W RF	5 x10^{-3} Torr	Floating	
499	Pt	500 mA DC	15 x10^{-3} Torr	60 V RF	
500	NiCoCrAlY	800 mA DC	15 x10^{-3} Torr	100 V RF	

Table 12.01 (c): Deposition parameters for coating runs in this study

Coating run number	Material	Deposition setting / mode	Deposition Pressure	Bias Setting / mode	Comments
570	NiCoCrAlY	800 mA DC	15 x10^{-3} Torr	Floating	Batch 2 samples
571	Pt	500 mA DC	15 x10^{-3} Torr	60 V RF	
572	Al_2O_3	2000 W PDC	4 x10^{-3} Torr	Floating	
573	NiCr	450 W DC	5 x10^{-3} Torr	Floating	
574	Al_2O_3	2000 W PDC	4 x10^{-3} Torr	Floating	
575	Ni	500 W RF	5 x10^{-3} Torr	Floating	
576	Pt	500 mA DC	15 x10^{-3} Torr	60 V RF	
577	NiCoCrAlY	800 mA DC	15 x10^{-3} Torr	100 V RF	
605	NiCoCrAlY	800 mA DC	15 x10^{-3} Torr	200 V RF	Batch 3 samples
606	Pt	500 mA DC	15 x10^{-3} Torr	60 V RF	
607	Al_2O_3	1800 W PDC	4 x10^{-3} Torr	Floating	
609	PdCr	500 mA DC	5 x10^{-3} Torr	Floating	
609	Al_2O_3	1800 W PDC	4 x10^{-3} Torr	Floating	
610	Cr	500 mA DC	5 x10^{-3} Torr	Floating	
611	Pt	500 mA DC	15 x10^{-3} Torr	60 V RF	
612	NiCoCrAlY	800 mA DC	15 x10^{-3} Torr	100 V RF	
618	NiCoCrAlY	800 mA DC	15 x10^{-3} Torr	200 V RF	Temperature measurement during deposition

Table 12.01 (d): Deposition parameters for coating runs in this study

The following techniques have been developed

Lift-off patterning process

Application method for photoresist on large components

Novel method of clamping mask to component

Calibration method for thin film thermocouples

Fabrication of a novel multilayer structure comprising sputtered bond coat, dielectric and metallic layers

12.2 Project conclusions

A solution to the problem of temperature and strain measurements on thermal barrier coated components has been demonstrated. The solution has proved to be a very complicated novel multilayer structure. The enabling technology for this sensor package has been evaluated and the results have been very encouraging. The high temperature coatings have been assembled into a sensor package consisting of seven layers on a turbine blade alloy substrate. Despite suffering interface failure due to contamination and residual stresses in the coatings, this work has shown that such a structure is feasible. Significant progress has been made to identify the best processing route. The main problems identified are the electrical insulation of the sensor and the formation of a dense well-adhered upper NiCoCrAlY layer. A programme has been established to solve these problems and a number of the main points from this are given later in this chapter.

The work has involved the development of a number of new processes. Specifically, the work has demanded innovation in the application of a magnetron-sputtered layer of NiCoCrAlY to replace the standard Vacuum Plasma Spray process that required subsequent shot peening. The use of a statistical experiment design has reduced the amount of experimentation necessary to yield valuable conclusions from the work. The effects of the deposition parameters on the coating structure, composition and deposition rate have been established. An excellent dense, well-adhered coating has been obtained. The deposition parameters that gave a dense coating resulted in a low aluminium content of the deposited film. This has been improved by the addition of aluminium studs to the NiCoCrAlY target. The effect of surface preparation method on the structure, adhesion and the number of interfacial voids have been established.

The Rolls-Royce facility was upgraded to allow the patterning and evaluation of the high temperature sensors. This has built up one of the most advanced facilities in this country for this type of application. A lift-off patterning technique has been developed to allow the formation of high temperature noble-metal sensors. The patterning process has also been improved to allow the patterning of large, heavy and

complex shaped components. This has also yielded benefit for lower temperature applications. Several examples of the use of this technology for the acquisition of data on engine development projects are reviewed in the thesis. One is for the application of strain gauges on a hydraulic pipe elbow fitting for Trent 700 flight test on an Airbus A330. The failure of this component by high cycle fatigue and the subsequent loss of hydraulic fluid, had caused engine shut down on several occasions whilst in service. The component size and complicated shape prohibited the use of conventional sensors. The application of thin film sensors allowed trials to be performed to alter the position of clamping of the hydraulic pipe to prevent vibration in the elbow fitting.

High temperature thin film sensors have been evaluated. A platinum-rhodium thermocouple has been fabricated and calibrated against a similar wire thermocouple. The results were very encouraging and show that high accuracy temperature measurements are possible. Several strain gauge alloys have been deposited and evaluated. Platinum-tungsten has been evaluated at temperature and a trial established to determine the effect of the deposition parameters and gauge design on sensor performance. A valuable conclusion can be drawn from this that the gauge sensitivity is highly dependent on the coating thickness and the sensitivity approaches that of wire gauges as the film thickness is increased.

An ENI pulsed dc power supply has been evaluated as a method for reducing arcing in the reactive sputtering of aluminium oxide compared with a RF supply. This work has identified the need to redesign the sputtering cathode to increase the utilisation of the target. This work has been performed by Gencoa Ltd and is awaiting evaluation. The coatings produced by the use of the pulsed dc supply with the existing cathode have been evaluated. These are stoichiometric and dense. The coatings have a number of surface features, which have been identified as nodular defects produced by imperfections on the substrate surface. These have been suppressed by the use of RF biasing during deposition.

The intended application for this work has been delayed from a test date in 1998 to the middle of the year 2000. This has caused financial budget alterations during the project, which shifted the facility resource towards the low temperature sensor applications. The high temperature development work has been further delayed by the loss of the Elton Road deposition system early in the programme and the need to order new sputtering targets. The work has however reached a point where significant conclusions can be drawn and future work identified to achieve the acquisition of data on thermal barrier coated components.

12.3 Recommendations for future work

Throughout the preceeding chapters attention has been drawn to areas which require further work. These are summarised in this section.

The survivability of the sensor package requires that a dense but well-adhered layer of NiCoCrAlY be deposited onto the component. The formation of a dense layer implies that the coating will have compressive residual stresses. The key to improving the adhesion lies in the elimination of the source of interfacial contamination and the use of chromium to promote adhesion between the oxide and metallic layers.

The top temperature capability of the sensor package needs to be improved. Specifically the arcing problem on the aluminium target needs to be resolved. Use of the new Gencoa cathode with the ENI power supply needs evaluation. The other identified source of defects in the oxide target is due to substrate imperfections. The polishing of the metallic coatings needs to be improved and a repeatable process established.

The next logical step would be the application of the TBC coating onto the sample by PVD. The sensor and coatings need to be examined for evidence of deterioration. The sensor package should then be subjected to temperature and strain cycling, to represent the environmental conditions in an engine during accelerations and

decelerations. The sensor package should be assembled on an actual CMSX-4 HP turbine blade. The structure of the coatings should be inspected due to the deposition on a complex shaped component. The high cycle fatigue and calibration of the sensor position against blade tip displacement amplitude can be performed by the excitation of the blade into a resonant vibration mode.

Fine wires should be attached to the sensor tracks by parallel gap welding. The high temperature properties of the sensor package can then be evaluated. A Lloyd Instruments tensile test machine has been purchased for the evaluation of the high temperature gauge sensitivity of the Pt-W and Pd-Cr sensors. The sensor package should be fabricated onto a CMSX-4 tensile test sample for this work.

New targets are required to further investigate the high temperature sensor characteristics and effect of deposition parameters on gauge performance.

Chapter 13: References

[1] Loftus P., Shepherd R.S., Stringfellow K., Surface mounted sensors for gas turbine R&D, SPIE Smart structures and materials conference, Albuquerque, New Mexico, 1993.

[2] The jet engine, Rolls-Royce publications, ISBN 0 902121 04 9, 1986.

[3] Smailes G., Vibration analysis of gas turbine blades, training document, Rolls-Royce, unpublished, 1993.

[4] Ashworth K., Private communication, Rolls-Royce, 1995.

[5] Ciureanu P., Middelhoek S., pp145-160, Thin film resistive sensors, Institute of Physics publishing, ISBN0750301, 1992.

[6] Bertodo R., Precious metal alloys for high temperature strain gauges, MRI Publication 68-RE-146, 1968.

[7] Hulse C.O., Bailey R.S., Grant H.P. Przyybyszewski J.S., High temperature static strain gauge development contract Interim report, Report number CR 180811, United Technologies Research Center, 1986.

[8] Lei J.F., Pd-Cr based high temperature static strain gauges, AIAA 5236, 1990.

[9] Lei J.F., High temperature thin film strain gauges, British Society of Strain Measurement conference proceedings, 1995.

[10] Shepherd R.S., Visit report to IHI, Japan, Rolls-Royce internal report EIR 01516, 1995.

[11] Gregory O.J., Dyer S.E., Cooke J.D., Overcoats for the improved performance of PdCr high temperature thin film strain gauges, AGARD Conference proceedings. 598, ISBN 92-836-0055X, 1997.

[12] Tong L., Guo J., Noble metal alloys as strain gauge materials, Platinum metals rev. 38, 98-108, 1994.

[13] Guo J., Tong L., Chen L., Platinum alloy strain gauge materials, Platinum metals rev. 41, 24-32, 1997.

[14] Wnuk S., Gauge factor considerations for platinum-tungsten alloy at elevated temperatures, Hitec Corporation publication, 1983.

[15] Mathers J., High temperature strain gauge parameters, Rolls-Royce report EIR 01467, 1993.

[16] Bethe K., Schon D., Thin film strain gauge transducers, Philips Tech. Rev.39, 94-101, 1980.

[17] Parrish C. J., Measurement uncertainty analysis for dynamic strain gauge measurement, Rolls-Royce report, EIR 01848, 1997.

[18] Mathers J., Strain measurement using resistance gauges-estimation of measurement errors, Rolls-Royce report, EIM 00078, 1992.

[19] Burke RT, Transduction errors in dynamic stress measurement, Rolls-Royce report EIR 00903, 1985

[20] Porter R., Experience of running thin film strain gauges on Rig 629/12, Rolls-Royce report EIR 01736, 1996.

[21] Slater T., Private communication, Rolls-Royce, 1997.

[22] Instrumentation standard and technique report number 03.05, Rolls-Royce unpublished material, 1988.

[23] Mathers J., Private communication, Rolls-Royce, 1997.

[24] Gregory O.J, Cooke J.D., Bienkiewicz J.M., High temperature-thin film strain gauges based on alloys of Indium Tin oxide, AGARD-CP-598, ISBN 92-836-0055, 1998.

[25] Larcombe R., Private communication, Rolls-Royce, 1997.

[26] Bird C., Mutton J.E., Shepherd R.S., Smith M.D.W., Watson H.M.L., Surface temperature measurements in turbines, AGARD CP-598, ISBN 92-836-0055, 1998.

[27] Childs P., Greenwood J., Long C, Techniques of temperature measurement and their selection, Rolls-Royce UTC report, 1998.

[28] Kaye G.W.C., Laby TH., Table of physical and chemical constants, 16th Edition, Longman Scientific & Technical, 1995.

[29] Finch D.I., General principals of thermoelectric thermometry, In temperature; Its measurement and control in science and industry, Editor: Herzfeld CM, Reinhold Pub Co, 3(2), pp 3-32, 1962.

[30] Lide D.R., Frederikse H.P.R., (editors) CRC handbook of chemistry and physics: a ready reference book of chemical and physical data, 77th edition, Handbook of chemistry and physics. Rubber handbook, CRCP Boca Raton, 1996.

[31] Michalski L., Eckersdorf K., Temperature Measurement, John Wiley & Sons, 1991.

[32] Greenwood J.R., Development of Robust Instrumentation for high speed rotating machinery, University of Sussex report, 1998.

[33] Caldwell F.R., Thermocouple materials: Temperature its measurement and control in science and industry, Herzfield C.M. (Editor) Rheinhold1-3, 1962.

[34] Serro J.A., Noble metal thermocouple wire, Engelhard Industries technical data sheet EM-6325-2. 1968

[35] Loftus P., High temperature applications of thermocouples, Von Karman Institute lecture series, 1996.

[36] Bedwell D.R., Introduction to Temperature measurements, Von Karman Institute lecture series, 1996.

[37] Kinzie P.A., Thermocouple temperature measurement, Wiley, 1973.

[38] Stringfellow K., HTDU4X Life of aerofoil embedded thermocouples, Rolls-Royce report EIR 00388, 1995.

[39] Parrish C., Uncertainty measurements in embedded thermocouple applications, Rolls-Royce internal report.

[40] Stein P.K., Advanced strain gauge techniques, Stein engineering services, 1962.

[41] Parrish C.P., Rig 629 build 1 instrumentation critique, Rolls-Royce report MER 43855, 1990.

[42] General Electric patent, Thin film gauges and method of fabrication, US patent 4, 104, 605, 1978.

[43] General Electric communication, 1995.

[44] Porter R.J., Trial of applied thin film strain gauges on Trent IPC Rig 821 build 4, Rolls-Royce internal report, EIR 01626, 1994.

[45] Grant H.P., Anderson W.L., Przybyszewski J.S., Rotating tests of advanced high temperature wire and thin film strain gauges, AIAA-88-3146, 1988.

[46] Gray D.R., Wood M.I., Lamb P.C., Thin film strain gauging on engineering components, ERA Technology Ltd, Report number 92-0726R, 1992.

[47] Gray D.R., Final report on development of thin film strain gauges for engine instrumentation, G V Planer Ltd, Report number D9378, 1980.

[48] Aona H., Shinohara J., Chikata T., Hagiwara Y., Thin film gauges for measuring dynamic strain on a compressor blade, SEM Las Vegas Meeting, 1985.

[49] Dennis A.J., Advanced structural instrumentation, AIAA-85-1470, 1985.

[50] Kayser P., Godefroy L., Sensors and Actuators, A37-A38, 328, 1993.

[51] Bethe K., Schon D., Thin film strain gauge transducers, Philips Tech Rev. 39, 94-101, 1980.

[52] Kuo T.C., Flattery J., Ghosh P.K., Kornreich P.G., Fabrication and calibration of integrated Cu-Cr thermocouple gauge, Rev. Sci. Instrum. 59 (10), 1988.

[53] Whiting R., Angadi M.A., Multilayer Cu/Cr films as strain gauges, Meas. Sci. Technol., 2, 879-881, 1991.

[54] Budhani R.C, Prakash S.,Bunshah R.F., Thin film temperature sensors for gas turbine engines: Problems and prospects, J. Vac. Sci. Technol., A4(6), 1986.

[55] Dunker R. (Editor), Advances in techniques for engine applications, Wiley & Sons, ISBN 0471953636, 1994.

[56] Kreider K.G., Semancik S., Olson C., Advanced thin film thermocouples, NBSIR-84/2949, 1984.

[57] Dils R.R., Follansbee P.S., High temperature sputtered surface sensors ISA ASI 75224 (127-132), 1975.

[58] Richardson P.E.C., Development of thin film dielectrics and thermocouples-engine and laboratory experience, Rolls-Royce report PD2134, 1980.

[59] Stowell W.R., Welse R.A., Application of thin film strain gauges and thermocouples for measurement on aircraft engine parts, General Electric company report, 1985.

[60] Rimai D.S., Anne R., The fabrication of thin-film thermocouples for determining the temperature and thermal conductivity within a flexible material, Rev. Sci. Instrum. 64 (6), 1993.

[61] Godefroy J.C., Gageant C., Francois D., Portat M., Thin film temperature sensors deposited by radio frequency cathodic sputtering, J. Vac. Sci. Technol., A5(5) 2917, 1987.

[62] Yoshida T., Taki M., Mimura F., High temperature thin film temperature sensors-current status of research and development, 67 Symposium of Japan Society of mechanical engineers, 1990.

[63] Huang H.L., Reliability consideration of thin film temperature sensors, AIAA 27th conference, 1991.

[64] Morel T., Wahiduzzamman S., Fort E.F. Tree D.R., DeWitt D.P., Kreider K.G., Heat transfer in a cooled and insulated diesel engine, SAE paper 890572,pp 185-195, 1989.

[65] Tong H.M., Arjavalingam G., Haynes R.D., Hyer G.N., Ritsko J.J., High temperature Pt-Ir thermocouple with fast time response, Rev. Sci. Instrum. 58 (5), 1987.

[66] Enomoto Y., Furuhama S., Study on thin film thermocouple for measuring instantaneous temperature on surface of combustion chamber wall in internal combustion engine, JSME. Vol. 28, No 235, 1985.

[67] Kreider K.G., Sputtered high temperature thin film thermocouples, J. Vac. Sci. Technol. A 11(4), 1993.

[68] General Electric information, Thin film transducers, unpublished, 1987.

[69] Shepherd R. S., Fabrication of hot film anemometer gauges for rig DT 32 build 2, Rolls-Royce report EIR 01322, 1994.

[70] Cook S.C.P, The development of thin film sensors at IHI, Japan, Rolls-Royce report EIR 01228, 1989.

[71] Barker A.J., Thin film sensors for aerospace applications, MSc report, University college, Swansea, 1993.

[72] Teer D.G., Evaporation and Sputter Techniques, Coatings for high temperature applications, edited by Lang E., Applied Science Publishers Ltd, ISBN0-85334-221-0, 1983.

[73] Westwood W.D., Sputter Deposition processes, MRS bulletin, 1998.

[74] CVC Products, Inc., Product information bulletin No 060282, 1982.

[75] Sigmund P., Phys. Rev. 184, 383, 1969.

[76] CVC training material, The basics of sputtering. unpublished, undated.

[77] Swann S., Magnetron sputtering, Physics Technol. 19, IOP publishing Ltd, 1988.

[78] Westwood W.D., Glow discharge sputtering, Progress in surface science, Vol. 7 pp71-111, Pergamon Press.

[79] Vossen J.L., J. Vac. Sci. Technol, 8, 751, 1971.

[80] Reichelt K., Nucleation and growth of thin films, Vacuum 38, pp1083-1099, 1998.

[81] Thornton J.A., Influence of apparatus geometry and deposition conditions on the structure and topography of thick sputtered coatings, J. Vac. Sci. Technol, Vol. 11, No4, 1974.

[82] van Kranenburg H., Lodder C., Tailoring growth and local composition by oblique-incidence deposition: a review and new experimental data, Materials Science and Engineering, R11, 295-354, 1994.

[83] Westwood W.D., Sputter deposition processes, MRS Bulletin, 1988.

[84] Godefroy J.C., Thin film temperature heat fluxmeters, Thin solid films, 193/194 924-934, 1990.

[85] Wang C.C., Akbar S.A., Chen W., Patton V.D., Review electrical properties of high temperature oxides, carbides and borides, J. Material Science, 30,1627-1641, 1995.

[86] Bauer A.A., Bates J.L., Variation of electric conductivity for insulation materials, Battelle Mem. Inst. Report., 1930.

[87] Elena M., Guzman L., Calliari L., Moro L., Steiner A., Miotello A., Bonnelli M., Capelletti M., Ossi P.M., Synthesis and structural characterisation of boron nitride thin films, Thin Solid Films, Vol. 253, No 1-2, 1994.

[88] Elena M., Guzman L., Production and characterisation of boron nitride films obtained by RF magnetron sputtering and reactive ion-beam assisted deposition, Surface and Coatings Technology, Vol. 36, No 1-2, 1988.

[89] Rickerby D. G., Gibson P.N., Gissler W., Haupt J., Structural investigation of reactively sputtered boron nitride films, Thin Solid films, 209, 155-160, 1992.

[90] Mieno M., Yoshida T., Preparation of cubic boron nitride films by radio frequency bias sputtering, Surface & Coatings Technology, Vol. 52, No 1, 1992.

[91] Goranchev B., Compressive stress of thin cubic BN films prepared by RF reactive sputtering on RF biased substrates, Thin Solid Films, Vol. 149, No1, 1987.

[92] Gissler W., Haupt J., Hoffman A., Gibson PN., Rickerby DG., Mixed phase nanocrystalline boron nitride films. Preparation and characterisation, Thin Solid Films, Vol. 199, No 1, 1991

[93] Tanabe N., Iwaki M., Influence of sputtering target material on the formation of cubic BN thin films by ion beam enhanced deposition, Diamond and related materials, Vol. 2, No 2-4, 1993.

[94] Shepherd R.S., Visit report to IHI, Japan, Rolls-Royce internal report EIR 01580, 1994.

[95] Richardson P.E.C., Directly deposited silicon nitride thin films: Deposition and evaluation, Rolls-Royce report, 1974.

[96] Godefroy J.C., Clery M., Gageant C., Francois D., Servouze Y., Thin film temperature heat fluxmeters, Thin solid films 193/194, pp924-934, 1990.

[97] Goranchev B., Structure of aluminium oxide films deposited by dc reactive sputtering, Thin solid films, 70, no 1, 1980.

[98] Kuwahara K., Sumomogi T., Kondo M., Internal stress in aluminium oxide, titanium carbide and copper films obtained by planar magnetron sputtering, Thin solid films, 78, no 1, 1981.

[99] Kreider K.G., Semancik S., Thermal and sputtered aluminium oxide coatings for high temperature electrical insulation, J. Vac. Sci. Technol. A3 (6), 1985.

[100] Olivera A., *et al.*, Production and characterisation of Si-N film obtained by RF magnetron sputtering, Surface & Coatings technology, 60, 463-467, 1993.

[101] Jones R.E, *et al.*, J.Vac. Sci. Technol., 5. 84, 1967

[102] Schiller S., *et al.*, Reactive dc high rate sputtering as production technology, Surface & Coatings technology, 33, 405, 1987.

[103] Strauder B., Perry F., Frantz C., Chemical and structural analysis of aluminium-oxide coatings obtained by dc magnetron reactive sputtering-some features of the process, Surface & Coatings technology, Vol. 74-75, Nos. 1-3, pp320-325, 1995.

[104] Mallins A., MSc project report, Loughborough University, 1995.

[105] Schiller S.,Goedicke K., Metzner C., Advances in pulsed magnetron sputtering, paper presented to International conference on metallurgical coatings and thin films, San Diego, April 1994.

[106] Schiller S, Goedicke K., Reschke J., Kirchhhoff V., Schneider S., Milde F., Pulsed magnetron sputter technology, Surface and Coatings Technology, 61, 331-337, 1993.

[107] Sellers J.C., Asymmetric bipolar pulsed DC, An enabling technology for reactive PVD, Soc. of Vacuum Coaters, 505/856-7188, 39th Annual technical conference proceedings, 1996.

[108] Shepherd R., Visit report to PA Consulting Ltd to obtain details of thin film polishing process, Rolls-Royce report EIR 01250, 1993.

[109] McCarter P.S., Private communication with project customer, Rolls-Royce, 1995.

[110] Gent J., Private communication, Rolls-Royce, 1995.

[111] Stringfellow K., Private communication, Rolls-Royce, 1995.

[112] Mathers J., Private communication, Rolls-Royce, 1995.

[113] Stringfellow K., HTDU4X Life of aerofoil embedded thermocouples, Rolls-Royce report EIR 00388, 1995.

[114] Rickerby D., Private communication, Rolls-Royce, 1995.

[115] Lewis R.G.O., Private communication, Rolls-Royce, 1995.

[116] Rickerby D., Private communication, Rolls-Royce, 1995.

[117] Larcombe R., Private communication, Rolls-Royce, 1996.

[118] Morell R., Handbook of properties of technical engineering ceramics, NPL, Her Majesty's stationary office, ISBN 0114800529, 1985.

[119] Unkel D.A., Elevated temperature strain gauges using resistive strain gauges, Strain gauge users handbook, Edited by Hannah RL & Reed SE, Elsevier Science publishers ltd.

[120] Shepherd RS., HTDU5 feasibility study report, Rolls-Royce internal report, EIR 016231, 1995.

[121] CVC operating manual, 1993.

[122] Weast R.C. (Editor), CRC handbook of chemistry and physics, CRC Press Inc, ISBN-0-8493-0460-8, 1962.

[123] Critchlow G.W., Instrumental Techniques for the surface analysis of materials, Trans IMF, 74 (3),108, 1996..

[124] Institute of Surface Science and Technology, Loughborough University, Course notes: Surface & Interface analysis applied to industrial problems, 1988.

[125] Institute of Surface Science and Technology, Loughborough University, Fact sheet.

[126] Elliot I. (Editor), Chemical characterisation, Institute of metals 444 seminar, ISBN 0-901462-50-0, 1988.

[127] Scott V.D., Love G., Quantitative electron-probe microanalysis, Ellis Horwood Ltd, ISBN 0-85312-514-7, 1983.

[128] Rank Taylor-Hobson Talysurf 10 operators handbook, 241-7.

[129] Rolls-Royce training course notes: Risk management facilitator, 1996.

[130] Rolls-Royce training course :Taguchi methodology, 1996.

[131] Davies L., Efficiency in research, development and production: The statistical design and analysis of chemical experiments, The Royal Society of Chemistry, ISBN 0-85186-137-7, 1993..

[132] Rolls-Royce information.

[133] Rolls-Royce information.

[134] Weast R.C (Editor), CRC Handbook of chemistry and physics, CRC Press Inc., ISBN 0-8493-0460-8, 1979.

[135] Rickerby D.S., Private communication, 1995.

[136] Gent J, Personal communication, 1996.

[137] Critchlow G., AES analysis of aluminium oxide films on glass, Institute of Surface Science and Technology report, AU/RRL/6479a.

[138] Brett M.J., Tait R.N., Dew S.K. Kamasz S., Labun A.H., Smy T., Nodular defect growth in thin films, J. Mat. Sci.: Materials in electronics 3, 64-70, 1992.

[139] Busfield R., Preliminary development studies of thin film PtRh, Rolls-Royce report EIR 01875, 1998.

[140] Englehard technical data sheet, Englehard Ltd, 1968.

[141] Rickerby D., Private communication, Rolls-Royce, 1996.

[142] Molyneux B., Process temperature monitor for use on the vacuum deposition rig, Rolls Royce report, EIM 00762, 1998.

Appendix 1: Substrate temperature measuring system

During the deposition of the metallic coatings or deposition onto temperature sensitive materials such as the photoresist layer, it was extremely valuable to have the ability to monitor the substrate temperature. Such a measurement is problematic, not least because of the complexity of movement of the substrates in the chamber, limited access to vacuum ports on the chamber and large voltages present on the substrate. One method would be to use an optical pyrometer to monitor the temperature, however line of sight from a view port to the substrate would not always be possible and the emisivity of the component would change as it was coated.

In order to measure the temperature of the substrate during deposition; a K-type thermocouple was attached directly to it. A K-type thermocouple vacuum feedthrough was purchased and fitted to a spare chamber port. This meant that the thermocouple and its monitoring equipment would experience the large radio frequency and dc common mode signals that are present on the substrate. These voltages would have constituted a hazard to the operator and would have caused conventional monitoring equipment to read erroneously or even be destroyed.

Although most of the target potential is across a region of a few millimetres in front of the target, some charged species would reach the sample causing it to charge up to a proportion of the target potential. To further control the coating properties, the sample could also be driven by a radio frequency source at 13.56MHz up to a power of 1000W. To protect the operator and equipment, a low pass filter was designed to fit close to the thermocouple feed-through. This removes any AC common mode signals present. These will be due predominately to the 13.56 MHz substrate drive but the filter also removes the 50-250kHz-signal leakage from the pulsed dc target drive. After filtering, a common mode of several hundred volts may be present to the asymmetrical nature of the drive waveforms. To accommodate this, the thermocouple amplifier and cold junction were designed to be fully floating and not referenced to earth. The output of the thermocouple amplifier was connected to an isolation amplifier whose output was earth referenced, effectively removing the common mode

voltage at this point. The output was then safely fed to the display unit. Brian Molyneux[142], an electrical systems designer, performed the design and construction of the filter and amplifier units. The author performed the specification and installation of the system.

The thermocouple gain was adjusted so that it displayed an accurate temperature. A small furnace was constructed from a ceramic tube wound with Nichrome V wire. This was insulated with a thermal insulation blanket. The system thermocouple and a calibrated reference thermocouple were clamped together and inserted into the furnace. The reference temperature was monitored through a k type thermocouple monitor box and the system thermocouple on the rack-mounted display, as the current applied to the furnace was increased. Both thermocouples gave similar readings at room temperature. However, the system thermocouple read 30°C lower at 250°C. The set gain potentiometer shown in figure A-2 was altered so that both thermocouples read the same at temperature.

Measurement of substrate temperature *during NiCoCrAlY deposition*

The substrate temperature was measured during a six hour coating run of NiCoCrAlY from an AJA cathode. The substrate was first ion cleaned at 200 Volts RF for 45 minutes. The deposition of the metallic coating was then started. Because of the complexity of the sample rotation system the substrate had to be fixed in place while the thermocouple was attached. Therefore the target could not be cleaned before the deposition onto the substrate. This is a useful technique for mapping the temperature profile during a deposition sequence but cannot be used for production coating work.

The NiCoCrAlY was deposited at a pressure of 15 $x10^{-3}$ Torr. The deposition current was 800mA and the bias set to 200 Volts. A graph of the substrate temperature is given in figure A-4. For this it can be seen that the substrate temperature becomes constant at 80°C after 30 minutes of ion cleaning. When the NiCoCrAlY deposition is started the temperature rises slowly and then becomes constant around 200°C.

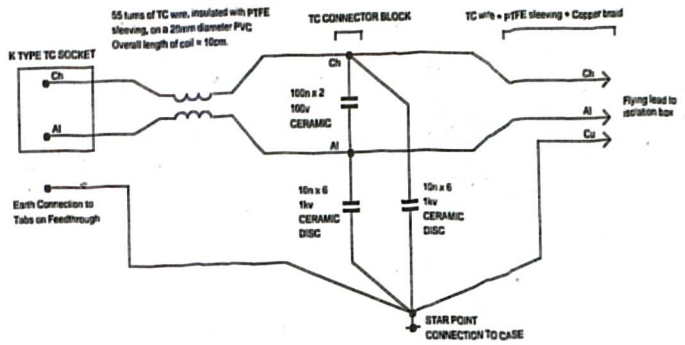

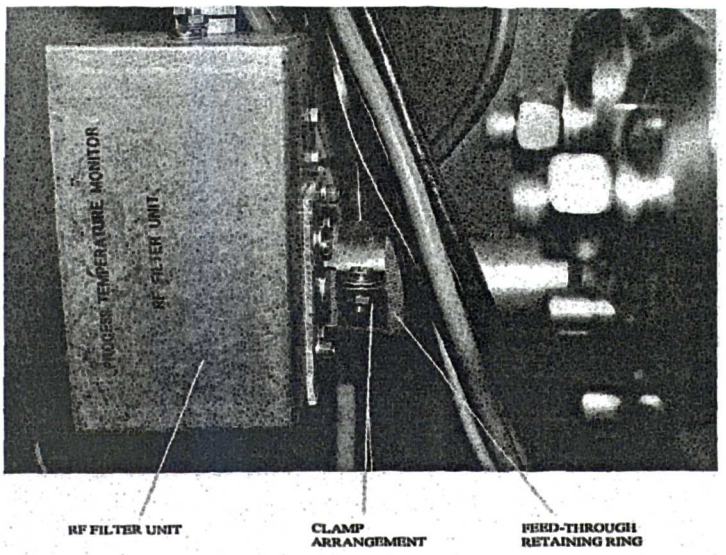

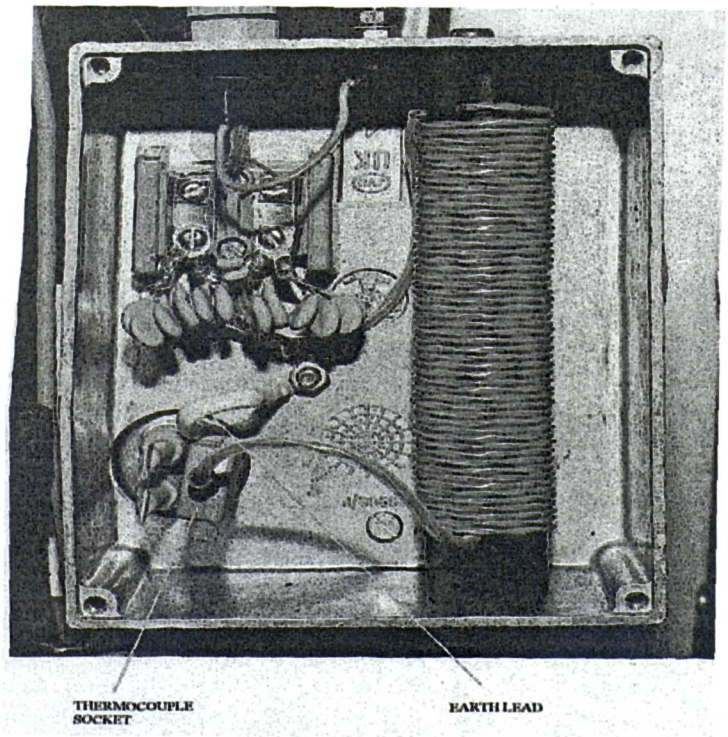

Figure A-1: RF filter unit

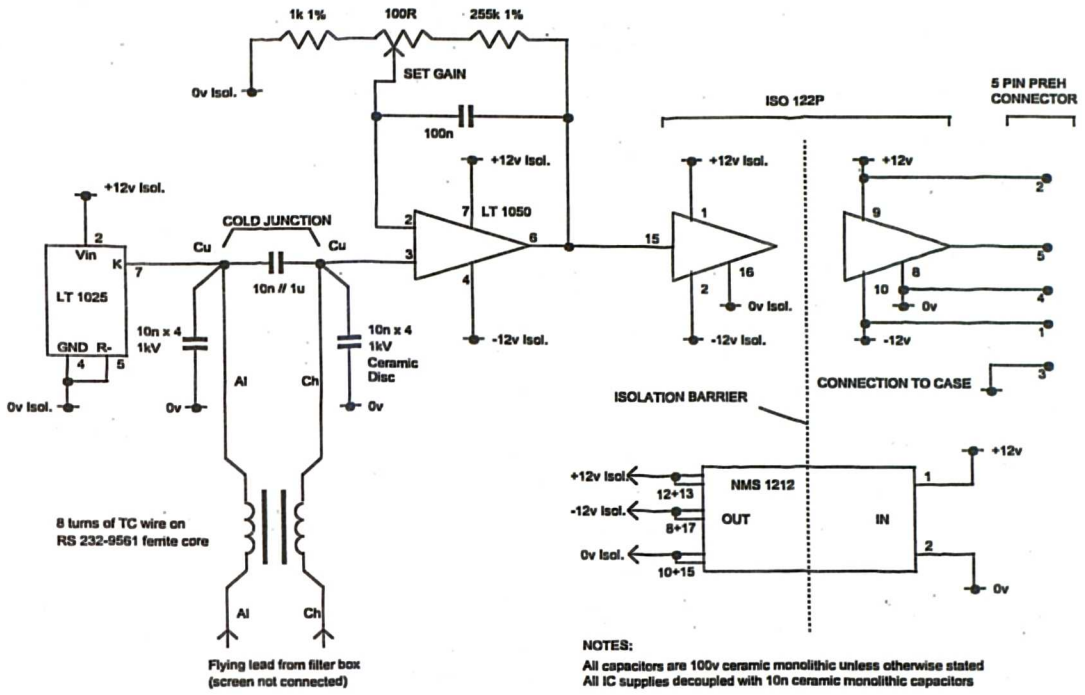

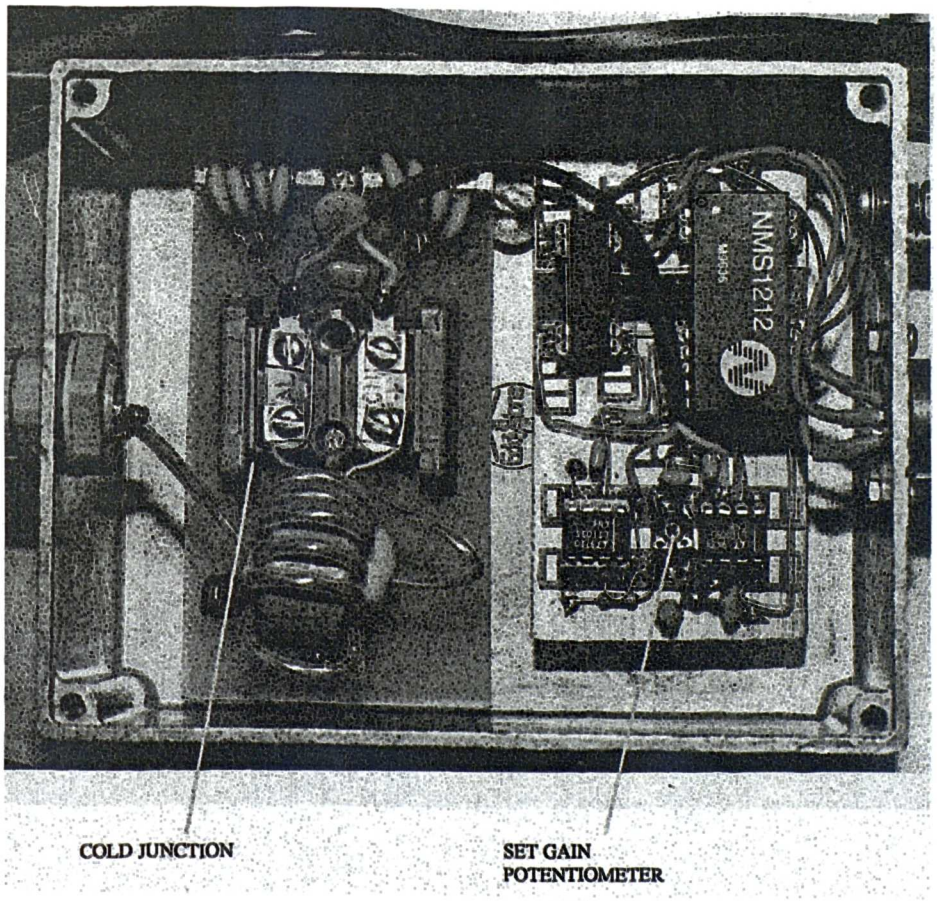

Figure A-2: Amplifier/Isolator unit

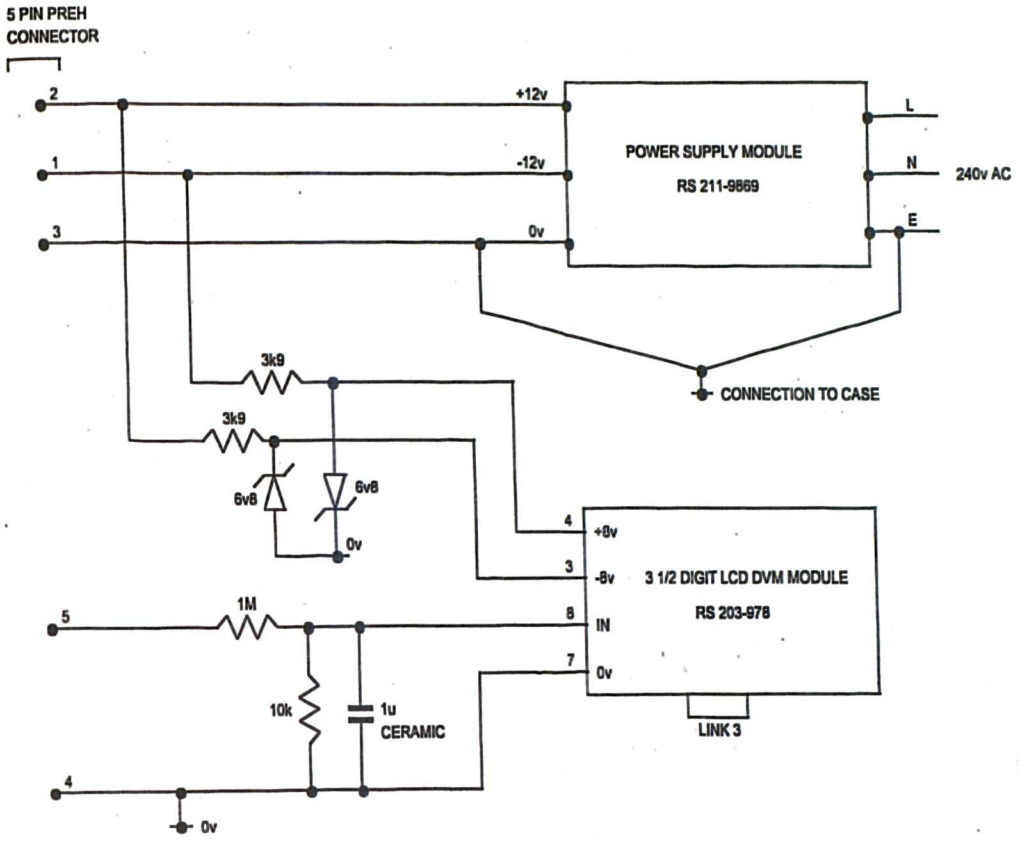

Figure A-3: Display/Power module

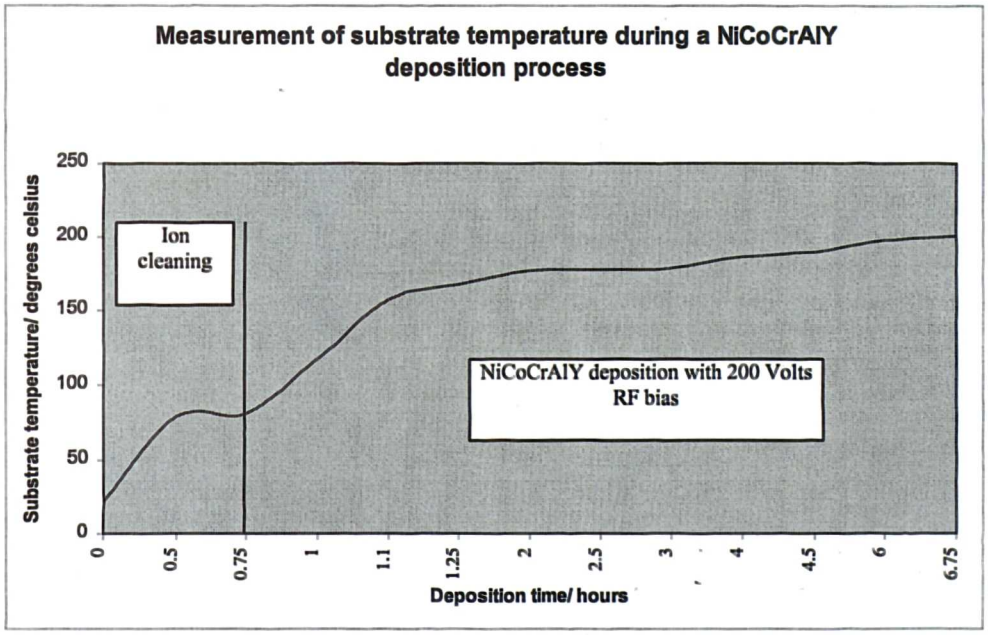

Figure A-4: Substrate temperature during a six-hour deposition of NiCoCrAlY